Publishing House ASV

begell house, inc. publishers

PAACH

Scientific coordination is carried out by the Russian Academy of Architecture and Construction Sciences (RAACS)

Volume 18 • Issue 2 • 2022

ISSN 2588-0195 (Online)
ISSN 2587-9618 (Print) Continues ISSN 1524-5845

International Journal for

Computational Civil and Structural Engineering

Международный журнал по расчету гражданских и строительных конструкций

http://raasn.ru/public.php
http://ijccse.iasv.ru/index.php/IJCCSE

DOI: 10.22337/2587-9618
GICID: 71.0000.1500.2830

PUBLISHER

ASV Publishing House
(ООО «Издательство АСВ»)
19/1,12, Yaroslavskoe Shosse, 120338, Moscow, Russia
Tel. +7(925)084-74-24; E-mail: iasv@iasv.ru; Интернет-сайт: http://iasv.ru/

ADVISORY EDITORIAL BOARD

TECHNICAL EDITOR

EDITORIAL TEAM

INVITED REVIEWERS

AIMS AND SCOPE

The aim of the Journal is to advance the research and practice in structural engineering through the application of computational methods. The Journal will publish original papers and educational articles of general value to the field that will bridge the gap between high-performance construction materials, large-scale engineering systems and advanced methods of analysis.

The scope of the Journal includes papers on computer methods in the areas of structural engineering, civil engineering materials and problems concerned with multiple physical processes interacting at multiple spatial and temporal scales. The Journal is intended to be of interest and use to researches and practitioners in academic, governmental and industrial communities.

ОБЩАЯ ИНФОРМАЦИЯ О ЖУРНАЛЕ

International Journal for Computational Civil and Structural Engineering

(Международный журнал по расчету гражданских и строительных конструкций)

Международный научный журнал "International Journal for Computational Civil and Structural Engineering (Международный журнал по расчету гражданских и строительных конструкций)" (IJCCSE) является ведущим научным периодическим изданием по направлению «Инженерные и технические науки», издаваемым, начиная с 1999 года (ISSN 2588-0195 (Online); ISSN 2587-9618 (Print) Continues ISSN 1524-5845). В журнале на высоком научно-техническом уровне рассматриваются проблемы численного и компьютерного моделирования в строительстве, актуальные вопросы разработки, исследования, развития, верификации, апробации и приложений численных, численно-аналитических методов, программно-алгоритмического обеспечения и выполнения автоматизированного проектирования, мониторинга и комплексного наукоемкого расчетно-теоретического и экспериментального обоснования напряженно-деформированного (и иного) состояния, прочности, устойчивости, надежности и безопасности ответственных объектов гражданского и промышленного строительства, энергетики, машиностроения, транспорта, биотехнологий и других высокотехнологичных отраслей.

В редакционный совет журнала входят известные российские и зарубежные деятели науки и техники (в том числе академики, члены-корреспонденты, иностранные члены, почетные члены и советники Российской академии архитектуры и строительных наук). Основной критерий отбора статей для публикации в журнале − их высокий научный уровень, соответствие которому определяется в ходе высококвалифицированного рецензирования и объективной экспертизы, поступающих в редакцию материалов.

Журнал входит в Перечень ВАК РФ ведущих рецензируемых научных изданий, в которых должны быть опубликованы основные научные результаты диссертаций на соискание ученой степени кандидата наук, на соискание ученой степени доктора наук по научным специальностям и соответствующим им отраслям науки:

- 1.1.8 – Механика деформируемого твердого тела (технические науки),
- 1.2.2 – Математическое моделирование численные методы и комплексы программ (технические науки),
- 2.1.1 – Строительные конструкции, здания и сооружения (технические науки),
- 2.1.2 – Основания и фундаменты, подземные сооружения (технические науки),
- 2.1.5 – Строительные материалы и изделия (технические науки),
- 05.23.07 – Гидротехническое строительство (технические науки),
- 2.1.9 – Строительная механика (технические науки)

В Российской Федерации журнал индексируется Российским индексом научного цитирования (РИНЦ).

Журнал входит в базу данных Russian Science Citation Index (RSCI), полностью интегрированную с платформой Web of Science. Журнал имеет международный статус и высылается в ведущие библиотеки и научные организации мира.

Издатели журнала – *Издательство Ассоциации строительных высших учебных заведений /АСВ/* (Россия, г. Москва) и до 2017 года *Издательский дом Begell House Inc*. (США, г. Нью-Йорк). Официальными партнерами издания является *Российская академия архитектуры и строительных наук* (РААСН), осуществляющая научное курирование издания, и *Научно-исследовательский центр СтаДиО* (ЗАО НИЦ СтаДиО).

Цели журнала – демонстрировать в публикациях российскому и международному профессиональному сообществу новейшие достижения науки в области вычислительных методов

решения фундаментальных и прикладных технических задач, прежде всего в области строительства.

Задачи журнала:

• предоставление российским и зарубежным ученым и специалистам возможности публиковать результаты своих исследований;

• привлечение внимания к наиболее актуальным, перспективным, прорывным и интересным направлениям развития и приложений численных и численно-аналитических методов решения фундаментальных и прикладных технических задач, совершенствования технологий математического, компьютерного моделирования, разработки и верификации реализующего программно-алгоритмического обеспечения;

• обеспечение обмена мнениями между исследователями из разных регионов и государств.

Тематика журнала. К рассмотрению и публикации в журнале принимаются аналитические материалы, научные статьи, обзоры, рецензии и отзывы на научные публикации по фундаментальным и прикладным вопросам технических наук, прежде всего в области строительства. В журнале также публикуются информационные материалы, освещающие научные мероприятия и передовые достижения Российской академии архитектуры и строительных наук, научно-образовательных и проектно-конструкторских организаций.

Тематика статей, принимаемых к публикации в журнале, соответствует его названию и охватывает направления научных исследований в области разработки, исследования и приложений численных и численно-аналитических методов, программного обеспечения, технологий компьютерного моделирования в решении прикладных задач в области строительства, а также соответствующие профильные специальности, представленные в диссертационных советах профильных образовательных организациях высшего образования.

Редакционная политика. Политика редакционной коллегии журнала базируется на современных юридических требованиях в отношении авторского права, законности, плагиата и клеветы, изложенных в законодательстве Российской Федерации, и этических принципах, поддерживаемых сообществом ведущих издателей научной периодики.

За публикацию статей плата с авторов не взымается. Публикация статей в журнале бесплатная. На платной основе в журнале могут быть опубликованы материалы рекламного характера, имеющие прямое отношение к тематике журнала.

Журнал предоставляет непосредственный открытый доступ к своему контенту, исходя из следующего принципа: свободный открытый доступ к результатам исследований способствует увеличению глобального обмена знаниями.

Индексирование. Публикации в журнале входят в системы расчетов индексов цитирования авторов и журналов. «Индекс цитирования» – числовой показатель, характеризующий значимость данной статьи и вычисляющийся на основе последующих публикаций, ссылающихся на данную работу.

Авторам. Прежде чем направить статью в редакцию журнала, авторам следует ознакомиться со всеми материалами, размещенными в разделах сайта журнала (интернет-сайт Российской академии архитектуры и строительных наук (http://raasn.ru); подраздел «Издания РААСН» или интернет-сайт Издательства АСВ (http://iasv.ru); подраздел «Журнал IJCCSE»): с основной информацией о журнале, его целями и задачами, составом редакционной коллегии и редакционного совета, редакционной политикой, порядком рецензирования направляемых в журнал статей, сведениями о соблюдении редакционной этики, о политике авторского права и лицензирования, о представлении журнала в информационных системах (индексировании), информацией о подписке на журнал, контактными данными и пр. Журнал работает по лицензии Creative Commons типа cc by-nc-sa (Attribution Non-Commercial Share Alike) – Лицензия «С указанием авторства – Некоммерческая – Копилефт».

Рецензирование. Все научные статьи, поступившие в редакцию журнала, проходят обязательное двойное слепое рецензирование (рецензент не знает авторов рукописи, авторы рукописи не знают рецензентов).

Заимствования и плагиат. Редакционная коллегия журнала при рассмотрении статьи проводит проверку материала с помощью системы «Антиплагиат». В случае обнаружения многочисленных заимствований редакция действует в соответствии с правилами COPE.

Подписка. Журнал зарегистрирован в Федеральном агентстве по средствам массовой информации и охраны культурного наследия Российской Федерации. Индекс в общероссийском каталоге РОСПЕЧАТЬ − 18076.

По вопросам подписки на международный научный журнал “International Journal for Computational Civil and Structural Engineering (Международный журнал по расчету гражданских и строительных конструкций)” обращайтесь в Агентство «Роспечать» (Официальный сайт в сети Интернет: http://www.rosp.ru/) или в издательство Ассоциации строительных вузов (АСВ) в соответствии со следующими контактными данными:

ООО «Издательство АСВ»

Юридический адрес: 129337, Россия, г. Москва, Ярославское ш., д. 26, офис 705;

Фактический адрес: 129337, Россия, г. Москва, Ярославское ш., д. 19, корп. 1, 5 этаж, офис 12 (ТЦ Соле Молл);

Телефоны: +7 (925) 084-74-24, +7 (926) 010-91-33;

Интернет-сайт: www.iasv.ru. Адрес электронной почты: iasv@iasv.ru.

Контактная информация. По всем вопросам работы редакции, рецензирования, согласования правки текстов и публикации статей следует обращаться к главному редактору журнала члену-корреспонденту РААСН *Сидорову Владимиру Николаевичу* (адреса электронной почты: sidorov.vladimir@gmail.com, sidorov@iasv.ru, iasv@iasv.ru, sidorov@raasn.ru) или к техническому редактору журнала советнику РААСН *Кайтукову Таймуразу Батразовичу* (адреса электронной почты: tkaytukov@gmail.com; kaytukov@raasn.ru). Кроме того, по указанным вопросам, а также по вопросам размещения в журнале рекламных материалов можно обращаться к генеральному директору ООО «Издательство АСВ» *Никитиной Надежде Сергеевне* (адреса электронной почты: iasv@iasv.ru, nsnikitina@mail.ru, ijccse@iasv.ru).

Журнал становится технологичнее. Издательство АСВ с сентября 2016 года является членом Международной ассоциации издателей научной литературы (Publishers International Linking Association (PILA)), осуществляющей свою деятельность на платформе CrossRef. Оригинальным статьям, публикуемым в журнале, будут присваиваться уникальные номера (индексы DOI – Digital Object Identifier), что значительно облегчит поиск метаданных и местонахождение полнотекстового произведения. DOI – это система определения научного контента в сети Интернет.

С октября 2016 года стал возможен прием статей на рассмотрение и рецензирование через онлайн систему приема статей Open Journal Systems на сайте журнала (электронная редакция): http://ijccse.iasv.ru/index.php/IJCCSE.

Автор имеет возможность следить за продвижением статьи в редакции журнала в личном кабинете Open Journal Systems и получать соответствующие уведомления по электронной почте.

В феврале 2018 года журнал был зарегистрирован в Directory of open access journals (DOAJ) (это один из самых известных поисковых сервисов в мире, который предоставляет открытый доступ к материалам и индексирует не только заголовки журналов, но и научные статьи), в сентябре 2018 года включен в продукты EBSCO Publishing.

В ноябре 2020 года журнал начал индексироваться в международной базе Scopus.

International Journal for
Computational Civil and Structural Engineering
(Международный журнал по расчету гражданских и строительных конструкций)
Volume 18, Issue 2 ***2022***

Scientific coordination is carried out by the Russian Academy of Architecture and Construction Sciences (RAACS)

CONTENTS

International Journal for
Computational Civil and Structural Engineering
(Международный журнал по расчету гражданских и строительных конструкций)
Volume 18, Issue 2 ***2022***

Scientific coordination is carried out by the Russian Academy of Architecture and Construction Sciences (RAACS)

СОДЕРЖАНИЕ

DOI:10.22337/2587-9618-2022-18-2-14-30

DEFORMATION MODEL AND ALGORITHM FOR CALCULATION OF REINFORCED CONCRETE STRUCTURES OF ROUND CROSS-SECTION UNDER TORSION WITH BENDING

Vladimir I. Travush [1], Vladimir I. Kolchunov [2], Sergey A. Bulkin [3], Maxim V. Protchenko [2]

[1] Research Institute of Building Physics of Russian Academy of Architecture and Construction Sciences, Moscow, RUSSIA
[2] Southwestern State University, Kursk, RUSSIA
[3] Urban planning institute of residential and public buildings (GORPROJECT), Moscow, RUSSIA

Abstract. Despite a fairly long period of research and a significant number of publications around the world on the problem of the complex resistance of reinforced concrete, the existing calculation models still remain far from perfect. This is especially true for structures with a non-rectangular cross section. The article presents a version of the model and an algorithm for the analytical calculation of reinforced concrete structures of a circular cross section in torsion with bending, which most fully reflects the specifics of the power resistance of such structures. The model takes into account all the components of external forces in a rod element of a circular cross section, the spatial nature of cracks, with the combined action of moments, various cases of the location of the compressed concrete zone, depending on the ratio of the acting forces in the calculated structure. For a spatial crack, calculated sections are taken in the form of diagonal large and small ellipses and a spatial surface bounded by concave and convex spatial parabolas. In compressed and stretched concrete, a broken section of three sections is considered, two in the form of longitudinal trapezoid and the third, middle section in the form of a small ellipse rotated at an angle to the longitudinal axis of the structure. The obtained analytical dependencies allow one to determine interconnected design parameters, such as stresses in the concrete of the compressed zone, the height of the compressed concrete, stresses in the longitudinal and transverse reinforcement, deformations in concrete and reinforcement, the length of the projection of a spatial inclined crack, and others. The deformation model and algorithm can be used in the design of reinforced concrete structures of circular and annular cross-section, working in bending with torsion.

Keywords: reinforced concrete, circular section, calculation scheme, bending moment, torsion, spatial crack, dangerous spatial crack, governing equations.

ДЕФОРМАЦИОННАЯ МОДЕЛЬ И АЛГОРИТМ РАСЧЕТА ЖЕЛЕЗОБЕТОННЫХ КОНСТРУКЦИЙ КРУГЛОГО ПОПЕРЕЧНОГО СЕЧЕНИЯ ПРИ КРУЧЕНИИ С ИЗГИБОМ

В.И. Травуш [1,3], Вл.И. Колчунов [2], С.А. Булкин [3], М.В. Протченко [2]

[1] Научно-исследовательский институт строительной физики РААСН, г. Москва, РОССИЯ
[2] Юго-Западный государственный университет, г. Курск, РОССИЯ
[3] Городской проектный институт жилых и общественных зданий, г. Москва, РОССИЯ

Аннотация. Несмотря на достаточно продолжительный срок исследований и значительное количество публикаций во всем мире по проблеме сложного сопротивления железобетона существующие расчетные модели до настоящего времени остаются далеко не совершенными. Особенно это относится к конструкциям непрямоугольного поперечного сечения. В статье представлен вариант модели и алгоритм аналитического расчета железобетонных конструкций

круглого поперечного сечения при кручении с изгибом наиболее полно отражающий специфику силового сопротивления таких конструкций. Модель учитывает все составляющие внешних усилий в стержневом элементе круглого поперечного сечения, пространственный характер трещин, при совместном действии моментов, различные случаи расположения сжатой зоны бетона в зависимости от соотношения действующих усилий в рассчитываемой конструкции. Для пространственной трещины приняты расчетные сечения в виде диагонального большого и малого эллипсов и пространственной поверхности ограниченной вогнутой и выпуклой пространственными параболами. В сжатом и растянутом бетоне рассмотрено ломанное сечение из трех участков, – два в виде продольных трапеции и третий, средний участок в виде малого эллипса, повернутого под углом к продольной оси конструкции. Полученные аналитические зависимости позволяют определять связанные между собой расчетные параметры, такие как напряжения в бетоне сжатой зоны, высоту сжатого бетона, напряжения в продольной и поперечной арматуре, деформации в бетоне и арматуре, длину проекции пространственной наклонной трещины и другие. Деформационная модель и алгоритм могут быть использованы при проектировании железобетонных конструкций круглого и кольцевого поперечного сечения, работающих на изгиб с кручением.

Ключевые слова: железобетонные конструкции, круглое сечение, расчетная схема, прочность, изгибающий момент, крутящий момент, пространственная трещина, разрешающие уравнения.

INTRODUCTION

It is known that the rational and safe design of building structures is largely determined by the availability of effective and relatively simple and understandable methods for their calculation. This is especially true for critical structures of buildings experiencing a complex stress state, which undoubtedly include structures that work on the simultaneous action of bending with torsion. Until now, this is one of the most complex and little-studied problems of the theory of reinforced concrete, since it is applied and used in domestic [10, 15, 18, 19, 23, 24] and foreign [2, 5–9, 13, 16, 17, 20, 21] research and in regulatory documents up to the present time, the methods remain extremely conditional and do not reflect the complex resistance of reinforced concrete structures at all levels of loading under such effects. Numerical solutions using software systems based on the finite element method and other numerical methods do not reflect the physics and all the specifics of the deformation of such structures, and the results of the solutions obtained are not unambiguous and are largely determined by the qualifications of the engineer. Known analytical solutions usually consider the calculation of structures of rectangular [2, 5, 7, 9, 13, 18, 20], and more recently box-shaped [26] sections and do not investigate the specifics of the calculation of structures of circular and annular sections. At the same time, structures with these cross-sectional shapes are often used in such critical structures as, for example, the stiffening core of high-rise buildings, bridge supports, cable cars, and the efficiency of their design solutions depends on the accuracy of the calculation. Therefore, the development of analytical methods for calculating building structures made of reinforced concrete, fiber- and steel-reinforced concrete and other similar multicomponent conglomerates remains in demand not only for verifying software systems and developing regulatory documents, but also when designing building objects that use fundamentally new design solutions and technologies that have not passed verification in the practice of construction and operation.

Therefore, the purpose of this study was to build a deformation model and an algorithm for calculating the complex resistance of reinforced concrete structures of a circular cross section under the combined action of torsional and bending moments, which most fully reflects the physical features of the force deformation of such structures.

Deformation model. In the development of studies [25], in which, to determine the calculated forces in reinforced concrete structures of the considered cross section, a general calculated scheme with spatial sections was proposed and the corresponding resolving

equilibrium equations and deformation equations were compiled that determine the stress-strain state in such structures under the considered effects on Based on the specification of these constitutive equations, here is an algorithm for determining all the calculated parameters used in this model.

It is assumed that the calculated reinforced concrete structure is conditionally divided into two blocks and in the space of these blocks there is a spatial crack limited along the length of the structure by normal cross sections 1-1 at the beginning and 3-3 at the end of the projection of this crack. The area of the beam covered by the crack, being projected onto the side surface of the structure, can be described by a large ellipse (Figure 1) with a projection length equal to **c**.

a)

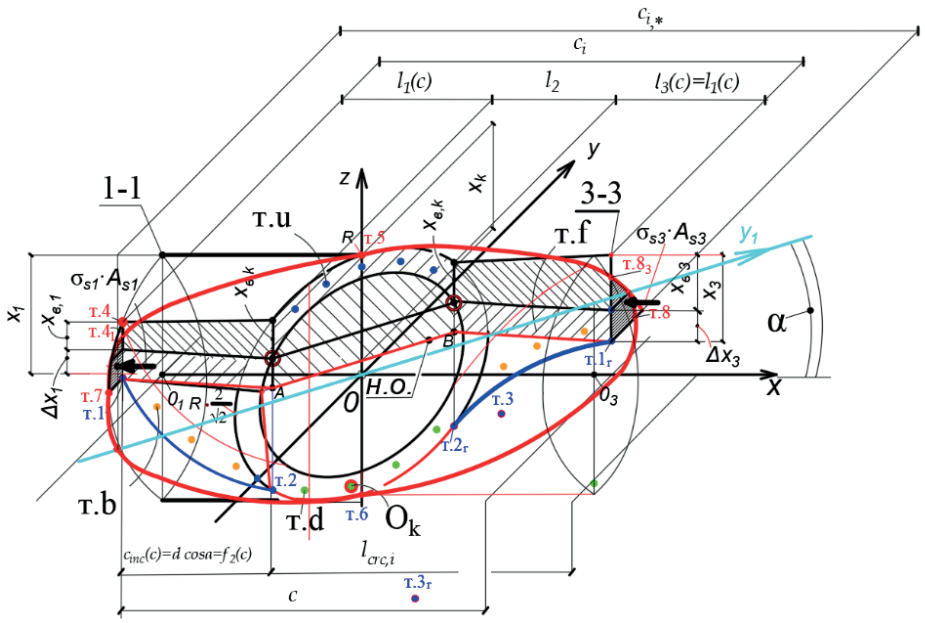

b)

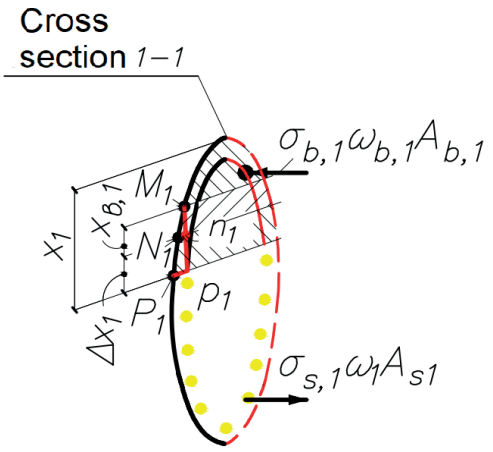

c)

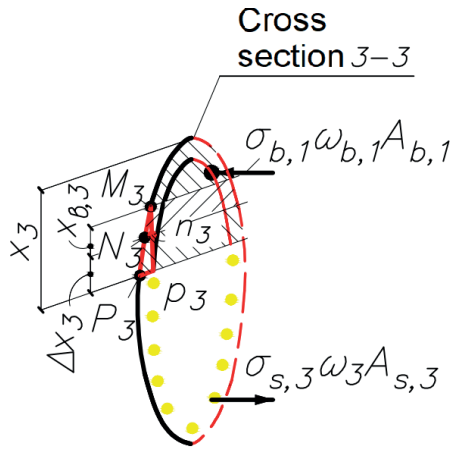

Figure 1. Calculatied scheme of a reinforced concrete element of a circular cross section under the action of bending and torque moments: a – block with small and large ellipses between normal sections I-I and 3-3; b, c – diagram of forces, compressed and stretched zones in section I-I and 3-3 respectively

In the compressed concrete of the design section within the projection of the inclined crack there are three characteristic sections with dimensions l_1, l_2, l_3, – longitudinal sections (l_1 and l_3), as well as a cross section of a small ellipse at a longitudinal distance l_2 (see Figure 1). In the stretched concrete there are the same three sections l_1, l_2, l_3, but in addition to the ellipse for the section l_2, there is also a parabola envelope in the sections l_1 and l_3.

The small ellipse equation for a spatial section is:

$$\frac{y^2}{2R^2}+\frac{z^2}{R^2}=1. \quad (1)$$

Then in stretched concrete in the first section we have a spatial curve $f_{par1,2,3}(x,y,z)$ and in the second section a spatial parabola $f_{par1_r,2_r,3_r}(x,y,z)$.

To construct the first spatial parabola $f_{par1,2,3}(x,y,z)$ we find the coordinates (x,y,z) of point 1 (T.1) along the axis x ($x=-l_1-0.5l_2$), the coordinate along the axis z ($z=R-x_1$) and, belonging to the circle in section 1-1, the coordinate along the axis y:

$$y=\pm\sqrt{R^2-(R-x_1)^2}. \quad (2)$$

Next, we find the coordinates (x,y,z) of point 2 (T. 2) along the x axis ($x=-0.5l_2$), the z coordinate ($z=-R+x_k-\Delta x_1-x_{b,k}$) and the y coordinate.

Let us write down the equation of the first spatial (in the form of a propeller curve) parabola:

$$f_{par1,2,3}(x,y,z)=\sqrt{z_1(x)^2+y_1(x)^2}. \quad (3)$$

where $z_1(x)^2$ and $y_1(x)$ – parabolas along respective coordinate axes.

The construction of the second spatial parabola $f_{par1_r,2_r,3_r}(x,y,z)$ is similar to the above scheme the auxiliary plane curve is defined $y_2(x)$ and the equation of the second spatial parabola is obtained accordingly:

$$f_{par1_r,2_r,3_r}(x,y,z)=\sqrt{z_2(x)^2+y_2(x)^2}. \quad (4)$$

CALCULATION ALGORITHM

In accordance with the accepted design scheme of the reinforced concrete structure of the beam of round cross section under the action of bending and torque moments and transverse forces, the most dangerous are spatial sections located at the support with maximum torque, bending moments and transverse forces.

In this scheme, the first block is separated by the cross section I-I passing at the end of the spatial crack, is in equilibrium under the action of external forces applied to it from the side of the support and internal forces arising at the place of the cross section.

When evaluating the complex resistance of the beam under consideration, the design scheme shown in Figure 1 is implemented in the following order.

1. The main one is an arbitrary vertical section k, passing through the end of the front of the spatial crack, in which the intensity of deformations is taken $\varepsilon_{i,u}=\varepsilon_{b,u}$.

2. We calculate the value of shear deformations $\varepsilon_{q,u}$ (Figure 2):

$$\varepsilon_{q,u}=2\cos\beta\sin\beta\left(\varepsilon_{1,u}-\varepsilon_{3,u}\right), \quad (5)$$

where angle β determines direction of main deformation of concrete shortening in vertical section *k*.

3. Using the diagram of the dependence proposed in [23] $a/h_0-\cos\beta$ (where a – is the distance from the support to the edge of the crack, h_0 – the working height of the section) the value of the shear stress limit is calculated R_q:

$$R_q = \tau = \tau_{z1,x1} = \frac{\sigma_{i,u}}{\varepsilon_{i,u}} \frac{1}{2[1+\mu(\lambda)]} \varepsilon_{q,u} . \quad (6)$$

4. For point 1 of state diagrams [23] of compressed zone concrete in the section under consideration using known dependencies of solid deformable body mechanics, strains and stresses are successively calculated:

$$\varepsilon_{x,1} = \varepsilon_{1,u} \cos^2\beta + \varepsilon_{3,u} \sin^2\beta ; \quad (7)$$

$$\varepsilon_{z,1} = \varepsilon_{1,u} \sin^2\beta + \varepsilon_{3,u} \cos^2\beta ; \quad (8)$$

$$\sigma_{x,1} = \frac{\sigma_{i,u}}{\varepsilon_{i,u}} \frac{1}{1-\mu^2(\lambda)} \left[\varepsilon_{x,1} + \mu(\lambda)\varepsilon_{z,1}\right]; \quad (9)$$

$$\sigma_{z,1} = \frac{\sigma_{i,u}}{\varepsilon_{i,u}} \frac{1}{1-\mu^2(\lambda)} \left[\varepsilon_{z,1} + \mu(\lambda)\varepsilon_{x,1}\right]. \quad (10)$$

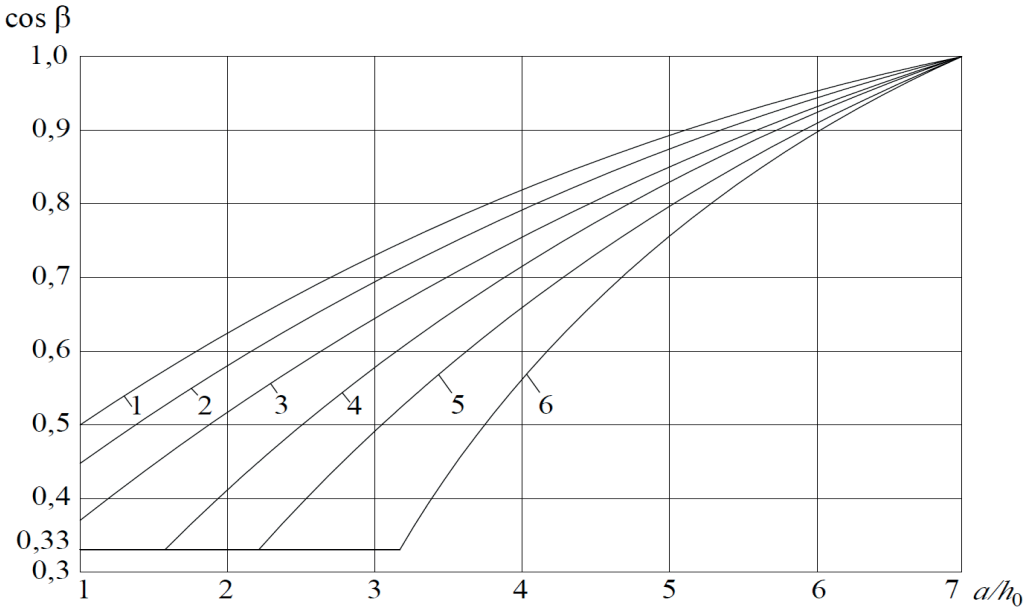

Figure 2. Diagram $a / h_0 - \cos\beta$: 1 - for ratio T/M = 0.1; 2 - for ratio T/M = 0.25; 3 - for ratio T/M = 0.5; 4 - for ratio T/M = 0.75; 5 - for ratio T/M = 1.0; 6 - for ratio T/M > 1.0

5. The transition from stresses in compressed concrete on the inclined site of the section under consideration to stresses on the normal site is carried out according to the known formulas of mechanics of the solid deformable body:

$$\sigma_{x,1} \cos^2\alpha + \sigma_{z,1} \sin^2\alpha + \tau_{x1z1} \sin 2\alpha ; \quad (11)$$

$$\tau_{xz,k} = \frac{\sigma_{x,1} - \sigma_{z,1}}{2} \sin 2\alpha - \tau_{z1,x1} \cos 2\alpha ; \quad (12)$$

$$\sigma_{bx,u,k} = \frac{\sigma_{x,k}}{\cos\alpha} ; \quad (13)$$

$$\tau_{xz,u} = \tau_{xz,u} = \frac{\tau_{xz,k}}{\cos\alpha} ; \quad (14)$$

$$\tau_{yx,k} = \sqrt{R_q^2 - \tau_{xz,k}^2} . \quad (15)$$

Here α – is the angle between the cross section normal to the longitudinal axis and the section *k-k* in question (see Figure 1).

In practical calculations, the direction of the main deformations of compressed concrete shortening (angle β) in the vertical section passing through the end of the front of the spatial crack can be determined using a graph of dependence $a / h_0 - \cos\beta$ (see Figure 2).

6. From equilibrium equation of projections of all forces acting in section I-I on axis x ($\sum X = 0$), height of compressed zone of concrete in normal section (unknown x):

$$\sigma_{bI,u} b_1 \varphi(x_k, x) x - \sigma_{s,I} m A_{s,I} = 0 . \quad (16)$$

Knowing the circumference radius of the circular cross section, the area of the compressed zone of concrete in this sections is calculated $A_{b,I}$ and then the height of the compressed zone x of concrete in this section is calculated.

From the hypothesis of proportionality of longitudinal deformations there are stresses in longitudinal working reinforcement $\sigma_{s,I}$ in section I-I:

$$\sigma_{s,I} = \frac{\varphi_{10,*}\sigma_{bu,x,I} \cdot E_s(\lambda)}{E_b(\lambda)} \cdot \frac{h_0 - x}{x} + \sigma_0 \le R_{s,I} . \quad (17)$$

If condition (17) is not met, voltage $\sigma_{s,I}$ is taken equal to R_s.

Normal shortening deformations along the x axis in compressed concrete at various points of design section k-k and in section I-I can be found on the condition of their proportionality to limit deformations $\varepsilon_{bu,k,rig,x}$ at the extreme point of section k-k (see Figure 1a):

– from right point (rig) to section I-I (similar to section 3-3)

$$\varepsilon_{b,I} = \frac{\varepsilon_{bu,k,rig,x} \cdot a}{a - l_1}; \quad (18)$$

– from right point (rig) to middle point (b_k)

$$\varepsilon_{b,k,x} = \frac{\varepsilon_{bu,k,rig,x} \cdot a_{m,b}}{a - l_1} = \frac{\varepsilon_{bu,k,rig,x} \cdot \left[a - \left(l_1 + \frac{\sqrt{2}}{2} l_2 \cdot \frac{1}{2} - \eta_{hor,b} \cdot l_2 \right) \right]}{a - l_1}; \quad (19)$$

– from right point (rig) to left point (lef)

$$\varepsilon_{bu,k,lef,x} = \frac{\varepsilon_{bu,k,rig,x} \cdot [a - (l_1 + l_2)]}{a - l_1}. \quad (20)$$

7. From the equilibrium equation of torques of all internal and external forces acting in section I-I, relative to the axis perpendicular to this section and passing through the point of application of equal forces in concrete of compressed zone ($\sum T = 0$), shear stresses from torque and transverse force (unknown $\tau_{T,I}$ and $\tau_{Q,I}$), are determined, where they are directed in opposite directions, and the ratio between them is taken equal to the ratio T_1 / Q_1 :

$$\omega_+ \omega_{1+} \tau_{\sum +} \frac{b_1}{2} b' x + \omega_- \omega_{1-} \tau_{\sum -} \frac{b_1}{2} b'' x - T_1 = 0; \quad (21)$$

$$\tau_{\sum +} = \tau_{T,I} \pm \tau_{Q,I}; \quad (22)$$

$$\frac{\tau_{T,I}}{\tau_{Q,I}} = \frac{T_1}{Q_I}. \quad (23)$$

Here b' (b'') – distance in radius from the center of gravity of the section to the arc of the section contour on the side where shear stresses $\tau_{T,I}$ and $\tau_{Q,I}$ are directed to one side (directed to opposite sides).

For total shear stresses calculated by the formula (22) the condition must be met:

$$\tau_{\sum +} \le \tau_{pl}. \quad (24)$$

Here $\tau_{pl} = 1.1 R_{bt}$.

The second support block is separated from the reinforced concrete element by a spatial section formed by a spiral-shaped crack and a vertical section passing along the compressed zone of concrete through the end of the front of the spatial crack (see Figure 1).

For a circular cross section, the torque in section 1-1 will be:

$$M_{t,I} = \tau_{pl,u} \cdot \lambda x_1 \cdot b_{cir} \cdot \varphi_{cir,\tau} \cdot (z_1 - 0.5 \cdot \lambda x_1) + 0.5 \cdot \tau_{pl,u} \cdot (x_1 - \lambda x_1) \cdot b_{cir} \cdot \left[0.5 \cdot \lambda x_1 + \frac{1}{3} \cdot (x_1 - \lambda x_1) \right] + Q_s (h_0 - z_1). \quad (25)$$

From the equilibrium equation of projections of internal and external forces acting in section I-I on the axis Y ($\sum Y = 0$):

$$-\tau_{pl,x} \cdot x \cdot b - \tau_{pl,x} \cdot k_{Q,m} \cdot (h_0 - x) \cdot b + K_M \cdot R_{sup} = 0 . \quad (26)$$

Here, it is assumed that the load forces in the working reinforcement on average between the cracks in the cross section I-I are zero.
The lateral force perceived by the compressed zone concrete will be:

$$Q_{I,b} = \tau_{pl,x} \cdot x \cdot b . \quad (27)$$

In turn, the transverse force perceived by the concrete of the stretched zone will be (Figure 4):

$$Q_{II,T} = \tau_{pl,x} \cdot k_{Q,m} (h_0 - x) \cdot b . \quad (28)$$

On the other hand, the value of the transverse force as part of the entire transverse force perceived by the design section is

$$Q_{II,T} = Q - Q_{I,b} . \quad (28)$$

The equation (26) can be used to determine a parameter $k_{Q,m}$, hat takes into account the presence of adjacent spatial cracks on the stressed-strain state of the stretched zone in the middle (between the cracks) of the calculated cross section I-I:

$$k_{Q,m} = \frac{K_M \cdot R_{sup} - \tau_{pl,x} \cdot x \cdot b}{\tau_{pl,x} (h_0 - x) \cdot b} . \quad (29)$$

8. From the equilibrium equation of bending moments of all internal and external forces acting in section I-I ($\sum M_B = 0$), a generalized reference reaction (unknown R_{sup}) is determined:

$$\sigma_{s,I} m A_{s,I} \left[h_{1,0} - \varphi(x_k, x) x \right] - M_I - R_{sup} a_1 = 0 \quad (30)$$

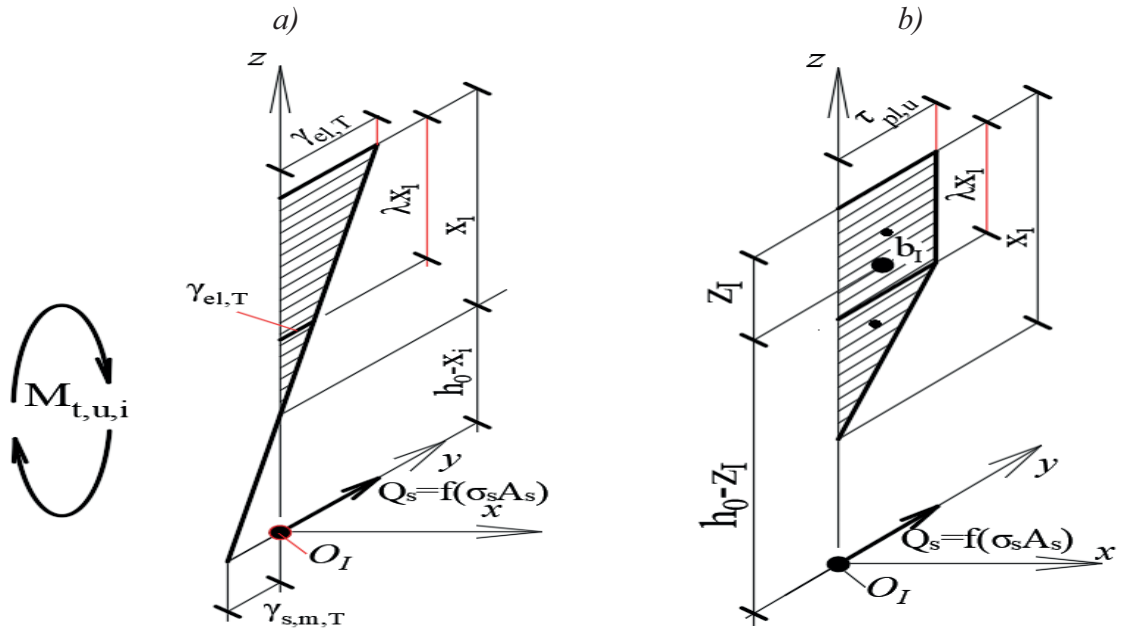

Figure 3. Schemes of distribution of shear strains and shear stresses in the cross section I-I (3-3)

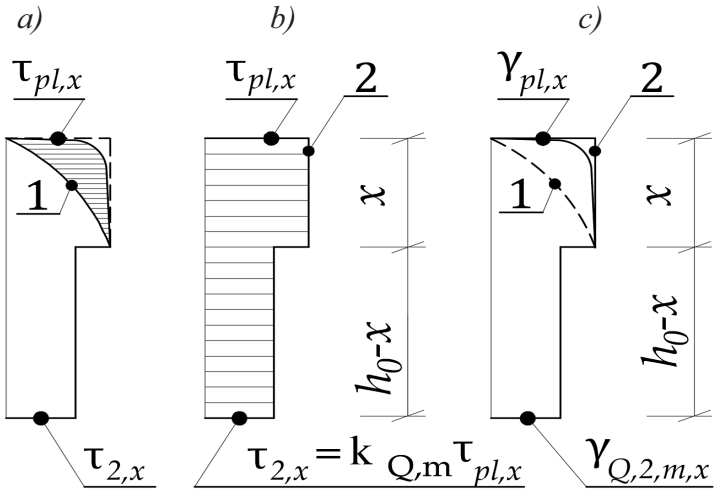

Figure 4. Diagram of transverse shear stresses τ_Q in medium cross sections I–I (3-3)

Where $\varphi(x_k, x)$ – coefficient of completeness of stress graphic in compressed concrete. For the limit states of the first group, the value of this coefficient can be taken to be 0.75); m is the number of rods of longitudinal working reinforcement in the section under consideration.

For a circular cross section from the equilibrium equation of moments of internal and external forces in section I-I relative to the y axis passing through the point of application of equal forces O_I in the stretched reinforcement ($\sum M_{O,I}=0$), we obtain the unknown $M_{bend,I}$:

$$M_{bend,I} = R_{sup,I,M} \cdot a_{m,I};\ \varphi_{10,*} \cdot \sigma_{bu,x,I} A_{b,I} [h_0 - \varphi_{z,cir} \cdot x] + +m \cdot R_{sc,I,up} \cdot \omega_{up,cir} \cdot A_{sc,up} \left(h_0 - a'_s\right) + \sum R_{sc,I,i,lef} \cdot \omega_{c,cir} \cdot A_{sc,I,i,lef} \left(h_0 - a'_{s,i,lef}\right) + + \sum R_{sc,I,i,rig} \cdot \omega_{c,cir} \cdot A_{sc,I,i,rig} \left(h_0 - a'_{s,i,rig}\right) - \sum R_{s,I,i,lef} \cdot \omega_{cir} \cdot A_{s,I,i,lef} \left(a_{s,i,lef} - a_{s,d}\right) - - \sum R_{s,I,i,rig} \cdot \omega_{cir} \cdot A_{s,I,i,rig} \left(a_{s,i,rig} - a_{s,d}\right) - K_M K_{pr,M} \cdot R_{sup,I} - R_{sup,I} \cdot a = 0, \quad (31)$$

and then lateral force from internal forces:

$$Q_I = R_{sup,I,M} = \frac{M_{bend,I}}{a_{m,I}} = \frac{M_{bend,I}}{a + K_M K_{pr,M}}. \quad (32)$$

9. From the condition of zero equality of the sum of projections of all forces on the x axis ($\sum X=0$, block II, see Figure 1) acting in space section k, an unknown parameter is determined - the height of the compressed zone in section k ($x_{B,k}$) :

$$-\sigma_{s,k} \cdot m_d \cdot A_{s,d} + \sum R_{sc,up,i} \cdot \omega_{up} \cdot A_{sc,up,i} - \sum R_{s,i,rig} \cdot \omega_{rig} \cdot A_{s,i,rig} - \sum R_{s,i,lef} \cdot \omega_{lef} \cdot A_{s,i,lef} + + \sum R_{sc,i,rig} \cdot \omega_{c,rig} \cdot A_{sc,i,rig} + \sum R_{sc,i,lef} \cdot \omega_{c,lef} \cdot A_{sc,i,lef} - \varphi_{10} \tau_{xy,u,Mt} \cdot A_{b,l_1} + \varphi_{10} \tau_{xy,u,Mt} \cdot A_{b,l_3} - \sigma_{b,1,rig} \cdot A_{b,*} - \sigma_{sc,1,rig} \cdot A_{sc,1,rig} - \sigma_{b,3,lef} \cdot A_{b,**} - \sigma_{sc,3,lef} \cdot A_{sc,3,lef} - - X_{b,k} \cdot A_{b,k,x_B} - \varphi_{10} \tau_{xy,u,Mt} \cdot A_{b,l_1,ad} + \varphi_{10} \tau_{xy,u,Mt} \cdot A_{b,l_3,ad} - \sigma_{b,1,rig} \cdot A_{b,*,cir,ad} - \sigma_{b,3,lef} \cdot A_{b,**,cir,ad} - X_{b,k} \cdot A_{b,k,core} = 0. \quad (33)$$

The following restrictions must be taken into account for $x_{B,k}$:

$$0.1h_0 \le x_{B,k} \le 0.3h_0; \quad (34)$$

$$x_{B,k} \le x_k. \quad (35)$$

In equation (34), $X_{b,k}$ – projection of the resulting directions in the grain of concrete on the axis x; A_{b,l_1} – area of compressed concrete on the site l_1; A_{b,l_3} – area of compressed concrete on the site l_3; $A_{b,*,cir}$ – concrete area of the right sector of broken section (sector with height $x_{B,1}$); $A_{b,**,cir}$ – concrete area of the left sector of broken section (sector with height $x_{B,3}$); $A_{b,l_1,ad}$ – concrete area with height Δx_1 at the site l_1; $A_{b,l_3,ad}$ – concrete area with height Δx_3 at the site l_3; $A_{b,*,cir,ad}$ – area of compressed concrete of part of the right sector with height Δx_1; $A_{b,**,cir,ad}$ – compressed concrete area of the left sector part with height Δx_3; $A_{b,k,core}$ – area of part of compressed zone of concrete in section k of small ellipse enclosed between points AB and section of arc of ellipse spaced from surface of small ellipse by height $x_{B,k}$ (see figure 1); A_{b,k,x_B} – area of part of compressed zone of concrete limited by sections of arcs of ellipses in section k-k, spaced from each other at a distance $x_{B,k}$; $\sum_{k=1}^{n_{rig}} R_{s,i,rig} \cdot \omega_{rig} \cdot A_{s,i,rig}$ ($\sum_{k=1}^{m_{rig}} R_{sw,i,rig} \cdot \omega_{rig} \cdot A_{sw,i,rig}$) – forces in stretched longitudinal reinforcement (transverse clamps) located in the area of the RH circuit of the first section of the spatial parabola $f_{par1,2,3}(x,y,z)$ (site l_1); $\sum_{k=1}^{m_{lef}} R_{sw,i,lef} \cdot \omega_{lef} \cdot A_{sw,i,lef}$ ($\sum_{k=1}^{n_{lef}} R_{s,i,lef} \cdot \omega_{lef} \cdot A_{s,i,lef}$) – forces in the stretched longitudinal reinforcement (transverse clamps) located in the area of the left contour of the second section of the spatial parabola $f_{par1_r,2_r,3_r}(x,y,z)$ (site l_3); h_0 – section working height, $\varphi_{7,lef}$, $\varphi_{7,rig}$, $\varphi_{8,lef}$, $\varphi_{8,rig}$, – parameters that take into account the components of the "heating" effect in the working reinforcement.

To determine the projection of component stresses in compressed concrete $X_{b,k}$ the x axis is previously calculated as the following unknown in the section k-k.

Deformations of longitudinal reinforcement in the left and right parts of the section $\varepsilon_{s,k,rig,x}$ and $\varepsilon_{s,k,lef,x}$ on condition of their proportionality in section x and section k-k:

$$\varepsilon_{s,k} = \frac{\varepsilon_{s,I} \cdot a_{m,s}}{a} = \frac{\varepsilon_{s,I} \cdot \left(a - \frac{h}{2h+b} \cdot c - \frac{2h+b}{c} \cdot 0.5 \cdot b \right)}{a}; \quad (36)$$

$$\varepsilon_{s,k,rig,x} = \frac{\varepsilon_{s,I} \cdot (a - l_1)}{a}; \quad (37)$$

$$\varepsilon_{s,k,lef,x} = \frac{\varepsilon_{s,k,rig,x} \cdot [a - (l_1 + l_2)]}{a - l_1}. \quad (38)$$

The relationship between angular deformations is recorded:

$$\gamma_{zx,pl} = k_* \cdot \gamma_{zx,Mt,el}; \quad (39)$$

where $k_* = M_t / M_{t,crc}$. In the first approximation for the crack torque we take $M_{t,crc} = 0,4M_t$.

We also take limit values of tangent stresses $\tau_{zx,pl} = R_q = R_{ch}$.

Knowing the angular deformations from the torque, the values of the tangent stresses from the action of the transverse force are determined

$$\tau_{zx,Q} = \tau_{zx} - \tau_{zx,Mt}; \quad (40)$$

$$k_{**} = \frac{\tau_{yx,Mt}}{\tau_{zx,Mt}} = \frac{\tau_{yx}}{\tau_{zx}}; \quad (41)$$

For the middle point (b_k) of the compressed zone of the broken design section k-k, the

projection of the component stresses in the compressed concrete $X_{b,k}$ on the x axis in the section l_2 is calculated by the formula:

$$X_{b,k}=\frac{\varphi_{z,1}\cdot\sigma_{bu,x,I}\cdot\varphi_{1,*}\cdot\left[a-\left(l_1+\frac{\sqrt{2}}{2}l_2\cdot\frac{1}{2}-\eta_{hor,b}\cdot l_2\right)\right]}{a}+\left(\varphi_{12}\cdot\tau_{zx,u,Q}\pm\varphi_{10}\cdot\tau_{xy,u,Mt}\right)\cdot\varphi_{3,*}; \quad (42)$$

The height of the compressed zone x_k in the section k-k between the cross sections I-I and III-III (see Figure 1) can be found from a linear proportion;

$$x_k=\frac{x_1+x_3}{2}, \quad (43)$$

where x_1 – is the height of the compressed zone in section I-I; x_3 – is the height of the compressed zone in section III-III.

By calculating the height of the compressed zone of concrete $x_{B,k}$ in section k-k from equation (34) and using the conditions of proportionality between the heights of the compressed zone in sections k-k and 1-1, the following ratios are written to determine the height of the compressed zone in section 1-1:

$$\Psi_1=\frac{x_{B,k}}{x_{B,k}+\Delta x_1}. \quad (44)$$

$$\Delta x_1=x_k-x_1. \quad (46)$$

$$\frac{x_{B,k}}{x_{B,k}+\Delta x_1}=\Psi_1=\frac{x_{B,1}}{x_{B,1}+\Delta x_1}$$

from which is calculated

$$x_{B,1}=\frac{\Psi_1\cdot\Delta x_1}{\Psi_1-1}. \quad (45)$$

Similarly, the height of the compressed zone is in another normal section $x_{B,3}$ (see Figure 1):

10. Intensity of load in clamps on the right side of round cross section is determined from equality of zero of sum of projections of all forces acting in space section k-k on z axis ($\sum Z=0$, refer to Figure 1):

$$\begin{aligned}q_{sw,rig}=\frac{tg\alpha}{h}\Big[&q_{sw,lef}\cdot\eta_q\cdot\frac{h}{tg\alpha_0}-\varphi_{7,*}R_s\sum\omega_{*,cir}A_{s,*,cir}-\varphi_{7,*,rig}R_s\sum\omega_{rig,*,cir}A_{s,rig}+\\&+\varphi_{7,*,lef}R_s\sum\omega_{lef,*}A_{s,lef}-Q+R_{sup}+\left(\varphi_{11}\tau_{zy,u,Mt}+\varphi_9\tau_{zy,u,Q}\right)\cdot A_{b,l_1}+\\&+\left(\varphi_{11}\tau_{zy,u,Mt}-\varphi_9\tau_{zy,u,Q}\right)\cdot A_{b,l_3}+\\&\left(\varphi_{14}\cdot\tau_{zx,u,Mt}+\varphi_{12}\cdot\tau_{zx,u,Q}\right)\cdot A_{b,*,cir}+\\&\left(\varphi_{14}\cdot\tau_{zx,u,Mt}-\varphi_{12}\cdot\tau_{zx,u,Q}\right)\cdot A_{b,**,cir}+Z_{b,k}\cdot A_{b,k,x_B}-\left(\varphi_{11}\tau_{zy,u,Mt}+\varphi_9\tau_{zy,u,Q}\right)\cdot A_{b,l_1,ad}+\\&\left(\varphi_{11}\tau_{zy,u,Mt}-\varphi_9\tau_{zy,u,Q}\right)\cdot A_{b,l_3,ad}+\left(\varphi_{14}\cdot\tau_{zx,u,Mt}+\varphi_{12}\cdot\tau_{zx,u,Q}\right)\cdot A_{b,*,cir,ad}+\\&+\left(\varphi_{14}\cdot\tau_{zx,u,Mt}-\varphi_{12}\cdot\tau_{zx,u,Q}\right)\cdot A_{b,**,cir,ad}+Z_{b,k}\cdot A_{b,k,core}.\end{aligned} \quad (46)$$

Here $\varphi_{7,lef}$, $\varphi_{7,rig}$ – parameters that take into account the components of the "heating" effect in the reinforcement. At each iteration step, these parameters are taken into account as constants, not as functions and are determined based on the second level model [25]; Q – the transverse force of the section from the support to the section k-k.

For the middle point (b_k) of the compressed zone of the broken design section k-k the projection of the component stresses in the compressed concrete on the z axis in the section l_2 is calculated by the formula:

$$Z_{b,k} = \left(\varphi_{12} \cdot \tau_{zx,u,Q} \pm \varphi_{14} \cdot \tau_{zx,u,Mt}\right) \cdot \frac{\sqrt{2}}{2} + \left(\varphi_9 \cdot \tau_{zy,u,Q} \pm \varphi_{11} \cdot \tau_{zy,u,Mt}\right) \cdot \frac{\sqrt{2}}{2} \quad (47)$$

Here, the components of tangent stresses in compressed concrete are calculated by analogy as in para. 9, with replacement by $\tau_{zx,u,Q}$ by $\tau_{zx,ad,Q}$, $\tau_{zx,u,Mt}$ by $\tau_{zy,ad,Q}$, $\tau_{zy,u,Mt}$ by $\tau_{zy,ad,Mt}$ etc.

The load intensity in the clamps on the left side of the round cross section $q_{sw,lef}$ is based on the ratio:

$$q_{sw,lef} = q_{sw,rig} - Ч_{11,*} \cdot \tau_Q; \quad (48)$$

It is assumed that the projections of inclined cracks on the left and right sides of the circular section are approximately the same $c_1 \approx c_2$ and then the value of the coefficient $Ч_{11,*} = Ч_{11} \cdot b$, where b is taken equal to the radius of the cross section of the calculated structure. Values of tangent stresses taking into account the action of transverse force on the left or right of section are performed with plus-minus sign ($\pm\tau_Q$) respectively.

At that, condition check is performed for load intensity in clamps $q_{sw,lef}$:

$$\frac{n \cdot R_{bt} \cdot A_{sw}}{u_s} \le q_{sw,lef} \le \frac{0.8 \cdot R_{sw} \cdot A_{sw}}{u_s} - Ч_{11,*} \cdot \tau_Q. \quad (49)$$

Values of parameters included in formula (51) are calculated by formulas:

$$\sigma_{sw} = \frac{E_{sw}}{E_b} \cdot \sigma_{bt} = n \cdot R_{bt};$$

$$\frac{n \cdot R_{bt} \cdot A_{sw}}{u_s} = q_{sw,lef,min}; \quad (50)$$

$$Ч_{11} \cdot \tau_Q = \psi_{Q,*} \cdot \tau_{pl,u} = \psi_{Q,*} \cdot R_{ch}\left(\frac{c}{h_0}\right); \quad (51)$$

At the same time, tangent stresses $\tau_{Q,k}$ are based on the condition of proportionality of relations of stresses and forces in section k and in section I-I:

$$\frac{\tau_{Q,I}}{\tau_{Q,k}} = \frac{Q_1}{Q_{k,m}}. \quad (52)$$

Here $\tau_{Q,1}$ and $\tau_{Q,k}$ – tangent stresses due to the action of the transverse force in the normal section I-I and in the center of the compressed zone of the spatial section k- k, respectively; Q_1 and $Q_{k,m}$ – a transverse force acting in the normal section I-I and in the center of the compressed zone of the space section k-k, respectively.

11. Stresses in longitudinal reinforcement σ_s are determined from the equation of moments of all internal and external forces ($\sum M_B = 0$), acting in the vertical longitudinal plane relative to the axis Z, passing through the point of application of equal forces in the concrete of the compressed zone:

$$\sigma_s m A_s \cdot \left(h_{1,0} - 0.5x_k\right) - M_k - R_{sup} a_{1,m} = 0 \quad (53)$$

This checks the condition:

$$\sigma_s \le m_{аз} R_s. \quad (54)$$

If this condition is not met, then σ_s we take it equal to $m_{аз} R_s$, where $m_{аз} = l_x / l_{anc}$), l_x – distance from the beginning of the stress transfer zone in the pre-stressed reinforcement to the section under consideration; If there is no prestress in the design, the factor $m_{аз} = 1$.

The bending moment, as a function of the calculated parameters of the section k-k, is from the

static condition of equal to zero moments of all internal and external forces acting in the vertical longitudinal plane relative to the y axis passing through the point of application of equal forces in the concrete of the compressed zone b_k ($\sum M_{b,k}$=0,see Figure 1) $M_{bend,k}(\sigma_{s,k}, \sigma_{s,rig}, \sigma_{s,lef}, h_0, x_{B,k}, A_{s,d}, R_{s,rig}, R_{s,lef} A_s, \omega_{*,cir}, \varphi_{5,*}, \varphi_{7,*}, \varphi_9, \varphi_{11}, q_{sw,rig}, q_{sw,lef}, A_{b,*,cir}, A_{b,**,cir}, l_1, l_2, l_3, \tau_{zy,u,Q}, \tau_{zy,u,Mt}, x_{B,k}, x_{B,1}, x_{B,3}, X_{b,k})$.

This constraint is detailed in [25].

The bending moment corresponding to the level of crack formation is from the following constraint

$$R_{bt} = \frac{M_{crc,k}}{0.85 W_{x,k}} = \frac{M_{crc,k}}{0.85 W_0 \cdot \gamma}; \quad (55)$$

Here, $R_{bt} = 2.2 МПа$ - design tensile strength of concrete; $\gamma = 2$ - a coefficient taken for a circular section equal to two; $W_{bend} = \pi D^3 / 32$.

The generalized reference reaction corresponding to the moment of crack formation is accepted $R_{sup,crc} = 0,4\ R_{sup,u}$.

From here, the transverse force from internal forces in the design section is determined:

$$Q_k = R_{sup,k,M} = \frac{M_{bend,k}}{a_{m,k}} = \frac{M_{bend,k}}{a_{m,b}(c) + K_M K_{pr,M}}. \quad (56)$$

12. Intensity of load in clamps located in lower stretched zone of round cross section is determined from equality of sum of projections of all forces acting in spatial section k- k on y axis equal to zero ($\sum Y$=0, refer to Figure 1) we have:

$$q_{sw,\sigma} = \frac{1}{\sqrt{l_2^2 + 4R^2}} \cdot \Big[-\varphi_{8,*,rig} R_s \sum \omega_{rig,cir} A_{s,rig} - -\varphi_{8,*,lef} R_s \sum \omega_{lef,cir} A_{s,lef} - \varphi_{8,*} \cdot R_s \sum \omega_* A_s + $$
$$+\varphi_{13} \cdot \tau_{yx,u,Mt} \cdot A_{b,*} + \varphi_{13} \cdot \tau_{yx,u,Mt} \cdot A_{b,**} + + Y_{b,k} \cdot x_{B,k} \cdot \sqrt{l_2^2 + b^2} + \varphi_{13} \cdot \tau_{yx,u,Mt} \cdot A_{b,*,ad} +$$
$$+\varphi_{13} \cdot \tau_{yx,u,Mt} \cdot A_{b,**,ad} + Y_{b,k} \cdot A_{b,k,x_B} + Y_{b,k} \cdot A_{b,k,core} \Big]. \quad (57)$$

Here, φ_{8*} – parameters, which take into account components of "heating" effect of reinforcement. At each iteration step, these parameters are taken into account as constants, not as functions, and are determined based on the second level model [25];

For the middle point (b_k) of the compressed zone of the broken design section k-k, the projection of the component stresses in the compressed concrete on the y axis in the section l_2 is calculated by formula:

$$Y_{b,k} = \varphi_9 \cdot \tau_{zy,u,Q} \cdot \frac{\sqrt{2}}{2} \pm \varphi_{13} \cdot \tau_{yx,u,Mt} \cdot \frac{\sqrt{2}}{2}. \quad (58)$$

Here, the components of tangent stresses in compressed concrete, by analogy with formula (49) with the replacement of the corresponding components of tangent stresses $\tau_{zy,ad,Q}$ instead of $\tau_{zy,u,Q}$ and $\tau_{yx,ad,Mt}$ instead of $\tau_{yx,u,Mt}$,

$\tau_{zy,ad,Q} = \tau_{zy,u,Q} - \tau_{zy,crc,Q}$;

$\tau_{yx,ad,Mt} = \tau_{yx,u,Mt} - \tau_{yx,crc,Mt}$.

13. The torque, as a function of the calculated parameters of the section k-k, is from the static condition of equal to zero moments of all internal and external forces acting in the vertical transverse plane relative to the x axis passing through the point of application of equal forces in the concrete of the compressed zone b_k ($\sum T_{b,k}$=0, see Figure 1)

$M_{t,k}(q_{sw,\sigma}, q_{sw,rig}, q_{sw,lef}, \eta_q, \eta_{hor,b}, \varphi_{7,*}, \varphi_{8,*}, R_s, A_s, x_{B,k}, h_0, A_{b,l_1}, A_{b,l_2}, A_{b,l_3}, \varphi_{11}, \varphi_9, \tau_{yz,u,Mt}, \tau_{yz,u,Q}, A_{b,*,cir}, A_{b,**,cir}, \eta_{hor,b})$.

This constraint is detailed in [25].

14. The length of the projection of the spatial crack is determined using the function $f(x,y,z)$ for the diagonal large ellipse of the circular cross-section structure introduced into the design scheme, with a smaller $b = R$ and larger diagonal $a = \frac{l(c) + R\sqrt{2} + l(c)}{2cos\alpha} = = \frac{2l(c) + R\sqrt{2}}{2\cos\alpha}$), respectively:

$$\frac{(y - y_0)^2}{(\frac{2l(c) + R\sqrt{2}}{2\cos\alpha})^2} + \frac{(z - z_0)^2}{R^2} = 1. \qquad (59)$$

Based on this, the size of the spatial crack for projecting it onto the horizontal axis is:

$$c = l_1(c) + l_2 + l_3(c) = \frac{2yR}{\sqrt{(R^2 - z^2)}}\cos\alpha \le R \cdot 3\sqrt{2}. \qquad (60)$$

where, $l_1(c) = l_3(c) = d\cos\alpha = d \cdot \cos 45° = d\frac{\sqrt{2}}{2}$; $z = 0$; $y = \frac{0.5l_2}{\cos\alpha} = \frac{0.5R\sqrt{2}}{\cos\alpha} = \frac{R\sqrt{2}}{2\cos\alpha}$.

$$c = l_1(c) + l_2 + l_3(c) = \frac{2yR}{\sqrt{(R^2 - z^2)}}\cos\alpha = \frac{2R^2\sqrt{2}}{2R} = R\sqrt{2} \le R \cdot 3\sqrt{2}\ \ R\sqrt{2} \le R \cdot 3\sqrt{2}$$

$$R \cdot 1.41 \le R \cdot 4.24$$

As a result, for the length boundary of the spatial crack, we can write:

$$1.41R \le c \le 4.24R.$$

In addition, for the length of the spatial crack, the limitation of the existing standards must be checked - no more than c_0, determined by the formula of paragraph 8.1.9 SP 63.13330.2018:

$$c_0 = \sqrt{\frac{R_s A_{s,I}(2h + b)}{q_{sw,1}}}, \qquad (61)$$

and take into account the limitation $c \le 2h + b$.

CONCLUSION

1. A block analytical calculated model and an algorithm for estimating the complex resistance of a reinforced concrete structure of a circular cross section from the action of bending with torsion, with modeling of the calculated sections by small and large ellipses and modeling of the calculation spatial crack by sections of specially constructed spatial parabolas.

2. Straining model equations for determination of unknown bending $M_{bend,k}$ and torque moment M_t, height of compressed zone of concrete $x_{B,k}$, deformations $\varepsilon_{s,k,rig,x}$, $\varepsilon_{s,k,lef,x}$ and stresses $\sigma_{s,k,rig,x}$, $\sigma_{s,k,lef,x}$ in reinforcement on the left and right of design section, intensity of load in clamps located respectively on the left and right side of design section $q_{sw,lef}$ $q_{sw,rig}$ and intensity of load in clamps located in lower stretched zone of section $q_{sw,\sigma}$ obtained using physical ratios for concrete and reinforcement and static conditions in spatial design section.

3. In the spatial section k, for the block cut off by a complex section passing along a spiral-shaped crack in the compressed zone, all reinforcement is taken into account, falling into this cross section and "heating" effect "in the stretched longitudinal and transverse reinforcement, falling into this spatial section, as well as normal and tangent stresses, located on sections normal to longitudinal axis at the distance x from support and that, as bending

moments increase, height of compressed zone of concrete in section k between first and third round normal cross sections decreases.

4. For dangerous spatial crack length of projection of this crack is found With projection on horizontal axis of diagonal large ellipse of function $f(x,y,z)$ with smaller diagonal $b = R$ and ellipse with larger diagonal $a = l_1(c) + l_2 + l_3(c)$ for which restriction is accepted $1.41R \le c \le 4.24R$.

REFERENCES

1. **Travush V.I., Karpenko N.I., Kolchunov Vl. I., Kaprielov S.S., Demyanov A.I., Bulkin S.A., Moskovtseva V.S.** Rezul'taty eksperimental'nyh issledovanij slozhnonapryazhennyh balok kruglogo poperechnogo secheniya iz vysokoprochnogo fibrozhelezobetona [Results of experimental studies of high-strength fiber reinforced concrete beams with round cross-sections under combined bending and torsion] // Structural Mechanics of Engineering Constructions and Buildings, 2020, Volume 16 (4), pp. 290-297 (in Russian).
2. **Khaldoun R.** Combined Torsion and Bending in Reinforced and Prestressed Concrete beams Using Simplified Method for Combined Stress-Resultants // ACI Structural Journal, 2007, Volume 104, pp. 402–411.
3. **Demyanov A.I., Salnikov A.S. Kolchunov Vl. I.** Experimental studies of reinforced concrete structures during torsion with bending and analysis of their results // Construction and reconstruction, 2017, Volume 4 (72), pp. 17–26 (in Russian).
4. **Thomas A., Hameed A.** An experimental study on combined flexural and torsional behaviour of RC beams // International Research Journal of Engineering and Technology, 2017, Volume 4, Issue 5, pp. 1367–1370.
5. **Kim C., Kim S., Kim K.-H., Shin D., Haroon M., Lee J.-Y.** Torsional behavior of reinforced concrete beams with high-strength steel bars // Structural Journal, 2019, Volume 116, pp. 251–233.
6. **Kandekar S.B., Talikoti R.S**. Study of torsional behavior of reinforced concrete beams strengthened with aramid fiber strips // International journal of advanced structural engineering, 2018, Volume 10, pp. 465-474.
7. **Křístek V., Průša J., Vítek J.L.** Torsion of reinforced concrete structural members // Solid state phenomena, 2018, Volume 272, pp. 178-184.
8. **Santhakumar R., Dhanaraj R., Chandrasekaran E.** Behaviour of retrofitted reinforced concrete beams under combined bending and torsion: A numerical study // Electronic journal of structural engineering, 2007, Volume 7, pp. 1–7.
9. **Kalkan I., Kartal S.** Torsional rigidities of reinforced concrete beams subjected to elastic lateral torsional buckling // International journal of civil and environmental engineering, 2017, Volume 11, pp. 969–972.
10. **Salnikov A., Kolchunov Vl., Yakovenko I.** The computational model of spatial formation of cracks in reinforced concrete constructions in torsion with bending // Applied mechanics and materials, 2015, Volume 725-726, pp. 784–789.
11. **Iakovenko I., Kolchunov Vl.** The development of fracture mechanics hypotheses applicable to the calculation of reinforced concrete structures for the second group of limit states // Journal of applied engineering science, 2017, Volume 15, Issue 455, pp. 370-380.
12. **Demyanov A.I., Kolchunov Vl.I., Yakovenko I.A.** Razrabotka universal'nogo korotkogo dvuhkonsol'nogo elementa k soprotivleniyu zhelezobetonnyh konstrukcij pri kruchenii s izgibom [The development of universal short dual-console ele-ment, for resistance of reinforced concrete structures under the action torsion with bending] // *Izvestiya vysshih uchebnyh zavedenij. Tekhnologiya tekstil'noj promyshlennosti*, 2017, Volume 367, pp. 258–263 (in Russian).

13. **Bernardo, L.** Modeling the full behavior of reinforced concrete flanged beams under torsion // Applied sciences, 2019, Volume 9 (13), p. 2750.
14. **Nahvi H., Jabbari M.** Crack detection in beams using experimental modal data and finite element model // International journal of mechanical sciences, 2005, Volume 47, pp. 1477-1497.
15. **Demyanov A., Kolchunov Vl.** The dynamic loading in longitudinal and transverse reinforcement at instant emergence of the spatial crack in reinforced concrete element under the action of a torsion with bending // Journal of applied engineering science, 2017, Volume 15, Issue 456, pp. 375–380.
16. **Vishnu H.J., Paresh V.P., Sharadkumar P.P.** Strengthening of RC beams subjected to combined torsion and bending with GFRP Composites // Procedia Engineering, 2013, Volume 51, pp. 282–289.
17. **Tsai H.-C., Liao M.-C.** Modeling torsional strength of reinforced concrete beams using genetic programming polynomials with building codes // KSCE Journal of Civil Engineering, 2019, Volume 23, pp. 3464-3475.
18. **Arzamastsev S.A., Rodevich V.V.** K raschetu zhelezobetonnyh elementov na izgib s krucheniem [To the calculation of reinforced concrete elements for bending with torsion] // *Izvestiya vysshih uchebnyh zavedenij. Stroitel'stvo*, 2015, Volume 9, pp. 99-109. (in Russian)
19. **Karpyuk V.M., Kostyuk A.I., Semina Y.A.** General case of nonlinear deformation-strength model of reinforced concrete structures //Strength of materials, 2018, Volume 50, pp. 453–454.
20. **Vítek J. L., Průša J., Křístek V.** Torsion of Rectangular Concrete Sections // ACI Symposium Publication, 2020, Volume 344, pp. 111–130.
21. **Rahal K.N.** Torsional strength of reinforced concrete beams // Canadian journal of civil engineering, 2000, Volume 27, pp. 445–453.
22. **Lin W.** Experimental investigation on composite beams under combined negative bending and torsional moments // Advances in Structural Engineering, 2020, Volume 24, pp. 1456–1465.
23. **Bondarenko V.M., Kolchunov V.I.** Raschetnye modeli silovogo soprotivleniya zhelezobetona [Computational models of the strength resistance of reinforced concrete]. Moscow: ACB, 2004, 472 pages (in Russian)
24. **Golyshev A. B., Kolchunov V.I.** Soprotivlenie zhelezobetona **[**Resistance of reinforced concrete]. Kiev: Osnova, 2009, 432 pages (in Russian).
25. **Kolchunov, V. I., Bulkin S. A.** Calculation scheme of reinforced concrete structures of circular cross-section under bending with torsion // International journal for computational civil and structural engineering, 2021, Volume 17, pp. 63-82.
26. **Karpenko N. I., Kolchunov Vl. I., Travush V. I.** Calculation model of a complex stress reinforced concrete element of a boxed section during torsion with bending // Russian journal of building construction and architecture, 2021, Volume 3(51), pp. 7-26.

СПИСОК ЛИТЕРАТУРЫ

1. **Травуш В.И., Карпенко Н.И., Колчунов Вл.И., Каприелов С.С., Демьянов А.И., Булкин С.А., Московцева В.С.** Результаты экспериментальных исследований сложно-напряженных балок круглого поперечного сечения из высокопрочного фиброжелезобетона // Строительная механика инженерных конструкций и сооружений, 2020, том 16. №4. с. 290-297.
2. **Khaldoun Rahal.** Combined Torsion and Bending in Reinforced and Prestressed Concrete beams Using Simplified Method for Combined Stress-Resultants // ACI Structural Journal, 2007, Volume 104, pp. 402–411.

3. **Демьянов А.И., Сальников А.С., Колчунов Вл.И.** Экспериментальные исследования железобетонных конструкций при кручении с изгибом и анализ их результатов // Строительство и реконструкция, 2017, №4(72), с. 17-26.
4. **Thomas A., Hameed A.** An experimental study on combined flexural and torsional behaviour of RC beams // International Research Journal of Engineering and Technology, 2017, Volume 4, Issue 5, pp. 1367–1370.
5. **Kim C., Kim S., Kim K.-H., Shin D., Haroon M., Lee J.-Y.** Torsional behavior of reinforced concrete beams with high-strength steel bars // Structural Journal, 2019, Volume 116, pp. 251–233.
6. **Kandekar S.B., Talikoti R.S**. Study of torsional behavior of reinforced concrete beams strengthened with aramid fiber strips // International journal of advanced structural engineering, 2018, Volume 10, pp. 465-474.
7. **Křístek V., Průša J., Vítek J.L.** Torsion of reinforced concrete structural members // Solid state phenomena, 2018, Volume 272, pp. 178-184.
8. **Santhakumar R., Dhanaraj R., Chandrasekaran E.** Behaviour of retrofitted reinforced concrete beams under combined bending and torsion: A numerical study // Electronic journal of structural engineering, 2007, Volume 7, pp. 1–7.
9. **Kalkan I., Kartal S.** Torsional rigidities of reinforced concrete beams subjected to elastic lateral torsional buckling // International journal of civil and environmental engineering, 2017, Volume 11, pp. 969–972.
10. **Salnikov A., Kolchunov Vl., Yakovenko I.** The computational model of spatial formation of cracks in reinforced concrete constructions in torsion with bending // Applied mechanics and materials, 2015, Volumes 725-726, pp. 784–789.
11. **Iakovenko I., Kolchunov Vl.** The development of fracture mechanics hypotheses applicable to the calculation of reinforced concrete structures for the second group of limit states // Journal of applied engineering science, 2017, Volume 15, Issue 455, pp. 370-380.
12. **Демьянов А.И., Колчунов Вл.И., Яковенко И.А.** Разработка универсального короткого двухконсольного элемента к сопротивлению железобетонных конструкций при кручении с изгибом // Известия ВУЗов. Технология текстильной промышленности, 2017, №4(367), с. 258–263.
13. **Bernardo, L.** Modeling the full behavior of reinforced concrete flanged beams under torsion // Applied sciences, 2019, Volume 9 (13), p. 2750.
14. **Nahvi H., Jabbari M.** Crack detection in beams using experimental modal data and finite element model // International journal of mechanical sciences, 2005, Volume 47, pp. 1477-1497.
15. **Demyanov A., Kolchunov Vl.** The dynamic loading in longitudinal and transverse reinforcement at instant emergence of the spatial crack in reinforced concrete element under the action of a torsion with bending. // Journal of applied engineering science, 2017, Volume 15, Issue 456, pp. 375–380.
16. **Vishnu H.J., Paresh V.P., Sharadkumar P.P.** Strengthening of RC beams subjected to combined torsion and bending with GFRP Composites // Procedia Engineering, 2013, Volume 51, pp. 282–289.
17. **Tsai H.-C., Liao M.-C.** Modeling torsional strength of reinforced concrete beams using genetic programming polynomials with building codes // KSCE Journal of Civil Engineering, 2019, Volume 23, pp. 3464-3475.
18. **Арзамасцев С.А., Родевич В.В.** К расчету железобетонных элементов на изгиб с кручением // Известия высших учебных заведений. Строительство, 2015, №9, с. 99-109.
19. **Karpyuk V.M., Kostyuk A.I., Semina Y.A.** General case of nonlinear

deformation-strength model of reinforced concrete structures //Strength of materials, 2018, Volume 50, pp. 453–454.
20. **Vítek J.L., Průša J., Křístek V.** Torsion of Rectangular Concrete Sections // ACI Symposium Publication, 2020, Volume 344, pp. 111–130.
21. **Rahal K.N.** Torsional strength of reinforced concrete beams // Canadian journal of civil engineering, 2000, Volume 27, pp. 445–453.
22. **Lin W.** Experimental investigation on composite beams under combined negative bending and torsional moments // Advances in Structural Engineering, 2020, Volume 24, pp. 1456–1465.
23. **Бондаренко В.М., Колчунов. В.И.** Расчетные модели силового сопротивления железобетона. – М.: АСВ, 2004. – 472 с.
24. **Голышев А.Б., Колчунов. В.И.** Сопротивление железобетона. – Киев: Основа, 2009. – 432 с.
25. **Kolchunov, V.I., Bulkin S.A.** Calculation scheme of reinforced concrete structures of circular cross-section under bending with torsion // International journal for computational civil and structural engineering, 2021, Volume 17, pp. 63-82.
26. **Karpenko N.I., Kolchunov Vl.I., Travush V.I.** Calculation model of a complex stress reinforced concrete element of a boxed section during torsion with bending // Russian journal of building construction and architecture, 2021, Volume 3(51), pp. 7-26.

Vladimir I. Travush, Full Member of Russian Academy of Architecture and Construction Sciences, Professor, Dr.Sc.; Vice-Director, Urban planning institute of residential and public buildings (GORPROJECT); Vice-President of the Russian Academy of Architecture and Construction Sciences; Research Institute of Building Physics of Russian Academy of Architecture and Construction Sciences, Lokomotivny pr., 21, Moscow; phone: +7 (495) 482-40-76, e-mail: travush@mail.ru. ORCID: eLibrary.ru SPIN-code: 6462-2331

Vladimir I. Kolchunov, Dr.Sc., Corresponding Member of the Russian Academy of Architecture and Construction Sciences, Professor, Department of unique building and structures, South-Western State University, 94, 50 let Oktyabrya street, Kursk, 305040, Russia phone: +7 (910) 317-93-55; e-mail: vlik52@mail.ru. ORCID: 0000-0001-5075-1134. eLibrary.ru SPIN-code:3990-0345

Sergey A. Bulkin, Chief Design Specialist of Urban planning institute of residential and public buildings (GORPROJECT), 105005, Russia, Moscow, Nizhny Susalny lane, 5, building 5A. ORCID: eLibrary.ru SPIN-код: 3925-7290

Maxim V. Protchenko, Southwestern State University, Kursk, Russia, engineer, E-mail: maxBROMmax@ya.ru. ORCID: 0000-0003-3406-8380. eLibrary.ru SPIN-code:5722-4434

Травуш Владимир Ильич, академик РААСН, профессор, доктор технических наук; профессор, заместитель генерального директора по научной работе, ЗАО «Городской проектный институт жилых и общественных зданий»; вице-президент Российской академии архитектуры и строительных наук; Научно-исследовательский институт строительной физики РААСН, Локомотивный пр., 21, г. Москва, 127238, Россия; тел.:+7 (495) 482-40-76, e-mail: travush@mail.ru. ORCID: eLibrary.ru SPIN-код: 6462-2331

Колчунов Владимир Иванович, член-корреспондент РААСН, доктор технических наук, профессор кафедры «Уникальные здания и сооружения», Юго-Западный государственный университет; 305040, Россия, г. Курск, ул. 50 лет Октября, дом 94; тел .: +7 (910) 317-93-55; e-mail: vlik52@mail.ru**.** ORCID: 0000-0001-5075-1134. eLibrary.ru SPIN-код:3990-0345

Булкин Сергей Александрович, главный специалист-конструктор ЗАО «Городской проектный институт жилых и общественных зданий», Россия, 105005, Россия, г. Москва, Нижний Сусальный пер., 5, стр. 5А, E-mail: sa.bulkin@gmail.com. ORCID: eLibrary.ru SPIN-код: 3925-7290

Протченко Максим Владимирович, ФГБОУ ВО «Юго-Западный государственный университет», г. Курск, Россия, инженер, E-mail: maxBROMmax@ya.ru. ORCID: 0000-0003-3406-8380. eLibrary.ru SPIN-код:5722-4434

International Journal for Computational Civil and Structural Engineering, 18(2) 31–42 (2022)

DOI:10.22337/2587-9618-2022-18-2-31-42

COMPRESSIVE CYLINDER STRENGTH AND DEFORMABILITY OF EXPANDED CLAY FIBER-REINFORCED CONCRETE WITH POLYPROPYLENE FIBER

Yulia G. Maskalkova, Valeryia A. Rzhevutskaya

Belarusian-Russian University, Mogilev, BELARUS

Abstract. This article presents the experimental studies results of the reinforcement effect with polypropylene fiber (0.5 %, 1 %, and 1.5 %) on the strength (compressive cylinder strength) and deformation (compressive strain) characteristics for expanded clay concrete. The most effective fiber percentage is the content of 1.5 % by weight of the cement mass, based on obtained experimental results. An increase in the compressive cylinder strength (up to 13 %), a significant increase in the value of ultimate compressive strain in concrete (corresponding to the peak stress) of the stress-strain diagram (up to 50 %), and the plastic failure of expanded clay fiber-reinforced concrete are noted.

Keywords: lightweight concrete, expanded clay concrete, dispersed reinforcement, polypropylene fiber, compressive cylinder strength, compressive strain, stress-strain diagram.

ЦИЛИНДРИЧЕСКАЯ ПРОЧНОСТЬ И ДЕФОРМАТИВНОСТЬ КЕРАМЗИТОФИБРОБЕТОНА НА ОСНОВЕ ПОЛИПРОПИЛЕНОВОЙ ФИБРЫ

Ю.Г. Москалькова, В.А. Ржевуцкая

Белорусско-Российский университет, г. Могилев, БЕЛАРУСЬ

Аннотация: В статье представлены результаты экспериментальных исследований влияния армирования полипропиленовой фиброй (0,5 %, 1 %, 1,5 %) на прочностные (цилиндрическая прочность при сжатии) и деформативные (деформации при сжатии) характеристики керамзитобетона. Наиболее эффективным процентом армирования полипропиленовой фиброй является 1,5 % по массе от массы цемента согласно полученным экспериментальным данным. На диаграмме деформирования отмечено увеличение цилиндрической прочности (до 13 %) и значительное увеличение (до 50 %) предельных относительных деформаций керамзитофибробетона, соответствующих пиковой точке диаграмме, а также пластический характер разрушения керамзитофибробетона.

Ключевые слова: легкий бетон, керамзитобетон, дисперсное армирование, полипропиленовая фибра, цилиндрическая прочность при сжатии, деформации при сжатии, диаграмма деформирования.

1. INTRODUCTION

Nowadays, expanded clay concrete is a promising building material since it can significantly reduce the self-weight in structures. However, the porosity of the coarse aggregate (expanded clay) imposes some restraints on the use of this material for the manufacture of the structure. One of the main features of expanded clay concrete under load is the absence of a descending branch in the stress-strain diagram '$\sigma_c - \varepsilon_c$'.

The specificity of the lightweight concrete deformation is taken into account in Eurocode 2 (Section 11, Table 11.3.1), where the ultimate compressive strain for lightweight aggregate

ε_{lcu1} are recommended to be taken equal to the compressive strain in the concrete at the peak stress ε_{lc1}, i.e. $\varepsilon_{lc1} = \varepsilon_{lcu1}$.

The absence of a descending branch in the stress-strain diagram is evidence of the brittle failure of the material. This negative factor can be eliminated by inclusion fiber to the concrete mix. Many articles are devoted to this topic, but they are often contradictory. This is probably due to the peculiarity of using special materials used to make specimens. According to the results of some investigations, the polymer fiber inclusion increases the compressive strength of LWAC. There are no changes in the compressive strength in other investigations. Following the results of some articles, it is empirically established, the dispersed reinforcement with polymer fibers significantly improves the deformability of lightweight concrete. Fiber promotes to eliminate of brittle failure of LWAC and improve mechanical characteristics, as evidenced in several studies [1–6].

The fiber effect on the strength characteristics of expanded clay concrete containing expanded clay aggregate 3–8 mm investigated by Fantilli et al. [7]. According to experimental data, the compressive strength of expanded clay concrete specimens was 21.51 MPa, 23.36 MPa, and 22.91 MPa with the polypropylene fiber contents (ρ_{PPf}) of 0 %, 1.4 %, and 2.0 % by cement mass, respectively. The maximum increase in strength (up to 8.6 %) was corresponded to $\rho_{PPf} = 1.4$ %.

The increase in the fiber content changes insignificantly the compressive strength of self-compacting expanded clay concrete (expanded clay aggregate 3–10 mm); it was experimentally established by Mazaheripour et al. [8]. The fiber percentage for all series investigations is considered sufficiently great ($\rho_{PPf} = 2.3$–2.5 %). It is assumed, the presence of fiber dispersed reinforcement prevents the brittle failure of lightweight concrete.

Similar results were obtained in [9, 10]. The experimental data showed the uneven change in the strength characteristics of the lightweight self-compacting concrete modified with polypropylene fiber as the result of an uneven distribution of fiber in the concrete mixture.

Badogiannis et al. [5] ascertained an increase in strength of 20 % and 29 % for LWAC containing polypropylene fiber of 0.5 % and 1 % by concrete volume, respectively. According to the test results, the following expression (1) was proposed (coefficient of determination $R^2 = 0.85$):

$$f_c^{FRLWC}/f_c^{LWC} = 1 + 1.01 \cdot V_f \cdot (l/d), \qquad (1)$$

where f_c^{FRLWC} – the compressive strength of the fiber-reinforced lightweight concrete, f_c^{LWC} – the compressive strength of the lightweight concrete ($V_f = 0$), V_f – the reinforcement percentage with polypropylene fiber by concrete volume, l/d – the fiber aspect ratio.

Polypropylene fiber content improves the strength and deformability properties of concrete, but exceeding a certain reinforcement percentage will negatively result [11]. Fallah et al. [12] evaluated the mechanical characteristics of concrete containing polypropylene fiber in an amount of 0.1–0.5 % by concrete volume. As a result, the fiber content of 0.1 % had a positive effect on the compressive strength of concrete (the compressive strength increase was up to 11.5 %).

The literature on fiber reinforced lightweight concrete shows that the content of polymer fiber in LWAC should be no more than 2 % of the cement mass [13–18]. Furthermore, if this value is exceeded, the strength of fiber-reinforced concrete is always lower than the strength of lightweight concrete without reinforcement. According to [15], the content of synthetic fibers (carbon fiber) should be in the range of 0.5–1.5 %. A similar conclusion can be derived from the test results of Singh [19], the maximum concrete strength is achieved with a polymer fiber content of 1.5 %, and the percentage of polymer fiber reinforcement of 0.5 % is not effective.

The descending branch of the stress-strain curve is an important keyword parameter for non-

linear structural analysis and design of reinforced concrete structures in compression. The use of fiber affects not only the descending branch but also the ascending one [20].

The use of dispersed reinforcement (steel, metal, plastic, polypropylene fiber, and a mixture of different fibers) slightly increased the compressive strength of expanded clay concrete specimens [3, 21, 22]. The value of the modulus of elasticity increased in all cases, except for the case for LWAC containing polypropylene fiber.

The increase in the value of the modulus of elasticity of LWAC was reported with a polymer fiber content of 0.1–0.3 % by concrete volume, while with higher fiber content, the value of the modulus of elasticity was decreased; it was noted in [12].

In a study [23] the dispersed reinforcement with basalt and polyacrylonitrile fiber (0.5 %, 1.0 %, and 1.5 % by concrete volume) of lightweight aggregate concrete present better compressive stress-strain test results than without reinforcement: the clear pronounced descending branch appears on the stress-strain curve.

2. METHODS

The purpose of the investigation is to evaluate the effect of dispersed reinforcement with polypropylene fiber on the strength and deformation characteristics of expanded clay concrete and to determine the optimal percentage of fiber reinforcement.

The aim of the investigation is to assign the reinforcement percentage of expanded clay concrete with polypropylene fiber, based on improvements not only in compressive strength but also in deformation characteristics of expanded clay concrete as a result of dispersed reinforcement.

For the manufacture of expanded clay concrete mixtures, the materials with the characteristics were used:

– expanded clay gravel with round shape and a particle size of 4–10 mm; bulk density of 390 kg/m^3; specific density of 2330 kg/m^3; particle density of 800 kg/m^3; cylinder compressive strength of 1.028 MPa; water absorption of 13.03 % (by mass); water absorption of 10.23 % (by volume); porosity of 83.23 %;

– ordinary Portland cement type I (CEM-I 42.5 N) manufactured by OJSC Krichevcementnoshifer; compressive strength at 28 days (the activity of cement) of 42.5 MPa; bulk density of 1136 kg/m^3; specific density of 3050 kg/m^3; water requirement of normal consistency 21–27 %; spread of cement paste of 106 mm;

– river sand was used as the fine aggregate with the fineness modulus of 2.132; specific density of 2460 kg/m^3; bulk density of 1667 kg/m^3; porosity of 32.32 %.

According to STB 943, river sand in terms of grain-size distribution is related to sand of medium size.

Polypropylene microfibers (PP microF) were used in the experimental study.

PP microF are made from granules of a high-modulus thermoplastic polymer by extraction. These polypropylene microfibers manufactured in the Russian Federation according to TU 2272-001-30726220-2015. Main characteristics of PP microF with 12 mm length: diameter of 50 μm; aspect ratio (length/diameter) of 240; shape is round; density of 910 kg/m^3 at 20 ºC; melting point is more than 160 ºC; electrical conduction is low; alkali resistance is high; chemical resistance is high.

Dispersed reinforcement was carried out with a polypropylene fiber contents of 0.5 %, 1 %, and 1.5 % by weight of the binder (cement) for Series 1–2. The percentage reinforcement of polypropylene fiber of 1.5 % by cement weight was considered for Series 3–4 as the most effective in accordance with the results obtained in [25]. The material components of the experimental specimens are shown in Table 1.

Table 1. Material components of the experimental expanded clay fiber-reinforced concrete and expanded clay concrete specimens

PP microF reinforcement percentage ρ_{PPf}, % (by binder weight)	Characteristics of materials (material components referred to 1 m^3 of expanded clay fiber-reinforced concrete, kg)			Mixture proportions of LWAC	
	Binder	Fine aggregate	Coarse aggregate	C : S : G	W/C
Series 1					
0	Portland cement (258)	River sand (716)	Expanded clay aggregate (333)	1 : 2.78 : 1.29	0.85
0.5					
1.0					
1.5					
Series 2					
0	Portland cement (428)	River sand (787)	Expanded clay aggregate (338)	1 : 1.84 : 0.79	0.52
0.5					
1.0					
1.5					
Series 3–4					
0	Portland cement (428)	River sand (787)	Expanded clay aggregate (338)	1 : 1.84 : 0.79	0.52
1.5					

The shape of the specimens for determining the strength and deformation characteristics of expanded clay fiber-reinforced concrete was in a form of a cylinder (diameter of 150 mm and a height of 300 mm). These specimens were tested for short term uniaxial loading on a hydraulic press in the laboratories of Belarusian-Russian University.

The fiber was added to the dry components and then mixed with water in Series 1. Adding polymer fiber to the dry mixture, thoroughly mixing, and then proportionally adding water is applicable for small batches in the laboratory. A batch with a volume of more than 0.3 m^3 using an inclined concrete mixer was used in that case. The strength of expanded clay fiber-reinforced concrete was less in all cases than the strength of expanded clay concrete without reinforcement (Series 1). In this regard, in the next Series of specimen's water was primarily poured into the drum of the concrete mixer, then the required amount of PP microF was added in portions to the water, after cement, sand, and expanded clay gravel were consistently added. Mixing time was increased by 15 %. This method of preparing a fiber-reinforced concrete mixture made it possible to obtain the strength of expanded clay fiber-reinforced concrete not lower than the strength of the expanded clay concrete without fiber (Series 2–4) [24].

3. RESULTS AND DISCUSSION

The characteristic compressive cylinder strength of expanded clay fiber-reinforced concrete at 28 days was determined from the test results taking into account the coefficient of variation $V < 13.5$ % with a confidence probability of 95 %. Characteristics of the experimental specimens are shown in Table 2.

The actual change in the characteristic compressive cylinder strength of expanded clay fiber-reinforced concrete at 28 days depending on PP microF reinforcement percentage is shown in Fig. 1 (the data are based on Table 1).

Table 2. Characteristics of the experimental cylinder specimens

ρ_{PPf} (by cement weight)	Mean value of density, kg/m^3	Cylinder compressive strength $f_{lc.cyl}$, MPa			The relative value of cylinder compressive strength in comparison with the control specimen	Remark
		Mean value f_{lcm}	The coefficient of variation *Var*, %	Characteristic value at 28 days f_{lck}		
Series 1						
0	1387	13.79	5.35	12.31	1.00	Fiber was added to dry mix
0.5	1412	11.92	5.64	10.57	0.86	
1.0	1398	9.48	6.98	8.15	0.69	
1.5	1363	10.57	10.05	8.43	0.77	
Series 2						
0	1387	11.62	5.10	10.50	1.00	Fiber was added to water
0.5	1567	11.83	4.44	10.83	1.02	
1.0	1475	11.61	5.28	10.45	1.00	
1.5	1421	13.12	7.09	11.47	1.13	
Series 3						
0	1536	11.76	5.41	10.56	1.00	Fiber was added to water
1.5	1413	12.65	4.67	11.57	1.10	
Series 4						
0	1475	11.45	4.84	10.44	1.00	Fiber was added to water
1.5	1474	12.39	4.53	11.40	1.09	

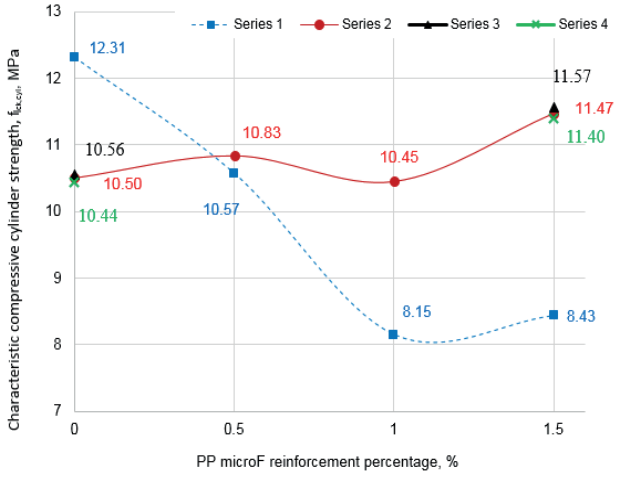

Figure 1. The change in the cylinder strength of expanded clay fiber-reinforced concrete depending on reinforcement percentage

The obtained results are in a good agreement with the results obtained earlier in the study of the cube compressive strength of expanded clay fiber-reinforced concrete [24, 25].

Compressive strength of expanded clay fiber-reinforced concrete can be determined based on the compressive strength of expanded clay concrete by introducing a partial safety factor k_{PPf}, taking into account the reinforcement percentage of polypropylene fiber ρ_{PPf}:

$$f_{lc,PPf} = f_{lc} \cdot k_{PPf}, \quad (2)$$

where $f_{lc,PPf}$ – compressive strength of expanded clay fiber-reinforced concrete, MPa, f_{lc} –

compressive strength of expanded clay concrete, MPa, k_{PPf} – partial safety factor for accounting the percentage of fiber reinforcement.

According to the data presented in Fig. 1, the relation between the characteristic compressive cylinder strength of expanded clay fiber-reinforced concrete at 28 days and the reinforcement percentage is not linear, but it can be expressed by a 2nd degree polynomial. This statement does not contradict the data obtained in [8–10].

The following expression (3) for the analytical determination of the coefficient k_{PPf} was obtained, based on the test results of Series 2–4:

$$k_{PPf} = 1.2 + 0.27\rho_{PPf} \cdot (\rho_{PPf} - 1.77), \quad (3)$$

where ρ_{PPf} – the percentage of polypropylene fiber content in the concrete mixture by cement weight, %.

A comparison of the experimental r_e and theoretical r_t values is shown in Fig. 2. All points are located close to the straight line $r_e = b \cdot r_t$ on the '$r_e - r_t$' diagram. Inclination of line is $\arctan 1.0015 = 45.04° \approx 45°$ (coefficient of determination $R^2 = 0.9969$).

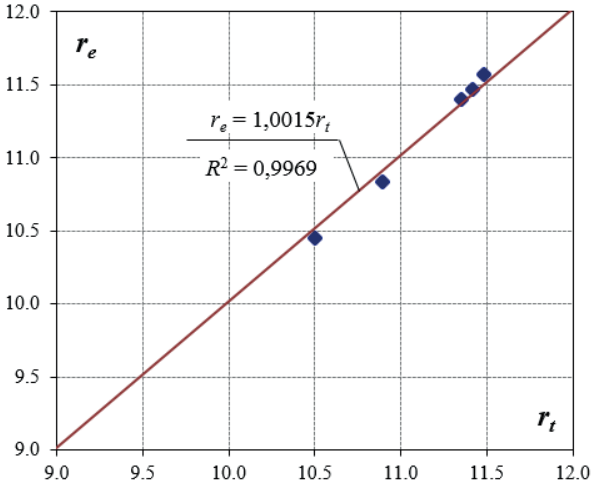

Figure 2. The '$r_e - r_t$' diagram

The proposed expression (3) is required elaboration based on the accumulated empirical data.

Plastic fracture in specimens reinforced by PP microF with a fiber contents of 1 % and 1.5 % by cement weight was observed (Fig. 3).

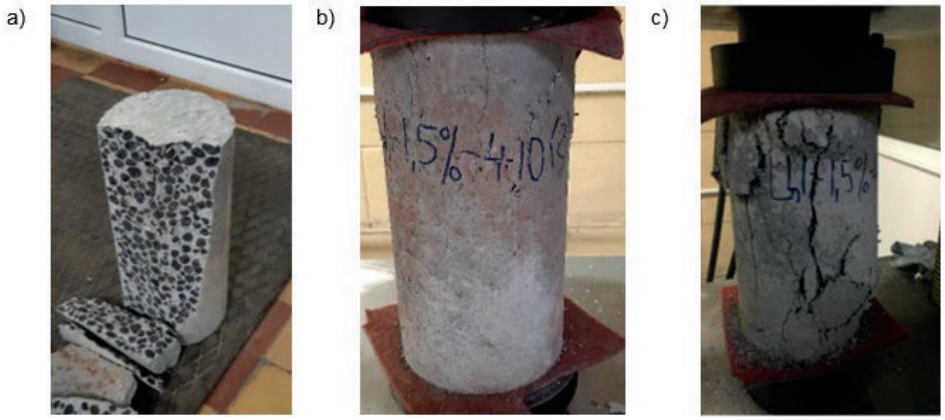

Figure 3. The failure behavior of expanded clay concrete cylinders: a) unreinforced $\sigma_c = f_{lc}$ (the peak stress in the stress-strain diagram), b) reinforced by PP microF $\sigma_c = f_{lc}$ (the peak stress in the stress-strain diagram), c) reinforced by PP microF $\sigma_c > f_{lc}$ (a descending branch in the stress-strain diagram)

In these cases, a descending branch appears in the stress-strain diagram (Fig. 4). Moreover, the actual recorded ultimate compressive strain increases with raising the fiber content. The appearance of a descending branch was not observed at a fiber content of 0.5 % by cement weight (Fig. 4).

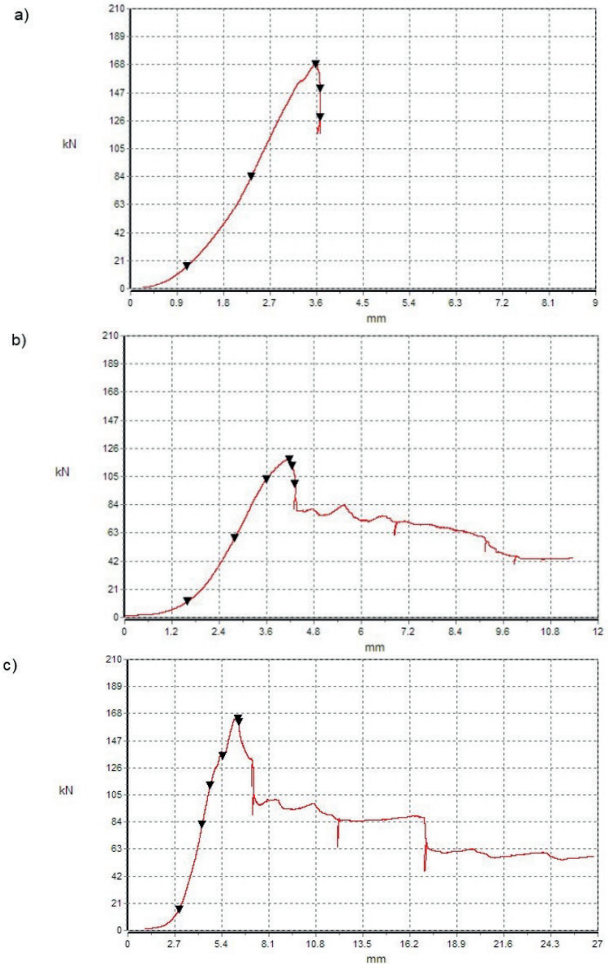

Figure 4. The actual stress-strain diagram of expanded clay fiber-reinforced concrete specimens containing polypropylene fiber: a) 0.5 %, b) 1 %, c) 1.5 %

Fiber forms structural bonds in the concrete mix and prevents segregation when mixing. The use of fiber enables to reduce the crack width and crack spacing, especially at an early age [20, 21]. The optimal effect of dispersed reinforcement is achieved when fibers are located in the sample in the direction perpendicular to the force [4]. As our investigations have shown, polypropylene fibers are predominantly located perpendicular to the vertical axis in cylindrical specimens in case of adherence to the technology of concrete mix preparation with the fiber addition and sufficient mixing time.

The influence of polypropylene and steel fiber (0.1 %, 0.2 %, and 0.3 % by concrete volume) on the deformation characteristics of expanded clay concrete was studied in [26]; it was noted the failure occurs as a result of pulling out or discontinuity of polymer fiber within the crack width (Fig. 5).

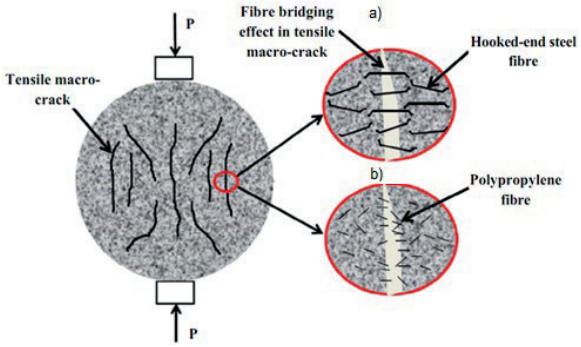

Figure 5. The effect of fibers on cracks in expanded clay concrete: a) steel fiber, b) polypropylene fiber [26]

However, our investigations contradict this statement. Polypropylene fibers restrained cracking, preventing brittle fracture of specimens. The fibers were stretched within the crack, but fiber discontinuity was not noted (Fig. 6).

Figure 6. Location of fibers within the crack at the moment of complete failure (see Fig. 3, c)

The investigation results of the effect of dispersed reinforcement with polypropylene fiber on the compressive strength and deformability of expanded clay concrete are shown in Table 3.

Table 3. The effect of the fiber reinforcement percentage on the compressive strength and deformability of expanded clay fiber-reinforced concrete

ρ_{PPf}	The effect on the compressive strength	Change in deformability	Justification
0.5 %	Compressive strength practically does not change.	The brittle failure. The value of compressive strain in the concrete at the peak stress ε_{lc1} practically does not change.	The fiber content is too low to have an appreciable effect on compressive strength and deformability.
1.0 %	Compressive strength decreases.	The plastic failure. The value of ε_{lc1} increases slightly (up to 10 %).	The fiber content is sufficient to prevent brittle failure, but not enough to inhibit the development of micro cracks. The fiber with low strength negatively affects the compressive strength.
1.5 %	Compressive strength increases (up to 13 %).	The plastic failure. The value of ε_{lc1} increases significantly (more than 50 %).	The fiber content is sufficient to prevent brittle fracture and inhibit the formation and internal micro crack development. The compressive strength of expanded clay concrete increases due to a later crippling of the cement stone

4. CONCLUSIONS

1. According to the obtained experimental data, dispersed reinforcement with polypropylene fiber does not have a significant effect on the strength of expanded clay fiber-reinforced concrete. When the content of polypropylene fiber is 1.5 % (by cement weight), the cylinder strength of expanded clay fiber-reinforced concrete increases up to 13 %. However, the increase of the strength can be due to the error of the testing machine during investigations.
2. The failure of expanded clay fiber-reinforced concrete occurs as a result of the failure of the expanded clay concrete matrix, and not as a result of pulling out or discontinuity of polypropylene fibers at all investigated percentages of reinforcement (0.5 %, 1 %, and 1.5 %).
3. Expanded clay concrete reinforced by polypropylene fiber with a reinforcement percentage of 1 % and 1.5 % by cement weight has a positive effect on the deformability of concrete. A pronounced descending branch appears on the stress-strain diagram; it is determined the plastic failure of expanded clay fiber reinforced concrete.
4. It is recommended to assign the percentage reinforcement of expanded clay concrete containing polypropylene fiber of 1.5 % by cement weight. In this case, it is possible to obtain the required compressive strength with a significant improvement in deformation characteristics, eliminating the brittle failure.
5. The technology of concrete mix preparation with the fiber addition requires clarification. Adding fiber to a dry mix and then mixing with water has a negative effect.
6. The compressive strength of expanded clay fiber-reinforced concrete $f_{lc,PPf}$ can be calculated based on the compressive strength of expanded clay concrete (unreinforced) f_{lc} by multiplying it by the partial safety factor for accounting the percentage of fiber reinforcement k_{PPf}.

5. ACKNOWLEDGEMENT

The authors would also like to express their sincere thanks to PhD. in Engineering S.V. Danilov for his help in organizing the investigation, manufacturing and testing of specimens.

REFERENCES

1. **Wu, F., Liu, C., Diao, Z., Feng, B., Sun, W., Li, X., Zhao, S.** Improvement of mechanical properties in polypropylene- and glass-fibre-reinforced peach shell lightweight concrete. Advances in Materials Science and Engineering. 2018. 2018 (s3). Pp. 1–11. DOI:10.1155/2018/6250941.
2. **Karaburc, S.N., Yildizel, S.A., Calis, G.C.** Evaluation of the basalt fiber reinforced pumice lightweight concrete. Magazine of Civil Engineering. 2020. 94(2). Pp. 81–92. DOI:10.18720/MCE.94.7.
3. **Ghasemzadeh Mousavinejad, S.H., Shemshad Sara, Y.G.** Experimental study effect of silica fume and hybrid fiber on mechanical properties lightweight concrete. Iranian Journal of Science and Technology – Transactions of Civil Engineering. 2019. 43(2). Pp. 263–271. DOI:10.1007/s40996-018-0137-9.
4. **Li, J.J., Niu, J.G., Wan, C.J., Jin, B., Yin, Y.L.** Investigation on mechanical properties and microstructure of high performance polypropylene fiber reinforced lightweight aggregate concrete. Construction and Building Materials. 2016. 118. Pp. 27–35. DOI:10.1016/j.conbuildmat.2016.04.116.
5. **Badogiannis, E.G., Christidis, I., Tzanetatos, G.E.** Evaluation of the mechanical behavior of pumice lightweight concrete reinforced with steel and polypropylene fibers. Construction and Building Materials. 2019. 196. Pp. 443–456. DOI:10.1016/j.conbuildmat.2018.11.109.
6. **Kayali, O., Haque, M., Zhu, B.** Some characteristics of high strength fiber reinforced lightweight aggregate concrete. Cement and Concrete Composites. 2003. 25(2). Pp. 207–213. DOI:10.1016/S0958-9465(02)00016-1.
7. **Fantilli, A.P., Chiaia, B., Gorino, A.** Ecological and mechanical assessment of lightweight fiber-reinforced concrete made with rubber or expanded clay aggregates. Construction and Building Materials. 2016. 127. Pp. 692–701. DOI:10.1016/j.conbuildmat.2016.10.020.
8. **Mazaheripour, H., Ghanbarpour, S., Mirmoradi, S.H., Hosseinpour, I.** The effect of polypropylene fibers on the properties of fresh and hardened lightweight self-compacting concrete. Construction and Building Materials. 2011. 25(1). DOI:10.1016/j.conbuildmat.2010.06.018.
9. **Altalabani, D., Linsel, S., Bzeni, D.K.H.** Fiber reinforced self-compacting lightweight concrete for the manufacture of floating structures. ZANCO Journal of Pure and Applied Sciences. 2019. 31(s3). Pp. 204–209. DOI:10.21271/zjpas.
10. **Altalabani, D., Bzeni, D.K.H., Linsel, S.** Mechanical properties and load deflection relationship of polypropylene fiber reinforced self-compacting lightweight concrete. Construction and Building Materials. 2020. 252. Pp. 119084. DOI:10.1016/j.conbuildmat.2020.11908.
11. **Blazy, J., Blazy, R.** Polypropylene fiber reinforced concrete and its application in creating architectural forms of public spaces. Case Studies in Construction Materials. 2021. 14. Pp. e00549. DOI: 10.1016/j.cscm.2021.e00549
12. **Fallah, S., Nematzadeh, M.** Mechanical properties and durability of high-strength concrete containing macro-polymeric and polypropylene fibers with nano-silica and silica fume. Construction and Building Materials. 2017. 132. Pp. 170–187. DOI:10.1016/j.conbuildmat.2016.11.100.
13. **Rabinovich, F.N.** Kompozity na osnove dispersno-armirovannykh betonov. Voprosy teorii i proyektirovaniya, tekhnologiya,

konstruktsii: monogr. [Composites based on dispersed-reinforced concrete. Questions of theory and design, technology, construction: monograph]. Moscow: ASV, 2004. 560 p. (rus)
14. **Ramujee, K.** Strength properties of polypropylene fiber reinforced concrete. International Journal of Innovative Research in Science, Engineering and Technology, 2013. 8(2). Pp. 3409–3413. URL: https://www.rroij.com/open-access/strength-properties-of-polypropylene-fiber-reinforced-concrete-.php?aid=46458.
15. **Nkem Ede, A., Oluwabambi Ige, A.** Optimal polypropylene fiber content for improved compressive and flexural stren gth of concrete. IOSR Journal of Mechanical and Civil Engineering. 2014. 11(3). Pp. 129–135. DOI:10.9790/1684-1134129135.
16. **Aulia, T.B.** Effects of polypropylene fibres on the properties of high strength concretes. [Online*]. System requirements: AdobeAcrobatReader. URL: https://www.researchgate.net/publication/292307093.
17. **Pothisiri, T., Soklin, C.** Effects of mixing sequence of polypropylene fibers on spalling resistance of normal strength concrete. Engineering Journal. 2014. 18(3). Pp. 55–63. DOI:10.4186/ej.2014.18.3.55.
18. **Korovkin, M.O., Yeroshkina, N.A., Yanbukova, A.R.** Issledovaniye effektivnosti polimernoy fibry v melkozernistom betone [Efficiency investigation of polymer fiber for fine concrete*] [Online*]. System requirements: AdobeAcrobatReader. URL: https://www.ivdon.ru/ru/magazine/archive/n2y2017/4164 (rus)
19. **Singh, S.K.** Polypropylene fiber reinforced concrete: an overview. [Online*]. System requirements: AdobeAcrobatReader. URL: https://www.nbmcw.com/tech-articles/concrete/26929-pfrc.html.
20. **Hassanpour, M., Shafigh, P., Mahmud, H. Bin.** Lightweight aggregate concrete fiber reinforcement – A review. Construction and Building Materials. 2012. 37(1). Pp. 452–461. DOI:10.1016/j.conbuildmat.2012.07.071.
21. **Khalil, W., Ahmed, H., Hussein, Z.** Behavior of high performance artificial lightweight aggregate concrete reinforced with hybrid fibers. MATEC Web of Conferences. 2018. 162. Pp. 1–8. DOI:10.1051/matecconf/201816202001.
22. **Li, J.J., Niu, J.J., Wan, C.J., Liu, X., Jin, Z.** Comparison of flexural property between high performance polypropylene fiber reinforced lightweight aggregate concrete and steel fiber reinforced lightweight aggregate concrete. Construction and Building Materials. 2017. 157. Pp. 729–736. DOI:10.1016/j.conbuildmat.2017.09.149
23. **Zeng, Y., Tang, A.** Comparison of effects of basalt and polyacrylonitrile fibers on toughness behaviors of lightweight aggregate concrete. Construction and Building Materials. 2021. 282. Pp. 122572. DOI: 10.1016/j.conbuildmat.2021.122572.
24. **Maskalkova, Yu.G, Rzhevutskaya, V.A.** Compressive strength of expanded clay fiber-reinforced concrete. AlfaBuild. 2021. 19(4). Pp. 1904. DOI: 10.34910/ALF.19.4.
25. **Maskalkova, Yu.G, Rzhevutskaya, V.A.** The effective reinforcement ratio of expanded clay concrete by polypropylene fiber. Construction of Unique Buildings and Structures. 2020. 93. Pp. 9303. DOI:10.18720/CUBS.93.3.
26. **Madandoust, R., Kazemi, M., Talebi, P.K., de Brito, J.** Effect of the curing type on the mechanical properties of lightweight concrete with polypropylene and steel fibres. Construction and Building Materials. 2019. 223. Pp. 1038–1052. DOI:10.1016/j.conbuildmat.2019.08.006.

СПИСОК ЛИТЕРАТУРЫ

1. **Wu, F., Liu, C., Diao, Z., Feng, B., Sun, W., Li, X., Zhao, S.** Improvement of mechanical properties in polypropylene- and glass-fibre-reinforced peach shell lightweight

concrete. Advances in Materials Science and Engineering. 2018. 2018 (s3). Pp. 1–11. DOI:10.1155/2018/6250941.

2. **Karaburc, S.N., Yildizel, S.A., Calis, G.C.** Evaluation of the basalt fiber reinforced pumice lightweight concrete. Magazine of Civil Engineering. 2020. 94(2). Pp. 81–92. DOI:10.18720/MCE.94.7.
3. **Ghasemzadeh Mousavinejad, S.H., Shemshad Sara, Y.G.** Experimental study effect of silica fume and hybrid fiber on mechanical properties lightweight concrete. Iranian Journal of Science and Technology – Transactions of Civil Engineering. 2019. 43(2). Pp. 263–271. DOI:10.1007/s40996-018-0137-9.
4. **Li, J.J., Niu, J.G., Wan, C.J., Jin, B., Yin, Y.L.** Investigation on mechanical properties and microstructure of high performance polypropylene fiber reinforced lightweight aggregate concrete. Construction and Building Materials. 2016. 118. Pp. 27–35. DOI:10.1016/j.conbuildmat.2016.04.116.
5. **Badogiannis, E.G., Christidis, I., Tzanetatos, G.E.** Evaluation of the mechanical behavior of pumice lightweight concrete reinforced with steel and polypropylene fibers. Construction and Building Materials. 2019. 196. Pp. 443–456. DOI:10.1016/j.conbuildmat.2018.11.109.
6. **Kayali, O., Haque, M., Zhu, B.** Some characteristics of high strength fiber reinforced lightweight aggregate concrete. Cement and Concrete Composites. 2003. 25(2). Pp. 207–213. DOI:10.1016/S0958-9465(02)00016-1.
7. **Fantilli, A.P., Chiaia, B., Gorino, A.** Ecological and mechanical assessment of lightweight fiber-reinforced concrete made with rubber or expanded clay aggregates. Construction and Building Materials. 2016. 127. Pp. 692–701. DOI:10.1016/j.conbuildmat.2016.10.020.
8. **Mazaheripour, H., Ghanbarpour, S., Mirmoradi, S.H., Hosseinpour, I.** The effect of polypropylene fibers on the properties of fresh and hardened lightweight self-compacting concrete. Construction and Building Materials. 2011. 25(1). DOI:10.1016/j.conbuildmat.2010.06.018.
9. **Altalabani, D., Linsel, S., Bzeni, D.K.H.** Fiber reinforced self-compacting lightweight concrete for the manufacture of floating structures. ZANCO Journal of Pure and Applied Sciences. 2019. 31(s3). Pp. 204–209. DOI:10.21271/zjpas.
10. **Altalabani, D., Bzeni, D.K.H., Linsel, S.** Mechanical properties and load deflection relationship of polypropylene fiber reinforced self-compacting lightweight concrete. Construction and Building Materials. 2020. 252. Pp. 119084. DOI:10.1016/j.conbuildmat.2020.11908.
11. **Blazy, J., Blazy, R.** Polypropylene fiber reinforced concrete and its application in creating architectural forms of public spaces. Case Studies in Construction Materials. 2021. 14. Pp. e00549. DOI: 10.1016/j.cscm.2021.e00549
12. **Fallah, S., Nematzadeh, M.** Mechanical properties and durability of high-strength concrete containing macro-polymeric and polypropylene fibers with nano-silica and silica fume. Construction and Building Materials. 2017. 132. Pp. 170–187. DOI:10.1016/j.conbuildmat.2016.11.100.
13. **Рабинович, Ф.Н.** Композиты на основе дисперсно-армированных бетонов. Вопросы теории и проектирования, технология, конструкции: моногр. Москва: Изд-во АСВ. 2004. 560 с.
14. **Ramujee, K.** Strength properties of polypropylene fiber reinforced concrete. International Journal of Innovative Research in Science, Engineering and Technology, 2013. 8(2). Pp. 3409–3413. URL: https://www.rroij.com/open-access/strength-properties-of-polypropylene-fiber-reinforced-concrete-.php?aid=46458.
15. **Nkem Ede, A., Oluwabambi Ige, A.** Optimal polypropylene fiber content for improved compressive and flexural stren gth of concrete. IOSR Journal of Mechanical and Civil Engineering. 2014.

11(3). Pp. 129–135. DOI:10.9790/1684-1134129135.
16. **Aulia, T.B.** Effects of polypropylene fibres on the properties of high strength concretes. [Online*]. System requirements: AdobeAcrobatReader. URL: https://www.researchgate.net/publication/292307093.
17. **Pothisiri, T., Soklin, C.** Effects of mixing sequence of polypropylene fibers on spalling resistance of normal strength concrete. Engineering Journal. 2014. 18(3). Pp. 55–63. DOI:10.4186/ej.2014.18.3.55.
18. **Коровкин, М.О. Ерошкина, Н.А., Янбукова, А.Р.** Исследование эффективности полимерной фибры в мелкозернистом бетоне. Инженерный вестник Дона: электронный научный журнал. 2017. № 2. Режим доступа: https://www.ivdon.ru/ru/magazine/archive/n2y2017/4164.
19. **Singh, S.K.** Polypropylene fiber reinforced concrete: an overview. [Online]. System requirements: AdobeAcrobatReader. URL: https://www.nbmcw.com/tech-articles/concrete/26929-pfrc.html.
20. **Hassanpour, M., Shafigh, P., Mahmud, H. Bin.** Lightweight aggregate concrete fiber reinforcement – A review. Construction and Building Materials. 2012. 37(1). Pp. 452–461. DOI:10.1016/j.conbuildmat.2012.07.071.
21. **Khalil, W., Ahmed, H., Hussein, Z.** Behavior of high performance artificial lightweight aggregate concrete reinforced with hybrid fibers. MATEC Web of Conferences. 2018. 162. Pp. 1–8. DOI:10.1051/matecconf/201816202001.
22. **Li, J.J., Niu, J.J., Wan, C.J., Liu, X., Jin, Z.** Comparison of flexural property between high performance polypropylene fiber reinforced lightweight aggregate concrete and steel fiber reinforced lightweight aggregate concrete. Construction and Building Materials. 2017. 157. Pp. 729–736. DOI:10.1016/j.conbuildmat.2017.09.149
23. **Zeng, Y., Tang, A.** Comparison of effects of basalt and polyacrylonitrile fibers on toughness behaviors of lightweight aggregate concrete. Construction and Building Materials. 2021. 282. Pp. 122572. DOI: 10.1016/j.conbuildmat.2021.122572.
24. **Maskalkova, Yu.G, Rzhevutskaya, V.A.** Compressive strength of expanded clay fiber-reinforced concrete. AlfaBuild. 2021. 19(4). Pp. 1904. DOI: 10.34910/ALF.19.4.
25. **Maskalkova, Yu.G, Rzhevutskaya, V.A.** The effective reinforcement ratio of expanded clay concrete by polypropylene fiber. Construction of Unique Buildings and Structures. 2020. 93. Pp. 9303. DOI:10.18720/CUBS.93.3.
26. **Madandoust, R., Kazemi, M., Talebi, P.K., de Brito, J.** Effect of the curing type on the mechanical properties of lightweight concrete with polypropylene and steel fibres. Construction and Building Materials. 2019. 223. Pp. 1038–1052. DOI:10.1016/j.conbuildmat.2019.08.006.

Yulia G. Maskalkova. PhD. in Engineering, Associate Professor, Associate Professor at the Department of Industrial and Civil Construction, Belarusian-Russian University, Mira Ave, 43, Mogilev, 212000, Belarus, e-mail: julia43@tut.by; ORCID ID: 0000-0002-4107-2452

Valeryia A. Rzhevutskaya. Postgraduate student at the Department of Industrial and Civil Construction, Belarusian-Russian University, Mira Ave, 43, Mogilev, 212000, Belarus, e-mail: valeriarzhevuckaya@gmail.com; ORCID ID: 0000-0001-8854-5408

Москалькова Юлия Георгиевна. К.т.н, доцент, доцент кафедры «Промышленное и гражданское строительство», Белорусско-Российский университет, пр. Мира, 43, Могилев, 212000, Беларусь, e-mail: julia43@tut.by; ORCID ID: 0000-0002-4107-2452

Ржевуцкая Валерия Андреевна. Аспирант кафедры «Промышленное и гражданское строительство», Белорусско-Российский университет, пр. Мира, 43, Могилев, 212000, Беларусь, e-mail: valeriarzhevuckaya@gmail.com; ORCID ID: 0000-0001-8854-5408

DOI:10.22337/2587-9618-2022-18-2-43-50

COMPARATIVE ANALYSIS OF STATIC AND DYNAMIC PILE TESTS IN DIFFICULT GROUNDS OF KAZAKHSTAN

Ascar Zh. Zhussupbekov [1], Ascar U. Yessentayev [1], Victor N. Kaliakin [2], Irina V. Drozdova[3]

[1] L.N. Gumilyov Eurasian National University, Nur-Sultan, KAZAKHSTAN
[2] University of Delaware, Newark, USA
[3] Saint Petersburg State University of Architecture and Civil Engineering, Saint Petersburg, RUSSIA

Abstract. A comparative analysis of the results of field tests to determine the bearing capacity of a pile at the facilitys in the Nur-Sultan city and Petropavlovsk city. The aim of the study was to carry out a comparative analysis of the results of dynamic and static tests in the two construction site in order to identify the difference in performance. This article provides programs and results of tests with static indentation load and dynamic load on a pile in different two of the construction site under different soil conditions. The results of the comparative analysis are the following: Dynamic tests are needed for a preliminary assessment of the dynamic bearing capacity and the possibility of driving piles in different soil conditions. The bearing capacity of the pile, determined by dynamic tests, is slightly lower than during static tests, the difference between the results is 11 and 17%.

Keywords: static test, dynamic tests, pile, comparative analysis, bearing capacity.

СРАВНИТЕЛЬНЫЙ АНАЛИЗ СТАТИЧЕСКИХ И ДИНАМИЧЕСКИХ ИСПЫТАНИЙ СВАИ В СЛОЖНЫХ ГРУНТОВЫХ УСЛОВИЯХ КАЗАХСТАНА

А.Ж. Жусупбеков [1], *А.У. Есентаев* [1], *В.Н. Калякин* [2], *И.В. Дроздова* [3]

[1] Евразийский Национальный Университет им. Л.Н.Гумилева, г. Нур-Султан, КАЗАХСТАН
[2] Университет Делавэра, г. Ньюарк, США
[3] Санкт-Петербургский государственный архитектурно-строительный университет, г. Санкт-Петербург, РОССИЯ

Аннотация. Проведен сравнительный анализ результатов натурных испытаний по определению несущей способности сваи на объектах г. Нур-Султан и г. Петропавловск. Целью исследования было провести сравнительный анализ результатов динамических и статических испытаний на двух строительных площадках с целью выявления разницы в эксплуатационных характеристиках. В данной статье приведены программы и результаты испытаний со статической вдавливающей нагрузкой и динамической нагрузкой на сваю на двух разных стройплощадках при разных грунтовых условиях. Результаты сравнительного анализа, следующие: Динамические испытания необходимы для предварительной оценки динамической несущей способности и возможности забивки свай в различных грунтовых условиях. Несущая способность сваи, определенная при динамических испытаниях, несколько ниже, чем при статических испытаниях, разница между результатами составляет 11 и 17 %.

Ключевые слова: статические испытания, динамические испытания, сваи, сравнительный анализ, несущая способность.

INTRODUCTION

The 800-bed Astana Medical University Hospital is being constructed on the right bank of the Esil River in the city of Nur-Sultan, Kazakhstan. The total area of the hospital will be 140 thousand square meters. It will house a consultative and diagnostic

center, round-the-clock and day facilities with 800 and 110 beds, respectively. The architectural rendering of the hospital complex is shown in Figure 1.

Figure 1. The architectural rendering of 800-bed Astana Medical University Hospital

Figure 2. The architectural rendering of the hospital complex in Petropavlovsk city

The hospital complex in Petropavlovsk city will be equipped with state-of-the-art equipment. Therefore, in order to improve their qualifications, 200 local doctors will undergo training abroad. The hospital is designed for 540 beds, dozens of modern departments. On the territory of the medical complex, there is a take-off platform for sanitary aviation. A separate conference building will be built here. The new multidisciplinary hospital will become a major medical center, attractive for citizens of other countries. The architectural rendering of the hospital complex is shown in Figure 2

1. PILE DYNAMIC TESTS

1.1. Pile dynamic tests in Nur-Sultan

Field tests of test piles C9-30 and C12-30 with dynamic load were carried out from September 21 to September 29, 2020 at the construction site "Construction and operation of the united university hospital for 800 beds at NJSC" Astana Medical University "in the city of Nur-Sultan. In axes X1-X70 and Y1-Y-60. Test piles C9-30 and C12-30 numbered 1, 2, 3, 4, 5, 6, 7, 8, 9, 10, 11, 12, 13, 14, 15, 16, 17 were subjected to dynamic tests. 18, 19 immersed in the ground to a depth of 8.5 m from the absolute elevation of the bottom of the pit 339.82 ÷ 340.22 m, indicated on the layout of the test piles. Driving and finishing of test piles was carried out from September 21 to September 23, 2020 using a Junttan PM-25HD piling rig with an NNK-8A hydraulic hammer with a shock mass of 8000 kg and a headband weighing 990 kg. When driving the piles, wooden spacers were used inside the metal head to prevent the destruction of the pile head. The drop height of the striking part of the hammer ranged from 0.3 ÷ 0.4 meters

The finishing of the piles was carried out on September 29, 2020 with two successive pledges of three and five blows, after 6 ÷ 8 days from the moment of the end of the pile driving. Before finishing, in order to accurately fix the movement, a measuring tape with a scale of 1 mm was glued to the pile. Observation of the sinking of the piles was carried out using a level.

Failures of piles during their finishing ranged from 0.26 cm to 0.42 cm with a hammer energy of 2.4 t* m.

To determine the bearing capacity, the largest average failure of three and five blows was taken, obtained when finishing the pile after their "rest" (MSP 5.01-101-2003), (SP RK 5.01-102-2013). The data obtained are given in the acts of dynamic tests of piles and are attached to the report

Figure 3. a) Junttan PM-25HD piling rig in Nur-Sultan city, b) test pile

The dynamic test results in Nur-Sultan are in the table 1.

Table 1. The dynamic test results in Nur-Sultan

№	Depth of driving piles into the ground, m	The height of the fall of the striking part during finishing, m	Failure of piles during finishing, cm	Partial value of ultimate resistance of piles, kN	Bearing capacity of piles, kN
1	9,50	0,30	0,34	813	
2	9,50	0,30	0,30	869	
3	9,50	0,30	0,27	919	
4	9,50	0,30	0,22	1025	
5	9,50	0,30	0,30	869	
6	9,50	0,30	0,20	1078	
7	9,50	0,30	0,60	590	
8	9,50	0,30	0,86	783	
9	9,50	0,30	0,46	682	813
10	9,50	0,30	0,70	542	
11	9,50	0,30	0,53	631	
12	9,50	0,30	0,84	789	
13	9,50	0,30	0,40	744	
14	9,50	0,30	0,30	869	
15	9,50	0,30	0,56	620	
16	9,50	0,30	0,30	869	
17	9,50	0,30	0,30	869	

1.2. Pile dynamic tests in Petropavlosk

Dynamic tests were carried out from September 26, 2020, using a Junttan PM-25HD pile driver.

The piles in these groups numbered 1, 2, 3, 4, 5, 6, 7, 8, 9, 10, 11, 12, 13, 14, 15, 16, 17 were subjected to dynamic tests. Additional information related to the piles is available in the report on dynamic testing prepared by KGS Astana LLP .

Figure 4. Junttan PM-25HD piling rig in Petropavlovsk

The dynamic test results in Petropavlovsk are in the table 2.

Table 2. The dynamic test results in Petropavlovsk

№	Depth of driving piles into the ground, m	The height of the fall of the striking part during finishing, m	Failure of piles during finishing, cm	Partial value of ultimate resistance of piles, kN	Bearing capacity of piles, kN
1	10,4	0,40	0,52	745	
2	10,4	0,40	0,54	730	
3	10,4	0,40	0,44	816	
4	10,4	0,40	0,50	761	
5	10,4	0,40	0,56	717	
6	10,4	0,40	0,48	779	
7	10,4	0,40	0,48	779	
8	10,4	0,40	0,52	745	
9	10,4	0,40	0,52	745	746
10	10,4	0,40	0,50	761	
11	10,4	0,40	0,48	779	
12	10,4	0,40	0,56	717	
13	10,4	0,40	0,50	761	
14	10,4	0,40	0,52	745	
15	10,4	0,40	0,56	717	
16	10,4	0,40	0,44	816	
17	10,4	0,40	0,48	779	

1.3. Summary about the dynamic tests

In the Nur-Sultan city:

1. The average load-bearing capacity of test piles in groups C9-30 and C12-30, driven to a depth of 8.50 m at the above construction site is 813 kN.
2. The permissible load on the pile, taking into account the safety factor $\gamma_k = 1.4$ in accordance with paragraph 3.10. of SNiP RK 5.01.-03-2002 “Pile foundations” should thus be taken equal to 580kN.

In the Petropavlovsk city:

1. The average load-bearing capacity of test piles in groups C12-30, driven to a depth of 10.40 m at the above construction site, is 746 kN.
2. The permissible load on the pile, taking into account the safety factor $\gamma_k = 1.4$ in accordance with paragraph 3.10. of SNiP RK 5.01.-03-2002 “Pile foundations” should thus be taken equal to 533 kN.

2. PILE STATIC TESTS

2.1. Pile static tests in Nur-Sultan

Field tests of S10-30 driven piles with static, vertical-indentation loads were carried out from December 02, 2020 to January 08, 2021 at the construction site of the Main Building and the Parking lot of the facility “Construction and operation of a united university hospital for 800 beds at NJSC“ Astana Medical University "In Nur-Sultan".

The tests were carried out on four driven test piles C10-30 numbered 29, 40 (Main building) and 62, 66 (Parking), immersed in the ground to a depth of 9.5 m, up to abs. the marks of their bottom are 330.28 ÷ 331.80 m. These test piles are shown in Figure 5.

Field tests were carried out after the piles “rest”, equal to 30 ÷ 60 days after their driving. According to fig. 3. The load on the pile was created using a 100-ton hydraulic jack "Enerpred DU100P150" with a pumping station "Enerpac P462", abutting against a test and loading stand, weighing 120.0 tons.

The process is described in detail in the articles previously published. [1,2]. Piles settlement graphs are show in Figure 6.

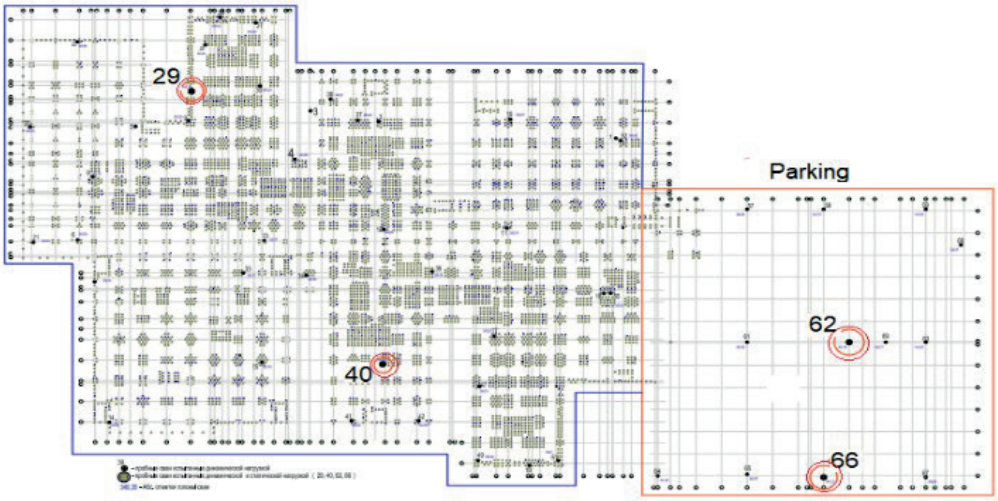

Figure 5. Test pile layout plan

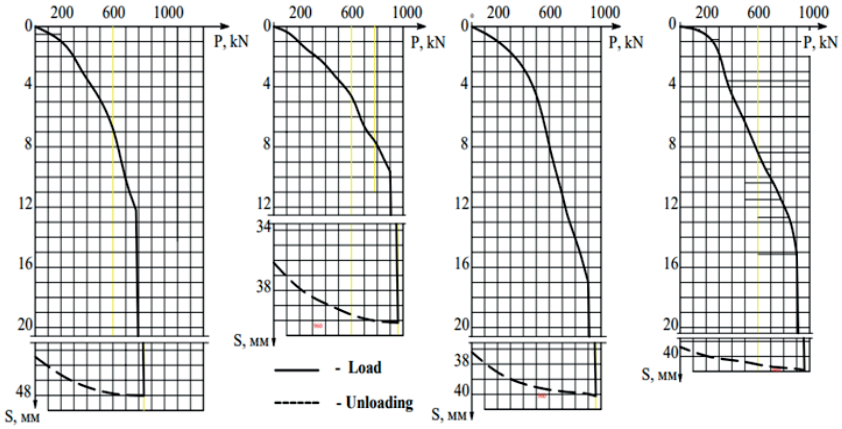

Figure 6. Pile settlement graphs in Nur-Siltan

Static pile tests results in Nur-Sultan:

1) The bearing capacity of the piles test at the locations of the main hospital building and the parking structure were 990 kN and 780 kN, respectively.

2) The permissible pile load, taking into account the safety factor γ_k = 1.2 in accordance with clause 4.4.1.11. SP RK 5.01-103-2013 "Pile foundations" should be taken equal to 750 kN and 650 kN for the main hospital building and parking structure locations, respectively.

Table 3. The static test results in Nur-Sultan

Pile №	Depth of immersion of piles in the ground, m	Maximum applied load, kN	Displacement at the highest applied load, mm	Partial value of ultimate resistance, kN	Bearing capacity of piles, kN
№ 62	9,5	840	48,01	780	780
№ 66	9,5	960	40,14	900	
№ 29	9,5	960	40,12	900	900
№ 40	9,5	960	40,91	900	

2.2. Pile static tests in Petropavlovsk

The movement of each pile was measured by two 6PAO deflectiometers with a scale division of 0.01 mm, and by four digital electronic displacement transducers of the type 027DG1, 027DG2, 027DG3, 027DG4 working in conjunction with the aforementioned SLT2 monitoring system.

Figure 7. Loading stand

The devices that are part of the SLT2 system are specially designed to monitor static load testing of piles in accordance with Eurocode 7. This system provides the ability to monitor static load testing of piles at a distance of up to 25 m, and allows personnel (testers) to remotely monitor behind the settlement of the piles and the actual load on the pile without approaching the potentially dangerous zone of the test site structure, where the system is under high pressure and load [3].

The piles were tested with static, stepwise increasing loads. This consisted of five load steps 166 kN (60 bar), next 111 kN (40 bar). The maximum load is 999 kN (pile №170), 1164 kN (piles №203, 157, 126, 492) и 1274 kN (pile №137).

The associated displacements of the piles were 48,10 mm, 39,99 mm, 41,30 mm, 41,33 mm, 42,29 mm и 41,84 mm, respectively.

Each pile was unloaded in steps, with each unloading step being observed for at least 15 minutes.

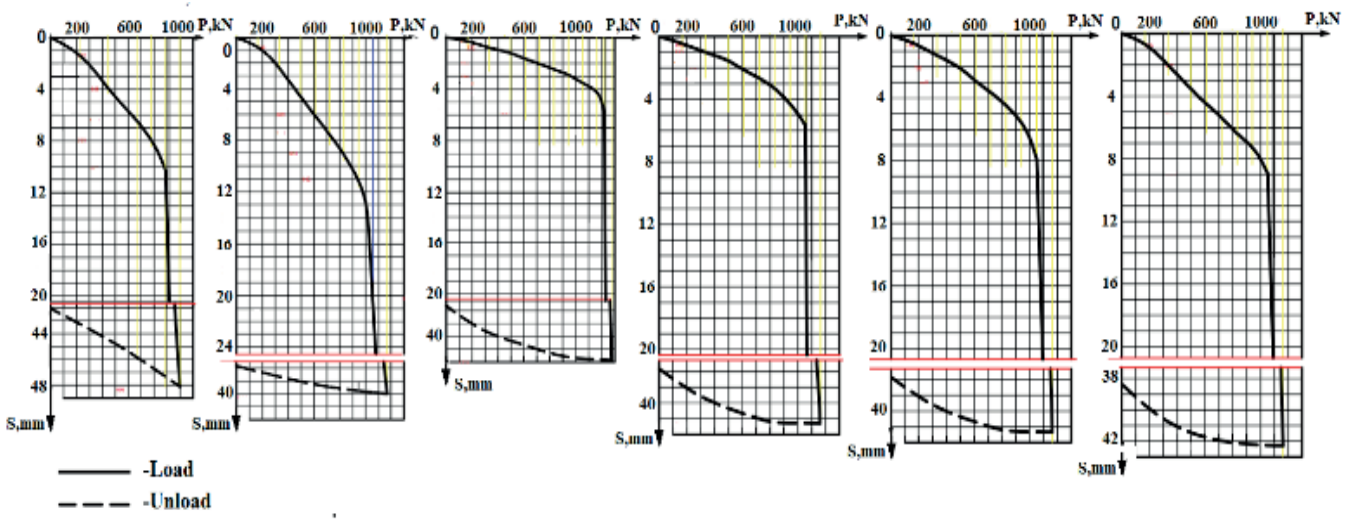

Figure 8. Pile settlements graphs in Petropavlovsk

After complete unloading (to zero), observation of the elastic displacements of the pile was carried out for 60 minutes, with the movement of the piles being recorded every 15 minutes [4,5]

Static pile tests results in Petropavlovsk

1) The bearing capacity of the piles test at the locations of the main hospital building was 995 kN.

2) The permissible pile load, taking into account the safety factor γ_k = 1.2 in accordance with clause 4.4.1.11. SP RK 5.01-103-2013 “Pile foundations” should be taken equal to 829 kN for the main hospital building.

Piles settlement graphs are show in Figure 8

Table 4. The static test results in Petropavlovsk

Pile №	Depth of immersion of piles in the ground, m	Maximum applied load, kN	Displacement at the highest applied load, mm	Partial value of ultimate resistance, kN	*Bearing capacity of piles, kN
№ 170	10,4	999	48,10	917	995
№ 203	10,4	1164	39,99	1053	
№ 137	10,4	1274	41,84	1230	
№ 157	10,4	1164	41,30	1063	
№ 126	10,4	1164	41,33	1093	
№ 492	10,4	1164	41,33	1090	

CONCLUSION

1. Based on the results of dynamic and static tests, it is possible to successfully determine the permissible load for piles.
2. Dynamic tests are needed for a preliminary assessment of the dynamic bearing capacity and the possibility of driving piles in different parts of a construction site under different soil conditions.
3. Static indentation test results must be considered when determining the correct pile length.
4. The bearing capacity of the piles, determined by a dynamic tests, is approximately 11% lower than during static tests in Nur-Sultan.
5. The bearing capacity of the piles, determined by a dynamic tests, is approximately 17% lower than during static tests in Petropavlovsk

REFERENCES

1. **Tulebekova A.S., Zhusupbekov A.Zh., Shakhmov Zh.A., Yenkebayev S.B.**. Opyt provedeniya ispytanij po mezhdunarodnomu standartu ASTM v slozhnyh gruntovyh usloviyah goroda Astany [Experience of testing according to international standard ASTM on problematical soil ground of Astana]. *Vestnik Evraziiskogo natsional'nogo universiteta imeni L.N. Gumileva*, 2012, publ. no. 2 (87), pp. 126-131. (In Russian).
2. **Zhussupbekov A.Zh., Syrlybaev M.K., Lukpanov R.E., Omarov A.R.** The applications of dynamic and static piling tests of Astana. The 15th Asian Regional conference on soil mechanics and geotechnical engineering. Fukuoka, Japan, 2015, pp. 508-508.
3. **Turashev A.S., Lukpanov R.E., Omarov A.R., Zhukenova G.A., Tanyrbergenova G.K.** The applications of dynamic (PDA and traditional) and traditional static piling tests of Astana city. *Vestnik Evraziiskogo natsional'nogo universiteta imeni L.N. Gumileva*, 2015, publ. no. 6 (109), part 1, pp. 244-249.
4. **Yenkebayev S.B**. Comparison results of static and dynamic load test at the construction site of Astana / S.B. Yenkebayev, R.E. Lukpanov, A.Zh.Zhussupbekov // Proc. of Korea-Kazakhstan Joint Geotechnical Seminar. – Incheon, Korea, 2012. pp. 115-121.
5. **Tulebekova A.S., and Zhussupbekov A.Zh**. Geotekhnicheskaya specifika mezhdunarodnyh trebovanij i tradicionnyh standartov pri ispytanii svaj [Geotechnical specificity of international requirements and traditional standards in pile testing]: Monograph. L.N. Gumilyov Eurasian National University. – Moscow: Moscow University Press, 2020, – 111 P. (in Russian).

СПИСОК ЛИТЕРАТУРЫ

1. **Тулебекова А.С., Жусупбеков А.Ж., Шахмов Ж.А., Енкебаев С.Б..** Опыт проведения испытаний по международному стандарту ASTM в сложных грунтовых условиях города Астаны. Вестник евразийского национального университета им. Л.Н.

Гумилева**,** 2012, – Изд. №. 2 (87), с. 126-131.
2. **Zhussupbekov A.Zh., Syrlybaev M.K., Lukpanov R.E., Omarov A.R.** The applications of dynamic and static piling tests of Astana. The 15th Asian Regional conference on soil mechanics and geotechnical engineering. Fukuoka, Japan, 2015, pp. 508-508.
3. The applications of dynamic (PDA and traditional) and traditional static piling tests of Astana city / A.S. Turashev, R.E. Lukpanov, A.R. Omarov, G.A. Zhukenova, G.K. Tanyrbergenova // Вестник Евразийского национального университета им. Л.Н. Гумилева. – 2015. – Изд. № 6 (109), ч. 1. – С. 244–249.
4. **Yenkebayev S.B**. Comparison results of static and dynamic load test at the construction site of Astana / S.B. Yenkebayev, R.E. Lukpanov, A.Zh. Zhussupbekov // Proc. of Korea-Kazakhstan Joint Geotechnical Seminar. – Incheon, Korea, 2012. – P. 115-121.
5. **Tulebekova A.S., and Zhussupbekov A.Zh**. Геотехническая специфика международных требований и традиционных стандартов при испытании свай : Монография. Евразийский национальный университет им. Л.Н. Гумилева. – М.: Издательство МГУ, 2020, – 111 Р.

Ascar Zh. Zhussupbekov, President of Kazakhstan Geotechnical Society, Dr.Sc., Academic of National Engineering Academy of Kazakhstan, Chair of TC 305 (ISSMGE) on Geotechnical Infrastructures of Megacities and New Capitals, Professor of Eurasian National University; 2, Satpayev Street Nur-Sultan, Kazakhstan, 010008, Phone: +7-701-5118382; email: astana-geostroi@mail.ru

Ascar U. Yessentayev, PhD Student of Eurasian National University; 2, Satpayev Street Nur-Sultan, Kazakhstan, 010008, Phone: +7-776-5730101; email: askaryess777@gmail.com

Victor N. Kaliakin, Professor, Department of Civil & Environmental Engineering, University of Delaware, 360F, Newark, DE 19716, U.S.A.; Phone: +01 302.831.2409; email: kaliakin@udel.edu

Irina V. Drozdova, Dr.Sc., Professor, Saint Petersburg State University of Architecture and Civil Engineering, 4, Vtoraya Krasnoarmeiskaya st., Saint Petersburg, 190005, Russia, Phone: +7(812)495-35-44; email: managment@spbgasu.ru

Жусупбеков Аскар Жагпарович, Президент Казахстанского геотехнического общества, д.т.н., академик Национальной Инженерной Академии Казахстана, председатель ТС 305 (ISSMGE) по Геотехническим Инфраструктурам Мегаполисов И Новых Столиц, профессор Евразийского национального Университета; ул. Сатпаева, 2, г. Нур-Султан, Казахстан, 010008, тел.: +7-701-5118382; email: astana-geostroi@mail.ru

Есентаев Аскар Уалиевич, докторант Евразийского Национального Университета; ул. Сатпаева, 2, г. Нур-Султан, Казахстан, 010008, тел.: +7-776-5730101; email: askaryess777@gmail.com

Калякин Виктор Николаевич, профессор кафедры гражданской и экологической инженерии, Делавэрский Университет, 360F, Ньюарк, Делавэр, 19716, США; Телефон: +01 302.831.2409; email: kaliakin@udel.edu

Дроздова Ирина Валерьевна, д.т.н., профессор Санкт-Петербургского Государственного Архитектурно-Строительного Университета, ул. 2 Красноармейская, д. 4, г. Санкт-Петербург, Россия, 190005 тел.: +7(812)495-35-44; email: managment@spbgasu.ru

International Journal for Computational Civil and Structural Engineering, 18(2) 51–61 (2022)

DOI:10.22337/2587-9618-2022-18-2-51-61

SEISMIC DESIGN OF EMBANKMENTS – NUMERICAL AND ANALYTICAL STUDY

Awwad Talal [1,2], *Alkayyal Hassan* [3]

[1] Saint Petersburg State University of Architecture and Civil Engineering, Saint Petersburg, RUSSIA
[2] Emperor Alexander I St. Petersburg State Transport University, Saint Petersburg, RUSSIA
[3] Department of soil mechanics and Foundation Engineering, University of the Federal Armed Forces Munich, GERMANY

Abstract: In this paper, a dynamic shear strength analysis was performed in a finite elements environment to evaluate the stability of embankments under seismic loadings. In addition, a dynamic factor of safety depending on the results of the numerical analysis was defined. To study these parameters' effects on the embankment's stability, a parametric study concerning the embankment inclination and the soil type was performed. Finally, the numerical analysis results were compared with the results of the pseudo-static analysis according to the EC8. The results of this study show the significance of the numerical seismic analyses in comparison with the analytical calculations.

Keywords: embankments, dynamic shear strength, seismic loadings, numerical analysis, stability, sound absorption coefficient.

ПРОЕКТИРОВАНИЕ НАСЫПЕЙ С УЧЕТОМ СЕЙСМИЧЕСКИХ ВОЗДЕЙСТВИЙ – ЧИСЛЕННО-АНАЛИТИЧЕСКОЕ ИССЛЕДОВАНИЕ

Аввад Талал [1, 2], *Аль-Хайал Хасан* [3]

[1] Санкт-Петербургский государственный архитектурно-строительный университет, г. Санкт-Петербург, РОССИЯ
[2] Санкт-Петербургский государственный университет транспорта им. императора Александра I, г. Санкт-Петербург, РОССИЯ
[3] Кафедра механики грунтов и фундаментостроения, Университет федеральных вооруженных сил, г. Мюнхен, ГЕРМАНИЯ

Аннотация: В статье выполнен анализ динамической сдвиговой прочности в программной среде метода конечных элементов для оценки устойчивости насыпей при сейсмических нагрузках. При этом, по результатам численного анализа определен динамический коэффициент запаса прочности. Для изучения влияния этих параметров на устойчивость насыпи проведено параметрическое исследование наклона насыпи и типа грунта. В завершении, результаты численного анализа сравнивались с результатами псевдостатического анализа в соответствии с ЕК8. Результаты этого исследования показывают значимость численного сейсмического анализа по сравнению с аналитическими расчетами.

Ключевые слова: насыпи, динамическая прочность на сдвиг, сейсмические нагрузки, численный анализ, устойчивость, коэффициент звукопоглощения.

INTRODUCTION

The propagation of the earthquake-induced waves due to an earthquake event affects the stability of geotechnical structures and causes different damages and ground settlements. The degree of influence depends on the geology, topography of the influenced area, and the behavior and properties of the local soil under cyclic loadings and it is highly related to the ground motion parameters. In the historical developments of the procedures to analyze the seismic stability of embankments, the pseudo-static approach of Terzaghi (1950) based on the

principle of D'Alembert in the mechanics was used very often. The effects of an earthquake in this approach and its following improvements are represented by constant horizontal and/or vertical accelerations, which produce inertial forces F_h and F_v acting through the centroid of the failure mass. The stability of the slope can be then evaluated by resolving the static and pseudo-static forces on the potential failure mass. Simultaneously, the permanent deformations can be estimated using the sliding block method developed by Newmark (1965). In this method, the permanent deformations can be calculated by time-dependent double integrating of the accelerations, which are above a determined value called the yield accelerationa_y, which makes the pseudo-static factor of safety equals to unity.

The above-mentioned methods are very simple to comprehend and to be applied due to their similarity to the static slope stability analyses and because they can be used to analyze the stability of slopes with sliding surfaces of different forms (planer, circular, or arbitrary failure surfaces). However, the simplification of the very complex effects of the earthquake using only pseudo-static accelerations is very rough. In addition, these methods assume the soil behavior to be rigid which means that they do not consider the realistic soil behavior. Furthermore, these analyses can be unreliable for soils that build up large pore pressures or show more than 15% degradation of strength due to earthquake shaking.

Despite the drawbacks and shortcomings of these methods, many regulations such as the Euro code (EC8) or the German standard (DIN EN 1998-5: 2010-12) suggest their applications to study the seismic stability of slopes and embankments taking into consideration their application limits.

In contrast to the conventional methods, the numerical methods consider the realistic behavior of the soil according to the utilized constitutive models. In addition, the analyses can be achieved in the time domain using real acceleration-time histories. Further, the values of the expected permanent deformations can be realistically determined.

Although the application of the finite element method is simple, it requires good knowledge of numerical modeling, an accurate understanding of the problem to be solved, and deep comprehension of the material laws, which govern the soil behavior. In the following, the most important requirements for numerical modeling under dynamic loading will be discussed.

1. THE APPLICATION OF THE FINITE ELEMENTS METHOD IN THE DYNAMIC ANALYSIS

The dynamic calculations are mainly concerned with the phenomenon of wave propagation. Therefore, the dimensions of the model must be chosen so that the wave reflections at the model boundaries won't influence the important area of the model, which includes the studied structure. This leads to a model with big size and a large number of elements. In addition, the movements of the soil at the model boundaries must be represented realistically using suitable boundary conditions. An additional, artificial, and a special type of boundary condition, which can absorb the earthquake-induced energy waves, must be also used. As a consequence of complying with the above-motioned requirements, the energy waves that propagate inside the model are continuously removed from it.

The mesh coarseness has also a great influence on the results. A coarse mesh with a small number of nodes causes the displacement components of high frequencies to be filtered. The proposed maximum dimension of an element must be between 1/8 Kuhlemeyer und Lysmer (1973) and 1/5 Lysmer et al. (1975) of the shortest wavelength.

After creating the model and generating the mesh, the mass, damping, and stiffness matrices of all elements are calculated and the global equation of motion of the model is time-dependent solved to determine the vectors of acceleration, velocity, and displacement of every node in the model.

2. THE MODEL DESCRIPTION

To achieve the main aims of this study, a plane strain model was created using the program PLAXIS 2D - version 9.0. The soil layers were simulated with volume elements of 15 nodes. The dimensions, boundary conditions, and the coarseness of the mesh were chosen so that the already mentioned requirements are met. The model has a total width of 305 m and a total height of 110 m. The width and the height of the slope are 105 m and 60 m and it has an angle of β=⟦30⟧^o, so that the lateral boundaries and the basis of the model are at distances of 100 m and 50 m away from the slope as shown in figure 1.
The option 'standard Fixities' was used to define the allowed movements at the model boundaries so that the lateral points of the model can only move vertically while the base points were totally fixed.
The seismic action was applied at the lower boundary of the model through prescribed displacement. Simultaneously, energy absorbent boundaries were added at the model vertical sides to eliminate the effects of the reflected waves on the model boundaries. Only the horizontal component of the earthquake was considered in the performed calculations. Figure 2 depicts the model with its boundary conditions. The mesh was generated with a fine coarseness.

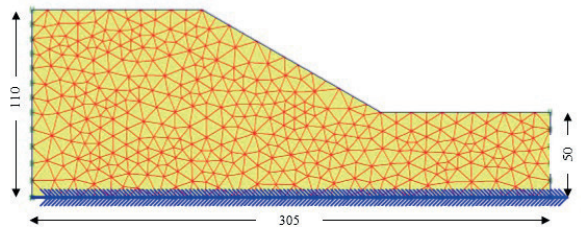

Figure 1. The created model, its dimensions and mesh (without scale, all units are in m)

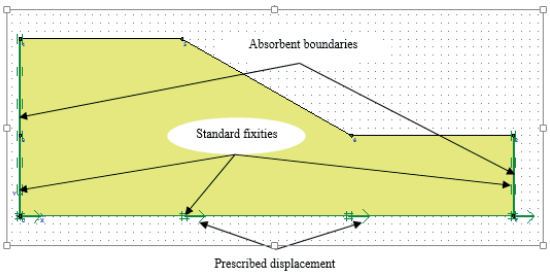

Figure 2. The boundary conditions of the model

3. THE CONSTITUTIVE MODEL HSS

The applied hardening soil small strain model (or abbreviated HSS-model) has the same features as the hardening soil model. In addition, it provides new features added by Benz (2007). The yield surface of the HSS-model can be extended depending on the plastic strain without exceeding the Mohr-Coulomb limit conditions. Due to the consideration of the double hardening, this model can't only account for the elastic and plastic strains (ε_e) and (ε_p), but it also divides the plastic strains into deviatoric and isotropic portions depending on the load direction. The soil stiffness calculated in every calculation step depends not only on the stress level but is also related to the level of the shear strain (γ) so that the value of the shear modulus (G) is greatly increased when the shear strain decreases as illustrated in Figure 3.
As it was observed from the laboratory experiments and the field tests, soil shows high stiffness under dynamic loads, which act within a short time and in a small strain domain. Since the HSS-model can take into account the dependency of the soil stiffness on the level of the shear strain, the use of this material model for the dynamic calculations is ideal. In addition, the HSS-model can also account for hysteretic damping according to the shear strain, so that the damping capacity of the soil (ψ) increases with the increase of the shear strain as shown in Figure 4.

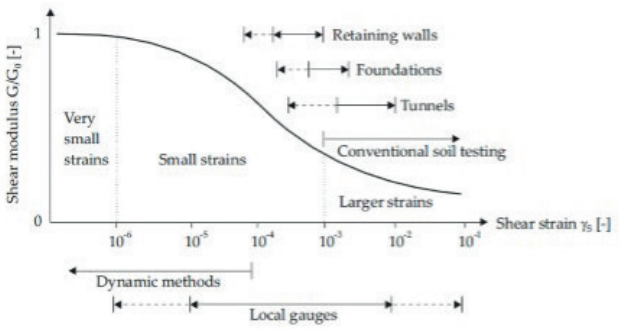

Figure 3. Characteristic stiffness-strain behavior of soil with typical strain ranges

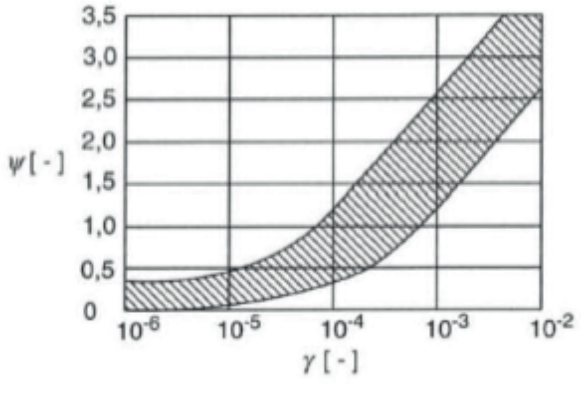

Figure 4. The soil damping capacity related to the shear strain

Depending on the previously mentioned explanations and features of the HSS-model, it can be concluded that this material law is suitable to analyze the studied problem. However, the shortcomings and the limitations of this model should also be taken into consideration. The HSS model cannot generate the accumulated strains due to multiple load cycles. In addition, it cannot generate the excess pore water pressures in the undrained calculations, which leads to the inability of the HSS-model to account for liquefaction, which is the most important phenomenon in the dynamic analysis.

4. THE DYNAMIC SHEAR STRENGTH REDUCTION ANALYSIS

The calculations were carried out stepwise. In the first step, the model has constructed then a static shear strength reduction (abbreviated SSR) analysis was performed to calculate the static factor of safety FS_{stat} and finally the seismic analysis was carried out. Table 1 shows the soil properties of the used dense, well-graded sand (SW).

The applied seismic acceleration-time history as depicted in figure 5 has a maximum acceleration of $PGA = -2.4\frac{m}{s^2}$, a duration of $T = 23.43s$, and a local magnitude of M=5.40.

Table 1. Properties of the SW soil

Soil property	Symbol	Unit	value
Soil unit weight	γ_b	[kN/m^3]	20
Secant stiffness in standard drained triaxial test	E_{50}^{ref}	[kN/m^2]	30000
Tangent stiffness for primary oedometer test	E_{oed}^{ref}	[kN/m^2]	30000
Unloading/reloading stiffness	E_{ur}^{ref}	[kN/m^2]	90000
Power for stress-dependency of stiffness	m	[-]	0.6
Cohesion	C_{ref}	[kN/m^2]	0.1
Friction angle	φ	[°]	40
Dilatancy angle	ψ	[°]	6
Shear strain at which $G_s = 0.772G_0$	$\gamma_{0,7}$	[-]	1.0*10^{-4}
Shear modulus at very small strain	G_0^{ref}	[kN/m^2]	1.0*10^5
Poisson's ratio	υ_{ur}	[-]	0.2
Reference stress for stiffness	p_{ref}	[kN/m^2]	100
Failure ration q_f/q_a	R_f	[-]	0.9
Interface strength	R_{inter}	[-]	1

In each subsequent calculation step, the previously done process (excluding the calculation of the static factor of safety) was repeated but using manually reduced shear parameters according to the Fellenius rule (Fellenius, 1927). The shear strength parameters were reduced using a reduction factor RF started from 1,000 (no reduction) and increased with a rate of 0,025 in each following step till the failure was observed. This analysis, in which the shear strength parameters were step by step reduced and the seismic analyses were carried out, is called the dynamic shear strength reduction analysis or abbreviated as dynamic SSR-Analysis. This analysis is just an extension of the static shear strength reduction analysis to the dynamic conditions based on the Fellenius rule.

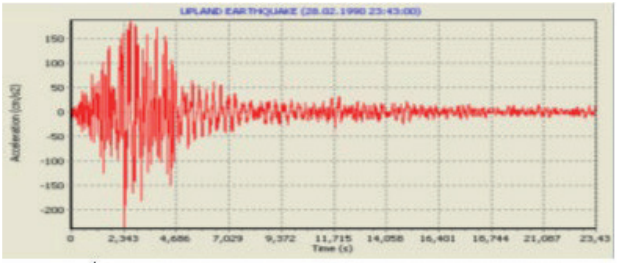

Figure 5. The applied acceleration-time history

To investigate the effect of embankment slope angle on the results, similar calculations with four different models with different slope angles ($\beta = 25^o, 28^o, 32^o$ and 35^o) were performed. Three new models with cohesive, stiff, high plasticity clay (CH) with different slope angles ($\beta = 21^o, 23^o$ and 25^o) were created to investigate the influence of the soil cohesion on the embankment stability under seismic conditions. In these models, the soil parameters listed in Table 2 were used.

Table 2. Properties of the CH soil

Soil property	Symbol	Unit	value
Soil unit weight	γ_b	[kN/m^3]	18
Secant stiffness in standard drained triaxial test	E_{50}^{ref}	[kN/m^2]	15000
Tangent stiffness for primary oedometer test	E_{oed}^{ref}	[kN/m^2]	15000
Unloading/reloading stiffness	E_{ur}^{ref}	[kN/m^2]	45000
Power for stress-dependency of stiffness	m	[-]	0.8
Cohesion	C_{ref}	[kN/m^2]	15
Friction angle	φ	[°]	25
Dilatancy angle	ψ	[°]	0
Shear strain at which $G_s = 0.772G_0$	$\gamma_{0,7}$	[-]	8.0*10^{-5}
Shear modulus at very small strain	G_0^{ref}	[kN/m^2]	60*10^3
Poisson's ratio	υ_{ur}	[-]	0.2
Reference stress for stiffness	p_{ref}	[kN/m^2]	100
Failure ration q_f/q_a	R_f	[-]	0.9
Interface strength	R_{inter}	[-]	1

5. ANALYSIS OF THE RESULTS

After the end of each calculation step, the developments of the plastic points (Mohr-Coulomb plastic points) and the incremental strains ($\Delta\varepsilon$) resulted from the seismic analyses were visually observed by creating time-dependent animations. In addition, the values of the total displacement at the top point of the model resulted from the seismic analyses ($U_{tot,dyn}$) were read and noted.

The development of failure surfaces inside the embankment body during the seismic phases of calculations was utilized to assess the stability of the embankment depending on the visual observations of the time-dependent developments of the plastic points and the incremental strains resulted from the dynamic SSR-analysis. According to these visual observations, the slope failed when a continuous failure surface appeared at a particular time during the dynamic analysis. In this context, the time-dependent development of the incremental strains must also be considered because the plastic points can't be used alone as a failure criterion.

Figures 6 and 7 show the failure surface resulted from the plastic points compared with the observation of incremental strains at the same time increment for the model with the slope angle of $\beta = 30^o$.

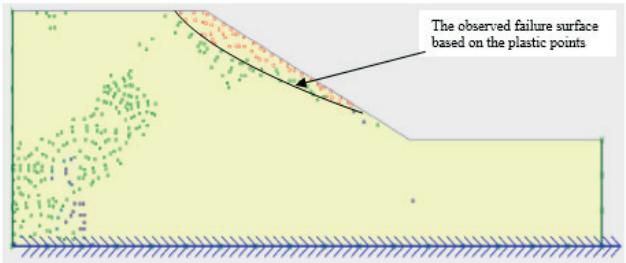

Figure 6. The failure surface resulted from the visual observations of the plastic points (the red points)

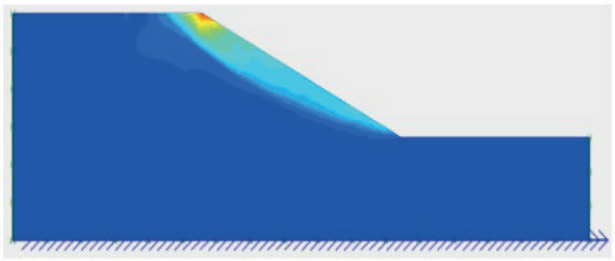

Figure 7. The failure surface resulted from the visual observations of the incremental strains

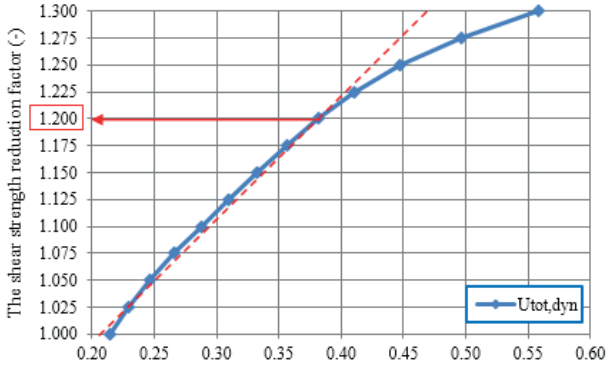

Figure 8. the development of the total dynamic displacement during the dynamic SSR-analysis

Furthermore, the development of the total dynamic displacements $U_{tot,dyn}$ with the increasing values of the reduction factor RF during the dynamic SSR-analysis was also observed. Figure 8 illustrates the curve representing this relationship for the model with the slope angle of $\beta = 30^o$.

Depending on the principles of the shear strength reduction analysis, a dynamic factor of safety (FS)_dyn, which represents an amount that can be used to evaluate the stability of an embankment under seismic conditions, can be defined as the shear strength reduction factor RF, at which a continuous failure surface during the dynamic SSR-analysis was observed. The dynamic factor of safety can also be obtained from the curve representing the development of the dynamic displacements during the SSR analysis. In this case, the dynamic factor of safety is defined as the shear strength reduction factor, at which this curve leaves its semi-linear development and turns into an exponential shape. At this value of RF, the values of the dynamic displacements increase suddenly very rapidly. This outcome was found out by noticing the coincidence between the appearance of a failure surface based on the plastic points and the incremental strains from one side and the development of the shape of the curve representing the development of the total dynamic displacements during the seismic SSR analysis on the other side.

6. THE ANALYTICAL ANALYSIS

The same models discussed in the SSR analyses were created again using the program "Phase02-Slide" in order to compare the results of the performed dynamic analyses with the results of the conventional pseudo-static method. Figure 9 depicts the model of the slope angle of $\beta = 30^o$. The pseudo-static analysis used in this paper benefited the slices method of Bishop (1955) in the pseudo-static conditions by adding inertial forces acting in the centroid of each slice within the potential failure body and resolving the static and pseudo-static forces to calculate the pseudo-static factor of safety FS_{ps}. To determine the value of the pseudo-static coefficient k_h, the response spectrum method according to Eurocode 08, Part 5 was utilized.

7. DISCUSSION OF THE RESULTS

Figures 9 and 10 show the changes in the values of the static FS_{stat}, pseudo-static $FS_{ps}$and dynamic FS_{dyn}factors of safety with the increasing values of the slope angle (β) for the previously described models.

It is clear that the values of the static factor of safety decrease when the values of the slope angle increase. This is also to be noticed in the values of dynamic and pseudo-static factors of safety, so that the steeper the slope is, the lower the dynamic safety level of the embankment is. Furthermore, the

cohesion of the soil plays an important role in increasing slope stability. This fact can be shown by observing the rate of reduction in the values of the dynamic factor of safety with the increasing values of the slope angle for the CH-clay models in comparison with the models of SW-sand.

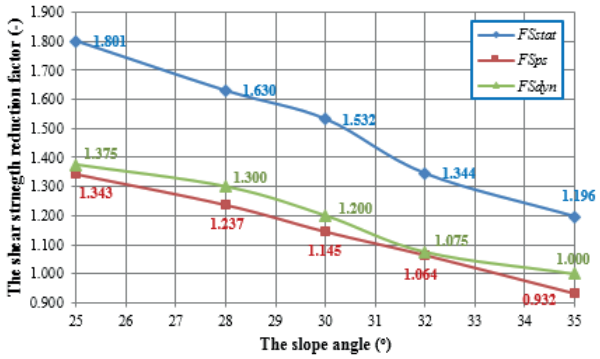

Figure 9. The decrease of the factors of safety with the increase of the slope angle for the models of the SW-soil

By comparing the results of the pseudo-static analysis with the result of the dynamic finite elements calculations, a rough coincidence can be noted between the results of both analyses, so that the pseudo-static analysis can only provide a rough prediction of the embankment slope stability under seismic conditions. It can also be noted that the results of the pseudo-static analysis may not always be on the safe side, since the results of this type of analysis are highly dependent on the input value of the pseudo-static coefficient

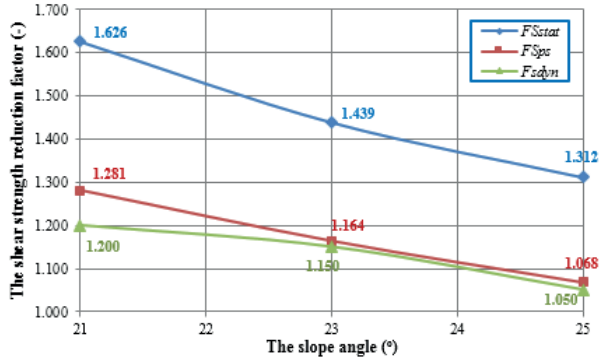

Figure 10. The decrease of the factors of safety with the increase of the slope angle for the models of the CH-soil

8. CONCLUSION

In this paper, a full description of the dynamic shear strength reduction analysis implemented in a finite elements environment was explained and applied to investigate the stability of embankments under seismic conditions. In addition, the paper provides information about the definition of a dynamic factor of safety as a measure for the evaluation of seismic slope stability. Furthermore, a parametric study containing the soil parameters and the embankment slope angle was carried out to predict the influences of these parameters on the stability of the embankments under seismic conditions. Finally, the results of the static, pseudo-static, and dynamic analyses were compared and the main features and interpretations of the results were discussed.

REFERENCES

1. **Alkayyal, H.** Analytische und numerische Berechnungen zur Erdbebenbemessung von Böschungen und Stützmauern, Masterarbeit, Institut für Geotechnik, Leibniz Universität Hannover, 2012
2. **Awwad T., Donia M. 2016.** The efficiency of using a seismic base isolation system for a 2D concrete frame founded upon improved soft soil with rigid inclusions. Earthquake Engineering and Engineering Vibration Volume 15, Issue 1, Cover Date 2016-03. Institute of Engineering Mechanics, China. SPRINGER pp 49-60. DOI: 10.1007/s11803-016-0304-6
3. **Awwad T., Donia M., Awwad L. 2017.** Effect of a stiff thin Foundation soil layer's depth on dynamic response of an embankment dam. Elsevier, Procedia Engineering, Volume 189, 2017, PP 525–532. DOI: 10.1016/j.proeng.2017.05.084
4. **Awwad T., Gruzin V., Kim V.** Sustainable Reconstruction in Conditions of Dense Urban Development. In: Weng MC., Lee J., Liu Y. (eds) Current Geotechnical Engineering Aspects of Civil

Infrastructures. GeoChina 2018. Sustainable Civil Infrastructures. Springer, Cham, 2019, pp 13-23 DOI:10.1007/978-3-319-95750-0_2.

5. **Awwad T., Mussabayev T., Tulebekova A., Jumabayev A.** "Development of the computer program of calculation of concrete bored piles in soil ground of Astana city". International Journal of GEOMATE Vol.17, Issue 60, 2019, pp.176-182, DOI:10.21660/2019.60.17339.
6. **Awwad T., Shakhmov Z.A., Lukpanov R.E., Yenkebayev S.B.** Experimental Study on the Behavior of Pile and Soil at the Frost Condition. In: El-Naggar H., Abdel-Rahman K., Fellenius B., Shehata H. (eds) Sustainability Issues for the Deep Foundations. GeoMEast 2018. Sustainable Civil Infrastructures. Springer, Cham, 2019, pp 69-76, DOI:10.1007/978-3-030-01902-0_7.
7. **Awwad T., Yenkebayev S.B., Tsigulyov D.V., Lukpanov R.E.** Analysis of Driven Pile Bearing Capacity Results by Static and Dynamic Load Tests. In: El-Naggar H., Abdel-Rahman K., Fellenius B., Shehata H. (eds) Sustainability Issues for the Deep Foundations. GeoMEast 2018. Sustainable Civil Infrastructures. Springer, Cham, 2019, pp 77-84. DOI: 10.1007/978-3-030-01902-0_8.
8. **Brinkgreve R.; Broere W.** Tutorial manual of PLAXIS 2D – Version 9.0, technical university of Delft, Netherlands, 2010.
9. **Brötzmannn, F.** 2012 Standsicherheitsuntersuchungen von Staudämmen unter seismischen Einwirkungen mittels dynamischer FE-Analysen, Beiträge der Spezialsitzung der Baugrundtagung in Mainz, Hrsg. Deutsche Gesellschaft für Geotechnik (DGGT), S. 23 – 28
10. **Derghoum, R. & Mohamed, M.** Numerical study for optimal design of soil nailed embankment slopes. International Journal of Geo-Engineering. 12. 2021. DOI:10.1186/s40703-021-00144-5
11. **Eurocode 8:** Auslegung von Bauwerken gegen Erdbeben – Teil 1: Grundlagen, Erdbebeneinwirkungen und Regeln für Hochbauten, Deutsche Fassung EN 1998-1:2004 + AC:2009, Dezember 2010
12. **Eurocode 8:** Auslegung von Bauwerken gegen Erdbeben – Teil 5: Gründungen, Stützbauwerke und geotechnische Aspekte, Deutsche Fassung EN 1998-5:2004, Dezember 2010
13. **Kodsi, S.A., Oda, K. & Awwad, T.** "Viscosity effect on soil settlements and pile skin friction distribution during primary consolidation," International Journal of GEOMATE, Dec., 2018 Vol.15, Issue 52, pp. 152-159. DOI: 10.21660/2018.52.52744.
14. **KRAMER, Steven L. 1996** Geotechnical Earthquake Engineering, Prentice Hall press,
15. **Lukpanov R.E., Awwad T., Orazova D.K., Tsigulyov D. 2019.** Geotechnical Research and Design of Wind Power Plant. In: Choudhury D., El-Zahaby K., Idriss I. (eds) Dynamic Soil-Structure Interaction for Sustainable Infrastructures. Sustainable Civil Infrastructures. Springer, Cham, pp 220-227. DOI: 10.1007/978-3-030-01920-4_19
16. **MEY, A.; VON WOLFFERSDORFF, P.-A. 2008.** Die Bedeutung der Stoffmodelle für dynamische Berechnungen zur Standsicherheit von Staudämmen mit der Finite-Elemente-Methode, Kolloquium "Bodenmechanik, Grundbau und bergbauliche Geotechnik" anl. 75. Geburtstag Prof. Förster, TU Bergakademie Freiberg, Veröffentl. Inst. Geotechnik, S. 111 – 133
17. **Nurakov, S. & Awwad, T.** Investigation on soil cutting by non-bucket bottom rotor end chisels. International Journal of GEOMATE, Vol.16, Issue 53, January 2019, pp.231-237. DOI: 10.21660/2019.53.96902

18. **TOWHATA, I. 2008.** Geotechnical Earthquake Engineering, Springer-Verlag, Berlin.
19. **Ulitsky V., Shashkin, A., Shashkin, K., Lisyuk, M., Awwad, T.** Numerical simulation of new construction projects and existing buildings and structures taking into account their deformation scheme. Proceedings of the 19th International Conference on Soil Mechanics and Geotechnical Engineering. Seoul, Korea, September 2017, pp 2061–2065, EID: 2-s2.0-85045466035
20. **VON WOLFFERSDORFF, P.-A. 2010.** Ausgewählte Probleme zu statischen und dynamischen Standsicherheitsberechnungen von Staudämmen, Beiträge zum 25. Christian Veder Kolloquium, Technische Universität Graz, Gruppe Geotechnik Graz, S. 163 – 182
21. **Zhang, W. & Wang, D.** Stability analysis of cut slope with shear band propagation along a weak layer. Computers and Geotechnics. 2020, 125. 103676. 10.1016/j.compgeo.2020.103676.
22. **Zhussupbekov A., Zhunisov T., Issina A., Awwad T.** "Geotechnical and structural investigations of historical monuments of Kazakhstan". Proceedings of Second International Symposium on Geotechnical Engineering for the Preservation of Monuments and Historic Sites, Naples, Italy, 2013. PP 779-784. EID: 2-s2.0-84878773734.
23. **Ziccarelli, M. & Rosone, M.** Stability of Embankments Resting on Foundation Soils with A Weak Layer. Geosciences. 2021.11.86. DOI:10.3390/geosciences11020086.

СПИСОК ЛИТЕРАТУРЫ

1. **Alkayyal, H.** Analytische und numerische Berechnungen zur Erdbebenbemessung von Böschungen und Stützmauern, Masterarbeit, Institut für Geotechnik, Leibniz Universität Hannover, 2012.
2. **Awwad T., Donia M.** (2016). The efficiency of using a seismic base isolation system for a 2D concrete frame founded upon improved soft soil with rigid inclusions. Earthquake Engineering and Engineering Vibration. Vol. 15, Issue 1, Cover Date 2016-03. Institute of Engineering Mechanics, China. SPRINGER pp. 49-60. DOI: 10.1007/s11803-016-0304-6.
3. **Awwad T., Donia M., Awwad L.** (2017). Effect of a stiff thin Foundation soil layer's depth on dynamic response of an embankment dam. Elsevier, *Procedia Engineering*, Vol. 189, pp. 525–532. DOI: 10.1016/j.proeng.2017.05.084.
4. **Awwad T., Gruzin V., Kim V.** Sustainable Reconstruction in Conditions of Dense Urban Development. In: Weng MC., Lee J., Liu Y. (eds) Current Geotechnical Engineering Aspects of Civil Infrastructures. GeoChina 2018. Sustainable Civil Infrastructures. Springer, Cham, 2019, pp. 13-23 DOI:10.1007/978-3-319-95750-0_2.
5. **Awwad T., Mussabayev T., Tulebekova A., Jumabayev A.** Development of the computer program of calculation of concrete bored piles in soil ground of Astana city. *International Journal of GEOMATE* Vol. 17, Issue 60, 2019, pp. 176-182, DOI:10.21660/2019.60.17339.
6. **Awwad T., Shakhmov Z.A., Lukpanov R.E., Yenkebayev S.B.** Experimental Study on the Behavior of Pile and Soil at the Frost Condition. In: El-Naggar H., Abdel-Rahman K., Fellenius B., Shehata H. (eds) Sustainability Issues for the Deep Foundations. GeoMEast 2018. Sustainable Civil Infrastructures. Springer, Cham, 2019, pp. 69-76, DOI:10.1007/978-3-030-01902-0_7.
7. **Awwad, T., Yenkebayev, S.B., Tsigulyov, D.V., Lukpanov, R.E.** (2019). Analysis of Driven Pile Bearing Capacity Results by Static and Dynamic Load Tests. In: El-Naggar, H., Abdel-Rahman, K., Fellenius,

B., Shehata, H. (eds) Sustainability Issues for the Deep Foundations. GeoMEast 2018. Sustainable Civil Infrastructures. Springer, Cham, pp. 77-84. DOI: 10.1007/978-3-030-01902-0_8.

8. **Brinkgreve R. Broere W.** Tutorial manual of PLAXIS 2D – Version 9.0, technical university of Delft, Netherlands, 2010.
9. **Brötzmannn F.** Standsicherheitsuntersuchungen von Staudämmen unter seismischen Einwirkungen mittels dynamischer FE-Analysen, Beiträge der Spezialsitzung der Baugrundtagung in Mainz, Hrsg. Deutsche Gesellschaft für Geotechnik (DGGT), 2012 S. 23 – 28.
10. **Derghoum, R., Meksaouine, M.** Numerical study for optimal design of soil nailed embankment slopes. *Geo-Engineering* 12, 15 (2021). DOI:10.1186/s40703-021-00144-5.
11. **Eurocode 8:** Auslegung von Bauwerken gegen Erdbeben – Teil 1: Grundlagen, Erdbebeneinwirkungen und Regeln für Hochbauten, Deutsche Fassung EN 1998-1:2004 + AC:2009, Dezember 2010.
12. **Eurocode 8:** Auslegung von Bauwerken gegen Erdbeben – Teil 5: Gründungen, Stützbauwerke und geotechnische Aspekte, Deutsche Fassung EN 1998-5:2004, Dezember 2010.
13. **Kodsi, S.A., Oda, K. & Awwad, T.** Viscosity effect on soil settlements and pile skin friction distribution during primary consolidation. *International Journal of GEOMATE*, Dec., 2018 Vol. 15, Issue 52, pp. 152-159. DOI: 10.21660/2018.52.52744.
14. **Kramer, Steven L. (**1996**)** Geotechnical Earthquake Engineering, Prentice Hall press,
15. **Lukpanov R.E., Awwad T., Orazova D.K., Tsigulyov D.** (2019) Geotechnical Research and Design of Wind Power Plant. In: Choudhury D., El-Zahaby K., Idriss I. (eds) Dynamic Soil-Structure Interaction for Sustainable Infrastructures. Sustainable Civil Infrastructures. Springer, Cham, pp. 220-227. DOI: 10.1007/978-3-030-01920-4_19.
16. **Mey, A., VON Wolffersdorff, P.-A.** (2008) Die Bedeutung der Stoffmodelle für dynamische Berechnungen zur Standsicherheit von Staudämmen mit der Finite-Elemente-Methode, Kolloquium "Bodenmechanik, Grundbau und bergbauliche Geotechnik" anl. 75. Geburtstag Prof. Förster, TU Bergakademie Freiberg, Veröffentl. Inst. Geotechnik, pp. 111–133.
17. **Nurakov, S. & Awwad, T.** Investigation on soil cutting by non-bucket bottom rotor end chisels. *International Journal of GEOMATE*, Vol.16, Issue 53, January 2019, pp.231-237. DOI: 10.21660/2019.53.96902.
18. **Towhata I. 2008.** Geotechnical Earthquake Engineering, Springer-Verlag, Berlin.
19. **Ulitsky V., Shashkin, A., Shashkin, K., Lisyuk, M., Awwad, T.** Numerical simulation of new construction projects and existing buildings and structures taking into account their deformation scheme. Proceedings of the 19th International Conference on Soil Mechanics and Geotechnical Engineering. Seoul, Korea, September 2017, pp 2061–2065, EID: 2-s2.0-85045466035.
20. **Von Wolffersdorff, P.-A.** (2010). Ausgewählte Probleme zu statischen und dynamischen Standsicherheitsberechnungen von Staudämmen, Beiträge zum 25. Christian Veder Kolloquium, Technische Universität Graz, Gruppe Geotechnik Graz, pp. 163–182.
21. **Zhang, W. & Wang, D.** Stability analysis of cut slope with shear band propagation along a weak layer. Computers and Geotechnics. 2020, 125. 103676. 10.1016/j.compgeo.2020.103676.
22. **Zhussupbekov A., Zhunisov T., Issina A., Awwad T.** Geotechnical and structural investigations of historical monuments of Kazakhstan. Proceedings of Second International Symposium on Geotechnical Engineering for the Preservation of

Monuments and Historic Sites, Naples, Italy, 2013. pp. 779-784. EID: 2-s2.0-84878773734.

23. **Ziccarelli M., Rosone M.** Stability of Embankments Resting on Foundation Soils with A Weak Layer. Geosciences. 2021.11.86. DOI:10.3390/geosciences11020086.

Talal Awwad, Dr. Ph.D., Professor of the Geotechnical Engineering Department, Civil Engineering faculty, Damascus University, Syria; Professor of the Soils and Foundations Department, Civil Engineering faculty, Emperor Alexander I St. Petersburg State Transport University, Russia; Professor of the Saint Petersburg State University of Architecture and Civil Engineering, St. Petersburg, Russia. Phone +79112216792; Email: dr.awwad.gfce@gmail.com.

Hassan Alkayyal, Department of soil mechanics and Foundation Engineering, University of the Federal Armed Forces Munich, Germany; M.Sc.; Project Manager. Boley Geotechnik GmbH; Phone +498960043474; Email: enghalkayyal@hotmail.com.

Талал Аввад, доктор технических наук, профессор кафедры геотехники строительного факультета Дамасского университета, Сирия; профессор кафедры грунтов и фундаментов строительного факультета Санкт-Петербургского государственного университета путей сообщения императора Александра I, Россия; профессор Санкт-Петербургского государственного архитектурно-строительного университета, Санкт-Петербург Санкт-Петербург, Россия. Телефон +79112216792; Электронная почта: dr.awwad.gfce@gmail.com .

Хасан Аль-Хайал, кафедра механики грунтов и строительства фундаментов, Университет Федеральных вооруженных сил, Мюнхен, Германия; M.Sc .; Руководитель проекта. Boley Geotechnik GmbH; Телефон +498960043474; Электронная почта: enghalkayyal@hotmail.com

DOI:10.22337/2587-9618-2022-18-2-62-73

MODEL OF STRESS-STRAIN STATE OF THREE-LAYERED REINFORCED CONCRETE STRUCTURE BY THE FINITE ELEMENT METHODS

Vu Dinh Tho [1], Elena A. Korol [2], Vladimir I. Rimshin [2], Pham Tuan Anh [1]

[1] University of Transport Technology (UTT), Ha Noi, VIETNAM

[2] National Research Moscow State University of Civil Engineering, Moscow, RUSSIA

Abstract. The object of the study is multi-layer reinforced concrete structures of concrete with various physical and mechanical characteristics of materials - concrete and reinforcement under the influence of loading. Analysis of the stress state of multilayer reinforced concrete beams by using different materials is a complex problem due to the different mechanical and physical characteristics of materials and the cracking behavior of concrete. This article presents an analysis of the stress-strain state of three-layered reinforced concrete structures using the finite element method in the program ANSYS Mechanical. Numerical modeling allows on ANSYS allows combining different combinations of loads, the variability of the strength and deformation characteristics of materials and various types of reinforcement in multilayer reinforced concrete beams. Comparison is made between the experimental results, numerical results and finite element analyses with respect to initial crack formation and the ultimate load capacity of beams. The results of the study were shown that as the grade of concrete in the external layer increases from B15 to B20 and the grade of lightweight concrete in the internal layer increases from B0.75 to B1.5, the crack resistance can be increased by 59.7% and the bearing capacity of the test beam is increased by 16.4%. When the thickness of the external layers varies from 40mm to 80mm, making the crack resistance increased by 47.5% and the bearing capacity of three-layer concrete beams greatly increased by 6.7%. The obtained scientific results enable to determine rational parameters for modeling various structural solutions of multilayer reinforced concrete structures.

Keywords: concrete buildings; reinforced concrete; multilayer structures; three-layer structures; contact interlayer; heat-insulating materials; stress analysis; ANSYS Mechanical.

МОДЕЛИРОВАНИЕ НАПРЯЖЕННО-ДЕФОРМИРОВАННОГО СОСТОЯНИЯ ТРЕХСЛОЙНОЙ ЖЕЛЕЗОБЕТОННОЙ КОНСТРУКЦИИ МЕТОДАМИ КОНЕЧНЫХ ЭЛЕМЕНТОВ

Ву Динь Тхо [1], Е.А. Король [2], В.И. Римшин [2], Фам Туань Ань [1]

[1] Университет транспортных технологий (UTT), факультет гражданского строительства и промышленного строительства, г. Ханой, ВЬЕТНАМ

[2] Национальный исследовательский Московский государственный строительный университет, г. Москва, РОССИЯ

Аннотация: Объектом исследования являются многослойные железобетонные конструкции из бетона с различными физико-механическими характеристиками материалов - бетона и арматуры под воздействием нагрузки. Анализ напряженного состояния многослойных железобетонных балок с использованием различных материалов представляет собой сложную проблему из-за различных механических и физических характеристик материалов и растрескивания бетона. В данной статье представлен анализ напряженно-деформированного состояния трехслойных армированных строительных конструкций с использованием метода конечных элементов в программе ANSYS Mechanical. Численное моделирование позволяет на ANSYS комбинировать различные комбинации нагрузок, изменчивость прочностных и деформационных характеристик материалов и различных типов арматуры в многослойных железобетонных балках. Проводится сравнение между экспериментальными результатами, численными результатами и анализом методом конечных

элементов в отношении начального образования трещин и предельной несущей способности балок. Результаты исследования показали, что по мере увеличения марки бетона во внешнем слое с B15 до B20 и сорт легкого бетона во внутреннем слое увеличивается с B0,75 до B1,5, трещиностойкость может быть увеличена на 59,7%, а несущая способность теста луч увеличен на 16,4%. При толщине наружных слоев от 40 мм до 80 мм трещиностойкость увеличивается на 47,5%, а несущая способность трехслойных бетонных балок значительно увеличивается на 6,7%. Полученные научные результаты позволяют определить рациональные параметры для моделирования различных конструктивных решений многослойных железобетонных конструкций.

Ключевые слова: бетонные здания; железобетон; многослойные конструкции; трехслойные конструкции; контактная прослойка; теплоизоляционные материалы; анализ напряжений; ANSYS Mechanical.

INSTRUCTION

Today, the development of technologies new materials from concrete has helped create many kinds of enclosing structures for civil and industrial buildings. Enclosing structures not only meet the requirements for bearing capacity but also meet other requirements such as thermal insulation, sound insulation, fire resistance, corrosion resistance, ... One of the effective solutions to solving this problem is the use of multilayer reinforced concrete structures with a middle layer of low thermal conductivity concrete, that consists of: the external layers made mainly of structural concrete to provide the load-bearing of elements such as: heavy concrete [1, 2], fine-grained concrete [3] or clay concrete [4, 5]; The internal layer of heat insulation and sound insulation is used by light concrete of low strength, such as foam concrete [6, 7], coarse-pored concrete [8], polystyrene concrete [1, 9], etc.

In this type of construction, made of non-uniform materials, under loadings, stress and strain distribution is a rather complex process, so the ratio between the modulus of elasticity of the middle and outer layers haves a strong influence on the stress and strain distribution. Various methods are used to calculate multilayer reinforced concrete structures. For calculating strength and deformation, the authors [10, 11] proposed to bring a three-layer reinforced concrete cross-section with a monolithic bond to an I-beam, based on the ratios of the initial elastic modulus of concrete of the layers using the hypothesis of flat sections. In the literature [12-14] a method for calculating a multilayer structure using a contact layer based on the Kirchhoff-Love hypothesis was used.

It was found that the stress–strain state of multilayer reinforced concrete structures was influenced by many factors. The influence of the physical and mechanical properties of concrete and the geometrical parameters of the layers was analyzed in references [15– 16]. The influence of geometric and physical nonlinearity, plastic and geological properties of concrete on the stress–strain state of multi-layer structures was studied in references [17, 18].

At present, the development of science and technology has allowed to perform a wide variety of researches using the finite element method and pro-vide results close to full-scale experiments. Meth-ods of debonding evaluation in FRP strengthened concrete beams based on finite element model (FEM)-modeling proposed in References [19–20]. In this study, the authors propose a solution to analyze the stress-strain state of three-layer reinforced concrete by using a finite element model (FEM) with the help of the program ANSYS.

1. MATERIALS AND METHODS

1.1 Model of tested samples and material properties

This article considers three-layered beams with a width of 160 mm, a height of 250 mm and a length of 3000 mm. For external layers, concrete of class B15, B20 and B25 (Table 1) is commonly

used, with a thickness from 40mm to 80mm. For the middle layer, lightweight concrete with low thermal conductivity is used, with polystyrene concrete class B0.75, B1 and B1.5, and with the thickness from 170mm to 90mm.

In the tested beam, armature is obtained with 2 rebars with a diameter of 8 mm (A-500), σ_y = 475.2 MPa, σ_u = 660.5 MPa, modulus of elasticity of the armature E_s = 206,000 MPa.

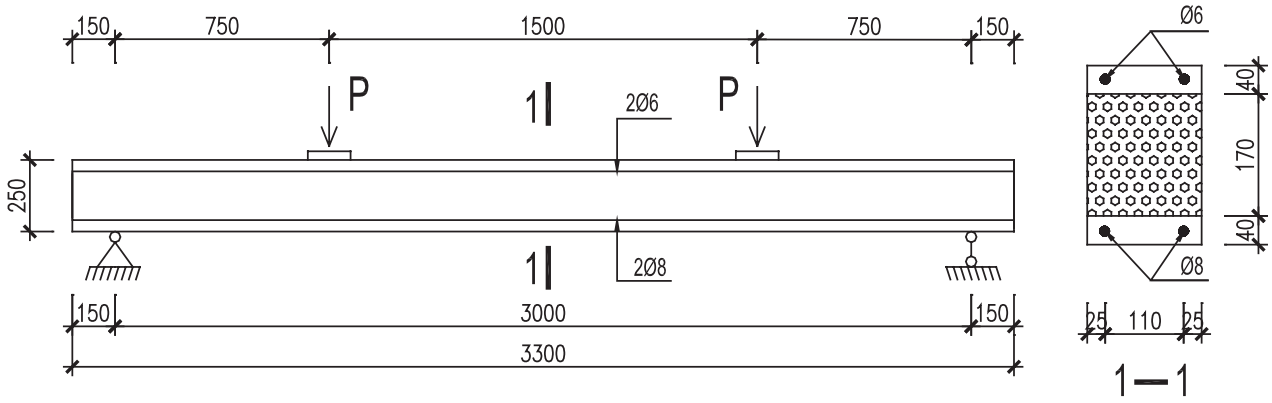

Figure 1. Three-layer concrete beam model of test

Table 1. Parameters and characteristics of concrete in tested beams

	External layer			Internal layer		
	B15	B20	B25	B0,75	B1	B1,5
R_b, (MPa)	11	15	18.5	0.84	1.1	1.61
R_{bt}, (MPa)	1.15	1.4	1.6	0.44	0.51	0.61
E_b, (MPa)	23000	27000	30000	650	850	1100
v	0.2	0.2	0.2	0.2	0.2	0.2

1.2 Finite element modeling for three-layers reinforced concrete beam on ANSYS

The research methods are based on numerical simulation of stresses and strains of multilayer reinforced concrete elements under the action of various load combinations. The use of modern software systems enables to carry out numerous variable studies, combining a different combination of loads and variability
of strength and deformation characteristics of materials – structural concrete, low-strength concrete for the middle layer, as well as to compare the results obtained from PC ANSYS with the theoretical results of the calculation. One of the most modern, universal software complexes ANSYS, based on finite element method was used in the article as well as volumetric eight-node finite elements of type SOLID65 and rod elements LINK180 [21].

The element Solid65 is used to model the concrete. This element has eight nodes with three degrees of freedom at each node –translations in the nodal x, y and z directions. This element is capable of plastic deformation, cracking in three orthogonal directions, and crushing. A schematic of the element is shown in Figure. 2 (a). The element Link8 is used to model steel reinforcement. This element is a 3D spar element and it has two nodes with three degrees of freedom – translations in the nodal x, y, and z directions. This element is also capable of plastic deformation. This element is shown in Figure. 2 (b).

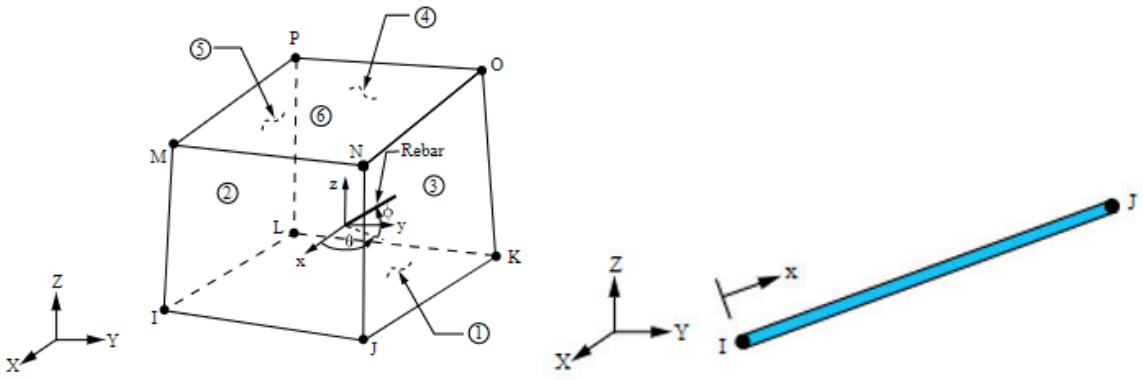

(a) *(b)*

Figure 2. (a) Solid65 Element and (b)Link8 element

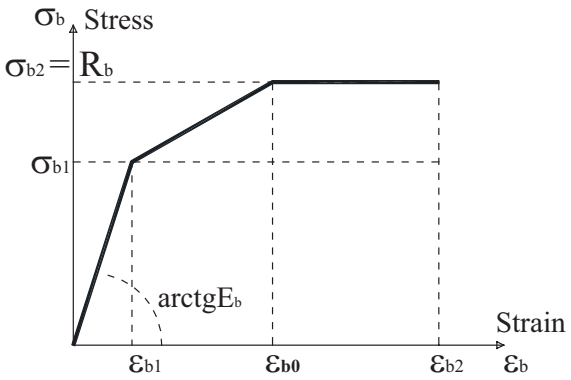

Figure 3. Stress-strain relationship for concrete

Where: σ_b - compressive stresses of concrete;
R_b - prismatic strength of concrete;
ε_b - the deformation of concrete;
ε_{b1}; ε_{b0}; ε_{b2} - the deformation of concrete corresponding to the stress $\sigma_{b1}= 0.6*R_b$; $\sigma_{b0}= R_b = \sigma_{b2}$

Figure. 3 shows the stress- strain relation of concrete [22]. Following equations are used to compute the multilinear isotropic stress-strain curve for the concrete (Figure. 3):

When $0 \leq \varepsilon \leq \varepsilon_{b1}$, with $\sigma_b = E_b.\varepsilon_b$ (1)

When $\varepsilon_{b1} \leq \varepsilon \leq \varepsilon_{b0}$, with

$$\sigma_b = \left[\left(1 - \frac{\sigma_{b1}}{R_b}\right)\frac{\varepsilon_b - \varepsilon_{b1}}{\varepsilon_{b0} - \varepsilon_{b1}} + \frac{\sigma_{b1}}{R_b}\right]R_b \quad (2)$$

When $\varepsilon_{b0} \leq \varepsilon \leq \varepsilon_{b2}$, with $\sigma_b = R_b$

The values of the stress σ_{b1} are determined by the following formula: $\sigma_{b1} = 0.6R_b$

$$\text{with } \varepsilon_{b1} = \frac{\sigma_{b1}}{E_b} \quad (3)$$

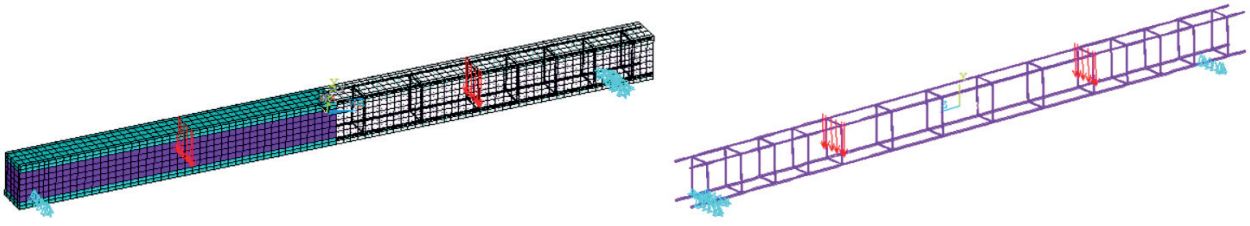

(a) *(b)*

Figure 4. Three-layers concrete beam model in ANSYS. a) Model of three-layer concrete beam b) Modeling of steel bars in concrete beams

2. RESULTS AND DISCUSSION

2.1 The results and analysis the stress-strain state of three- layered reinforced concrete structures of experiment and on ANSYS

The analysis and comparison of stress and deformation of the three-layer beam under the effect of load between finite element method with using software complexes ANSYS, numerical method and experiment is done on three-layer beams in Figure. 1. The parameters and properties of materials are shown in Table. 2.

The analysis results of moment (M) and deflection (f) of three-layer beam on ANSYS are shown in Figure 5 and Table 3.

Beam start to crack and to be damaged, are shown in Figure. 6 and Figure. 7.

Table 2. Parameters and characteristics of concrete in tested beams

The layers of beam	External layer	Internal layer
The thickness of the layers h, cm	0.04	0.17
Prismatic strength of concrete R_b, (MPa)	21.5	1.54
Tensile strength of concrete R_{bt}, (MPa)	1.8	0.36
The initial modulus of elasticity E_b, (MPa)	12100	1310
Coefficient Poisson v = 0.00189 $\|R_b\|$+ 0.12	0.16	0.122
Shear modulus G = $E_0/(2(1 + \nu))$, MPa	5216	346
The average density of concrete, kg/m^3	1800	440

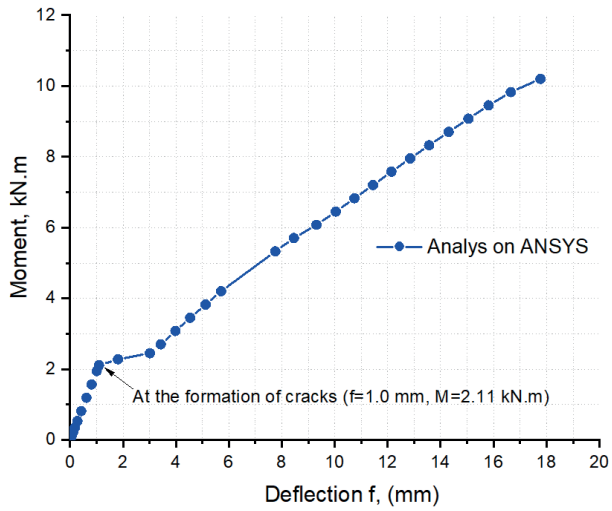

Figure 5. Load-Displacement curve for tested beam

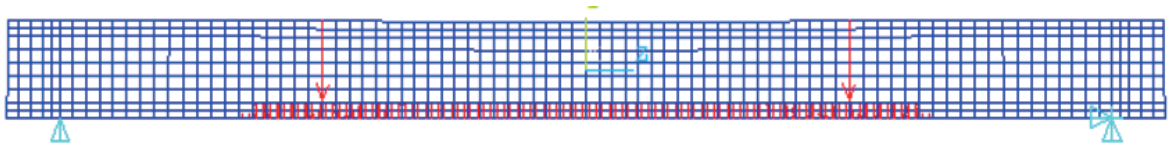

Figure 6. Beam start to crack, at moment M_{crc} = 2.11 kN.m

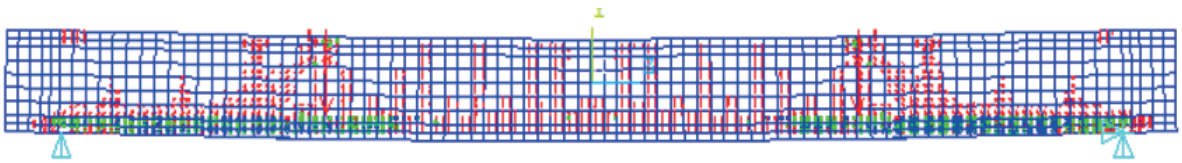

Figure 7. Beam is damaged, at moment M_{ult} = 10.20 kN.m

Table 3. Comparation of the results of analysis

Model	At the formation of cracks		At failure of beam	
	Moment M_{crc} (kN.m)	Deflection f, (mm)	Moment M_{ult} (kN.m)	Deflection f, (mm)
On ANSYS	2.11	1.10	10.20	17.7
Experimental study [1]	2.23	1.12	9.6	8.30
Numerical study based on the monolith converter of cross-section [1]	2.09	1.20	11.1	17.96

The analysis results in Table. 3 are shown that moment (M) and deflection (f) of the three-layer beam at the crack's formation and at the beam's failure on ANSYS near experimental results than results by using numerical models. The difference of the results of the beam bearing capacity analysis between the ANSYS model and experiment is 1% at the crack's formation and 5.8% at the beam's failure. This difference between the numerical and experimental models respectively is 6.3% và 13.5%.

The analysis results of stress and deformation of three-layer beams on ANSYS are close to the experimental results, it allows to use this method in the research and evaluation of bearing capacity of the three-layer beam under the effect of load.

2.2 Effect of concrete grade changes in external and internal layers on the bearing capacity of three-layer concrete beams

The three-layer reinforced concrete beams in Figure. 1 are used to analyze the effect of concrete grade changes in external and internal layers on the bearing capacity of three-layer concrete beams. The heavy concrete class B15, B20 and B25 are used in external layers thickness 40mm. The lightweight concrete class B0.75, B1 and B1.5 are used in internal layers thickness 170mm.

Table 4 presents the cases of investigating changes in concrete grades in the external and internal layers:

Table 4. Concrete grade in cases investigated

Case	Layer 1: NC layer	Layer 2: LW layer	Layer 3: NC layer
1	B15	B0.75	B15
2	B15	B1	B15
3	B15	B1.5	B15
4	B20	B0.75	B20
5	B20	B1	B20
6	B20	B1.5	B20
7	B25	B0.75	B25
8	B25	B1	B25
9	B25	B1.5	B25

Where: The normal concrete layer below is layer 1; the lightweight concrete layer in the middle is layer 2; the normal concrete layer above is layer 3.

For three-layer concrete beams, the vertical displacement spectrum and moment at the formation of cracks and at the failure of the beam are shown in Table. 5, Figure. 8 and Figure. 9.

Table 5. Comparation of the results of analysis

Model	At the formation of cracks		At failure of beam	
	Moment M_{crc} (kN.m)	Deflection f, (mm)	Moment M_{crc} (kN.m)	Deflection f, (mm)
Case-1	1.16	0.43	9.07	22.06
Case-2	1.18	0.41	9.82	19.96
Case-3	1.19	0.39	10.19	17.36
Case-4	1.52	0.57	9.44	23.07
Case-5	1.54	0.54	10.19	18.85
Case-6	1.57	0.51	10.37	16.26
Case-7	1.74	0.52	9.65	23.24
Case-8	1.81	0.51	10.48	18.67
Case-9	1.90	0.51	10.55	17.13

For three-layer reinforced concrete beams, as the grade of concrete in the external layer increases from B15 to B20, the bearing capacity of the test beam is increased. The moment at the crack's formation increased from 1.16 kN.m to 1.74 kN.m (increase by 50%), on the beams using lightweight concrete B0.75 in the internal layer; and increased from 1.19 kN.m to 1.9 kN.m (increase by 59.7%), on beams using lightweight concrete B1.5 in the internal layer (in Figure.8). The moment at the beam's failure can be increased from 9.07 kN.m to 10.55 kN.m (increase by 16.4%), is shown in Table.5 and Figure. 9.

When the concrete grade in the external layers is the same, the grade of lightweight concrete in the internal layer increases from B0.75 to B1.5, the moment at the beam's failure can be increased from 9.07 kN.m to 10.19 kN.m (increase by 12.4%) (in Figure.9).

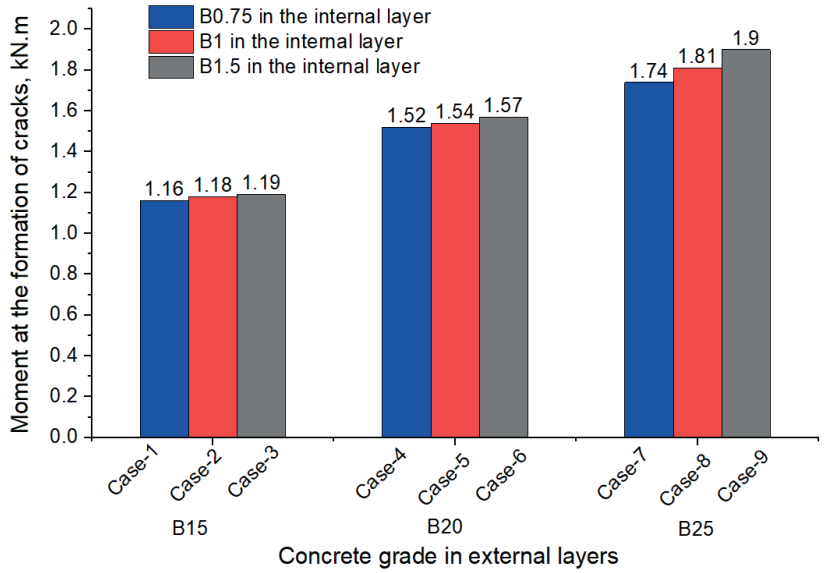

Figure 8. Chart of the relationship between crack's moment and concrete grade in external layers

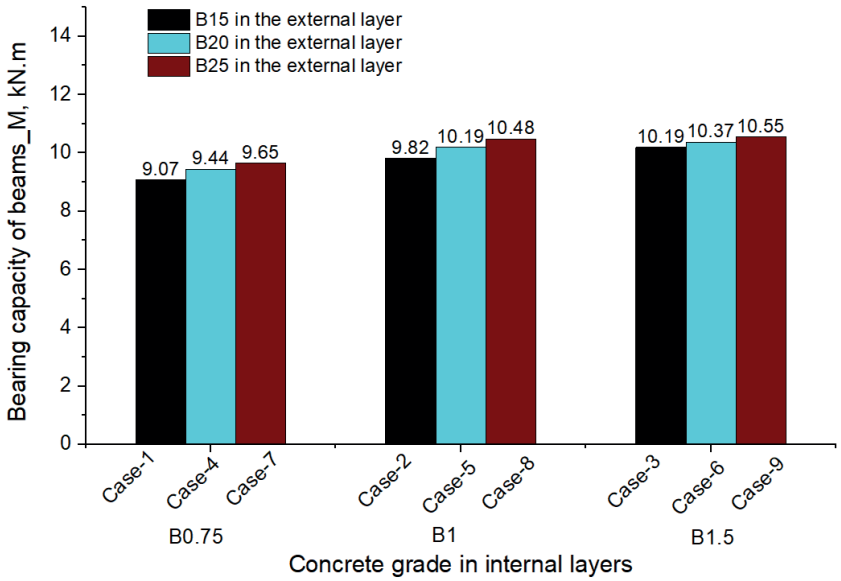

Figure 9. Chart of the relationship between bearing capacity of beams and concrete grade in internal layers

2.3 Effect of thickness of the external and internal layers on the bearing capacity of three-layer concrete beams.

In this case, three-layered beams with width 160mm, height 250mm and length 3000 mm, shown in Figure1, are studied. The external layers of tested beams made by heavy concrete (normal concrete) grade B15, with changes of thickness from 40mm to 80mm and the internal layers of tested beams made by lightweight concrete grade B1, with changes of thickness from 170mm to 90mm.

Table 6 presents the cases of investigating changes of thickness of the external and internal layers on bearing capacity of three-layer reinforced concrete beams.

The results of the analysis the stress and deformation state on the beams are shown in Table. 7 and Figure.10.

Table 6. Thickness of layers in cases investigated

Case	Layer 1: NC layer	Layer 2: LW layer	Layer 3: NC layer
10	40 mm	170 mm	40 mm
11	60 mm	130 mm	60 mm
12	80 mm	90 mm	80 mm

Where: The normal concrete (B15) layer below is layer 1; the lightweight concrete (B1) layer in the middle is layer 2; the normal concrete (B15) layer above is layer 3.

Table 7. Comparation of the results of analysis

Model	At the formation of cracks		At failure of beam	
	Moment M_{crc} (kN.m)	Deflection f, (mm)	Moment M_{crc} (kN.m)	Deflection f, (mm)
Case-10	1.18	0.41	9.82	19.96
Case-11	1.57	0.44	10.19	20.26
Case-12	1.74	0.46	10.46	19.15

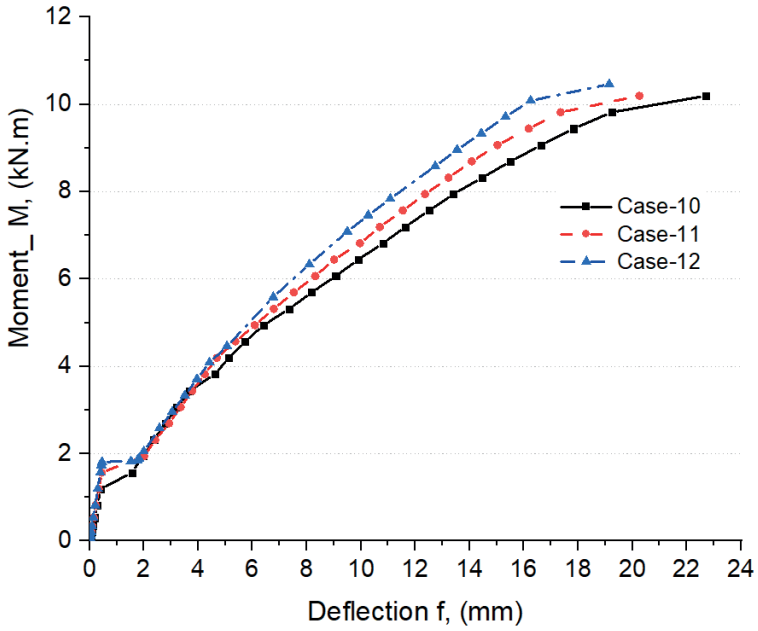

Figure 10. Load-displacement curve for tested beams

In the beam samples case-10; 11 and case-12, the material used by the external and internal layers of the three-layered beams remains constants, when thickness of the external layers varies from 40mm to 80mm, making the crack resistance and the bearing capacity of three-layer concrete beams greatly changed. The moment at the crack's formation increased from 1.18 kN.m to 1.74 kN.m (increase by 47.5%), the bearing capacity of tested beams increased from 9.82 kN.m to 10.46 kN.m (increase by 6.7%).

3. CONCLUSION

The obtained experimental and theoretical results lead to the following conclusions:
(1) The final analysis shows similar results obtained by numerical methods using the ANSYS PC, compared to experimental studies and theoretical calculations. The results of analysis of moments and deflections of multilayer reinforced concrete beams of ANSYS are usually lower compared to the result of moments and deflections when calculated according to the theory scheme (from 1 to 5.8%).
(2) The analysis of concrete grade changes in the layers shows that as the grade of concrete in the external layer increases from B15 to B20, the crack resistance can be increased in 59.7% and the bearing capacity of the test beam is increased in 16.4%. When the concrete grade in the external layers is the same, the grade of lightweight concrete in the internal layer increases from B0.75 to B1.5, the moment at the beam's failure can be increased in 12.4%.
(3) The analysis of changes thickness of the external and internal layers shows that when the thickness of the external layer varies from 40mm to 80mm, making the crack resistance increased in 47.5% and the bearing capacity of three-layer concrete beams greatly increased 6.7%.

REFERENCES

1. **Korol E.A.** Trekhsloynyye ograzhdayushchiye zhelezobetonnyye konstruktsii iz legkogo betona i osobennosti ikh rascheta [Three-layer fencing reinforced concrete structures made of lightweight concrete and features of their calculation]. Moscow, ASV, 2001, 395 pages (in Russian).
2. **Tho V.D., Korol E.A.** Vliyaniye kontaktnykh sloyev na treshchinostoykost' izgibayemykh trekhsloynykh konstruktsii [Influence of contact layers on the crack resistance of bent three-layer structures] // *Vestnik MGSU*, 2020, Vol. 15, pp. 988–998 (in Russian).
3. **Lam T.V., Vu D.T., Dien V.K., Bulgakov B.I., Korol E.A.** Properties and thermal insulation performance of lightweight concrete. // Magazine of Civil Engineering, 2018, Vol. 84, Issue 8, pp. 173–191.
4. **Korol E.A., Marina Berlinova.** Calculation of multilayer enclosing structures with middle layer of polystyrene concrete. // MATEC Web Conf, 2018, Volum 193, 7 pages.
5. **Korol E.A., Kharkin Y.A**. To the question of choosing a software package for modeling the stress-strain state of three-layer reinforced concrete elements and structures with a monolithic bond of layers. // Scientific and technical journal on construction and architecture (The Bulletin), 2010, Vol. 3, pp.156-163.
6. **Korol E.A, Vu Dinh Tho., Kustikova Y**. Model of stressed-strained state of multilayered reinforced concrete structure with the use of composite reinforcement. // IOP Conference Series: Materials Science and Engineering, 2017, Vol. 365, Issue 5, 11 pages.
7. **Fernando P.L.N., Jayasinghe M.T.R., Jayasinghe C**. Structural feasibility of Expanded Polystyrene (EPS) based lightweight concrete sandwich wall panels. // Construction and Building Materials, 2017, Volume 139, pp. 45–51.
8. **Diamond S.** Aspects of concrete porosity revisited. // Cement and Concrete Research, 1999, Vol. 29, Issue 8, pp. 1181-1188.
9. **Tho V.D., Korol E.A.** Influence of geometrical parameters of the cross section, strength and deformability of the materials used on stress strain state of three-layered reinforced concrete. // IOP Conference Series: Materials Science and Engineering, 2019, Vol. 661, 10 pages.
10. **Shendy M.E**. A comparative study of LECA concrete sandwich beams with and without core reinforcement. // Cement and

Concrete, Compos, 1991, Vol. 13, pp. 143–149.
11. **Korol E.A**. The choice of the rational parameters of three-layer reinforced concrete enclosing structures with the monolithic bond of layers by computer simulation. // IOP Conference Series: Materials Science and Engineering, 2018, Vol. 456, 7 pages.
12. **Shams A., Horstmann M., Hegger J**. Experimental investigations on Textile-Reinforced Concrete (TRC) sandwich sections. // Composite Structures, 2014, Vol. 118, Pages 643-653.
13. **Andreev V.I., Turusov R.A., Tsybin N.Y**. Application of the Contact Layer in the Solution of the Problem of Bending the Multilayer Beam. // Procedia Engineering, 2016, Vol. 153, pp. 59–65.
14. **Gara F., Ragni L., Roia D., Dezi L**. Experimental behaviour and numerical analysis of floor sandwich panels. // Eng. Struct, 2012, Vol. 36, pp. 258–269.
15. **Gara F., Ragni L., Roia D., Dezi** L. Experimental tests and numerical modelling of wall sandwich panels. // Eng. Struct, 2012, Vol. 37, pp. 193–204.
16. **Tho V.D., Korol E.A**. Influence of geometrical parameters of the cross section, strength and deformability of the materials used on stressstrain state of three-layered reinforced concrete. // IOP Conference Series: Materials Science and Engineering, 2019, Vol. 661, pages 10.
17. **Yue Z., Xiao H**. Generalized Kelvin Solution based boundary element method for crack problems in multilayered solids. // Engineering Analysis with Boundary Elements, 2002, Vol. 26, pp. 691–705.
18. **Marčiukaitis G., Juknevičius L**. Influence of the Internal Layer Cracks on the Cracking of Flexural Three-Layer Concrete Members. // Journal of Civil Engineering and Management, 2002, Vol. 8, pp. 153–158.
19. **Funari M.F., Spade, S., Fabbrocino F., Luciano R. A**. Moving Interface Finite Element Formulation to Predict Dynamic Edge Debonding in FRP-Strengthened Concrete Beams in Service Conditions. // Fibers, 2020, Vol. 8, pages 42.
20. **Funari M.F., Greco F., Lonetti P**. 2016. A cohesive finite element model based ALE formulation for z-pins reinforced multilayered composite beams. // Procedia Struct. Integr, 2016, Vol. 2, pp. 452–459.
21. **S. Moaveni**. Finite element analysis: Theory and application with ANSYS, 2015, (in London).
22. SP 63.13330.2012. 2012.Concrete and reinforced concrete structures.

СПИСОК ЛИТЕРАТУРЫ

1. **Король Е.А.** Трехслойные ограждающие железобетонные конструкции из легкого бетона и особенности их расчета. – М.; АСВ 2001. – 255 с.
2. **Tho V.D., Kopol E.A.** Влияние контактных слоев на трещиностойкость изгибаемых трехслойных конструкции. // *Вестник МГСУ*, 2020, Том 15, с. 988–998.
3. **Lam T.V., Vu D.T., Dien V.K., Bulgakov B.I., Korol E.A.** Properties and thermal insulation performance of lightweight concrete. // Magazine of Civil Engineering, 2018, Volume 84, Issue 8, pp. 173–191.
4. **Korol E.A., Marina Berlinova.** Calculation of multilayer enclosing structures with middle layer of polystyrene concrete. // MATEC Web Conf, 2018, Volum 193, pages 7.
5. **Korol E.A., Kharkin Y.A**. To the question of choosing a software package for modeling the stress-strain state of three-layer reinforced concrete elements and structures with a monolithic bond of layers. // Scientific and technical journal on construction and architecture (The Bulletin), 2010, Volume 3, pp.156-163
6. **Король Е. А., Vu Dinh Tho., Kustikova Y**. Model of stressed-strained state of multilayered reinforced concrete structure with the use of composite reinforcement. // IOP Conference Series: Materials Science and

Engineering, 2017, Volume 365, Issue 5, pages 11.
7. **Fernando P.L.N., Jayasinghe M.T.R., Jayasinghe C**. Structural feasibility of Expanded Polystyrene (EPS) based lightweight concrete sandwich wall panels. // Construction and Building Materials, 2017, Volume 139, pp. 45–51.
8. **Diamond S.** Aspects of concrete porosity revisited. // Cement and Concrete Research, 1999, Volume 29, Issue 8, Pages 1181-1188.
9. **Tho V.D., Korol E.A.** Influence of geometrical parameters of the cross section, strength and deformability of the materials used on stressstrain state of three-layered reinforced concrete. // IOP Conference Series: Materials Science and Engineering, 2019, Volume 661, 10 pages.
10. **Shendy M.E**. A comparative study of LECA concrete sandwich beams with and without core reinforcement. // Cement and Concrete, Compos, 1991, Volume 13, pp. 143–149.
11. **Korol E.A**. The choice of the rational parameters of three-layer reinforced concrete enclosing structures with the monolithic bond of layers by computer simulation. // IOP Conference Series: Materials Science and Engineering, 2018, Volume 456, 7 pages.
12. **Shams A., Horstmann M., Hegger J**. Experimental investigations on Textile-Reinforced Concrete (TRC) sandwich sections. // Composite Structures, 2014, Volume 118, Pages 643-653.
13. **Andreev V.I., Turusov R.A., Tsybin N.Y**. Application of the Contact Layer in the Solution of the Problem of Bending the Multilayer Beam. // Procedia Engineering, 2016, Volume 153, pp. 59–65.
14. **Gara F., Ragni L., Roia D., Dezi L**. Experimental behaviour and numerical analysis of floor sandwich panels. // Eng. Struct, 2012, Volume 36, pp. 258–269.
15. **Gara F., Ragni L., Roia D., Dezi** L. Experimental tests and numerical modelling of wall sandwich panels. // Eng. Struct, 2012, Volume 37, pp. 193–204.
16. **Tho V.D., Korol E.A**. Influence of geometrical parameters of the cross section, strength and deformability of the materials used on stressstrain state of three-layered reinforced concrete. // IOP Conference Series: Materials Science and Engineering, 2019, Volume 661, pages 10.
17. **Yue Z., Xiao H**. Generalized Kelvin Solution based boundary element method for crack problems in multilayered solids. // Engineering Analysis with Boundary Elements, 2002, Volume 26, pp. 691–705.
18. **Marčiukaitis G., Juknevičius L**. Influence of the Internal Layer Cracks on the Cracking of Flexural Three-Layer Concrete Members. // Journal of Civil Engineering and Management, 2002, Volume 8, pp. 153–158.
19. **Funari M.F., Spade, S., Fabbrocino F., Luciano R. A**. Moving Interface Finite Element Formulation to Predict Dynamic Edge Debonding in FRP-Strengthened Concrete Beams in Service Conditions. // Fibers, 2020, Volum 8, 42 pages.
20. **Funari M.F., Greco F., Lonetti P**. 2016. A cohesive finite element model based ALE formulation for z-pins reinforced multilayered composite beams. // Procedia Struct. Integr, 2016, Volume 2, pp. 452–459.
21. **S. Moaveni**. Finite element analysis: Theory and application with ANSYS, 2015, (in London).
22. SP 63.13330.2012. 2012.Concrete and reinforced concrete structures.

Vu Dinh Tho. Candidate of Technical Sciences, Teacher of the Department of Construction of civil engineering and industrial engineering « University of transport technology (UTT)» (Vietnam), 100000, 54-Trieu Khuc, Thanh Xuan, Ha Noi, Vietnam.

Ву Динь Тхо. Канд. техн. наук, преподаватель кафедры "Промышленное и гражданское строительство", Университет транспортных технологий; 100000, 54- Чиеу Хук, Тхань Суан, Ха Ной, Вьетнам; e-mail: thovd@utt.edu.vn; (+84)986961858; 0000-0001-7374-9424.

Elena A. Korol. Doctor of Technical Sciences, Professor, Professor of the Department "Housing and Communal Complex", National Research Moscow State University of Civil Engineering" (NIU MGSU); 129337, 26, Yaroslavskoye Shosse, Moscow, Russia; e-mail: KorolEA@mgsu.ru; 0000-0002-5019-3694.

Vladimir I. Rimshin. Doctor of Technical Sciences, Professor, Professor of the Department "Housing and Communal Complex", National Research Moscow State University of Civil Engineering" (NIU MGSU); 129337, 26, Yaroslavskoye Shosse, Moscow, Russia; e-mail: RimshinVI@mgsu.ru.

Pham Tuan Anh. Candidate of Technical Sciences, Teacher of the Department of Construction of civil engineering and industrial engineering « University of transport technology (UTT)» (Vietnam), 100000, 54-Trieu Khuc, Thanh Xuan, Ha Noi, Vietnam.

Король Елена Анатольевна. Доктор технических наук, профессор, профессор кафедры «Жилищно-коммунальный комплекс», Федеральное государственное бюджетное образовательное учреждение высшего образования «Национальный исследовательский Московский государственный строительный университет» (ФГБОУ ВО «НИУ МГСУ»); 129337, г. Москва, Ярославское шоссе, д. 26; e-mail: KorolEA@mgsu.ru.; 0000-0002-5019-3694.

Римшин Владимир Иванович. Доктор технических наук, профессор, профессор кафедры «Жилищно-коммунальный комплекс», Федеральное государственное бюджетное образовательное учреждение высшего образования «Национальный исследовательский Московский государственный строительный университет» (ФГБОУ ВО «НИУ МГСУ»); 129337, г. Москва, Ярославское шоссе, д. 26; e-mail: RimshinVI@mgsu.ru.

Фам Туань Ань. Канд. техн. наук, преподаватель кафедры "Промышленное и гражданское строительство", Университет транспортных технологий; 100000, 54- Чиеу Хук, Тхань Суан, Ха Ной, Вьетнам; e-mail: anhpt@utt.edu.vn; 0000-0001-9484-1916.

International Journal for Computational Civil and Structural Engineering, 18(2) 74–84 (2022)

DOI:10.22337/2587-9618-2022-18-2-74-84

THE MODEL OF FREE SPREADING A FLOW RAPID BEHIND A RECTANGULAR PIPE

Olga A. Burtseva [1], Viktor N. Kohanenko [1], Sergey I. Evtushenko [2], Maria S. Alexandrova [1]

[1] Platov South Russian State Polytechnic University (NPI), Novocherkassk, RUSSIA
[2] National Research University Moscow State University of Civil Engineering, Moscow, RUSSIA

Abstract. The article considers the free spreading of a turbulent stationary two-dimensional open potential water flow into a wide diverting riverbed behind a non-pressure pipe of a rectangular section. A system of nonlinear partial differential equations of motion has been adopted as the mathematical model of the flow in the physical plane. When moving to the plane of the velocity hodograph, the nonlinear system of equations is transformed into a linear system with respect to partial derivatives. Using the obtained system of equations, various problems along the flow of two-dimensional water streams have been solved analytically. The paper determines the flow kinetics parameter τ and the angle θ characterizing the direction of the local flow velocity vector at the intersection points of an arbitrary equipotential and an arbitrary current line. The *X*, *Y* coordinates of these points are found. The peculiarities of changing the angle θ during the transition of the vertical front of the X_D are taken into account. Article proposes a module for the transition from a two-dimensional water flow model to a one-dimensional one. This module is necessary for using the laws of flow resistance and taking into account the resistance forces. The model proposed in this paper is a development of analytical methods for calculating potential flows with previously unknown boundaries and before the flow expands. It allows determining the entire range of geometric and kinematic parameters of the flow with an error not exceeding 10%. The adequacy of the model for all flow parameters improves the accuracy of previously existing methods. This allows the designers of road culverts to increase its reliability.

Keywords: mathematical model, two-dimensional flow, motion equations, resistance forces, flow energy equations, line flow, hydrodynamic pressure, flow spread parameters, free spreading of the flow into the diverting riverbed.

МОДЕЛЬ СВОБОДНОГО РАСТЕКАНИЯ БУРНОГО ПОТОКА ЗА ПРЯМОУГОЛЬНОЙ ТРУБОЙ

О.А. Бурцева [1], В.Н. Коханенко [1], С.И. Евтушенко [2], М.С. Александрова [1]

[1] Южно-Российский государственный политехнический университет (НПИ) имени М.И. Платова, г. Новочеркасск, РОССИЯ
[2] Национальный исследовательский Московский государственный строительный университет, г. Москва, РОССИЯ

Аннотация. Рассматривается свободное растекание бурного, стационарного, двухмерного в плане, открытого, потенциального, водного потока в широкое отводящее русло за безнапорной трубой прямоугольного сечения. Математическая модель потока в физической плоскости описывается в виде системы нелинейных дифференциальных уравнений движения в частных производных. При переходе в плоскость годографа скорости нелинейная система уравнений трансформируется в линейную систему относительно частных производных. Пользуясь полученной системой уравнений аналитически решены различные задачи по течению двухмерных водных потоков. Определены параметр кинетичности τ потока и угол θ, характеризующий направление вектора местной скорости потока в точках пересечения произвольной эквипотенциали и произвольной линии тока. Найдены координаты X, Y этих точек. Учтены особенности изменения угла θ при переходе вертикального фронта $X_Д$. Предложен модуль перехода от двумерной в плане модели течения водного потока к одномерной. Этот модуль необходим для использования законов сопротивления потоку и учету сил сопротивления. Модель, предложенная в работе представляет собой развитие аналитических методов расчёта потенциальных потоков с заранее неизвестными границами и до расширения потока $\beta = 7 \div 10$. Позволяет с погрешностью не превышающую 10% определять весь спектр геометрических и

кинематических параметров потока. Адекватность модели по всем параметрам потока до расширения β = 7÷10 улучшает адекватность по ранее существующим методам, что позволяет проектировщикам ГТС дорожных водопропускных сооружений повышать их надёжность.

Ключевые слова: математическая модель, двухмерный в плане водный поток, уравнения движения, силы сопротивления, уравнения энергии потока, линия тока, гидродинамический напор, параметры растекания потока, свободное растекание потока в отводящее русло.

INTRODUCTION

This work is devoted to the development of I.A. Sherenkov's ideas [1] for solving a practical problem concerning the turbulent flow behind the voluntary flow into a wide discharge channel. The flow parameters behind the non-pressure pipe are necessary for the road water conduit structures' design under roads and railways [2]. On the basis of the characteristic theory, I.A. Sherenkov carried out the solution to the problem [3, 4] and supplemented it with the analytical studies.

I.A. Sherenkov developed a theory for calculating the flow parameters, based on which he proposed a universal schedule as it was shown in the work [5]. Previously, this theory provided a powerful impetus for the culverts' calculation development. However, it turned out to be very approximate due to the graphical methods of the characteristic theory use, borrowed from the gas dynamics [6]. Thereby, t**he purpose of this work** is development of the same problem solution based on the analytical methods.

1. RESEARCH METHODS

1.1. Equations of water flow motion in the physical plane of its streaming.

The motion basic equations of a two-dimensional plan water flow have the form [7, 8]:

$$\begin{cases} X - \dfrac{1}{\rho}\dfrac{\partial p}{\partial x} - T_x = \dfrac{du_x}{dt}; \\ Y - \dfrac{1}{\rho}\dfrac{\partial p}{\partial y} - T_y = \dfrac{du_y}{dt}; \\ Z - \dfrac{1}{\rho}\dfrac{\partial p}{\partial z} - T_z = \dfrac{du_z}{dt}, \end{cases} \qquad (1)$$

where X, Y, Z are the volumetric force components; T_x, T_y, T_z are the components of resistance forces per liquid mass unit; ρ denotes liquid density; p is the local pressure.

For the steady-state water flow with vertical axis direction z and the action of a single volume force (gravity) in liquid, the system (1) takes the following form [9, 10]:

$$\begin{cases} -\dfrac{1}{\rho}\dfrac{\partial p}{\partial x} - T_x = u_x\dfrac{\partial u_x}{\partial x} + u_y\dfrac{\partial u_x}{\partial y} + u_z\dfrac{\partial u_x}{\partial z}; \\ -\dfrac{1}{\rho}\dfrac{\partial p}{\partial y} - T_y = u_x\dfrac{\partial u_y}{\partial x} + u_y\dfrac{\partial u_y}{\partial y} + u_z\dfrac{\partial u_y}{\partial z}; \\ -\dfrac{1}{\rho}\dfrac{\partial p}{\partial z} - T_z = u_x\dfrac{\partial u_z}{\partial x} + u_y\dfrac{\partial u_z}{\partial y} + u_z\dfrac{\partial u_z}{\partial z}. \end{cases} \qquad (2)$$

Without considering the resistance forces to the flow

$$T_x = T_y = T_z = 0$$

and taking into account:

$$u_z = 0;$$

$$\frac{\partial u_z}{\partial x} = \frac{\partial u_z}{\partial y} = \frac{\partial u_z}{\partial z} = 0; \quad \frac{\partial u_x}{\partial z} = \frac{\partial u_y}{\partial z} = 0$$

the system (2) transforms to the following one:

$$\begin{cases} -\dfrac{1}{\rho}\dfrac{\partial p}{\partial x} - T_x = u_x\dfrac{\partial u_x}{\partial x} + u_y\dfrac{\partial u_x}{\partial y} + u_z\dfrac{\partial u_x}{\partial z}; \\ -\dfrac{1}{\rho}\dfrac{\partial p}{\partial y} - T_y = u_x\dfrac{\partial u_y}{\partial x} + u_y\dfrac{\partial u_y}{\partial y} + u_z\dfrac{\partial u_y}{\partial z}; \\ -g - \dfrac{1}{\rho}\dfrac{\partial p}{\partial z} = 0. \end{cases} \qquad (3)$$

From the third equation of the system (3), it follows:

$$p = -\gamma z + f(x, y),$$

where $f(x, y)$ denotes the arbitrary function. Since $z = z_n$, $p = p_n = \text{const}$ on a free surface, we arrive to the hydrostatic law of pressure distribution on the vertical:

$$p - p_n = \gamma(z_n - z).$$

Denoting the watercourse bottom coordinate with z_0, we get:

$$\frac{\partial p}{\partial x} = \gamma \frac{\partial}{\partial x}\left(z_0 + h\right), \quad \frac{\partial p}{\partial y} = \gamma \frac{\partial}{\partial y}\left(z_0 + h\right).$$

The Eqs. (3) under these conditions is written in the form:

$$\begin{cases} u_x \dfrac{\partial u_x}{\partial x} + u_y \dfrac{\partial u_x}{\partial y} = -\mathrm{g} \dfrac{\partial}{\partial x}(z_0 + h); \\ u_x \dfrac{\partial u_y}{\partial x} + u_y \dfrac{\partial u_y}{\partial y} = -\mathrm{g} \dfrac{\partial}{\partial y}(z_0 + h). \end{cases}$$

Having supplemented this system of equations with the continuity equation for a two-dimensional flow

$$\frac{\partial}{\partial x}(hu_x) + \frac{\partial}{\partial y}(hu_y) = 0$$

we obtain the system of equations:

$$\begin{cases} u_x \dfrac{\partial u_x}{\partial x} + u_y \dfrac{\partial u_x}{\partial y} = -\mathrm{g} \dfrac{\partial}{\partial x}(z_0 + h); \\ u_x \dfrac{\partial u_y}{\partial x} + u_y \dfrac{\partial u_y}{\partial y} = -\mathrm{g} \dfrac{\partial}{\partial y}(z_0 + h); \\ \dfrac{\partial}{\partial x}(hu_x) + \dfrac{\partial}{\partial y}(hu_y) = 0. \end{cases} \quad (4)$$

In case of the discharge channel horizontal bottom z_0, Eqs. (4) can be written as follows:

$$\begin{cases} u_x \dfrac{\partial u_x}{\partial x} + u_y \dfrac{\partial u_x}{\partial y} + \mathrm{g} \dfrac{\partial h}{\partial x} = 0; \\ u_x \dfrac{\partial u_y}{\partial x} + u_y \dfrac{\partial u_y}{\partial y} + \mathrm{g} \dfrac{\partial h}{\partial y} = 0; \\ \dfrac{\partial}{\partial x}(hu_x) + \dfrac{\partial}{\partial y}(hu_y) = 0. \end{cases} \quad (5)$$

The system of partial differential equations (5) describes the two-dimensional flow in terms of open stationary flows in a horizontal conduit without taking into account the flow resistance forces. This system is a system of essentially nonlinear equations isolated with respect to the unknown functions:

$$u_x = u_x(x, y); \quad u_y = u_y(x, y); \quad h = h(x, y).$$

Introducing an additional condition for the flow potentiality:

$$\Omega = \frac{\partial u_y}{\partial x} - \frac{\partial u_x}{\partial y} = 0,$$

where Ω is the velocity vortex for a two-dimensional flow, we are convinced that there exists such a potential function $\phi = \phi(x, y)$ that:

$$u_x = \frac{\partial \phi}{\partial x}; \quad u_y = \frac{\partial \phi}{\partial y}.$$

In this particular case, the system (5) is reduced to the form:

$$\begin{cases} \dfrac{u_x^2 + u_y^2}{2\mathrm{g}} + h = H_0; \\ \dfrac{\partial}{\partial x}(hu_x) + \dfrac{\partial}{\partial y}(hu_y) = 0; \\ u_x = \dfrac{\partial \phi}{\partial x}; \quad u_y = \dfrac{\partial \phi}{\partial y}, \end{cases} \quad (6)$$

where H_0 is a constant for the whole flow.
The system of equations is the main one for solving the problem of planned flows directly in the flow physical plane.

1.2. The flow equations in the velocity hodograph plane.
The system of equations (6) accepts a transition to the velocity hodograph plane as suggested by S.A. Chaplygin for the gas flows study [11, 12]. As a result of this transformation, the nonlinear system of equations (6) transformed into a linear system with respect to partial derivatives.
Introducing the squared velocity coefficient

$$\mathrm{t} = \frac{V^2}{2gH_0},$$

where $V^2 = u_x^2 + u_y^2$; angle "θ" characterizing the local flow velocity vector direction; current function $\psi = \psi(\tau, \theta)$; potential function $\phi = \phi(\tau, \theta)$, we obtain a system of equations in the velocity hodograph plane $\Gamma(\tau, \theta)$

$$\begin{cases} \dfrac{\partial \phi}{\partial \tau} = \dfrac{h_0}{2H_0} \dfrac{3\tau - 1}{\tau(1-\tau)^2} \dfrac{\partial \psi}{\partial \theta}; \\ \dfrac{\partial \phi}{\partial \theta} = 2\dfrac{h_0}{H_0} \dfrac{\tau}{(1-\tau)} \dfrac{\partial \psi}{\partial \tau}, \end{cases} \qquad (7)$$

where τ, θ are the independent variables.
Wherein:

$$h = H_0(1 - \mathrm{t}); \quad V = \mathrm{t}^{\frac{1}{2}}\sqrt{2gH_0}, \ \frac{1}{3} < \tau \le 1;$$

$$H_0 = h_0 + \frac{V_0^2}{2g},$$

where h_0, V_0 are define depth and flow velocity at some characteristic point.
The system solution (7) is reduced to solving the following equation

$$\frac{\partial}{\partial \tau}\left(\frac{2\tau}{1-\tau}\frac{\partial \psi}{\partial \tau}\right) + \frac{1-3\tau}{2\tau(1-\tau)^2}\frac{\partial^2 \psi}{\partial \theta^2} = 0.$$

Moreover, there is a complex differential link between the planes $\Phi(x, y)$ and $\Gamma(\tau, \theta)$ [8]:

$$d(x+iy) = \left[d\phi + i\frac{h_0}{H_0(1-\tau)} d\psi \right] \frac{e^{i\theta}}{\tau^{\frac{1}{2}}\sqrt{2gH_0}}, \qquad (8)$$

where $i = \sqrt{-1}$ - is an imaginary unit; x, y are the coordinates of a liquid flow particle in terms of its flow; τ, θ are the independent variables of a liquid particle flow in the velocity hodograph plane; $\phi = \phi(\tau, \theta)$ is a potential function; $\psi = \psi(\tau, \theta)$ is a stream function.
Eqs. (7) makes it possible solving the boundary problem of flow spreading first in the velocity hodograph plane $\Gamma(\tau, \theta)$, and then using the relation (8) to obtain a solution to the problem in the physical plane $\Phi(x, y)$.
In the works [7, 8], a whole spectrum of the system's analytical solutions (7) has been obtained. However, it was proved that the system solution (7)

$$\psi = A\frac{\sin\theta}{\tau^{\frac{1}{2}}}; \ \phi = A\frac{h_0}{H_0}\frac{\cos\theta}{\tau^{\frac{1}{2}}(1-\tau)} \qquad (9)$$

is the solution providing sufficient adequacy to the real flow for the flow outlet vicinity in the range from the rectangular pipe up to the flow expansion:

$$\beta = \frac{y}{b/2} = 7 \div 10,$$

where b is the culvert width; y defines the transverse coordinate of the extreme streamline, see Fig.1.

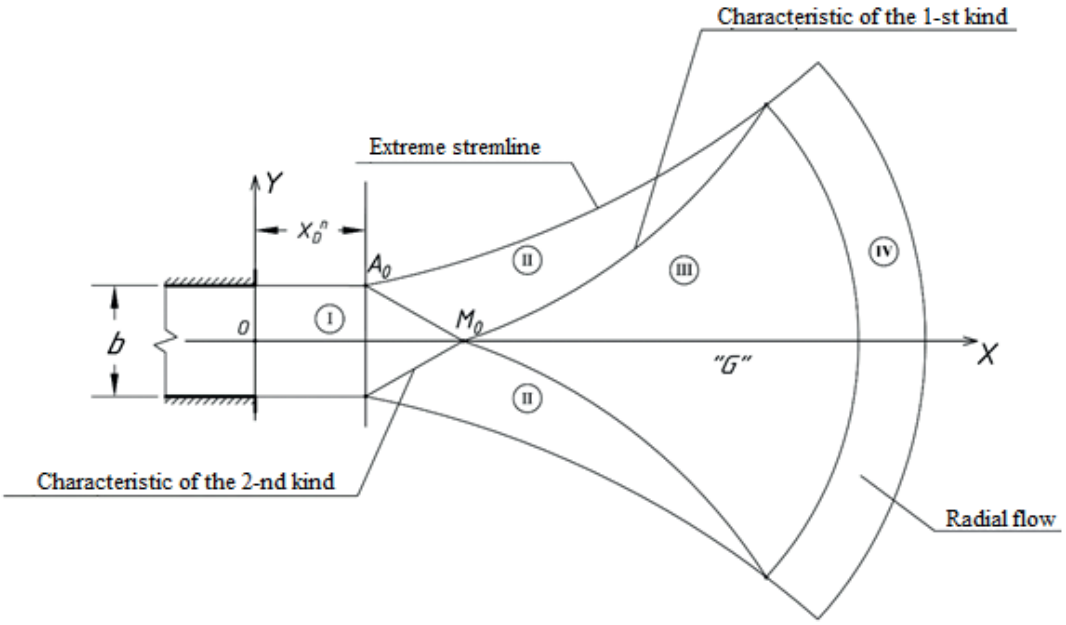

Figure 1. The plan of the flow

2. THE PROBLEM SOLUTION IN THE VELOCITY HODOGRAPH PLANE

Solving the boundary problem in the velocity hodograph plane means determining the constant "A" in the formulas (9) and determining the flow parameters τ, θ at the intersection points of an arbitrary streamline and an arbitrary equipotential.

2.1. The constant A definition.

The extreme streamline cuts off 50% of the application rate (referred to «h_0») from the longitudinal symmetry axis. Therefore:

$$\psi = \frac{V_0 b}{2} = A\frac{\sin\theta}{\tau^{1/2}}.$$

At infinity $\tau = 1;\ \theta = \theta_{\max}$. Then

$$A = \frac{V_0 b}{2\sin\theta}.$$

The angle $\theta_{\max}$ is determined by the formulas following from the characteristic theory [3, 4]:

$$\theta_{\max} = C_1 + (\sqrt{3}-1)\frac{\pi}{2};$$

$$C_1 = arctg\sqrt{\frac{3\tau_0 - 1}{1-\tau_0}} - \sqrt{3}arctg\left(\frac{1}{\sqrt{3}}\sqrt{\frac{3\tau_0 - 1}{1-\tau_0}}\right).$$

2.2. Defining the flow parameters τ, θ at the arbitrary streamline intersection points with an arbitrary equipotential.

According to the equations (9), the following equalities are completed along the arbitrary streamline:

$$\begin{cases} \dfrac{\sin\theta}{\tau^{1/2}} = K\sin\theta_{\max}; \\ \dfrac{\cos\theta}{\tau^{1/2}(1-\tau)} = \dfrac{1}{\tau_{oc}^{1/2}(1-\tau_{oc})}, \end{cases} \qquad (10)$$

where $K \in [0,1]$ is the flow coefficient along the streamline under consideration; τ_{oc} is the parameter "τ" at the intersection of the equipotential under consideration with the longitudinal symmetry flow axis.

The system of equations (10) is solved analytically with the standard methods by reducing it to solving a cubic equation [13]. In this case, the equation root should satisfy the condition:

$$\tau_0 < \tau \le 1 .$$

Next, it is necessary to move to the physical region of the streams with known parameters τ, θ at the intersection point of an arbitrary line flow with an arbitrary equipotential.

3. DETERMINATION OF THE X, Y COORDINATES IN THE PLANE $\Phi(x, y)$ CORRESPONDING TO THE POINT τ, θ IN THE VELOCITY HODOGRAPH PLANE $\Gamma(\tau, \theta)$.

When inspecting the arbitrary streamline, starting from the culvert, one can reach the given point with the coordinates τ, θ. Therefore, we consider $d\psi = 0$ in the equation (8). Moreover,

$$d\left(x + iy\right) = d\phi \frac{e^{i\theta}}{\tau^{1/2}\sqrt{2gH_0}} \qquad (11)$$

follows from (8).
Separating the variables in Eq. (11), we obtain:

$$\begin{cases} dx = \dfrac{d\phi \cos\theta}{\tau^{1/2}\sqrt{2gH_0}}; \\ dy = \dfrac{d\phi \sin\theta}{\tau^{1/2}\sqrt{2gH_0}}. \end{cases} \qquad (12)$$

Eqs. (12) confirm that along the streamline:

$$\frac{dy}{dx} = \mathrm{tg}\theta .$$

The velocity vector along the streamline is inclined with angle "θ" to the flow symmetry axis *Ox*, i.e., it is tangential to streamline.

From the first equation of the system (10), we determine:

$$\sin\theta = K\tau^{1/2}\sin\theta_{\max} . \qquad (13)$$

Substituting the right-hand part of Eq. (13) instead of $\sin\theta$ into the second equation of the system (12), we obtain:

$$dY = \frac{d\phi K\tau^{1/2}\sin\theta_{\max}}{\tau^{1/2}\sqrt{2gH_0}} = \frac{d\phi K\sin\theta_{\max}}{\sqrt{2gH_0}} . \qquad (14)$$

Additional information from the experimental research.
It was experimentally revealed in the work [12-17] that there is a vertical front with a length "X_D" along the flow symmetry axis, along which the flow parameters do not change (Fig.1).
There is an abrupt change in angle "θ" from zero to $\theta_н$ after point "*K''*". "X_D" length was determined by processing more than a hundred experiments. The following formula of which has been obtained:

$$X_D = \mathrm{trunc}\left[\frac{\sqrt{F_0 - 1}}{\sin\theta_{\max}(F_0 + 2)} h_0\right] + 1,$$

where $F_0 = \dfrac{V_0^2}{gh_0}$ is the Froude number at the flow outlet from the pipe; h_0 denotes flow depth at the pipe outlet; $\theta_{\max}$ is the maximum flow angle; values of X_D, h_0 are determined experimentally and given in cm.
Integrating the Eq. (14), we obtain:

$$Y_M - Y_T = \frac{K\sin\theta_{\max}}{\sqrt{2gH_0}}\left(\phi_M - \phi_T\right), \qquad (15)$$

where $\phi_M = A\dfrac{h_0}{H_0}\dfrac{\cos\theta_M}{\tau_M^{1/2}(1-\tau_M)}$;

$$\phi_{\mathrm{T}} = A\frac{h_0}{H_0}\frac{\cos\theta_{\mathrm{T}}}{\tau_{\mathrm{T}}^{1/2}(1-\tau_{\mathrm{T}})};$$

$\theta_{\mathrm{T}}, \tau_{\mathrm{T}}$ are the flow parameters defining the initial equipotential.

The system's first equation integration (12) leads to the following one:

$$X_{\mathrm{M}} = X_{\mathrm{D}} + X_{\mathrm{T}} + \frac{Ah_0}{H_0\sqrt{2gH_0}}\left[J_1 - K^* J_2 - K^* J_3\right]\Bigg|_{\tau_{\mathrm{T}}}^{\tau_{\mathrm{M}}},$$

where $K^* = \sin^2\theta_{\max}^{\mathrm{T}}$, $\theta_{\max}^{\mathrm{T}}$ defines the maximum angle of the flow spreading along the selected streamline;

$$J_1 = \frac{1+\tau}{\tau(1-\tau)} + \ln\frac{\tau}{1-\tau};$$

$$J_2 = \frac{2}{1-\tau} + \ln\frac{1-\tau}{\tau};\ J_3 = \ln\frac{\tau}{1-\tau}. \quad (16)$$

In a particular case from Eq. (15) and Eq. (16), it follows that, along the flow symmetry axis, the relationship between X and τ takes the form:

$$X = X_{\mathrm{D}} + \tilde{X}_{\mathrm{D}} + \frac{Ah_0}{H_0\sqrt{2gH_0}}\left[\frac{1+\tau}{\tau(1-\tau)} - \ln\frac{1-\tau}{\tau} - \frac{1+\tau_0}{\tau_0(1-\tau_0)} + \ln\frac{1-\tau_0}{\tau_0}\right],$$

where $\tilde{X}_{\mathrm{D}} = \frac{b}{2}\mathrm{tg}\frac{\theta_k}{2}$. The angle θ_k and the parameter τ_k are determined from the system:

$$\begin{cases} \dfrac{\sin\theta_k}{\tau_k^{1/2}} = \sin\theta_{\max}; \\ \dfrac{\cos\theta_k}{\tau_k^{1/2}(1-\tau_k)} = \dfrac{1}{\tau_0^{1/2}(1-\tau_0)}. \end{cases}$$

Along the extreme streamline, it follows from Eq. (15) and Eq. (16) that:

$$X = X_{\mathrm{D}} + \frac{Ah_0}{H_0\sqrt{2gH_0}}\left[\frac{1+\tau}{\tau(1-\tau)} - \frac{2\sin^2\theta_{\max}}{1-\tau} - \ln\frac{1-\tau}{\tau} - \frac{1+\tau_k}{\tau_k(1-\tau_k)} + \ln\frac{1-\tau_k}{\tau_k} + \frac{2\sin^2\theta_{\max}}{1-\tau_k}\right]; \quad (17)$$

$$Y = \frac{b}{2} + A\frac{h_0\sin^2\theta_{\max}}{H_0\sqrt{2gH_0}}\left[\frac{\cos\theta}{\tau^{1/2}(1-\tau)} - \frac{\cos\theta_k}{\tau_k^{1/2}(1-\tau_k)}\right]. \quad (18)$$

We determined depths and flow rates with the known parameter "τ" according to the formulas:

$$h = H_0(1-\tau);\quad V = \tau^{1/2}\sqrt{2gH_0}.$$

4. THE TRANSITION FROM A TWO-DIMENSIONAL MODEL TO A ONE-DIMENSIONAL

This module is necessary to use the flow resistance laws and takes into account the resistance forces.

We use the flow rate conservation equation

$$Q = BVH,$$

where

$$V = \tau^{1/2}\sqrt{2gH_0};\quad h = H_0(1-\tau)$$

or in other form:

$$Q = BH_0(1-\tau)\sqrt{2gH_0}\tau^{1/2} \quad (19)$$

Assuming the known width of the flow $B = 2Y$, where Y is taken from a two-dimensional flow model, it is possible to determine the parameter "τ_{cp}" from the solution of the cubic equation:

$$(1-\tau_{\mathrm{cp}})\tau_{\mathrm{cp}}^{1/2} = \frac{Q}{2YH_0\sqrt{2gH_0}}.$$

For $\tau_0 \le \tau_{cp} \le 1$, the root of τ_{cp} can be determined from the equation:

$$(1-\tau_{cp})^2 \tau_{cp} = \frac{Q^2}{4Y^2 H_0^3 2gH_0}.$$

We will further define the parameters of a conditionally one-dimensional flow with the characteristics:

$$h_{cp} = H_0(1-\tau_{cp}); \quad V_{cp} = \tau_{cp}^{1/2}\sqrt{2gH_0}. \quad (20)$$

The corresponding X coordinate is determined by equation (17). Therefore, the parameter "τ" is determined for the abscissa "X" given. Further, $Y(\tau)$ is determined from equation (18). And the average depths and velocities h_{cp}, V_{cp} in the considered non-pressure flow line are determined by formulas (20).

THE RESULTS OF THE STUDY

1. The model proposed in the work represents the analytical methods' development for calculating the potential flows with the previously unknown boundaries. This allows determining the entire range of geometric and kinematic flow parameters with an error not exceeding 10% up to the flow expansion $\beta = 7 \div 10$.
2. The model adequacy for all flow parameters up to the flow expansion $\beta = 7 \div 10$ improves the accuracy of the previously existing methods, which allows the designers of the road culverts' hydraulic structures to increase its reliability using the results of the structure fastening designers' work.
3. This model can be applied as an initial model for calculating the real flows behind the culverts taking into account the fluid resistance.
4. The authors propose an additional module to take into account the fluid resistance.
5. The transition to a one-dimensional model allow us to take into account the action of the fluid resistance and recalculate the flow parameters required by the designers of the hydraulic structure. The paper indicates only the direction for possible consideration of the fluid resistance, which will be further developed and detailed.
6. The package of applied programs is available at the Department of General Engineering Disciplines of the Platov South-Russian State Polytechnic University.

CONCLUSIONS

The model proposed in the paper represents the development of analytical methods for calculating potential flows with previously unknown boundaries and before the flow $\beta = 7 \div 10$ expands. It allows determining the entire range of geometric and kinematic parameters of the flow with an error not exceeding 10%. The substantiation of this position is confirmed by experimental experiments and numerical calculations given in [8, 12].
The adequacy of the model in all parameters of the flow before $\beta = 7 \div 10$ expansion improves the accuracy of previously existing methods, which allows the designers of the hydraulic structure of road culverts to increase its reliability using the results of the work of the designers of the fastening of the structure.
The article proposes a module of transition from a two-dimensional water flow model to a one-dimensional one. This module is necessary for using the laws of fluid resistance and takes into account the fluid resistance.

REFERENCES

1. **Sherenkov I.A.** O planovoj zadache rastekaniya strui burnogo potoka neszhimaemoj zhidkosti [On the planned problem of the spreading of a jet of a stormy flow of an incompressible fluid] // *Izv. AN SSSR,* 1958, Issue 1, Pp. 72-78 (in Russia).
2. **Spravochnik** po gidravlike [Handbook on hydraulics] /2nd edition, remastered and

added. – Kiev, Vishcha shkola, 1984, 343 pages (in Russia).
3. **Sherenkov I.A.** Eksperimental'nye issledovaniya rastekaniya burnogo potoka za vyhodnymi ogolovkami vodopropusknyh sooruzhenij [Experimental studies of the growth of a turbulent flow behind the output heads of culverts] // *Trudy ob"edinennogo seminara po gidroenergeticheskomu i vodohozyajstvennomu stroitel'stvu* [Proceedings of a single seminar on hydropower and water management construction]. Har'kov, 1959, Issue 1. (in Russia).
4. **Sherenkov I.A.** O roli normal'nyh turbulentnyh napryazhenij v formirovanii plana techenij [On the role of normal turbulent stresses in the formation of plane flows] // *Gidravlika i gidrotekhnika*. Kiev, Tekhnika, 1973. Vol. 17 (in Russia).
5. **Sherenkov I.A.** Prikladnye planovye zadachi gidravliki spokojnyh potokov [Applied planning tasks for hydraulics of calm flows. Moscow, Energiya, 1978 (in Russia).
6. **Lojcyanskij L.G.** Mekhanika zhidkosti i gaza [Fluid and Gas Mechanics] / 5th edition. Moscow, Nauka, 1978, 736 pages (in Russia).
7. **Kohanenko V.N.** Modelirovanie odnomernyh i dvuhmernyh otkrytyh vodnyh potokov [Modeling of one-dimensional and two-dimensional open water flows]: monograph. Rostov n/D, YUFU, 2007, 168 pages (in Russia).
8. **Kohanenko V.N., Volosuhin YA.V.** et al. Modelirovanie burnyh dvuhmernyh v plane vodnyh potokov [Modeling of stormy two-dimensional in the plane of water flows]: monograph, Rostov na Donu, YUFU, 2013, 180 pages (in Russia).
9. **Vysockij L.I.** Upravlenie burnymi potokami na vodosbrosah [Management of stormy flows at spillways]. Moscow, Energiya, 1977, 280 pages (in Russia).
10. **Shterenliht D.V.** Gidravlika [Hydraulics] /Edition 3rd, remastered. Moscow, Kolos, 2005, 656 pages (in Russia).
11. **Kohanenko V.N.** O planovoj zadache rastekaniya burnogo potoka neszhimaemoj zhidkosti [On the planned spreading problem of a turbulent flow of an incompressible fluid] // *Izvestiya vuzov. Seriya: Tekhnicheskie nauki,* 2012, № 6, Pp. 82-88 (in Russia).
12. **Kohanenko V.N.** Dvuhmernye v plane burnye stacionarnye potoki za vodopropusknymi sooruzheniyami v usloviyah svobodnogo rastekaniya [Two-dimensional in an airplane turbulent stationary flows behind culverts in conditions of free spreading]: Doctoral diss.: 05.23.16: Kohanenko Viktor Nikolaevich, Moscow, 1997, 238 pages (in Russia).
13. **Korn G.**, **Korn T.** Spravochnik po matematike dlya nauchnyh rabotnikov i inzhenerov [Handbook on Mathematics for scientists and engineers], Moscow, Nauka, 1970, 720 pages (in Russia).
14. **Kohanenko V.N., Kelekhsaev D.B.** Reshenie zadachi opredeleniya uravneniya krajnej linii toka i parametrov vdol' nee s uchetom uchastka Xd [Solving the problems of determining the equation of the extreme streamline and parameters along with the counting section Xd] // Rezul'taty issledovanij – 2019: materialy IV Nacional'noj konf. professorsko-prepodavatel'skogo sostava i nauch. rabotnikov [Research results – 2019: materials of the IV National Conf. teaching staff and scientific. Workers], 14th may 2019, Novocherkassk / Yuzh.-Ros. gos. politekhn. un-t (NPI) im. M.I. Platova. – Novocherkassk, YURGPU (NPI), 2019. – Pp. 113-117 (in Russia).
15. **Posobie** po gidravlicheskim raschetam malyh vodopropusknyh sooruzhenij [Manual on hydraulic calculations of small culverts]. Moscow, Transport, 1992. - 408 pages (in Russia).

16. **Bahvalov, N.S.** Chislennye metody [Numerical methods]. Moscow, Binom, 2003, 633 pages (in Russia).
17. **Esin A.I.** Zadachi tekhnicheskoj mekhaniki zhidkosti v estestvennyh koordinatah [Problems of technical fluid mechanics in natural coordinates]. Saratov, Publishing of Saratovskij GAU, 2003, 144 pages (in Russia).

СПИСОК ЛИТЕРАТУРЫ

1. **Шеренков И.А.** О плановой задаче растекания струи бурного потока несжимаемой жидкости // *Изв. АН СССР. ОТН,* 1958, №1, С. 72–78.
2. **Справочник** по гидравлике / 2-е изд., перераб. и доп. – Киев: Вища школа, 1984. – 343 с.
3. **Шеренков И.А.** Экспериментальные исследования растекания бурного потока за выходными оголовками водопропускных сооружений // Труды объединенного семинара по гидроэнергетическому и водохозяйственному строительству. – Харьков, 1959. Вып. 1.
4. **Шеренков И.А.** О роли нормальных турбулентных напряжений в формировании плана // Гидравлика и гидротехника. – Киев: Техника, 1973. Вып 17.
5. **Шеренков И.А.** Прикладные плановые задачи гидравлики спокойных потоков. – М.: Энергия, 1978.
6. **Лойцянский Л.Г.** Механика жидкости и газа. - М.: Наука, 1978. – 736 с.
7. **Коханенко В.Н**. Моделирование одномерных и двухмерных открытых водных потоков: монография. – Ростов н/Д: Изд-во ЮФУ, 2007. – 168 с.
8. **Коханенко В.Н., Волосухин Я.В.** и др. Моделирование бурных двухмерных в плане водных потоков: монография. – Ростов на Дону: Издательство Южного федерального университета, 2013. -180 с.
9. **Высоцкий Л.И.** Управление бурными потоками на водосбросах. – М.: Энергия, 1977. – 280 с.
10. **Штеренлихт Д.В.** Гидравлика. – М.: Колос, 2005. – 656 с.
11. **Коханенко В.Н.** О плановой задаче растекания бурного потока несжимаемой жидкости // *Известия вузов. Серия: Технические науки.* № 6. 2012. – С. 82–88.
12. **Коханенко В.Н.** Двухмерные в плане бурные стационарные потоки за водопропускными сооружениями в условиях свободного растекания: дисс. на соиск. уч. степ, д-ра техн. наук: 05.23.16: Коханенко Виктор Николаевич. – М., 1997. – 238с.
13. **Корн Г.** Справочник по математике для научных работников и инженеров. – М.: Наука, 1970. – 720 с.
14. **Коханенко В.Н., Келехсаев Д.Б.** Решение задачи определения уравнения крайней линии тока и параметров вдоль нее с учетом участка Хд // Результаты исследований – 2019: материалы IV Национальной конф. профессорско-преподавательского состава и науч. работников, 14 мая 2019 г., г. Новочеркасск / Юж.-Рос. гос. политехн. ун-т (НПИ) им. М.И. Платова. – Новочеркасск: ЮРГПУ (НПИ), 2019. – С. 113–117.
15. **Пособие** по гидравлическим расчетам малых водопропускных сооружений / Под общей редакцией Г.Я. Волченкова, ВНИИ транспортного строительства (ЦНИИС), Главное управление проектирования и капитального строительства (ГУПиКС) Минтрансстроя СССР. – М.: Транспорт, 1992. – 408 с.
16. **Бахвалов Н.С.** Численные методы. – М.: Бином, 2003, – 633 с.
17. **Есин А.И.** Задачи технической механики жидкости в естественных координатах. – Саратов: Изд-во ФГОУ ВПО «Саратовский ГАУ», 2003. 144 с.

Olga A. Burtseva, Candidate of Technical Sciences, Associate Professor of the Department of General Engineering Disciplines South Russian State Polytechnic University (NPI) named after M. I. Platov, 132 Prosveshcheniya str., Novocherkassk, 346428, Russia; phone: +7(951) 511-33-59; E-mail: kuzinaolga@yandex.ru.

Viktor N. Kohanenko, Doctor of Technical Sciences, Professor of the Department of General Engineering Disciplines South Russian State Polytechnic University (NPI) named after M. I. Platov, 132 Prosveshcheniya str., Novocherkassk, 346428, Russia; phone: +7(951) 490-70-09; e-mail: victorkohanenko@yandex.ru.

Sergey I. Evtushenko Doctor of Technical Sciences, Professor, Honorary Worker of Higher Education of the Russian Federation, Adviser of the RAASN, member of the ROMGGiF, Professor of the Department "Information Systems, Technology and Automation of Construction" of the National Research University Moscow State University of Civil Engineering, Yaroslavskoe shosse, 26, Moscow, 129337, Russia; phone: 8(928)901-70-69; E-mail: evtushenkosi@mgsu.ru.

Maria S. Alexandrova Postgraduate student of the Department of General Engineering Disciplines of the South Russian State Polytechnic University (NPI) named after M. I. Platov; 132 Prosveshcheniya str., Novocherkassk, 346428, Russia; phone: 8(985)245-34-62; E-mail: e_masha@mail.ru.

Бурцева Ольга Александровна, кандидат технических наук, доцент кафедры общеинженерных дисциплин Южно-Российского государственного политехнического университета (НПИ) имени М.И. Платова; 346428, Россия, г. Новочеркасск, ул. Просвещения, 132; телефон: +7(951) 511-33-59; E-mail: kuzinaolga@yandex.ru.

Коханенко Виктор Николаевич доктор технических наук, профессор кафедры общеинженерных дисциплин Южно-Российского государственного политехнического университета (НПИ) имени М.И. Платова; 346428, Россия, г. Новочеркасск, ул. Просвещения, 132; телефон: +7(951) 490-70-09; E-mail: victorkohanenko@yandex.ru.

Евтушенко Сергей Иванович доктор технических наук, профессор, почетный работник высшего образования Российской Федерации, советник РААСН, член РОМГГиФ, профессор кафедры «Информационные системы, технология и автоматизация строительства» Национального исследовательского Московского государственного строительного университета; телефон: 8(928)901-70-69; E-mail: evtushenkosi@mgsu.ru.

Александрова Мария Сергеевна, аспирант кафедры общеинженерных дисциплин Южно-Российского государственного политехнического университета (НПИ) имени М.И. Платова; 346428, Россия, г. Новочеркасск, ул. Просвещения, 132; телефон: 8(985)245-34-62; E-mail: e_masha@mail.ru.

International Journal for Computational Civil and Structural Engineering, 18(2) 85–97 (2022)

DOI:10.22337/2587-9618-2022-18-2-85-97

DEFINITION OF THE BEAMS FROM A NONLINEARLY DEFORMED MATERIAL BY THE RITZ-TIMOSHENKO METHODS AND FINITE DIFFERENCES TAKING INTO ACCOUNT THE DEGRADATION RIGIDITY FUNCTIONS

Vladimir P. Selyaev, Sergey Yu. Gryaznov, Delmira R. Babushkina

National Research Mordovia State University, Saransk, RUSSIA

Abstract. The article solves the problem of determining the deflections of a beam made of a nonlinearly deformable material – a polyester composite held in water using the numerical methods of Ritz-Timoshenko and finite differences. The influence of an aggressive environment on the material of the structure was taken into account by introducing the degradation function of stiffness into the calculation algorithms of the above methods. The problem of determining the time and conditions for the onset of the limiting state of the structure in the second group in accordance with the current norms and rules has been solved.

Keywords: beam, nonlinearity, deflection, Ritz-Timoshenko method, finite difference method, stiffness, degradation function, limiting state.

ОПРЕДЕЛЕНИЕ ПРОГИБОВ БАЛКИ ИЗ НЕЛИНЕЙНО ДЕФОРМИРУЕМОГО МАТЕРИАЛА МЕТОДАМИ РИТЦА-ТИМОШЕНКО И КОНЕЧНЫХ РАЗНОСТЕЙ С УЧЕТОМ ДЕГРАДАЦИОННЫХ ФУНКЦИЙ ЖЕСТКОСТИ

В.П. Селяев, С.Ю. Грязнов, Д.Р. Бабушкина

Национальный исследовательский Мордовский государственный университет, г. Саранск, РОССИЯ

Аннотация. В статье решена задача определения прогибов балки из нелинейно деформируемого материала – полиэфирного композита, выдержанного в воде, численными методами Ритца-Тимошенко и конечных разностей. Влияние агрессивной среды на материал конструкции было учтено введением деградационной функции жесткости в расчетные алгоритмы, вышеназванных методов. Решена задача по определению времени и условий наступления предельного состояния конструкции по второй группе согласно действующим нормам и правилам.

Ключевые слова: балка, нелинейность, прогиб, метод Ритца-Тимошенко, метод конечных разностей, жесткость, деградационная функция, предельное состояние.

INTRODUCTION

Construction materials and structures may be subject to the destructive effects of aggressive environments at any stage of the life cycle of the object. The probability of occurrence of some adverse events is taken into account at the design stage of structures by the introduction of conditional reserve coefficients that guarantee the impossibility of the occurrence of limit states. However, in practice, emergency situations often occur in which the structure can go into the limit state in a fairly short period of time. For example, numerous studies have proved the nonlinearity of the development of chemical degradation processes [1-8].

Consequently, in the existing mathematical models, all unreasonable coefficients should

be replaced by functional dependencies that take into account the influence of complex stochastic and chronological processes [9-11]. Among the known approaches to assessing durability and reliability [12-20], the most accurate, perfect and experimentally reasonable is the method of assessing the chemical resistance of construction materials and structures using degradation functions [10, 21-24].

The purpose of the work: to determine the change in deflections of a polyester composite operating under the combined effects of mechanical loads and an aggressive environment; to determine the conditions for the onset of the limit state for group 2, using the method of degradation functions.

MATERIALS AND METHODS

It has been experimentally established [10] that the process of destruction of the material within the cross-sectional area of the element has an uneven character. The aggressive medium begins to penetrate deep into the material through weak areas, through pores, capillaries, amorphous particles. Consequently, the elastic-strength characteristics will change non-linearly along the cross-section, which can be traced on the corresponding graphs – isochrones of degradation (Fig. 1, *b*). The position of the degradation isochrones is characterized by three parameters: the coordinate of the destruction front – the depth index (a), the characteristic of the linearity of the degradation mechanism – (φ), and the chemical resistance coefficient of the material – (β).

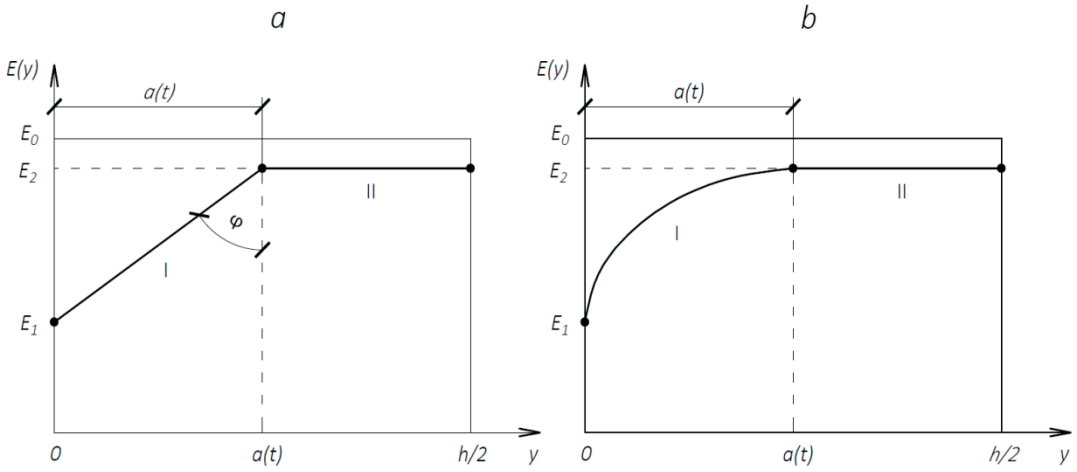

Figure 1. Basic models of deformation modulus change: a – linear, b – nonlinear

It has been experimentally established that the numerical values of the modulus of deformation and micro-hardness, determined with high accuracy by sclerometric methods, have a directly proportional relationship. Therefore, the degradation function of stiffness $F(B)$, characterize by the law of variation of the modulus of deformation over the section of the element, was determined as the basic one. It is important to note that in this work, the process of transferring an aggressive medium into the sample was studied only along the y axis.

Let is consider a single-span, pivotally supported beam with a length $l = 10\ m$ c with a constant cross-section $b \times h = 0{,}3 \times 0{,}4\ m$ of polyester composite (Table. 1), loaded along the entire length with a uniformly distributed load $q = 17\ kN/m$ (Fig. 2).

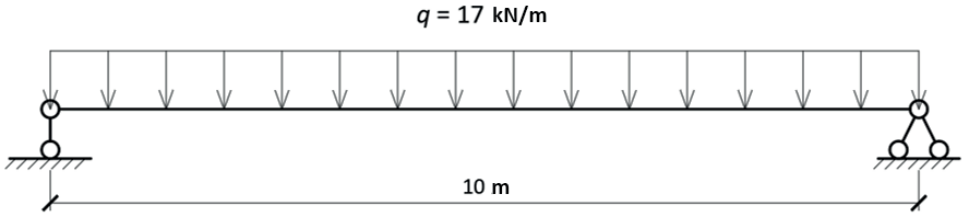

Figure 2. The design scheme of the beam

For bendable elements, the degradation stiffness function, based on a combined power approximation of the isochron of degradation, in relative coordinates has the following form:

$$F(B) = k_{\text{x.c.2}} - (k_{\text{x.c.2}} - k_{\text{x.c.1}}) \cdot \left(\frac{a}{h}\right)^3 \cdot \frac{2p}{p+3}\ , (1)$$

where is $k_{\text{x.c.1}} = \beta_1 = H_1/H_0 = E_1/E_0$ – the coefficient of chemical resistance of the material, determined by the degradation isochrones, using numerical values of the change in micro-hardness over time on the sample surface [25];

$k_{\text{x.c.2}} = \beta_2 = H_2/H_0 = E_2/E_0$ – the coefficient of chemical resistance of the material, determined at the depth a of the damaged material layer;

h – the height of the cross section of the element;

$a = k(\xi)\sqrt{Dt}$ – coordinate of the leading edge of corrosion, characterizing the depth of damage to the material (depth indicator);

$k(\xi) = 0{,}1$ – a coefficient that takes into account the instrumental accuracy of determining the coordinate$a$;

$D = 0{,}02\ cm^2/day$ – the diffusion coefficient of the aggressive medium into the material determined experimentally;

t – time of exposure to aggressive solution;

a/h – relative characteristics of the corrosion front.

In formula (1), the parameter p characterizes the type of isochron degradation, their position and shape. It can be determined experimentally from the analysis of isochron degradation, or selected from a pre-formed statistical database of compliance of materials, conditions of physico-chemical and mechanical effects, as well as the duration of the aggressive environment. Numerically, the parameter p can be equal to any positive rational number, provided the inequality is one.

For the polyester composite exposed in water, the values of elastic strength characteristics, as well as the values of degradation functions (1), were obtained at each time point under consideration t (Table 1).

To solve the problem of bending a beam from a non-linearly deformable material, an analytical function of the following form approximating the deformation diagram «σ – ε», was chosen:

$$\sigma_i = \alpha \cdot \varepsilon_i - \beta \cdot {\varepsilon_i}^5\ , \qquad (2)$$

where the constants $\alpha = E_0(t_0) \approx 3{,}16 \cdot 10^4\ MP\text{a}$, $\beta = (E_b - E_{bu})/\varepsilon_{bu}^4 \approx 5{,}12 \cdot 10^{12}\ MP\text{a}$ are determined from the condition of conformity of the approximating function (2) to the normalized indicators [26].

RESULTS AND DISCUSSION

To solve the problem of determining the deflections of the beam, 2 methods were used: the Ritz-Timoshenko method (MRI) and the finite difference method (MD). Both options were automated in Microsoft Excel 2010. To verify the software algorithms, additional calculations were performed in the Lira-CAD 2013 software package (Fig. 3).

Table 1. Elastic strength characteristics of polyester composite

Parameter	Exposure time of samples in water t, day					
	0	15	30	175	265	400
1	2	3	4	5	6	7
σ_{ue}, MPa	132.853	122.581	117.153	84.819	74.592	60.477
ε_{ue}	0.0042	0.0047	0.0051	0.005	0.005	0.0049
E_0, MPa	31631.667	26081.064	22971.176	16963.8	14918.4	12342.245
σ_{bu}, MPa	150	140.572	135.304	99.773	93.466	82.197
ε_{bu}	0.006	0.0065	0.0066	0.0076	0.0083	0.0097
E_{bu}, MPa	25000	21626.462	20500.606	13128.026	11260.964	8473.918
$k_{x.c.1}$	1	0.825	0.726	0.536	0.472	0.39
$k_{x.c.2}$	1	1	1	1	1	1
a, cm	0	5.5	7.7	18.7	23	28.3
a/h	0	0.1375	0.1925	0.4675	0.575	0.7075
$F(B)$	1	1	0.998	0.962	0.92	0.827

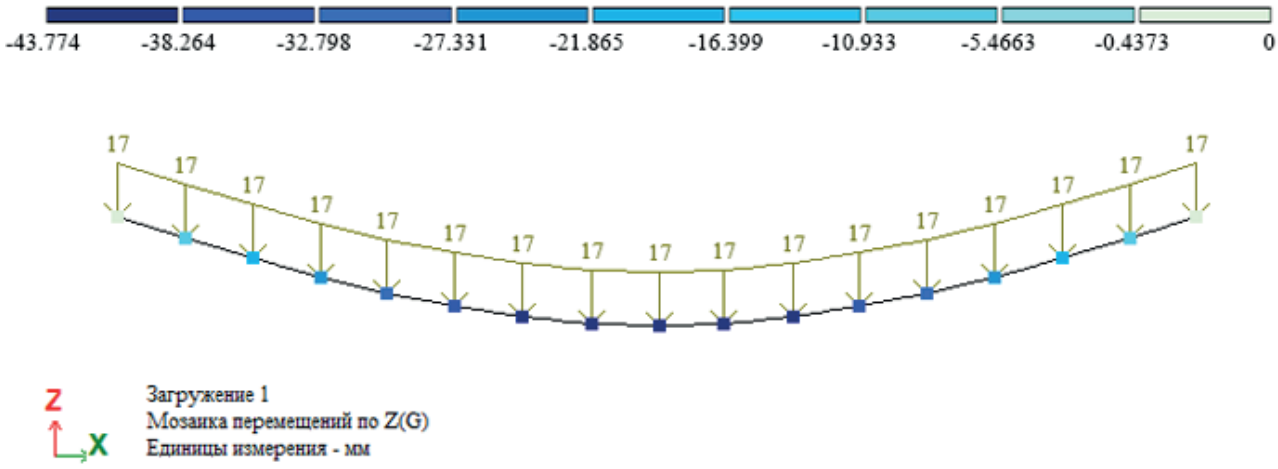

Figure 3. Linear calculation of beam deflections in the Lira-CAD 2013 PC

Table 2. Comparison of the results of linear calculations of Lira, MRI and MD at $F(B) = 1$

Cross-section coordinate x, m	Deflections w, mm				
	Lira	MRI	Δ%	MD	Δ%
0	0	0	0	0	0
0.625	8.680	8.681	0.01	8.707	0.31
1.25	16.980	16.982	0.01	17.029	0.29
1.875	24.566	24.570	0.01	24.635	0.28
2.5	31.158	31.162	0.01	31.241	0.27
3.125	36.524	36.529	0.01	36.619	0.26
3.75	40.485	40.491	0.01	40.588	0.26
4.375	42.913	42.919	0.01	43.021	0.25
5	43.730	43.737	0.01	43.840	0.25
| max |	43.730	43.737	0.01	43.840	0.31

Table 3. Comparison of the results of linear calculations of Lira, MRI and MD at $F(B) = 0{,}827$

Cross-section coordinate x, m	Deflections w, mm				
	Lira	MRI	Δ%	MD	Δ%
0	0	0	0	0	0
0.625	10.495	10.497	0.02	10.527	0.30
1.25	20.531	20.535	0.02	20.590	0.29
1.875	29.704	29.710	0.02	29.785	0.27
2.5	37.674	37.681	0.02	37.774	0.26
3.125	44.163	44.171	0.02	44.275	0.26
3.75	48.952	48.961	0.02	49.075	0.25
4.375	51.888	51.897	0.02	52.0160	0.25
5	52.876	52.886	0.02	53.007	0.25
| max |	52.876	52.886	0.02	53.007	0.30

Note to Tables 2 and 3: the beam is symmetrical relative to the middle of the span, so the results are presented in abbreviated form.

The introduction of the degradation stiffness function into the algorithm for solving the problem by the Ritz-Timoshenko method (MRI) was implemented as follows.

This method is based on the Lagrange-Dirichlet theorem on the minimum of the total potential energy of a body in equilibrium. Taking into account formula (2), the expression for the total potential energy of the beam will be written as follows:

$$V = \frac{1}{2}\alpha J_o \int_0^l \left(\frac{d^2w}{dx^2}\right)^2 dx - \frac{1}{6}\beta J_n \int_0^l \left(\frac{d^2w}{dx^2}\right)^6 dx\,, \qquad (3)$$

where is $J_o = bh^3/12$ и $J_n = bh^7/448$ – the moments of inertia of the beam section (axial and higher order, respectively).

In equation (3), the multipliers αJ_o and βJ_n represent nothing else than the stiffness of the beam, linear and higher order, respectively. Multiplying them by the value $F(B)$ obtain formulas for recording the stiffness of the beam taking into account the degradation function:

$$B_o = \alpha J_o F(B)\,;\; B_n = \beta J_n F(B)\,. \qquad (4)$$

The operation of an external distributed load $q(x)$ is determined by the formula:

$$A_q = \int_0^l q(x)w dx\,. \qquad (5)$$

Adding (5) and (3) taking into account (4), obtain a formula for determining the total bending energy of the beam

$$Э(W) = \frac{1}{2}B_o \int_0^l (w'')^2 dx - \frac{1}{6}B_n \int_0^l (w'')^6 dx - \int_0^l q(x)w dx\,. \qquad (6)$$

The deflection of a beam can be represented as a series with a finite number of terms:

$$w(x) = \sum_{n=1}^{N} K_n \varphi_n(x), \quad (n = 1, 2, \dots N), \qquad (7)$$

where is K_n – the desired constants (generalize coordinates);

$\varphi_n(x)$ – approximating functions (constructed by the method of initial parameters), each of which must satisfy geometric boundary conditions.

Formula (6) from the generalize coordinates [27] will be written as:

$$Э(K) = f_1K^2 - f_2K^6 - f_3K\,. \qquad (8)$$

From the condition of the minimum of the total potential energy of the beam, obtain the following nonlinear algebraic equation with respect to the deflection amplitude K:

$$\frac{dЭ}{dK} = 2f_1K - 6f_2K^5 - f_3 = 0\,. \qquad (9)$$

Here the coefficients f_1, f_2, f_3 are determined by the formulas:

$$f_1 = \frac{1}{2}B_o \int_0^l (\varphi'')^2 dx\;;\; f_2 = \frac{1}{6}B_n \int_0^l (\varphi'')^6 dx\;;\; f_3 = \int_0^l q(x)\varphi dx\,. \qquad (10)$$

The final resolving equation will be written as:

$$a \cdot K^5 + b \cdot K + c = 0\,. \qquad (11)$$

It follows from formula (7) that in order to determine the deflections of the beam, it is necessary to find at least one real root of equation (11), at which the identical equality of this equation is fulfilled. However, this equation is not solved in radicals, i.e. there are no formulas that would make it possible to calculate the roots by coefficients. This was first proved by the Norwegian mathematician Nils Abel. However, the roots of the 5th degree equation can be found with any predetermined accuracy using numerical methods. In this case, the actual roots were calculated with $1 \cdot 10^{-5}$ precision. Thus, the maximum deflection of the beam, determined by the above method (MRI), taking into account the degradation function $F(B) = 0{,}827$ was $w_{max} = 52{,}888\, mm$. At the same time, the root of equation (11) was $K \approx 1{,}69 \cdot 10^{-5}$.

To solve this problem by the finite difference method (MD), the following algorithm for introducing the degradation function of stiffness into the calculation is proposed.

The basic differential equation of bending of a beam made of a nonlinear elastic material has the form:

$$J_c(w)\frac{d^4w}{dx^4} + 2\frac{dJ_c(w)}{dx}\cdot\frac{d^3w}{dx^3} + \frac{d^2J_c(w)}{dx^2}\cdot\frac{d^2w}{dx^2} = q(x)\,. \quad (12)$$

Equation (12) includes both the stiffness variable along the length of the beam and its derivatives. In this case, they can be calculated only numerically using finite-difference approximation formulas [28].

After a series of transformations, equation (12), written in finite-difference form, can be transformed relative to the deflection value w_i by the following formula:

$$w_i = \frac{q_i^* - w_{i-2}\cdot A_i - w_{i-1}\cdot B_i - w_{i+1}\cdot E_i - w_{i+2}\cdot F_i}{C_i}\,, \quad (13)$$

where the variable coefficients depending on the stiffness will be recalculated at each new iteration stage according to the formulas:

$$A_i = \frac{J_{ci}}{\Delta x^4} - \frac{J'_{ci}}{\Delta x^3}\,;\; B_i = -4\frac{J_{ci}}{\Delta x^4} + 2\frac{J'_{ci}}{\Delta x^3} + \frac{J''_{ci}}{\Delta x^2}\,;\; C_i = -6\frac{J_{ci}}{\Delta x^4} - 2\frac{J''_{ci}}{\Delta x^2}\,;$$
$$E_i = -4\frac{J_{ci}}{\Delta x^4} - 2\frac{J'_{ci}}{\Delta x^3} + \frac{J''_{ci}}{\Delta x^2};\; F_i = \frac{J_{ci}}{\Delta x^4} + \frac{J'_{ci}}{\Delta x^3}\,. \quad (14)$$

Consequently, the smaller the step of dividing the beam lengthwise into finite elements Δx, the smaller the error value of the finite-difference approximation. Thus, to take into account the stiffness degradation process, it is proposed to multiply formulas (14) by the value of the degradation function $F(B)$.

Then the main equation (13) will be written as:

$$w_i = \frac{q_i^* - (w_{i-2}\cdot A_i - w_{i-1}\cdot B_i - w_{i+1}\cdot E_i - w_{i+2}\cdot F_i)\cdot F(B)}{C_i\cdot F(B)}\,. \quad (15)$$

Solving the system of finite-difference equations (15) with respect to deflections w_i in each section of the beam under consideration (we take $\Delta x = 0{,}625\, m$), we determine the deflections along the entire length, taking into account the degradation function.

The boundary conditions in the finite-difference form when the beam length is split (hinted along the edges, Fig. 4) into n = 16 parts will be determined by the formulas [28]:

$$w_a = w_b = 0\,;\; w_{a-1} + w_{a+1} = 0\,;$$
$$w_{a-2} + w_{a+2} = 0\,;\; w_{b-1} + w_{b+1} = 0\,;$$
$$w_{b-2} + w_{b+2} = 0\,. \quad (16)$$

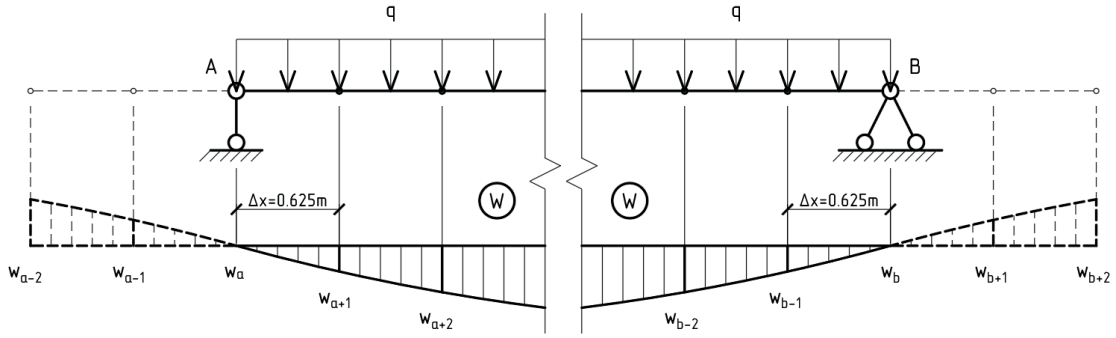

Figure 4. Accounting for boundary conditions in a finite difference scheme

The solution of a system of linear algebraic equations involves an iterative calculation process. This task was solved using the built-in iterative processor in Microsoft Excel 2010. The maximum number of iterations was 32767 with the accuracy of the calculation $1 \cdot 10^{-6}$. Thus, the maximum deflection of the beam, determined by the above method (MKR), taking into account the degradation function $F(B) = 0{,}827$ was $w_{max} = 53{,}013\ mm$.

The discrepancies in the values with the previous calculations turned out to be insignificant, however, it is important to note that the beam was loaded by 16,91% of the destructive load, as evidenced by the magnitude of the relative deformations in the middle of the span $\varepsilon = 0{,}00101$, while the limit deformations for this material $\varepsilon_{bu} = 0{,}006$. That is, the beam material under such a load works linearly elastic.

According to clause 15.1.1 of SP 20.13330.2016, when calculating building structures for the second group of limit states, the condition must be met:

$$w \le w_u\,, \qquad (17)$$

where is w – the deflection and displacement of the structural element (or the structure as a whole), determined taking into account the factors affecting their values;

w_u – the maximum deflection or displacement established by the norms. For a beam with a span of 10 m, the maximum deflection is 0,0478 m.

In order to predict the moment of the onset of the limit state for the 2 group of limit states, as a result of the influence of an aggressive environment, taken into account with the help of the degradation function, the formula can be used:

$$w_{F(B)} = \frac{w_0}{F(B)}\,, \qquad (18)$$

where is w_0 – the initial deflection (before the start of the aggressive environment).

Therefore, solving the inverse problem, it is possible to determine the critical value of the degradation function at which the limiting state occurs:

$$F(B)_{cr} = \frac{w_0}{w_u} = \frac{0{,}0437}{0{,}0478} = 0{,}914\,. \qquad (19)$$

The graph of the change in the degradation function $F(B)$ over time (Fig. 5) can be approximated with a high degree of accuracy by higher-order polynomial dependencies, however, for this particular case, the accuracy of the approximation turns out to be high already when using the quadratic equation.

Substituting the limiting value of the degradation function (19) into the quadratic equation shown in the graph (Fig. 5) instead of the value y, obtain an expression for determining the approximate moment of time x of the onset of the limiting state:

$$y = 9{,}5712 \cdot 10^{-7} \cdot x^2 - 5{,}0601 \cdot 10^{-5} \cdot x + 8{,}6421 \cdot 10^{-2} = 0\,. \qquad (20)$$

Solving the quadratic equation (20) obtain $x \approx 275\ day$ (Fig. 5).

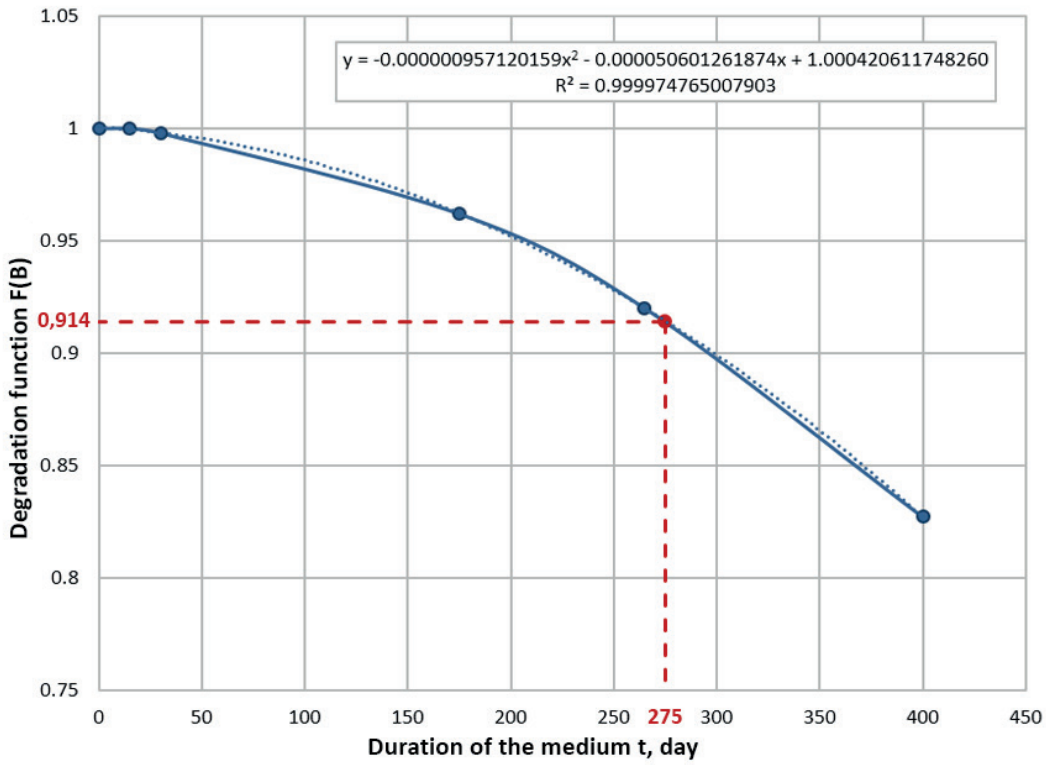

Figure 5. Dependence of the degradation function $F(B)$ on the duration of the medium t, day for the conditions according to Table 1

CONCLUSIONS

Thus, based on the above, the following conclusions can be made:

1. In the work, numerical methods of Ritz-Timoshenko and finite differences were used to determine the deflections of a polyester composite beam. The control calculation of the design in question was performed in the Lira-CAD 2013 PC, thereby confirming the correctness of the proposed automation algorithms for MRI and MD in the Microsoft Excel 2010 program.
2. In the calculation formulas of the methods under consideration, an additional mathematical dependence was introduced, which is a degradation function of the stiffness of the bent element. Thanks to this, it was possible to determine the deflections of the beam taking into account the aggressive effects of the environment, in this particular case – water.
3. It was found that the limit state for the second group, for a polyester composite beam, taking into account a given uniformly distributed load, occurs already at the linear elastic stage of the material. Thus, it can be concluded that the geometric parameters of the bent element under consideration are not optimal, therefore, the solution of the optimization problem is required.
4. In the work, the value of the limiting degradation function of stiffness was determined, at which the limit state for the structure occurs in the second group.
5. The construction of a graphical interpretation of the dependence of the degradation function of stiffness on the duration of the aggressive medium, followed by approximation by polynomial dependencies, allowed us to determine with a sufficient degree of accuracy the moment of the onset of the limiting state of the structure for the second group.

REFERENCES

1. **Selyaev V.P., Selyaev P.V., Sorokin E.V., Kechutkina E.L.** Forecasting the durability of reinforced concrete bending elements by the method of degradation functions. // Housing construction Vol. 12, 2014, pp. 8-12.
2. **Selyaev V.P., Selyaev P.V., Sorokin E.V., Kechutkina E.L.** Evaluation of the strength of structural elements made of cement composites exposed to the action of an aggressive environment. // Bulletin of the Volga State Technological University. Ser.: Materials. Constructions. Technologies Vol. 1(5), 2018, pp. 58-64.
3. **Selyaev V.P., Selyaev P.V., Sorokin E.V., Kechutkina E.L.** Assessment of the influence of chemically active aggressive media on the degradation of composites. // Durability of building materials, products and structures, 2018, pp. 170-174.
4. **Yao Y., Wang Z., Wang L.** Durability of concrete under combined mechanical load and environmental actions: A review. // Journal of Sustainable Cement-Based Materials Vol. 1(2), 2012, pp. 2-15.
5. **Vorechovska D., Somodikova M., Podrouzek J., Lehky D., Teply B.** Concrete structures under combined mechanical and environmental actions: Modelling of durability and reliability. // Computers and Concrete Vol. 1, 2017, pp. 99-110.
6. **Wittmann F.H., Zhao T., Jiang F., Wan X.** Influence of combined actions on durability and service life of reinforced concrete structures exposed to aggressive environment. // Restoration of Buildings and Monuments Vol. 2, 2012, pp. 105-112.
7. **Glasser F.P., Marchand J., Samson E.** Durability of concrete – Degradation phenomena involving detrimental chemical reactions. // Cement and Concrete Research Vol. 2, 2008, pp. 226-246.
8. **Basheer L., Kropp J., Cleland D.J.** Assessment of the durability of concrete from its permeation properties: a review. // Construction and building materials Vols. 2-3, 2001, pp. 93-103.
9. **Rzhanitsyn A.R.** Teoriya rascheta stroitel'nykh konstruktsiy na nadezhnost' [The theory of calculating building structures for reliability]. Moscow, Stroyizdat, 1978, 239 pages (in Russian).
10. **Solomatov V.I., Selyaev V.P., Sokolova Yu.A.** Khimicheskoye soprotivleniye materialov [Chemical resistance of materials]. Moscow, RAASN, 2001, 284 pages (in Russian).
11. **Karpenko N.I., Karpenko S.N., Yarmakovsky V.N., Erofeev V.T.** On modern methods of ensuring the durability of reinforced concrete structures. // Academia. Architecture and construction Vol. 1, 2015, pp. 93-102.
12. **Pujonto L.M.** Dolgovechnost' zhelezobetonnykh konstruktsiy sooruzheniy [Durability of reinforced concrete structures of structures]. Moscow, ASV, 2004, 423 pages (in Russian).
13. **Stepanova V.F., Falikman V.R.** Problems of ensuring the durability of concrete and reinforced concrete structures today. // Second Polakov Readings: Collection of scientific articles based on the materials of the international scientific and technical conference dedicated to the 105th anniversary of the birth of prof. Alexei Filippovich Polak, 2017, pp. 97-111.
14. **Stepanova V.F., Falikman V.R., Koroleva E.N.** Monitoring and analysis of regulatory documents in the field of design of reinforced concrete structures according to their life cycle. // Construction Materials Vol. 7, 2018, pp. 14-19.
15. **Bolotin V.V.** Metody teorii veroyatnostey i teorii nadezhnosti v raschetakh sooruzheniy [Methods of the theory of probability and the theory of reliability in the calculations of structures]. Moscow, Stroyizdat, 1982, 351 pages (in Russian).
16. **Selyaev V.P., Selyaev P.V., Petrov I.S.** Probabilistic methods for assessing the durability of reinforced concrete bending ele-

ments. // Academia. Architecture and construction Vol. 3, 2009, pp. 87-90.
17. **Solomatov V.I., Selyaev V.P.** Chemical resistance of concrete. // Concrete and reinforced concrete Vol. 8, 1984, pp. 16-17.
18. **Petrov V.V., Ovchinnikov I.G., Shikhov Yu.M.** Raschet elementov konstruktsiy, vzaimodeystvuyushchikh s agressivnoy sredoy [Calculation of structural elements interacting with an aggressive environment]. Saratov, Izdatel'stvo Saratovskogo universiteta, 1987, 288 pages (in Russian).
19. **Tuutti K.** Korroziya stali v betone. Shvedskiy institut issledovaniy tsementa i betona [Corrosion of steel in concrete]. Stockholm, Shvedskiy institut issledovaniy tsementa i betona, 1982, 469 pages (in Russian).
20. **Bazant Z.** Physical model for steel corrosion in concrete sea structures theory. // Journal of the Structural Division Vol. 105 (ST6), 1979, pp. 1137-1153.
21. **Zhuravleva V.N., Selyaev V.P., Solomatov V.I.** Calculation of flexible polymer concrete elements interacting with aggressive media. // Technology and mechanization of waterproofing works of industrial, civil and energy structures, 1983, pp. 78-80.
22. **Zhuravleva V.N., Selyaev V.P., Solomatov V.I.** Experimental method for determining degradation functions for polymer concrete. // Improving the durability of concrete transport structures, 1980, pp. 86-95.
23. **Selyaev V.P.** Osnovy teorii rascheta kompozitsionnykh konstruktsiy s uchetom deystviya agres-sivnykh sred: Avtoreferat dissertatsii doktora tekhnicheskikh nauk [Fundamentals of the theory of calculation of composite structures taking into account the action of aggressive area: Abstract of the dissertation of Doctor of Technical Sciences]. Moscow, 1984, 36 pages (in Russian).
24. **Zhuravleva V.N., Selyaev V.P., Solomatov V.I.** Degradation models for structural polymer concrete. // Improving the durability of concrete of transport structures, 1982, pp. 27-31.
25. **Selyaev V.P., Selyaev P.V.** Fiziko-khimicheskiye osnovy mekhaniki razrusheniya tsementnykh kompozitov: monografiya **[**Physicochemical foundations of fracture mechanics of cement composites: monograph]. Saransk, Izdatel'stvo Mordovskogo universiteta, 2018, 220 pages (in Russian).
26. **Selyaev V.P., Selyaev P.V., Gryaznov S.Yu., Babushkina D.R.** Verification of dependencies approximating the deformation diagrams of cement and polymer concretes by the method of standardized indicators. // Construction and reconstruction Vol. 1(93), 2021, pp. 125-133.
27. **Selyaev V.P., Utkina V.N., Gryaznov S.Yu., Babushkina D.R.** Determination of deflections of a beam from a nonlinear elastic material by the Ritz-Timoshenko method when approximating deformation diagrams by combined power dependences. // Expert: theory and practice Vol. 2(11), 2021, pp. 42-50.
28. **Petrov V.V., Krivoshein I.V.** Metody rascheta konstruktsiy iz nelineyno-deformiruyemogo materiala [Methods for calculating structures made of nonlinearly deformable material]. Moscow, ASV, 2008, 208 pages (in Russian).

СПИСОК ЛИТЕРАТУРЫ

1. **Селяев В.П., Селяев П.В., Сорокин Е.В., Кечуткина Е.Л.** Прогнозирование долговечности железобетонных изгибаемых элементов методом деградационных функций. // Жилищное строительство, 2014, №12, с. 8-12.
2. **Селяев В.П., Селяев П.В., Сорокин Е.В., Кечуткина Е.Л.** Оценка прочности элементов конструкций из цементных композитов, подверженных действию агрессивной среды. // Вестник Поволжского государственного технологического университета. Сер.: Материалы. Кон-

струкции. Технологии, 2018, № 1(5), с. 58-64.
3. **Селяев В.П., Селяев П.В., Сорокин Е.В., Кечуткина Е.Л.** Оценка влияния химически активных агрессивных сред на процесс деградации композитов. // Долговечность строительных материалов, изделий и конструкций, 2018, с. 170-174.
4. **Yao Y., Wang Z., Wang L.** Durability of concrete under combined mechanical load and environmental actions: A review. // Journal of Sustainable Cement-Based Materials, 2012, № 1(2), pp. 2-15.
5. **Vorechovska D., Somodikova M., Podrouzek J., Lehky D., Teply B.** Concrete structures under combined mechanical and environmental actions: Modelling of durability and reliability. // Computers and Concrete, 2017, № 1, pp. 99-110.
6. **Wittmann F.H., Zhao T., Jiang F., Wan X.** Influence of combined actions on durability and service life of reinforced concrete structures exposed to aggressive environment. // Restoration of Buildings and Monuments, 2012, № 2, pp. 105-112.
7. **Glasser F.P., Marchand J., Samson E.** Durability of concrete – Degradation phenomena involving detrimental chemical reactions. // Cement and Concrete Research, 2008, № 2, pp. 226-246.
8. **Basheer L., Kropp J., Cleland D.J.** Assessment of the durability of concrete from its permeation properties: a review. // Construction and building materials, 2001, № 2-3, pp. 93-103.
9. **Ржаницын А.Р.** Теория расчета строительных конструкций на надежность. – М.: Стройиздат, 1978. – 239 с.
10. **Соломатов В.И., Селяев В.П., Соколова Ю.А.** Химическое сопротивление материалов, 2-е изд., перераб. и дополн. – М.: РААСН, 2001. – 284 с.
11. **Карпенко Н.И., Карпенко С.Н., Ярмаковский В.Н., Ерофеев В.Т.** О современных методах обеспечения долговечности железобетонных конструкций. // Academia. Архитектура и строительство, 2015, № 1, с. 93-102.
12. **Пухонто Л.М.** Долговечность железобетонных конструкций сооружений. – М.: АСВ, 2004. – 423 с.
13. **Степанова В.Ф., Фаликман В.Р.** Проблемы обеспечения долговечности бетонных и железобетонных конструкций сегодня. // Вторые Полаковские чтения: Сб. науч. статей по материалам международной науч.-тех. конференции, посвященной 105-летию со дня рождения проф. Алексея Филипповича Полака, 2017, с. 97-111.
14. **Степанова В.Ф., Фаликман В.Р., Королева Е.Н.** Мониторинг и анализ нормативных документов в области проектирования железобетонных конструкций по их жизненному циклу. // Строительные материалы, 2018, № 7, с. 14-19.
15. **Болотин В.В.** Методы теории вероятностей и теории надежности в расчетах сооружений. – М.: Стройиздат, 1982. – 351 с.
16. **Селяев В.П., Селяев П.В., Петров И.С.** Вероятностные методы оценки долговечности железобетонных изгибаемых элементов. // Academia. Архитектура и строительство, 2009, № 3, с. 87-90.
17. **Соломатов В.И., Селяев В.П.** Химическое сопротивление бетонов. // Бетон и железобетон, 1984, № 8, с. 16-17.
18. **Петров В.В. Овчинников И.Г., Шихов Ю.М.** Расчет элементов конструкций, взаимодействующих с агрессивной средой. – Саратов: Сарат. ун-т, 1987. – 288 с.
19. **Tuutti K.** Corrosion of stel in concrete. Swedish Cement and Concrete Research Inst. – Stockholm, 1982. – 469 p.
20. **Bazant Z.** Physical model for steel corrosion in concrete sea structures theory. // Journal of the Structural Division, 1979, № 105 (ST6), pp. 1137-1153.
21. **Журавлева В.Н., Селяев В.П., Соломатов В.И.** Расчет изгибаемых полимербетонных элементов, взаимодействующих с агрессивными средами. // Технология и механизация гидроизоляцион-

ных работ промышленных, гражданских и энергетических сооружений, 1983, с. 78-80.
22. **Журавлева В.Н., Селяев В.П., Соломатов В.И.** Экспериментальный метод определения деградационных функций для полимербетонов. // Повышение долговечности бетона транспортных сооружений, 1980, с. 86-95.
23. **Селяев В.П.** Основы теории расчета композиционных конструкций с учетом действия агрессивных сред: Автореф. дисс. д-ра техн. наук. – М., 1984. – 36 с.
24. **Журавлева В.Н., Селяев В.П., Соломатов В.И.** Модели деградации конструкционных полимербетонов. // Повышение долговечности бетонов транспортных сооружений, 1982, с. 27-31.
25. **Селяев В.П., Селяев П.В.** Физико-химические основы механики разрушения цементных композитов: монография. – Саранск: Изд-во Мордов. ун-та, 2018. – 220 с.
26. **Селяев В.П., Селяев П.В., Грязнов С.Ю., Бабушкина Д.Р.** Верификация зависимостей, аппроксимирующих диаграммы деформирования бетонов цементного и полимерного методом нормируемых показателей. // Строительство и реконструкция, 2021, № 1(93), с. 125-133.
27. **Селяев В.П., Уткина В.Н., Грязнов С.Ю., Бабушкина Д.Р.** Определение прогибов балки из нелинейно-упругого материала методом Ритца-Тимошенко при аппроксимации диаграмм деформирования комбинированными степенными зависимостями. // Эксперт: теория и практика, 2021, № 2(11), с. 42-50.
28. **Петров В.В., Кривошеин И.В.** Методы расчета конструкций из нелинейно-деформируемого материала. – М.: АСВ, 2008. – 208 с.

Vladimir P. Selyaev, Academician of the Russian Academy of Architectural and Construction Sciences, Professor, Doctor of Technical Sciences, National Research Ogarev Mordovian State University, Head of the Department of Building Structures; 430006, Russia, Saransk, Bolshevistskaya St., 68; phone: +7 (8342) 47-71-56, e-mail: ntorm80@mail.ru.

Sergey Yu. Gryaznov, Postgraduate student of the Department of Building Structures, National Research Ogarev Mordovian State University; 430006, Russia, Saransk, Bolshevistskaya St., 68; e-mail: sergey.gryaznov.97@mail.ru.

Delmira R. Babushkina, Postgraduate student of the Department of Building Structures, National Research Ogarev Mordovian State University; 430006, Russia, Saransk, Bolshevistskaya St., 68; e-mail: delmira2009@yandex.ru.

Селяев Владимир Павлович, Академик РААСН, профессор, доктор технических наук, Национальный исследовательский Мордовский государственный университет им. Н.П. Огарёва, заведующий кафедрой строительных конструкций; 430006, Россия, г. Саранск, ул. Большевистская, д. 68; тел.: +7 (8342) 47-71-56, e-mail: ntorm80@mail.ru.

Грязнов Сергей Юрьевич, аспирант кафедры строительных конструкций, Национальный исследовательский Мордовский государственный университет им. Н.П. Огарёва; 430006, Россия, г. Саранск, ул. Большевистская, д. 68; e-mail: sergey.gryaznov.97@mail.ru.

Бабушкина Дельмира Рафиковна, аспирант кафедры строительных конструкций, Национальный исследовательский Мордовский государственный университет им. Н.П. Огарёва; 430006, Россия, г. Саранск, ул. Большевистская, д. 68; e-mail: delmira2009@yandex.ru.

International Journal for Computational Civil and Structural Engineering, 18(2) 98–111 (2022)

DOI:10.22337/2587-9618-2022-18-2-98-111

TEMPERATURE DEFORMATIONS OF PVC WINDOW PROFILES WITH REINFORCEMENT

Ivan S. Aksenov, Aleksandr P. Konstantinov

National Research Moscow State University of Civil Engineering, Moscow, RUSSIA

Abstract. Modern window structures made of PVC profiles can experience significant temperature deformation during both winter and summer operation. This effect is not considered in the current engineering methods of PVC windows calculation, which causes a number of problems in their operation (freezing and blowing through the windows, the failure of fittings, etc.). The use of laboratory methods of testing windows for temperature loads is limited due to their labor intensity and the high cost of testing equipment. We propose to develop an engineering method for calculating the mechanical operation of PVC windows under the action of temperature loads, which can be used at an early stage of design. One of the stages of its creation is a theoretical description of the temperature deformation of a PVC window profile when it works together mechanically with a reinforcing core. The article describes the nature of the forces transmitted by the PVC profile on the core during thermal bending (the case of temperature deformation at negative outside temperatures is considered). It was proposed to decompose these forces into two components: longitudinal, caused by different values of temperature shrinkage of PVC profile and reinforcing core, and transverse, caused by thermal bending of PVC profile. Mathematical models have been developed to calculate both force components and temperature deformation of the profile at different numbers and spacing of attachment points. A physical model has been proposed for implementation in the numerical calculation program, which allows a more accurate description of the temperature deformation of a long profile. Calculation of the test problem according to the proposed methodology and by means of full-fledged three-dimensional finite-element modeling in the COMSOL Multiphysics program was performed. A comparison of the results showed a discrepancy of less than 10%. It was found that the key influence on the deformations of PVC window profiles with a reinforcing core will have characteristics of the outermost joints "PVC profile – reinforcing core", because the greatest forces arise in them under the action of temperature loads.

Keywords: PVC windows, temperature deformation, finite-element modeling, COMSOL Multiphysics, PVC profiles.

ТЕМПЕРАТУРНЫЕ ДЕФОРМАЦИИ ОКОННЫХ ПРОФИЛЕЙ ПВХ С УЧЕТОМ АРМИРОВАНИЯ

И.С. Аксенов, А.П. Константинов

Национальный исследовательский Московский государственный строительный университет, г. Москва, РОССИЯ

Аннотация. Современные оконные конструкции из ПВХ профилей могут испытывать значительные температурные деформации как в зимний, так и летний период эксплуатации. Данный эффект не учитывается в действующих инженерных методах расчета окон ПВХ, что становится причиной ряда проблем при их эксплуатации (промерзание и продувание окон, нарушение работы фурнитуры и т.д.). Применение лабораторных методов испытаний окон на действие температурных нагрузок носит ограниченный характер из-за их трудоемкости и высокой стоимости испытательного оборудования. Предлагается к разработке инженерный метод расчета механической работы ПВХ окон при действии температурной нагрузки, который может быть использован на ранней стадии проектирования подобных конструкций. Одним из этапов его создания является теоретическое описание температурных деформаций оконного ПВХ профиля при его совместной механической работе с армирующим сердечником. В статье описан характер усилий, передаваемых ПВХ профилем на сердечник при температурном изгибе (рассмотрен случай температурных деформаций при отрицательных температурах наружного воздуха). Предложено разложить эти усилия на две

компоненты: продольную, обусловленную различной величиной температурной усадки ПВХ профиля и армирующего сердечника, и поперечную, обусловленную температурным изгибом ПВХ профиля. Разработаны математические модели, позволяющие рассчитать как обе компоненты усилий, так и температурные деформации профиля при различном количестве и шаге точек крепления. Предложена физическая модель для реализации в программе численного расчета, позволяющая более точно описать температурные деформации профиля большой длины. Выполнен расчет тестовой задачи по предложенной методике и средствами полноценного трехмерного конечно-элементного моделирования в программе COMSOL Multiphysics. Сравнение результатов показало расхождение менее 10%. Установлено, что ключевое влияние на деформации оконных профилей ПВХ с армирующим сердечником будут оказывать характеристики крайних узлов соединения «ПВХ профиль – армирующий сердечник», т.к. именно в них возникают наибольшие усилия при действии температурных нагрузок.

Ключевые слова: ПВХ окна, температурные деформации, конечно-элементное моделирование, COMSOL Multiphysics, ПВХ профили.

1. INTRODUCTION

Currently, the quality assessment of windows is based on the use of declared (nominal) values of their technical and operational characteristics. Nominal technical and operational characteristics of windows are determined under standard laboratory test conditions without reference to the actual climatic conditions of operation [1]. Thus, most standards for test methods of air permeability of windows (EN 1026 in Europe, ASTM E283 – in North America, GOST 26602.2 – in Russia) requires tests at the same and constant temperature on both sides of the window [2–4]. This approach is reasonable and appropriate for the purpose of comparing the products of individual manufacturers with each other. However, this does not correspond to the real operating conditions of windows during the cold season, when their tightness becomes an important factor influencing the quality of the microclimate in the room [5–8]. Temperature loads lead to deformation of the profile elements of the window. This leads to a decrease in the compression force of window seals, which violates the tightness of the window and can increase its air permeability by several times compared with the results of standard tests [9,10]. For the first time this phenomenon was studied in 1970 in the work [11] where it was found experimentally that the air permeability of windows with double vertical sliding sash increases with decreasing outside air temperature. A very important work in the topic under study is the work [12]. It discusses the disadvantages of the method used in the USA (at the time of 1985 year) for determining the air permeability of window structures (ASTM E283). One of the criticism points is precisely the lack of consideration of temperature loads. The author proposed to develop a new method for testing the air permeability of windows, taking into account the temperature load. This method has been implemented in the new ASTM E1424 – 91 standards, which now runs parallel to ASTM E283. In the Russian Federation, the methodology for determining the air permeability of window structures with regard to temperature effects was patented in 2012 [13], but it has never become mandatory.

Studies on the subject in Western Europe and North America have ceased since the publication of the work [10] in 1998. The work evaluated the effect of changes in the air permeability of windows when the outside temperature decreases on the energy balance of the building. As a result, it was concluded that this phenomenon has an insignificant effect on the energy balance of the building and therefore in the daily design activities it can be neglected. However, these results were obtained at the design temperature of the outside air during the heating period of -5°C, which is acceptable for the countries of Europe, but unacceptable for countries with cold climate [14–16]. In the Russian Federation the

problem of temperature deformation of window structures and their impact on air permeability, on the contrary, began to receive attention in recent years. A number of experiments have been conducted, which confirm the conclusions of earlier studies – the air permeability of window structures may increase 3-10 times when the outside air temperature decreases to -30...-50°C [17–20]. The works [21,22] show that temperature deformation of modern PVC and aluminum windows in winter conditions can be comparable to deformations from wind load. In the work [23], which was the result of a large number of laboratory tests, it is proposed to develop a set of criteria for the applicability of windows for different climatic operating conditions, and the temperature deformation are considered in this case as one of the mandatory factors to be taken into account.

Methods of experimental investigation of window temperature deformation, with all their obvious advantages, have significant limitations: the complexity and high cost of the necessary test equipment, significant time and labor costs to conduct tests. Accordingly, it seems appropriate to develop a theoretical method for calculating the temperature deformation of windows, which would allow the engineer to make effective design decisions. To date, only a limited number of papers have attempted to study the temperature deformation of modern windows by analytical or numerical methods. The authors of this paper previously published an article [24] in which they examined in detail the bending process of unreinforced PVC window profile from the action of temperature load, taking into account the actual temperature distribution in its cross section. The present article deals with the joint operation of the PVC profile and the reinforcing core.

2. METHODS

In winter conditions, there are temperature differences on different sides of the window. Its value depends on the climatic region of construction, and in the Russian Federation can reach up to 60°C. As a consequence, the profile elements of the window undergo a bend in the direction of the warm room. The presence of steel reinforcing core significantly affects the nature of deformation of PVC window profile under temperature load. PVC profile is connected to the core by means of self-tapping screws, the number and pitch of self-tapping screws may vary depending on the length of the profile. As it was found out [24], the temperature field arising in the cross section of the steel core is practically homogeneous (due to the large value of the thermal conductivity coefficient of steel [25]). This means that the core experiences only longitudinal temperature deformations and remains straight, while the PVC profile tends to bend. For simplicity, let us assume that the forces between the core and the PVC profile are transmitted only at the joints of the self-tapping screws (in other words, we will not consider the contact interactions, which in the general case may occur in the problem under consideration). Since the stiffness of the reinforcing core is many times greater than the stiffness of the PVC profile, at the first stage we will consider the core as an absolutely rigid body. Let us also neglect the fact that the locations of the self-tapping screws (and, therefore, the forces occurring in them) are eccentric with respect to the neutral axes of the PVC profile and the core, and we will consider these forces to be centrally applied. The forces occurring at the connection points of the profile and the core will have both longitudinal and transverse components (see figure 1). Transverse components are due to the tendency of the PVC profile to bend, they compensate for this bend. The longitudinal components are due to the difference in longitudinal temperature deformations of the profile and the core.

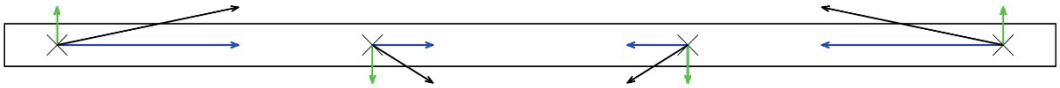

Figure 1 – Forces transmitted from PVC profile to reinforcing core (at 4 attachment points)

To determine the magnitude of these forces, we use the superposition principle. Let us assume that due to the smallness of the deformations of the PVC profile, their longitudinal and transverse components can be found independently of each other.

2.1 Determining the longitudinal force components

Assume that the profile and the reinforcing core experience only longitudinal temperature deformations. We will look for the solution in general form (see Figure 2). Let the PVC profile has an arbitrary length and is connected to the reinforcing core with m fasteners (the distances between the fasteners can also be arbitrary). Each fastener has two points: one referring to the core (we will denote the coordinate of this point by a capital letter *"X"*), the other referring to the PVC profile (we will denote the coordinate of this point by a lowercase letter *"x"*). Initially, the X and x coordinates are the same in each fixture: $X_i = x_i$

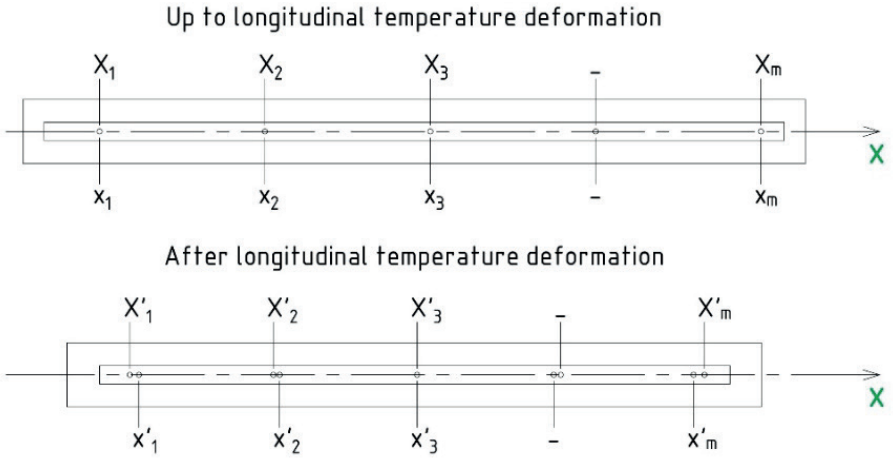

Figure 2. Physical model for determining the longitudinal forces at the attachment points

As a result of temperature stresses, the reinforcing core changes its length (its corresponding attachment points move and occupy a new position *X'*). Since the core is regarded as an absolutely rigid body, then:

$$X'_i = X_i(1+\alpha_s(T_m - T_{ref})) \quad (*)$$
$$X_1 = 0 \Rightarrow X'_1 = 0$$

PVC has a much higher coefficient of linear thermal expansion than steel, so when PVC cools down, the profile shrinks much more than the core (in the problem at hand we calculate exactly for winter operating conditions). Free shrinkage of the PVC profile is prevented by the forces generated at the fixing points. The PVC profile is stretched in this process. As a result of the deformation, the attachment points belonging to the PVC profile move from the old position x to the new position *x'*. At the same time, due to the supposed suppleness of the mount, the points *X'* and *x'* belonging to the same mount can move relative to each other, and a force occurs between them $|H_i| = \xi_x \cdot |X'_i - x'_i|$. The

conditions described above are mathematically expressed by the following system of equations:

$$\begin{cases} x'_2 - x'_1 = (x_2 - x_1)k_{ax}^{unc}\left(\dfrac{N_1}{E_{PVC}A} + 1\right) \\ x'_3 - x'_2 = (x_3 - x_2)k_{ax}^{unc}\left(\dfrac{N_2}{E_{PVC}A} + 1\right) \\ \vdots \\ x'_m - x'_{m-1} = (x_m - x_{m-1})k_{ax}^{unc}\left(\dfrac{N_{m-1}}{E_{PVC}A} + 1\right) \quad (**) \\ N_1 = \xi_x(x'_1 - X'_1) \\ N_2 - N_1 = \xi_x(x'_2 - X'_2) \\ \vdots \\ N_{m-1} - N_{m-2} = \xi_x(x'_{m-1} - X'_{m-1}) \\ -N_{m-1} = \xi_x(x'_m - X'_m) \end{cases}$$

where $k_{ax}^{unc} = \varepsilon_{ax}^{unc} - 1$ is the coefficient of longitudinal deformation of the PVC profile axis at unconstrained temperature deformation (see [24]) and N_i is the longitudinal force between the i and i+1 attachment points.

Equations (**) with account of (*) form a linear closed system that can be solved by the matrix method. By solving this system, we can find the vector of unknown quantities and determine the magnitude of longitudinal forces arising in the PVC profile.

2.1 Determining the traverse force components

Assume that the PVC profile attachment points to the reinforcing core can slide freely along the core axis. Then, when bending the PVC profile at the connection points only transverse forces will occur. Consider a few cases:

1. PVC profile is connected to the core with 2 self-tapping screws (true for short profiles);
2. PVC profile is connected to the core with 3 self-tapping screws;
3. PVC profile is connected to the core with 4 self-tapping screws;
4. PVC profile is connected to the core with more than 4 self-tapping screws.

2.2.1 Two attachment points

In the first case, no transverse force will occur at the two connection points. PVC profile will curve freely with the curvature K_{unc} (profile curvature at unconstrained temperature deformation – see [24]), the distance between the mounting points will be reduced (because they can freely slide along the core). Now apply a force N to the sliding attachment points, determined by the method described in the previous section. This takes into account that the PVC profile at the same time as bending also experiences tension. After the longitudinal force is applied, the deflection of the PVC rod will decrease. Calculation of deflections, in which the influence of the longitudinal force is taken into account, will give more accurate results, but will also lead to more complex calculation formulas. On the contrary, neglecting the influence of the longitudinal force will result in simpler calculation formulas, but at the same time a less accurate result Table 1 shows a comparison of the analytical solution for bending of the profile axis in two these statements. The calculation scheme of the problem is shown in Figure 3. The calculation takes into account that in the case of small displacements, the curvature of the profile is equal to the second derivative of the deflection function.

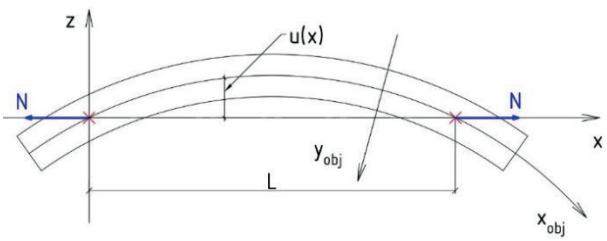

Figure 3 – Calculation scheme

Table 1. Analytical solution for different formulations of the problem

	Taking into account N (1)	Excluding N (2)
The analytical solution	$u(x)=\frac{K_{unc}EI}{N}\left(\frac{e^{\omega x}+e^{\omega(L-x)}}{1+e^{\omega L}}-1\right)$	$u(x)=\frac{K_{unc}}{2}x^2-\frac{K_{сб}L}{2}x$
The maximum deflection	$u_{\text{m}}=-\frac{K_{unc}EI}{N}\cdot\frac{(1-e^{\frac{\omega L}{2}})^2}{1+e^{\omega L}};\ \omega=\sqrt{\frac{N}{EI}}$	$u_{\text{m}}=-\frac{K_{unc}L^2}{8}$

The maximum possible step between the screws when attaching the reinforcing core to PVC profiles is determined by the technological recommendations of PVC profile manufacturers, but usually not more than 400 mm. Comparative calculations on specific examples showed that the difference between the values of maximum deflection calculated according to formulas (1) and (2) of Table 1 is the greater the parameter L is. At L = 0.4 m this difference is about 1.5% (the maximum deflection in this case reaches about 1 mm). Such a difference can be neglected and the deflections can be calculated using the simpler formulas (2) in Table 1. Note that if the maximum deflection of the PVC profile is less than the gap that exists between the reinforcing core and the PVC profile, then there will be no contact between them, otherwise the PVC profile will be pressed (central part) into the wall of the reinforcing core and the calculation scheme will change, in the joints there will be transverse forces.

2.2.2 Three attachment points

In the second case, the central fixing point will prevent the free bending of the PVC profile. This will result in balanced lateral forces at the attachment points (see Figure 4).

In the previous example, it was found that the longitudinal force does not significantly affect the deflections of the profile. In this and the following sections of the paper, in addition to deflections, the transverse reaction forces (R) at the attachment points will also be determined. The attachment points of the PVC profile to the reinforcing core may in general also be malleable in the transverse direction. This allows them to shift relative to the center line of attachment. Let us assume that the value of this displacement is proportional to the shear force occurring in the anchorage $|R_i|=\xi_z|u_i|$. To estimate the most significant factors in determining the transverse reaction forces, the problem will be solved in 4 formulations:

1. Without taking into account N / Without taking into account compliance
2. Without taking into account N / Taking into account compliance
3. Taking into account N / Without taking into account compliance
4. Taking into account N / Taking into account compliance

Since the problem is symmetrical, there will be no longitudinal force at the central attachment point: the same tensile force N will act throughout the PVC profile. Due to the symmetry of the problem, it is sufficient to consider only half of the profile. Results of the analytical solution for the described statements of the problem are shown below, computational schemes are shown in Figure 4.

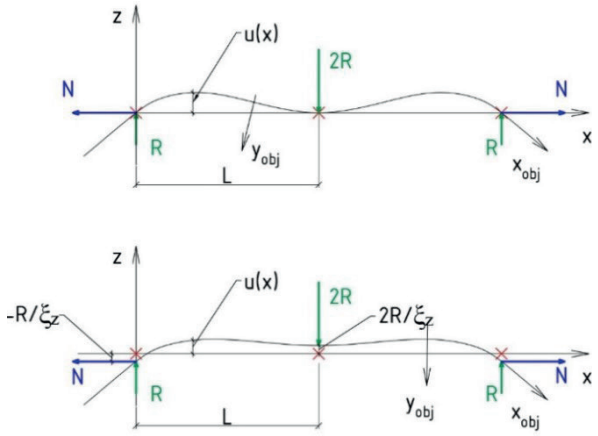

Figure 4. Calculation diagram (top – without taking into account compliance, bottom – taking into account compliance)

The equation for determining R:
1. Without consideration of compliance / without consideration of N:

$$R = -\frac{3K_{unc}EI}{2L}$$

2. Without consideration of compliance / with consideration of N:

$$R = -\frac{K_{unc}EI}{L}\cdot\frac{\left(1-e^{\omega L}\right)^2}{e^{2\omega L}+1-\dfrac{e^{2\omega L}-1}{\omega L}};\ \omega = \sqrt{\frac{N}{EI}}$$

3. With consideration of compliance / without consideration of N:

$$R = -\frac{K_{unc}EI}{L}\cdot\left(\frac{2}{3}+\frac{6EI}{L^3\xi_z}\right)^{-1}$$

4. With consideration of compliance / with consideration of N:

$$R = -\frac{K_{unc}EI}{L}\cdot\frac{\left(1-e^{\omega L}\right)^2}{\left(e^{2\omega L}+1\right)\left(1+\dfrac{3N}{\xi_z L}\right)-\dfrac{e^{2\omega L}-1}{\omega L}}$$

A comparative calculation on specific examples showed that the longitudinal forces have little effect, including on the values of transverse reaction forces (difference of about 3%). That is why here and in the following calculations they can be disregarded. At the same time, the joint compliance significantly reduces the value of transverse forces (by ≈30%), so it must be taken into account in the calculation.

2.2.3 Four attachment points

The calculation scheme for the considered case is shown in Figure 5. As justified above, the longitudinal forces will not be taken into account in determining the transverse reaction forces. The analytical solution for R is following:

$$R = -\frac{K_{unc}EI}{L_1}\cdot\frac{L_1+L_2}{\dfrac{4EI}{\xi_z {L_1}^2}+\dfrac{2}{3}L_1+L_2}$$

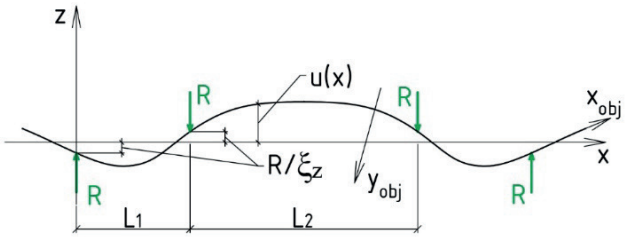

Figure 5. Calculation scheme

2.2.4 Joint compliance factor

In this article, two coefficients of the joint compliance "PVC profile – reinforcing core" were introduced in the calculations: longitudinal ξ_x and transverse ξ_z. The longitudinal compliance coefficient is caused by deformations of the connection node (local deformation of the profile wall, rotation of the screw under the action of the shear force). Calculations of the mechanical work of the profile together with the reinforcing core in the elastic formulation using a three-dimensional finite-element model allowed to estimate the value of ξ_x. It can be taken as $4.3\ldots5\cdot10^6$ N/m. The question of the effect of PVC plastic properties on the value of ξ_x remains open. The transverse compliance coefficient is due in large part to the bending stiffness of the reinforcing core itself – with transverse loads, the core bends and the attachment points shift relative to the center line. The value of this displacement is directly proportional to the value of the shear force (which corresponds to the introduced definition of the value ξ_z). These considerations allow us to obtain the equations for ξ_z:

for three attachment points – $\xi_z = 9\dfrac{E_s I_s}{L^3}$

for four attachment points – $\xi_z = \dfrac{E_s I_s}{{L_1}^3}\cdot\dfrac{12}{2+3\dfrac{L_2}{L_1}}$

With this in mind, the equations for R can be rewritten.

$$Rl_1 = -K_{unc}EI \Rightarrow R = -\frac{K_{unc}EI}{l_1}$$

2.2.5 More than 4 attachment points

With a larger number of attachment points, the outermost two (at the opposite ends of the profile) remain the most stressed, while there are almost no transverse forces at the central points. However, the redistribution of forces between the attachment points leads to a change in the shear forces arising at the extreme points with respect to those values determined by the formulas from the previous sections. The appearance of new attachment points violates the linear character of ξ_z, results in its increase (the core bends less at the same temperature moment), also the pairing of forces is violated: in the second attachment point from the edge, the shear force module will be slightly higher than in the first (by 8% tentatively). If this difference is neglected, then in first approximation we can assume that the pair of forces arising between the first attachment points fully compensates the temperature moment in the PVC profile section:

A more accurate determination of the transverse components of the reaction forces with a large number of attachment points is possible using a numerical solution. We can use the same physical model from which the formulas in section 2.2.4 were derived: two rods with different bending stiffness are connected at the attachment points by hinges, one of the rods tends to bend under the temperature load and bends the second rod by acting on it through the attachment points

3. RESULTS AND DISCUSSION

To check the correctness of the proposed methodology, a comparative calculation of the reinforced profile Veka system SL70 (see figure 6) on the temperature load was carried out. The same problem was solved analytically, as well as in the finite element modeling program COMSOL Multiphysics.

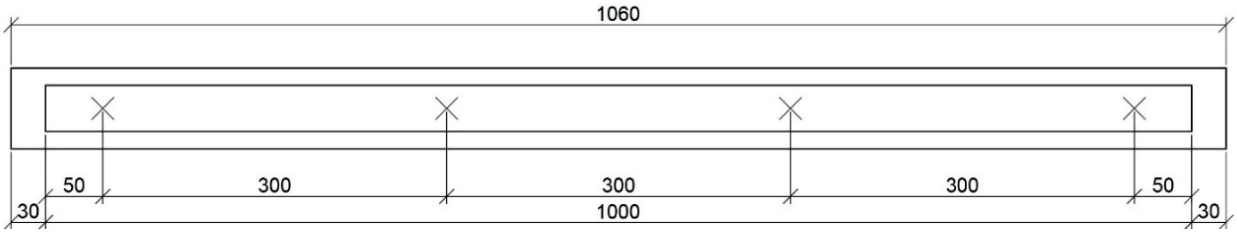

Figure 6. PVC profile with a length of 1,060 mm with a core of 1,000 mm, fastened with self-tapping screws in 4 places with the pitch of 300 mm

The calculation was performed for the following conditions: t_{ex} = -20°C; t_{in} = 20°C; $\alpha_в$ = 8.7 W/(m^2 °C); $\alpha_н$ = 23 W/(m^2 °C). For the profile in question its thermal resistance is known R_0 = 0.77 (m^2 °C)/W. The paper [24] described in detail how to use these data to calculate the temperature field in the cross section of the PVC profile (taking into account the reinforcing core) and to determine its parameters of free temperature deformation under the effect of this temperature field: the curvature (K_{unc}) and the longitudinal deformation coefficient (k_{ax}^{unc}). The results of the calculation using this method are shown in Figure 7. In this case, K_{unc} = -0,02567 1/m; $k_{ax}^{unc} = 0.998348$.

Let us write down all other necessary data for the calculation (see table 2).

Table 2. Calculation data

l_1	0.3 m	A_{PVC}	9.05 cm^2
l_2	0.3 m	E_{PVC}	$2.7\cdot10^9$ Pa
I_s	2.13 cm^4	α_{PVC}	$7\cdot10^{-5}$ K^{-1}
E_s	$2\cdot10^{11}$ Pa	ξ_x	$4.3\cdot10^6$ N/m
α_s	$1.2\cdot10^{-5}$ K^{-1}	T_m	-1.54 °C
I_{PVC}	58.62 cm^4	T_{ref}	20 °C

Solving the system of equations (*) and (**), we find: $N_1 = 1446$ N; $N_2 = 1855$ N; $N_3 = 1446$ N. Next, we determine the transverse force components:

$$R = -\frac{-0.02567\cdot2.7\cdot10^9\cdot58.62\cdot10^{-8}}{0.3}\cdot\frac{0.3+0.3}{\left(\frac{2}{3}\cdot0.3+0.3\right)\left(1+\frac{2.7\cdot58.62}{200\cdot2.13}\right)} = 118.5 \text{ N}$$

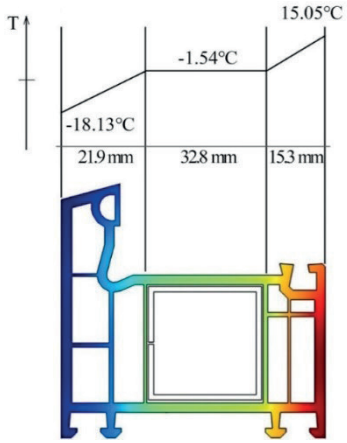

Figure 7. Temperature field

Thus, the forces acting on the reinforcing core from the PVC profile side will have the value shown in Figure 8.

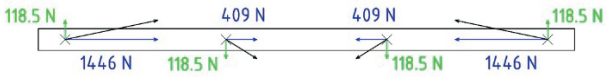

Figure 8. Forces acting on the core from the PVC profile side

In the COMSOL Multiphysics program (hereafter COMSOL), a similar problem was posed. The model created in COMSOL reflected the real three-dimensional geometry of the PVC profile and the core, all elements in it were considered to be perfectly elastic, at the points of self-tapping between the PVC profile and the core were given hinged connections. In the cross section of the profile elements, a temperature field similar to that shown in Figure 7 was set (see Figure 9).

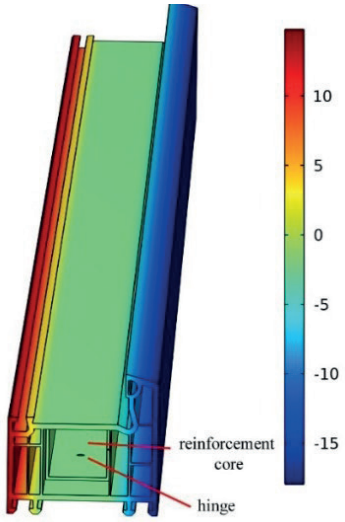

Figure 9. 3D model of the reinforced profile and the temperature field in it (legend in °C)

To ensure the uniqueness of the solution, the boundary conditions of the "Rigid Connector" type were imposed on the end faces of the PVC profile in a flexible type of connection: on one end, connections were imposed for movements in all directions and for rotation around the longitudinal axis of the profile (x axis), on the other end, only for movements along the y and z axes (free rotations). Such boundary conditions do not create any obstacles for internal deformations of the profile, but provide its fixed position in space. The results of the simulation are shown in Figure 10. The reaction forces in the joints connecting the PVC profile and the core are shown in the table 3.

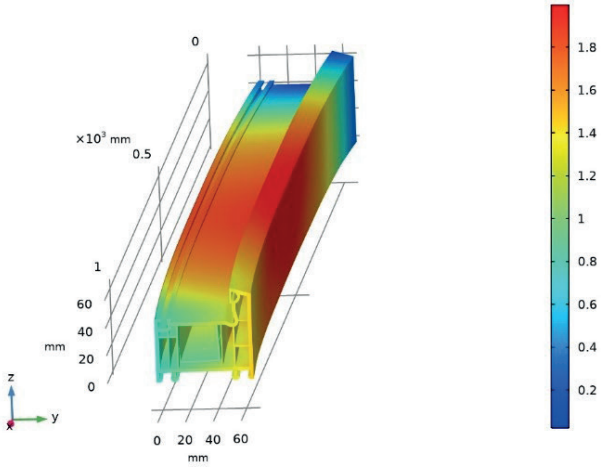

Figure 10. Deformations (legend in mm)

As can be seen, the results of the manual calculation according to the proposed method are in good agreement with the results of numerical modeling. The observed discrepancies are primarily due to the fact that the attachment points of the profile to the core (and consequently the application points of the reaction forces) are eccentric with respect to the neutral axes of the core and the profile itself, which causes: torsion (to which the metal core is more subject) and bending of the profiles not only around the z axis (axis position – see Figure 10), but also around the y axis. However, as part of the structure of the window, the PVC profile has less free deformation conditions. In this way the end edges of PVC profiles are rigidly connected to each other by welding, such a connection prevents the torsion of the profiles and their bending around the second axis (thereby bringing the real picture of the stress-strain state of the profile even closer to the model that was developed in this article). These prerequisites will make it possible to determine the forces occurring in the corner joints of PVC windows, which will be a topic for further work by the authors.

Table 3. Comparison of calculation results

No. of joint	Based on simulation results		Based on manual calculation results		Divergence, %	
	Longitudinal component	Transverse component	Longitudinal component	Transverse component	Longitudinal component	Transverse component
1	1325 H	110.3 H	1446 H	118.5 H	-9.1	-7.4
2	447 H	-110.3 H	409 H	-118.5 H	8.5	-7.4
3	-447 H	-110.3 H	-409 H	-118.5 H	8.5	-7.4
4	-1325 H	-110.3 H	-1446 H	118.5 H	-9.1	-7.4

4. CONCLUSION

In this work, a method of analytical calculation of the temperature deformation of a PVC profile reinforced with a metal core was proposed, thus:
1. The nature of the forces occurring at the attachment points of the reinforcing core to the PVC profile was described. The greatest forces occur in the extreme fasteners that fix the PVC profile to the reinforcing core. The compliance of these joints has a decisive influence on the deformation of PVC profiles under the action of temperature loads.
2. A mathematical model was developed to calculate the longitudinal components of the forces in the attachment points due to different values of temperature shrinkage of PVC profile and reinforcing core;
3. A mathematical model was developed to calculate the longitudinal components of the forces in the attachment points caused by the thermal bending of the PVC profile;
4. In order to increase the calculation accuracy with a large number of attachment points (for long profiles), a physical model of the joint mechanical operation of PVC profile and core

was proposed, this model is planned to be implemented in the numerical calculation program;

5. A comparative calculation of the bending of a reinforced PVC profile with a length of 1 m using the proposed methodology, as well as with the full three-dimensional finite-element modeling in the program COMSOL Multiphysics was carried out. Comparison of the calculation results showed convergence with an error of less than 10%.

The theoretical conclusions proposed in this article are part of a more extensive, currently under development methodology for calculating the mechanical operation of modern window structures with regard to temperature loads. This methodology will allow engineers to make effective decisions early in the design process and greatly reduce the amount of expensive and time-consuming laboratory testing.

In what follows, the authors propose to consider the following issues:

1. Influence of plastic properties of PVC on the value of the coefficient of transverse compliance of joints "PVC profile – reinforcing core" ξ_z;
2. Oblique bending of PVC profiles (this problem is especially acute for PVC profiles with a marked asymmetry of the cross-section);
3. Static operation of the nodes connecting the profile elements of the window with each other;
4. Influence of rigidity of translucent filling (insulating glass unit) and bracing elements of fittings on deformations of profile window elements.

REFERENCES

1. **Klems, J.H.** Methods of estimating air infiltration through windows. Energy and Buildings. 1983. 5(4). Pp. 243–252. DOI:10.1016/0378-7788(83)90012-9.
2. **Provan, T.F., Younger, J.D.** Air infiltration characteristics of windows. Energy and Buildings. 1986. 9(4). Pp. 281–292. DOI:10.1016/0378-7788(86)90033-2.
3. **Van Den Bossche, N., Huyghe, W., Moens, J., Janssens, A., Depaepe, M.** Airtightness of the window-wall interface in cavity brick walls. Energy and Buildings. 2012. 45. Pp. 32–42. DOI:10.1016/j.enbuild.2011.10.022. URL:
4. **Van Den Bossche, N., Janssens, A.** Airtightness and watertightness of window frames: Comparison of performance and requirements. Building and Environment. 2016. 110. Pp. 129–139. DOI:10.1016/j.buildenv.2016.09.034.
5. **Schiepel, D., Westhoff, A.** Study on the Influence of Turbulence on Thermal Comfort for Draft Air. New Results in Numerical and Experimental Fluid Mechanics XIII. STAB/DGLR Symposium 2020. Notes on Numerical Fluid Mechanics and Multidisciplinary Design. 2021. Pp. 494–503. DOI:https://doi.org/10.1007/978-3-030-79561-0_47.
6. **Van Craenendonck, S., Lauriks, L., Vuye, C., Kampen, J.** Local effects on thermal comfort: Experimental investigation of small-area radiant cooling and low-speed draft caused by improperly retrofitted construction joints. Building and Environment. 2019. 147(October 2018). Pp. 188–198. DOI:10.1016/j.buildenv.2018.10.021.
7. **Manz, H., Frank, T.** Analysis of thermal comfort near cold vertical surfaces by means of computational fluid dynamics. Indoor and Built Environment. 2004. 13(3). Pp. 233–242. DOI:10.1177/1420326X04043733.
8. **Hou, Y.** Effect of wind speed on human thermal sensation and thermal comfort. AIP Conference Proceedings. 2018. 1971. Pp. 1–6. DOI:10.1063/1.5041131.
9. **Fleury, G., Thomas, M.** Variations to window air permeability according to outside temperature. Cahiers Du Centre Scientifique et Technique Du Batiment. 1972. 132(1129).
10. **Henry, R., Patenaude, A.** Measurements of window air leakage at cold temperatures and impact on annual energy performance

of a house. ASHRAE Transactions. 1998. 104(Pt 1B). Pp. 1254–1260.
11. **Bursey, T., Green, G.H.** Combined Thermal and Air Leakage Performance of Double Windows. ASHRAE Transactions. 1970. 76 p 2(2157). Pp. 215–226.
12. **Kehrli, D.** Window air leakage performance as a function of differential temperatures and accelerated environmental aging. Thermal performance of exterior envelopes of building III. 1985. Pp. 872–890. URL: https://web.ornl.gov/sci/buildings/conf-archive/1985 B3 papers/066.pdf.
13. **Verkhovskij, A.A., Shubin, I.L., Shekhovtsov, A.V.** Method of determining air permeability of building enclosing structures. RU 2 445 610 C1. 2010.
14. **Takada, K., Hayama, H., Mori, T., Kikuta, K.** Influence of the thermal performance of pvc windows for residential buildings onto heating load of windows for cold regions. AIJ Journal of Technology and Design. 2020. 26(62). Pp. 173–178. DOI:10.3130/aijt.26.173.
15. **Feng, G., Wang, Y., Xu, X., Wang, K.** Test and Analysis of Airtightness of External Windows for the Nearly Zero-Energy Building in Severe Cold Area. 11th International Symposium on Heating, Ventilation and Air Conditioning, ISHVAC 2019. 2020. Pp. 739–747. DOI:10.1007/978-981-13-9528-4_75.
16. **Li, H.X., Zhang, R., Feng, G.H., Huang, K.L., Cao, C.H.** The Test and Analysis of Air Tightness for Zero Energy Building in Cold Region. Procedia Engineering. 2016. 146. Pp. 239–243. DOI:10.1016/j.proeng.2016.06.381.
17. **Shekhovtsov, A.** Air permeabillity of an PVC-window when exposed to freezing temperatures. 2011. (3(1)). Pp. 263–269. URL: http://vestnikmgsu.ru/ru/component/sjarchive. (rus).
18. **Verkhovsky, A.A., Zimin, A.N., Potapov, S.S.** The applicability of modern translucent walling for the climatic regions of Russia. Zhilishchnoe Stroitel'stvo [Housing Construction]. 2015. (6). Pp. 16–19. URL: https://elibrary.ru/item.asp?id=23754563 (rus).
19. **Kunin, Y.S., Alekperov, R.G., Potapova, T.V.** Dependence of air permeability of translucent structures on temperature impacts. Promyshlennoe i Grazhdanskoe Stroitelstvo [Industrial and civil engineering]. 2018. (10). Pp. 114–120. URL: http://www.pgs1923.ru/ru/index.php?m=4&y=2018&v=10&p=00&r=19 (rus).
20. **Konstantinov, A., Verkhovsky, A.** Assessment of the Negative Temperatures Influence on the PVC Windows Air Permeability. IOP Conference Series: Materials Science and Engineering. 2020. 753(2). DOI:10.1088/1757-899X/753/2/022092.
21. **Konstantinov, A., Verkhovsky, A.** Assessment of the Wind and Temperature Loads Influence on the PVC Windows Deformation. IOP Conference Series: Materials Science and Engineering. 2020. 753(3). DOI:10.1088/1757-899X/753/3/032022.
22. **Verkhovskiy, A., Bryzgalin, V., Lyubakova, E.** Thermal Deformation of Window for Climatic Conditions of Russia. IOP Conference Series: Materials Science and Engineering. 2018. 463(3). DOI:10.1088/1757-899X/463/3/032048.
23. **Verkhovskiy, A., Umnyakova, N., Savich, A.** Especially the Use of Windows and Curtain Wall in Climatic Conditions of Russia. IOP Conference Series: Materials Science and Engineering. 2018. 463(3). DOI:10.1088/1757-899X/463/3/032033.
24. **Aksenov, I.S., Konstantinov, A.P.** An analytical method for calculating the stress-strain state of PVC window elements under a temperature load. Vestnik MGSU (Monthly Journal on Construction and Architecture). 2021. 16(11). Pp. 1437-1451 DOI: 10.22227/1997-0935.2021.11.1437-1451 (rus).
25. **Yafei, S., Yongjun, T., Jing, S., Dongjie, N.** Effect of temperature and composition on thermal properties of carbon steel. 2009

Chinese Control and Decision Conference, CCDC 2009. 2009. (2). Pp. 3756–3760. DOI:10.1109/CCDC.2009.5191721.

СПИСОК ЛИТЕРАТУРЫ

1. **Klems, J.H.** Methods of estimating air infiltration through windows. Energy and Buildings. 1983. 5(4). Pp. 243–252. DOI:10.1016/0378-7788(83)90012-9.
2. **Provan, T.F., Younger, J.D.** Air infiltration characteristics of windows. Energy and Buildings. 1986. 9(4). Pp. 281–292. DOI:10.1016/0378-7788(86)90033-2.
3. **Van Den Bossche, N., Huyghe, W., Moens, J., Janssens, A., Depaepe, M.** Airtightness of the window-wall interface in cavity brick walls. Energy and Buildings. 2012. 45. Pp. 32–42. DOI:10.1016/j.enbuild.2011.10.022. URL:
4. **Van Den Bossche, N., Janssens, A.** Airtightness and watertightness of window frames: Comparison of performance and requirements. Building and Environment. 2016. 110. Pp. 129–139. DOI:10.1016/j.buildenv.2016.09.034.
5. **Schiepel, D., Westhoff, A.** Study on the Influence of Turbulence on Thermal Comfort for Draft Air. New Results in Numerical and Experimental Fluid Mechanics XIII. STAB/DGLR Symposium 2020. Notes on Numerical Fluid Mechanics and Multidisciplinary Design. 2021. Pp. 494–503. DOI:https://doi.org/10.1007/978-3-030-79561-0_47.
6. **Van Craenendonck, S., Lauriks, L., Vuye, C., Kampen, J.** Local effects on thermal comfort: Experimental investigation of small-area radiant cooling and low-speed draft caused by improperly retrofitted construction joints. Building and Environment. 2019. 147(October 2018). Pp. 188–198. DOI:10.1016/j.buildenv.2018.10.021.
7. **Manz, H., Frank, T.** Analysis of thermal comfort near cold vertical surfaces by means of computational fluid dynamics. Indoor and Built Environment. 2004. 13(3). Pp. 233–242. DOI:10.1177/1420326X04043733.
8. **Hou, Y.** Effect of wind speed on human thermal sensation and thermal comfort. AIP Conference Proceedings. 2018. 1971. Pp. 1–6. DOI:10.1063/1.5041131.
9. **Fleury, G., Thomas, M.** Variations to window air permeability according to outside temperature. Cahiers Du Centre Scientifique et Technique Du Batiment. 1972. 132(1129).
10. **Henry, R., Patenaude, A.** Measurements of window air leakage at cold temperatures and impact on annual energy performance of a house. ASHRAE Transactions. 1998. 104(Pt 1B). Pp. 1254–1260.
11. **Bursey, T., Green, G.H.** Combined Thermal and Air Leakage Performance of Double Windows. ASHRAE Transactions. 1970. 76 p 2(2157). Pp. 215–226.
12. **Kehrli, D.** Window air leakage performance as a function of differential temperatures and accelerated environmental aging. Thermal performance of exterior envelopes of building III. 1985. Pp. 872–890. URL: https://web.ornl.gov/sci/buildings/conf-archive/1985 B3 papers/066.pdf.
13. **Верховский А.А., Шубин И.Л., Шеховцов А.В.** Патент РФ 2445610 C1. Способ определения воздухопроницаемости строительных ограждающих конструкций // Заявление № 2010151153/28 от 15.12.2010.
14. **Takada, K., Hayama, H., Mori, T., Kikuta, K.** Influence of the thermal performance of pvc windows for residential buildings onto heating load of windows for cold regions. AIJ Journal of Technology and Design. 2020. 26(62). Pp. 173–178. DOI:10.3130/aijt.26.173.
15. **Feng, G., Wang, Y., Xu, X., Wang, K.** Test and Analysis of Airtightness of External Windows for the Nearly Zero-Energy Building in Severe Cold Area. 11th

International Symposium on Heating, Ventilation and Air Conditioning, ISHVAC 2019. 2020. Pp. 739–747. DOI:10.1007/978-981-13-9528-4_75.
16. **Li, H.X., Zhang, R., Feng, G.H., Huang, K.L., Cao, C.H.** The Test and Analysis of Air Tightness for Zero Energy Building in Cold Region. Procedia Engineering. 2016. 146. Pp. 239–243. DOI:10.1016/j.proeng.2016.06.381.
17. **Шеховцов А.В.** Воздухопроницаемость оконного блока из ПВХ профилей при действии отрицательных температур // Вестник МГСУ. 2011. № 3-1. С. 263-269.
18. **Верховский А.А., Зимин А.Н., Потапов С.С.** Применимость современных светопрозрачных ограждающих конструкций для климатических регионов России // Жилищное строительство. 2015. № 6. С. 16-19.
19. **Кунин Ю.С., Алекперов Р.Г., Потапова Т.В.** Зависимость воздухопроницаемости светопрозрачных конструкций от температурных воздействий // Промышленное и гражданское строительство. 2018. № 10. С. 114-120.
20. **Konstantinov, A., Verkhovsky, A.** Assessment of the Negative Temperatures Influence on the PVC Windows Air Permeability. IOP Conference Series: Materials Science and Engineering. 2020. 753(2). DOI:10.1088/1757-899X/753/2/022092.
21. **Konstantinov, A., Verkhovsky, A.** Assessment of the Wind and Temperature Loads Influence on the PVC Windows Deformation. IOP Conference Series: Materials Science and Engineering. 2020. 753(3). DOI:10.1088/1757-899X/753/3/032022.
22. **Verkhovskiy, A., Bryzgalin, V., Lyubakova, E.** Thermal Deformation of Window for Climatic Conditions of Russia. IOP Conference Series: Materials Science and Engineering. 2018. 463(3). DOI:10.1088/1757-899X/463/3/032048.
23. **Verkhovskiy, A., Umnyakova, N., Savich, A.** Especially the Use of Windows and Curtain Wall in Climatic Conditions of Russia. IOP Conference Series: Materials Science and Engineering. 2018. 463(3). DOI:10.1088/1757-899X/463/3/032033.
24. **Aksenov, I.S., Konstantinov, A.P.** An analytical method for calculating the stress-strain state of PVC window elements under a temperature load. Vestnik MGSU (Monthly Journal on Construction and Architecture). 2021. 16(11). Pp. 1437-1451 DOI: 10.22227/1997-0935.2021.11.1437-1451 (rus).
25. **Yafei, S., Yongjun, T., Jing, S., Dongjie, N.** Effect of temperature and composition on thermal properties of carbon steel. 2009 Chinese Control and Decision Conference, CCDC 2009. 2009. (2). Pp. 3756–3760. DOI:10.1109/CCDC.2009.5191721.

Ivan S. Aksenov, lecturer of the Department of Design of Buildings and Structures; Moscow State University of Civil Engineering (National Research University) (MGSU); 26 Yaroslavskoe shosse, Moscow, 129337, Russian Federation. E-mail: ivanak1995@mail.ru.

Aleksandr P. Konstantinov, Candidate of Technical Sciences, Associate Professor, Associate Professor of the Department of Design of Buildings and Structures; Moscow State University of Civil Engineering (National Research University) (MGSU); 26 Yaroslavskoe shosse, Moscow, 129337, Russian Federation. E-mail: apkonst@yandex.ru.

Иван Сергеевич Аксенов, преподаватель кафедры проектирования зданий и сооруже ний; Национальный исследовательский Московский государственный строительный университет (НИУ МГСУ); 129337, г. Москва, Ярославское шоссе, д. 26. E-mail: ivanak1995@mail.ru;

Александр Петрович Константинов, кандидат технических наук, доцент, доцент кафедры проектирования зданий и сооружений; Национальный исследовательский Московский государственный строительный университет (НИУ МГСУ); 129337, г. Москва, Ярославское шоссе, д. 26. E-mail: apkonst@yandex.ru.

DOI:10.22337/2587-9618-2022-18-2-112-120

INFLUENCE OF STAGE-BY-STAGE CONSTRUCTION OF A CYLINDRICAL SHELL ON STRESS-STRAIN STATES OF AN EXISTING NEARBY SHELL IN A SOIL BODY

Sergey B. Kosytsyn, Vladimir Y. Akulich

Russian University of Transport (MIIT), Moscow, RUSSIA

Abstract: a study was carried out on influence of stage-by-stage construction of a cylindrical shell on stress-strain states of an existing nearby shell in a soil body. Additionally, a case is considered in which the stage-by-stage construction of shells was not taken into account. The obtained results were analyzed by the authors.

Keywords: construction stages, soil body, shell, finite elements, contact elements.

О ВЛИЯНИИ ПОЭТАПНО ВОЗВОДИМОЙ ЦИЛИНДРИЧЕСКОЙ ОБОЛОЧКИ НА НДС СУЩЕСТВУЮЩЕЙ БЛИЗЛЕЖАЩЕЙ ОБОЛОЧКИ И ИХ ЕДИНОГО ОКРУЖАЮЩЕГО ОСНОВАНИЯ

С.Б. Косицын, В.Ю. Акулич

Российский университет транспорта (МИИТ), г. Москва, РОССИЯ

Аннотация: в работе проведено исследование влияния поэтапно возводимой цилиндрической оболочки на напряженно-деформированные состояния существующей близлежащей оболочки и их единого окружающего основания. Дополнительно рассмотрен случай без учета этапности сооружения оболочек. Полученные результаты проанализированы авторами.

Ключевые слова: стадии строительства, грунтовый массив, оболочка, плоские и пространственные конечные элементы, контактные конечные элементы.

1. INTRODACTION

There is a problem of evaluating the impact of potential future construction of the cylindrical shell of a new tunnel on the stress-strain state of the cylindrical shell of an existing tunnel built earlier. Similar problems emerged when designing the first variant (with two tube tunnels) of the Lefortovo tunnel in Moscow. Calculations of such systems are known in two-dimensional formulation. For example, S. B. Kositsyn and D. B. Dolotkazin explored the effect of some features of the Lefortovo tunnel on its stress-strain state by the finite element method [4].

2. NUMERICAL ANALYSIS OF STRESS-STRAIN STATES OF CYLINDRICAL SHELLS IN A SOIL BODY

The calculation of the stress-strain state of shells was performed by the finite element method in the ANSYS Mechanical software package [2, 3, 6, 8, 11, 12].

The developed spatial computational models includes two parallel cylindrical shells and a soil body. The purpose of the study is to determine how the phased construction of a new cylindrical shell affects the stress-strain state of the existing shell built earlier. The geometric characteristics of cylindrical shells in the

computational model are close to the initial data of the work [4]. The diameter of the shell D = 13.5 m, the thickness of the shell t = 0.7 m, depth of cylindrical shells Z = 25.0 m, distance between the axes of shells – $2D$. The distance between the shell and the left and right sides of the soil body is $W = 5D$. The distance between the shell and the upper side of the soil body is $H = 5D$. Both cylindrical shells consists of 32 separate rings with a width of 2.8 m.

The material of the cylindrical shell is presented by a linear-elastic model with the following characteristics: density ρ – 2300 kg/m3, elastic modulus E – 30000 MPa, Poisson's ratio μ – 0.2. The material of the soil body [9] is presented by an elastic-plastic model of Mohr–Coulomb with the following parameters: density ρ – 2000 kg/m^3, deformation modulus E_{def} – 10 MPa, Poisson's ratio μ – 0.3, cohesion C_u – 10 kPa, friction angle φ – 25°. These material models require a physically nonlinear calculation.

The soil body has constraint on the side faces and on the bottom face. The load consists of the own weight of the soil body and the cylindrical shells. In addition, there is a gap between the shell and the soil body in the computational model [7, 10], which takes into account the influence of a slurry shield during the construction of the cylindrical shell (the friction coefficient f = 0.6) [5].

The calculation was done geometrically, structurally and physically nonlinear statement.

The design case consists of 65 stages of determining the stress-strain state of the cylindrical shell and the soil body: the first (zero) stage calculates the natural state of the soil body without the shell, the next 64 stages calculate the stress-strain state of the model after activating each individual ring of shells (thirty-two stages for each shell). The change in the stress-strain state is considered for the elements of the shell installed first. This makes it possible to evaluate the impact of the construction of the second shell on the first.

The spatial computational model is shown in figure 1. The cylindrical shells are shown in figure 2.

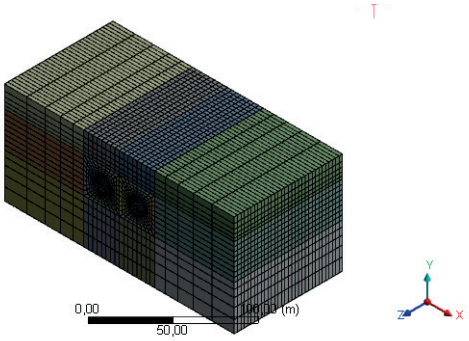

Figure 1. Spatial computational model in ANSYS Mechanical

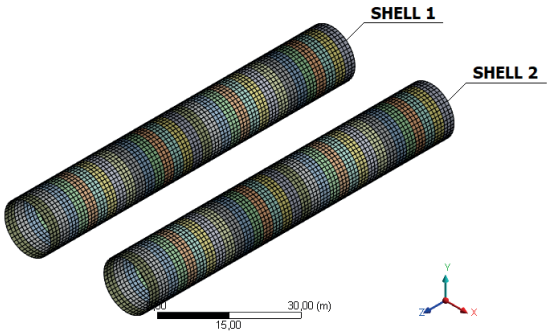

Figure 2. View of cylindrical shells

The equivalent stresses curves according to the IV strength theory (von Mises) [1] of the cylindrical shell rings are shown in figures 3 – 11. Vertical green lines on the graphs separate the stages of construction of the first and second shells.

Table 1 shows the values of the stress increase caused by the construction of the second shell, and their percentage share for the considered rings of the first shell.

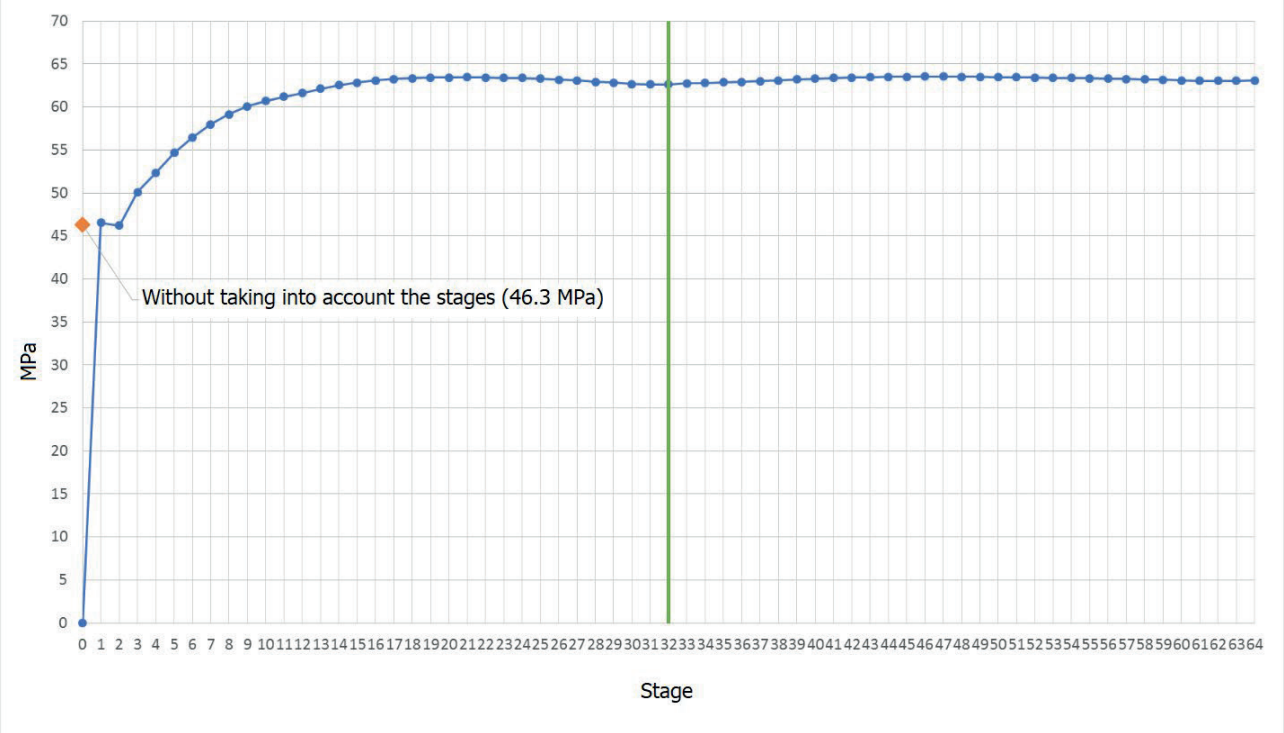

Figure 3. The maximum equivalent stresses according to the IV strength theory (von Mises) of 01 ring of the first shell

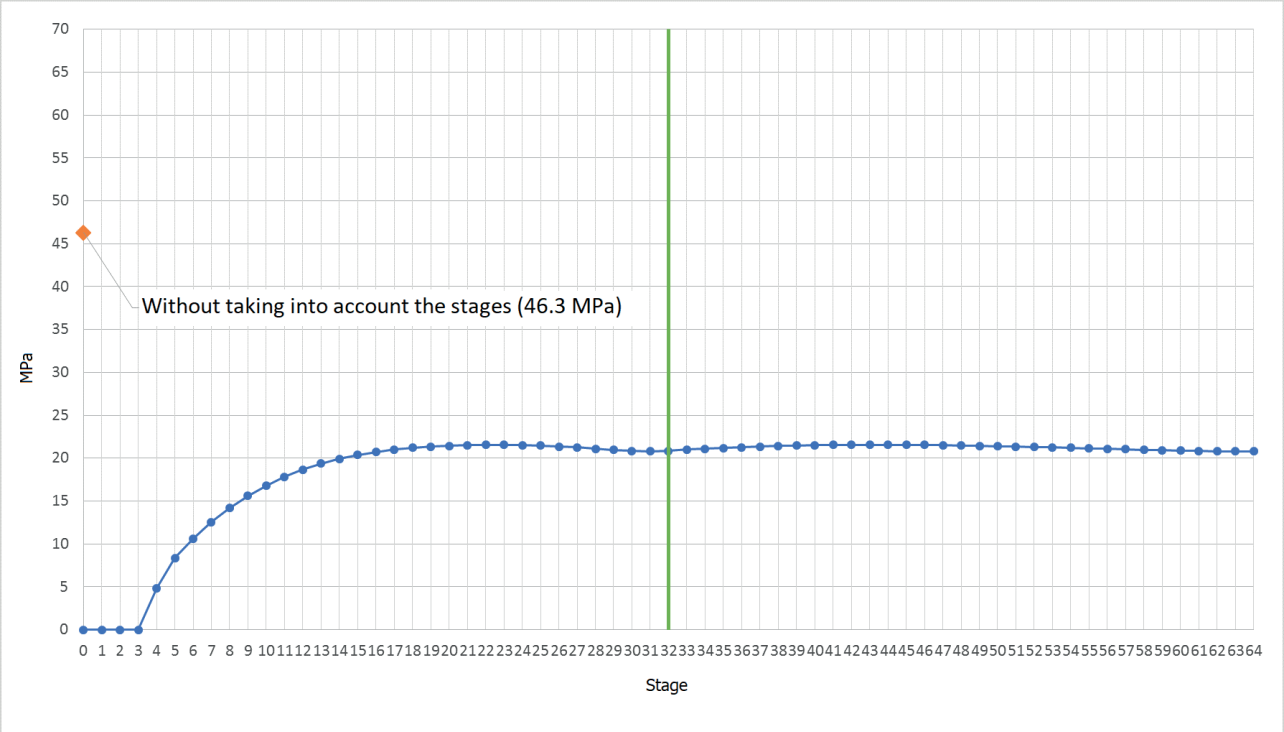

Figure 4. The maximum equivalent stresses according to the IV strength theory (von Mises) of 04 ring of the first shell

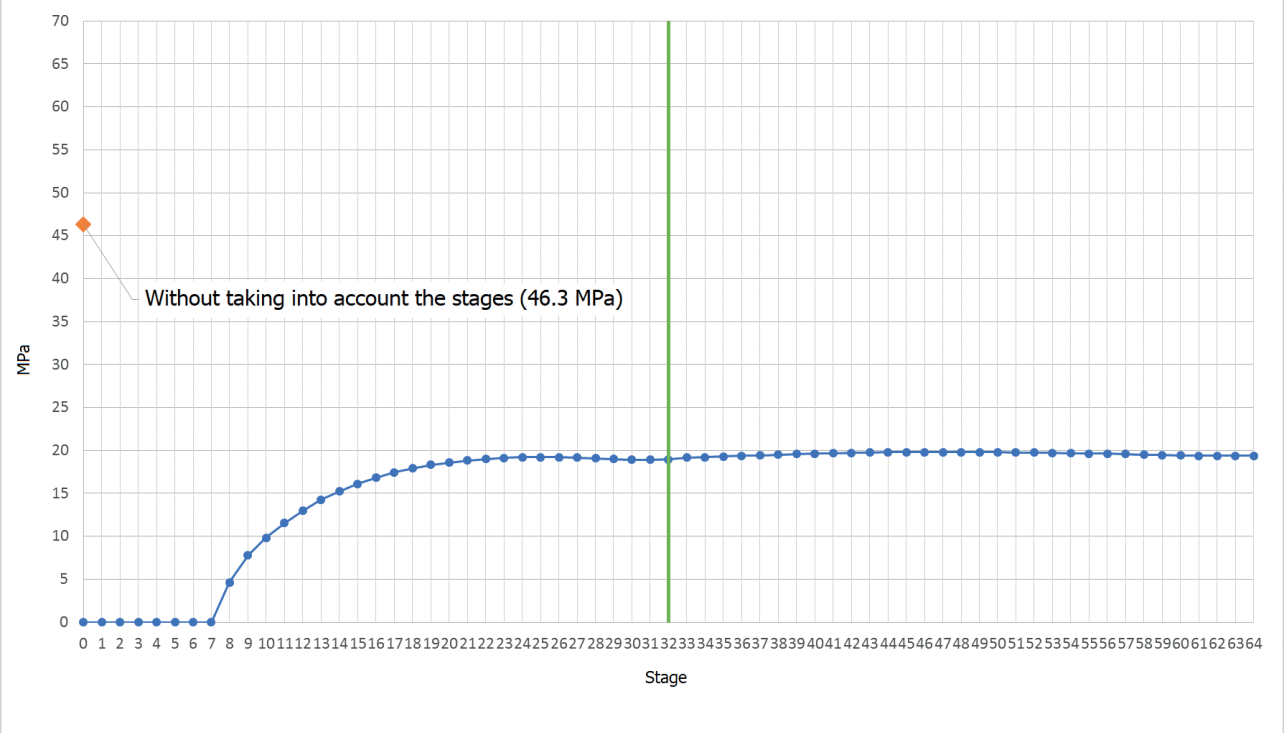

Figure 5. The maximum equivalent stresses according to the IV strength theory (von Mises) of 08 ring of the first shell

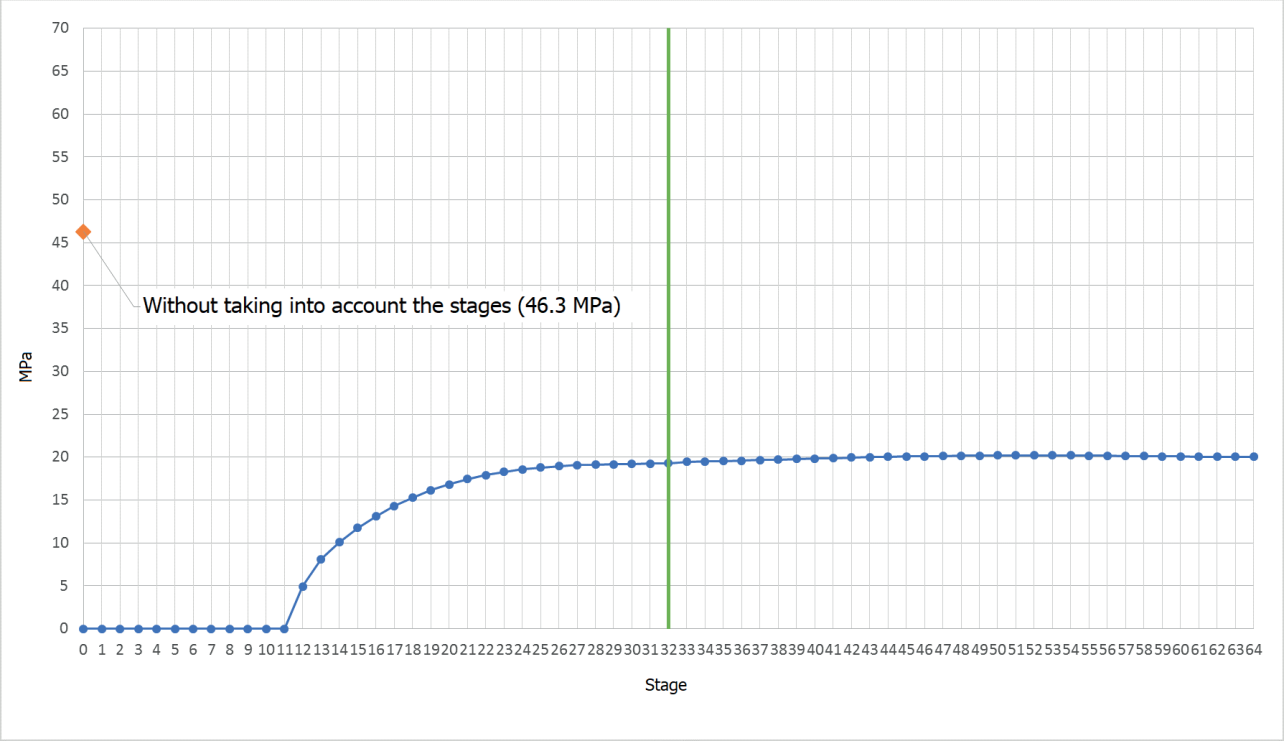

Figure 6. The maximum equivalent stresses according to the IV strength theory (von Mises) of 12 ring of the first shell

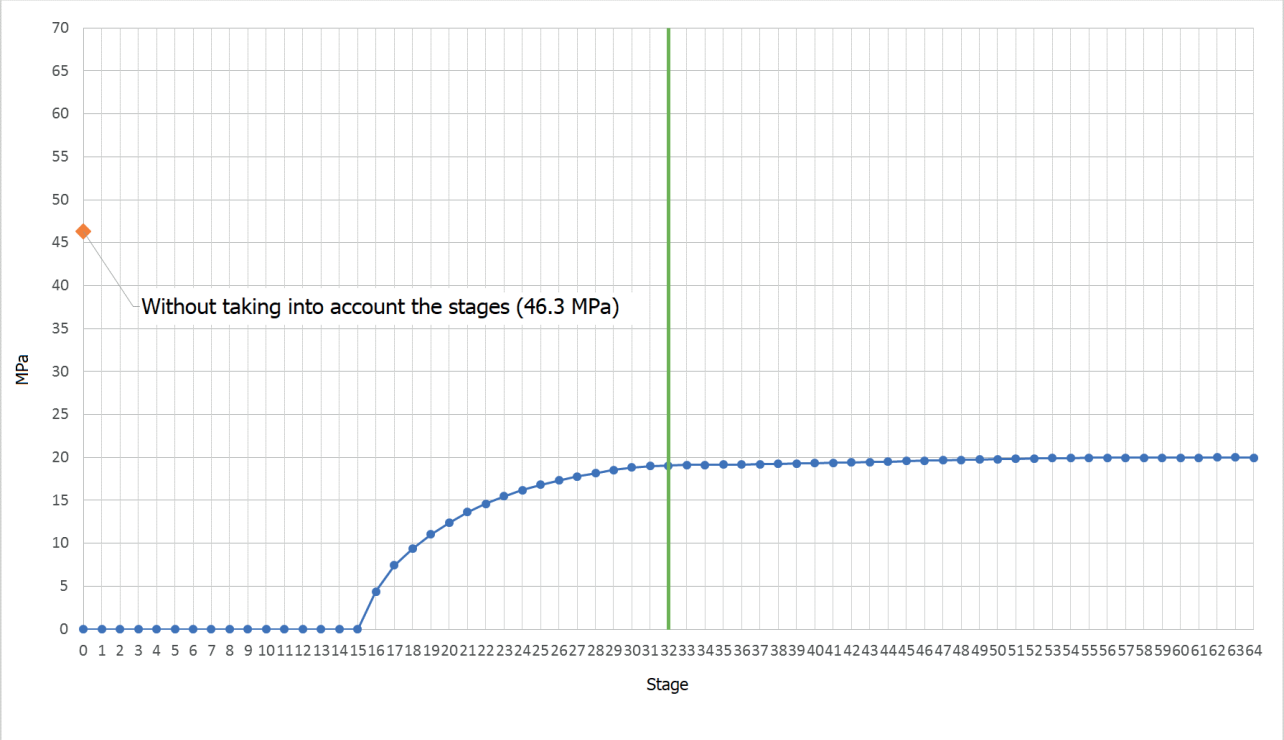

Figure 7. The maximum equivalent stresses according to the IV strength theory (von Mises) of 16 ring of the first shell

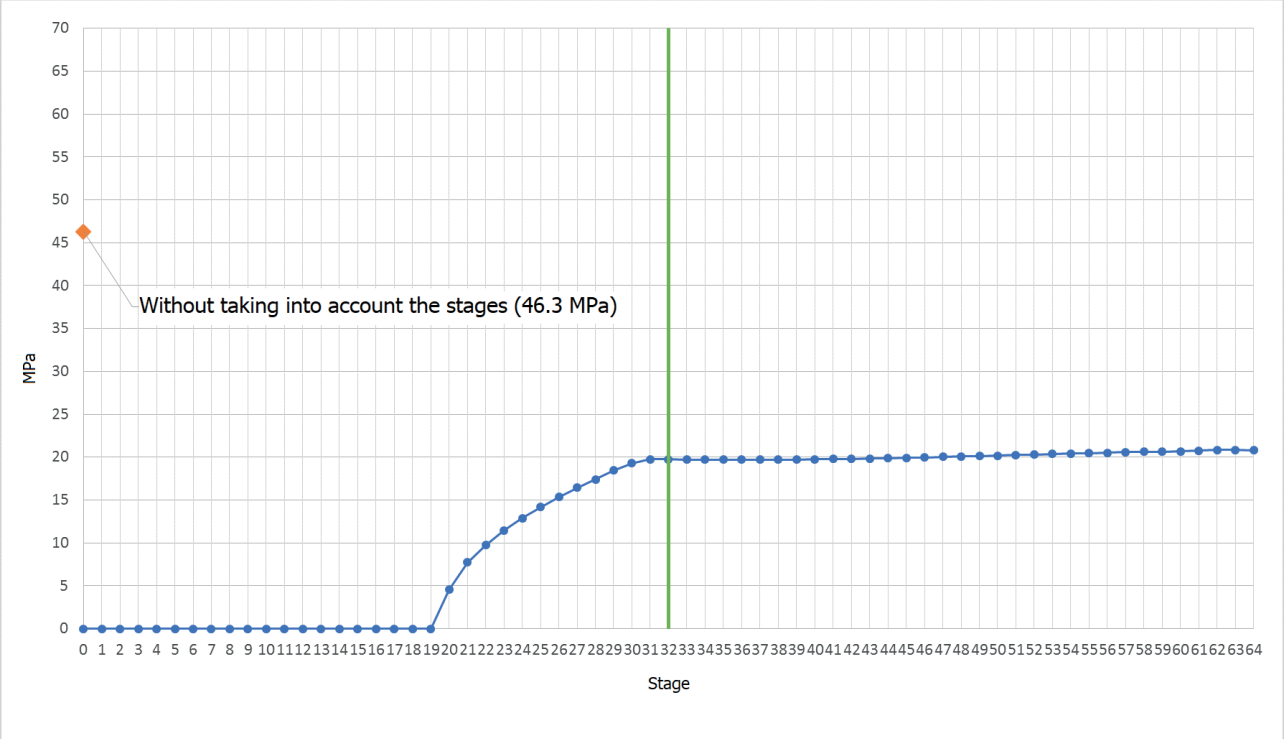

Figure 8. The maximum equivalent stresses according to the IV strength theory (von Mises) of 20 ring of the first shell

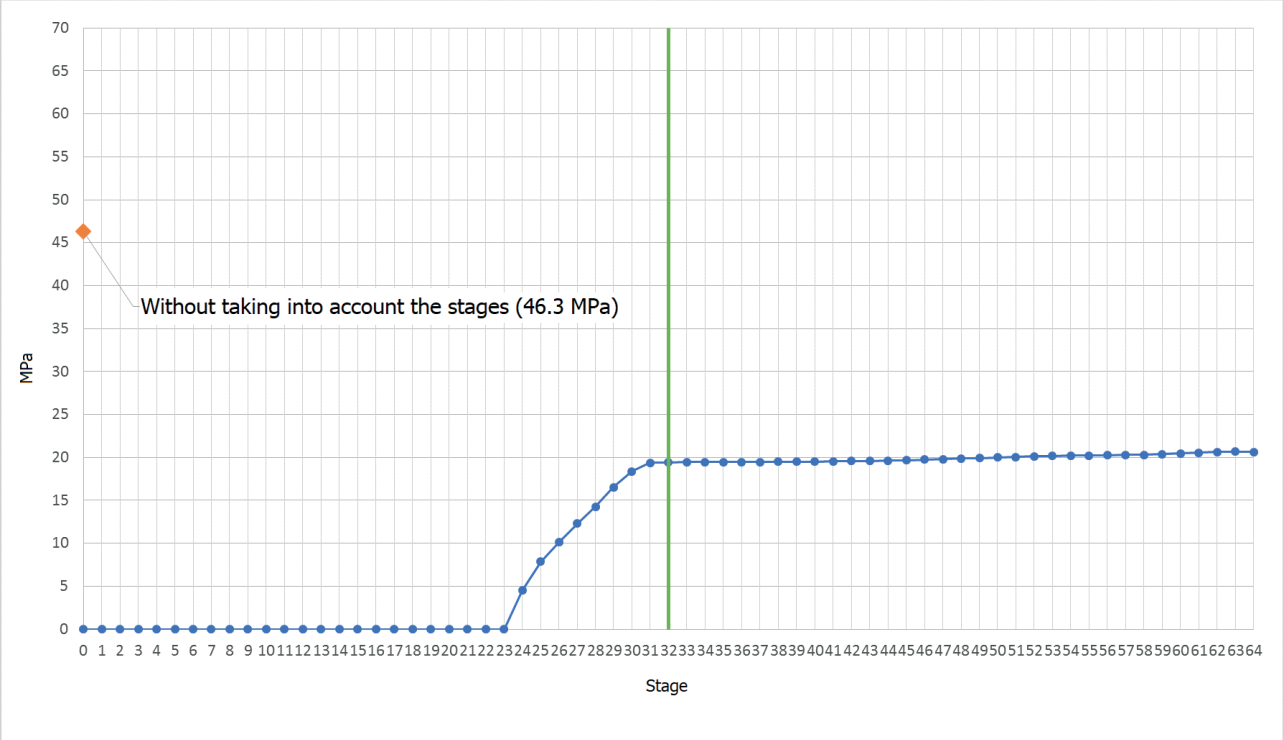

Figure 9. The maximum equivalent stresses according to the IV strength theory (von Mises) of 24 ring of the first shell

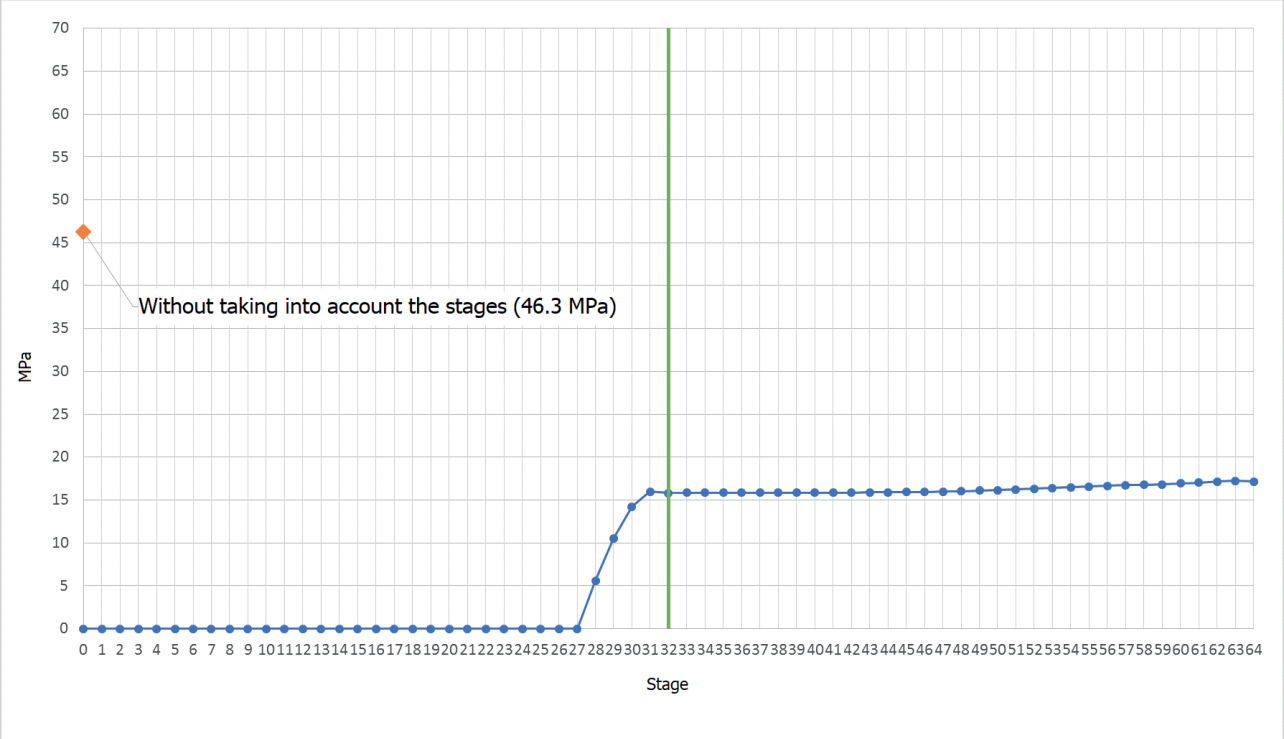

Figure 10. The maximum equivalent stresses according to the IV strength theory (von Mises) of 28 ring of the first shell

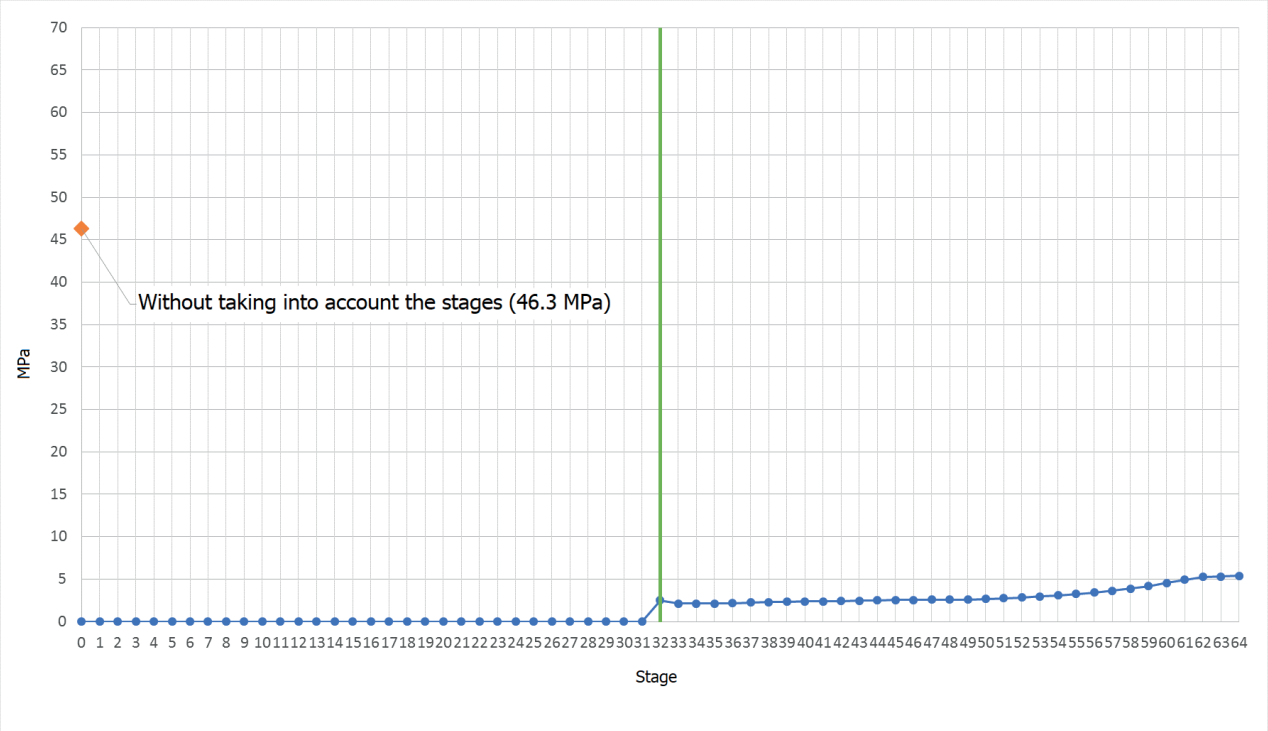

Figure 11. The maximum equivalent stresses according to the IV strength theory (von Mises) of 32 ring of the first shell

Table 1. The increase in the equivalent stresses according to the IV strength theory (von Mises) in the considered rings of the first shell

Shell ring	Increase in equivalent stresses, MPa	%
1	0.08	0.1
4	0.04	0.2
8	0.59	3.1
12	0.91	4.7
16	0.94	4.9
20	1.11	5.6
24	1.26	6.5
28	1.25	7.8
32	2.89	116.8

The results show that the construction of the second shell has little impact on the existing shell. The increase in equivalent stresses is 116.8 % only in the last ring. This is due to the fact that the last ring is underloaded more than the others during the construction of the first shell. However, this ring takes a new load equally with the others during the construction of the second shell. The stresses increase does not exceed 7.8 % in rings from 1 to 28. The maximum equivalent stresses in the shells are 46.3 MPa in the calculations without taking into account the construction stages. Table 2 shows the stresses in the first shell from the calculated cases, taking into account and without taking into account the stages of construction, as well as the difference of these stresses as a percentage. Higher stresses were obtained in all the shell rings without taking into account the construction stages, except for the first one.

Table 2. The maximum equivalent stresses according to the IV strength theory (von Mises) for the calculated cases with and without taking into account the stages

Shell ring	Maximum equivalent stresses, MPa		The difference of the maximum equivalent stresses, %
	Without taking into account the stages	With taking into account the stages	
1	46.3	63.5	37 %
4	46.3	21.6	– 53 %
8	46.3	19.8	– 57 %
12	46.3	20.2	– 56 %
16	46.3	20.0	– 57 %
20	46.3	20.8	– 55 %
24	46.3	20.7	– 55 %
28	46.3	17.2	– 63 %
32	46.3	5.4	– 88 %

3. CONCLUSION

The authors consider the features of the stress-strain state of a system consisting of two parallel cylindrical shells and a soil body. In this paper it is shown how the phased construction of a new cylindrical shell affects the existing nearby shell. The results obtained showed that this effect is insignificant. The stress increase for all the considered rings of the first shell does not exceed 7.8 %, except for the last ring, where the stress increase is 116.8 %.

Additionally, the stress-strain state of the first shell is compared with and without taking into account the stages of construction. The comparison showed that it is necessary to take into account the stages of construction of cylindrical shells in such tasks.

REFERENCES

1. **Alexandrov A.V., Potapov V.D.** Osnovy teorii uprugosti i plastichnosti [Foundations of the theory of elasticity and plasticity]. Moscow, High school, 1990, 400 pages (in Russian).
2. **Bate K., Wilson E.** Chislennye metody analiza i metod konechnyh elementov [Numerical analysis methods and finite element method]. Moscow, Stroizdat, 1982, 446 pages (in Russian).
3. **Gallagher R.** Metod konechnyh elementov. Osnovy [The finite element method. Basics]. Moscow, Mir, 1984, 429 pages (in Russian).
4. **Kositsyn S.B., Dolotkazin D.B.** Issledovanie vliyaniya nekotoryh osobennostej tonnel'nogo perekhoda v Lefortovo v g. Moskve na ego napryazhenno-deformirovannoe sostoyanie [Investigation of the influence of some features of the Lefortovo tunnel in Moscow on its stress-strain state]. // RUDN Journal Of Engineering Researches, 2002, Issue 1, pp. 90-94 (in Russian).
5. **Kositsyn S.B., Akulich V.Y.** Numerical analysis of the account of the stages in the calculation of the shell together with the soil massif // *International Journal for Computational Civil and Structural Engineering*, 2019, Volume 15, Issue 3, pp. 84-95.
6. **Perelmuter A.V., Slivker V.I.** Raschetnye modeli sooruzhenij i vozmozhnosti ih analiza [Design models of structures and possibilities of their analysis]. Kiev, Steel, 2002, 445 pages (in Russian).
7. **Prevo R.** Raschet na prochnost' truboprovodov zalozhennyh v grunt **[**Strength calculation of pipelines laid in the ground]. Moscow, Stroyizdat, 1964, 123 pages (in Russian).
8. **Trushin S.I.** Metod konechnyh elementov. Teoriya i zadachi [The finite element

method. Theory and tasks]. Moscow, ACB, 2008, 256 pages (in Russian).
9. **Shaposhnikov N.N.** Raschet krugovyh tonnel'nyh obdelok na uprugom osnovanii, harakterizuemom dvumya koefficientami posteli [Calculation of circular tunnel linings in elastic foundation characterized by the two coefficients of elastic foundation]. // *Scientific Proc. of Moscow state university of railway engineering*, 1961, Issue 131, pp. 296-305 (in Russian).
10. **Attewell P.B.** Ground movements caused by tunnelling in soil // Large ground movements and structures. London: Pentech Press, 1978, pp. 120–140.
11. **Zienkiewicz O.C.** The finite element method. 5-th edition. Volume 2: Solid mechanics. Butterworth-Heinemann, 2000, 479 pages.

СПИСОК ЛИТЕРАТУРЫ

1. **Александров А.В., Потапов В.Д.** Основы теории упругости и пластичности.– М.: Высш. шк., 1990. – 400 с.
2. **Бате К., Вилсон Е.** Численные методы анализа и метод конечных элементов. – М.: Стройиздат, 1982. – 446 с.
3. **Галлагер Р.** Метод конечных элементов. Основы. – М.:Мир, 1984. – 429 с.
4. **Косицын С.Б., Долотказин Д.Б.** Исследование влияния некоторых особенностей тоннельного перехода в Лефортово в г. Москве на его напряженно-деформированное состояние // Вестник Российского университета дружбы народов. Специальный выпуск «Геометрия и расчет тонкостенных пространственных конструкций», 2002, № 1, с. 90-94.
5. **Kositsyn S.B., Akulich V.Y.** Numerical analysis of the account of the stages in the calculation of the shell together with the soil massif // *International Journal for Computational Civil and Structural Engineering*, 2019, Volume 15, Issue 3, pp. 84-95.
6. **Перельмутер А.В., Сливкер В.И.** Расчетные модели сооружений и возможности их анализа. – Киев: Сталь, 2002. – 445 с.
7. **Прево Р.** Расчет на прочность трубопроводов заложенных в грунт. – М.: Стройиздат, 1964. –123 с.
8. **Трушин С.И.** Метод конечных элементов. Теория и задачи. – М.: Издательство АСВ, 2008. – 256 с.
9. **Шапошников Н.Н.** Расчет круговых тоннельных обделок на упругом основании, характеризуемом двумя коэффициентами постели // Научн. тр. Московского института инженеров железнодорожного транспорта, 1961, Вып. 131, с. 296-305.
10. **Attewell P.B.** Ground movements caused by tunnelling in soil // Large ground movements and structures. London: Pentech Press, 1978, pp. 120–140.
11. **Zienkiewicz O.C.** The finite element method. 5-th edition. Volume 2: Solid mechanics. Butterworth-Heinemann, 2000, 479 pages.

Sergey B. Kosytsyn, Advisor of RAASN, Dr. Sc., Professor, Head of Department of Theoretical Mechanics, Russian University of Transport (MIIT); 127994, Russia, Moscow, 9b9 Obrazcova Street; phone/fax: +7(499) 978-16-73; E-mail: kositsyn-s@yandex.ru, kositsyn-s@mail.ru

Vladimir Y. Akulich, PhD student of Department of Theoretical Mechanics, Russian University of Transport (MIIT); 127994, Russia, Moscow, 9b9 Obrazcova Street; phone/fax: +7(499) 978-16-73; E-mail: vladimir.akulich@gmail.com

Косицын Сергей Борисович, советник РААСН, доктор технических наук, профессор, заведующий кафедрой «Теоретическая механика» Российского университета транспорта (МИИТ); 127994, г. Москва, ул. Образцова, 9, стр. 9; тел./факс +7(499) 978-16-73; E-mail: kositsyn-s@yandex.ru, kositsyn-s@mail.ru

Акулич Владимир Юрьевич, аспирант кафедры «Теоретическая механика» Российского университета транспорта (МИИТ); 127994, г. Москва, ул. Образцова, 9, стр. 9; тел./факс +7(499) 978-16-73; E-mail: vladimir.akulich@gmail.com

DOI:10.22337/2587-9618-2022-18-2-121-130

STUDY OF THE INFLUENCE OF THE KINETICS OF HYDROGEN SATURATION ON THE STRESS-DEFORMED STATE OF A SPHERICAL SHELL MADE FROM TITANIUM ALLOY

Aleksander A. Treshchev, Violetta O. Kuznetsova

Tula State University, Tula, RUSSIA

Abstract. In this paper, a mathematical model is considered that allows one to determine the stress-strain state of a spherical shell made of titanium alloy VT1-0, the external load is assumed to be transverse uniformly distributed, acting on the outer surface, the medium is assumed to act on the inner surface of the shell. For this, a nonlinear model was used, presented in normalized stress spaces. Fastening along the contour of the shell is rigid. Nonlinear resolving equations for calculating a spherical shell are obtained. An algorithm for solving the problem of hydrogenation of titanium alloy shells has been developed. A practical solution was made by a two-step method of sequential perturbations of parameters using the MatLab and Maple software packages. To solve the system of the obtained differential equations, the method of finite differences is applied. The calculation of the stress-strain state of the shell is obtained taking into account the diffusion process of an aggressive hydrogen-containing medium, and the obtained solution is compared with the results of the classical nonlinear theory without taking into account the aggressive medium. The results of comparing these solutions demonstrate quantitative differences in the parameters of the shell deformation process, which are explained by a more accurate account of the influence of the type of stress state. This approach has a rather flexible mechanism for considering the initial and induced differential resistance, demonstrates a high accuracy of matching the obtained theoretical results with empirical data on loading a wide range of materials under complex types of stress state.

Keywords: flat shell, titanium alloy, finite differences, nonlinear equations, initially isotropic material, large deflections.

ИССЛЕДОВАНИЕ ВОЗДЕЙСТВИЯ КИНЕТИКИ НАВОДОРОЖИВАНИЯ НА НАПРЯЖЕННО-ДЕФОРМИРОВАННОЕ СОСТОЯНИЕ СФЕРИЧЕСКОЙ ОБОЛОЧКИ ИЗ ТИТАНОВОГО СПЛАВА

А.А. Трещев, В.О. Кузнецова

Тульский государственный университет, г. Тула, РОССИЯ

Аннотация. В данной работе рассмотрена математическая модель, позволяющая определять напряжённо-деформированное состояние сферической оболочки из титанового сплава ВТ1-0, внешняя нагрузка принята поперечной равномерно распределённой, действующей на внешнюю поверхность, среда принята действующей на внутренную поверхность оболочки. Для этого использована нелинейная модель, представленная в нормированных пространствах напряжений. Закрепление по контуру оболочки жёсткое. Получены нелинейные разрешающие уравнения расчёта сферической оболочки. Разработан алгоритм решения задачи наводороживания оболочек из титанового сплава. Практическое решение производилось двухшаговым методом последовательных возмущений параметров с использованием пакетов прикладных программ MatLab и Maple. Для решения системы полученных дифференциальных уравнений применён метод конечных разностей. Получен расчет НДС оболочки с учетом процесса диффузии агрессивной водородосодержащей среды, произведено сравнение полученного решения с результатами классической нелинейной теории без учета агрессивной среды. Результаты сравнения указанных решений демонстрируют количественные различия в параметрах процесса деформирования оболочки, которые объясняются более точным учетом влияния вида напряженного состояния. Данный подход имеет

достаточно гибкий механизм учета изначальной и наведенной разносопротивляемости, демонстрирует высокую точность согласования получаемых теоретических результатов с эмпирическими данными по нагружению широкого круга материалов при сложных видах напряженного состояния.

Ключевые слова: пологая оболочка, титановый сплав, конечные разности, нелинейные уравнения, начально изотропный материал, большие прогибы.

INTRODUCTION

One of the first theories for calculating structural elements operating in aggressive hydrogen-containing media, taking into account the change in material properties over time, apparently, should be noted the model proposed in the works [1 – 4].

In previous studies, to construct a mathematical model of the behavior of materials in a hydrogen-containing medium, it was proposed to use the theory of Yu.N. Rabotnov [5, 6] taking into account physical and chemical effects on the surface and in the volume of the deformable But, as practice has shown, this theory does not take into account a number of effects inherent in the problem under consideration, such as the presence of triple nonlinearity, as well as induced differential resistance, which undoubtedly leads to a decrease in the accuracy of the results. This study also considers the change in the properties of materials under the influence of a changing concentration of an aggressive medium, but initially nonlinear relationships were used built in normalized stress spaces, which consider a continuous change in the state of a structural material depending on the type of stress state and quantitative characteristics at a point. A more effective mathematical model for solving the problem of the effect of hydrogenation on the stress-strain state of a flat spherical shell made of titanium alloy is proposed, a numerical solution of the problem is constructed based on the finite difference method. To solve the problem with triple nonlinearity, a two-step method of sequential perturbations of parameters was adopted [7], which allows linearizing the resolving equations and also has a high accuracy. The numerical implementation of this approach was carried out by the finite difference method of increased accuracy. The integration of the functions of the stress-strain state and rigidity parameters over the thickness was carried out by the Simpson method [8].

FORMULATION OF THE PROBLEM

The object of research is a flat spherical shell made of titanium alloy VT1-0, loaded with an external uniformly distributed transverse load with an intensity of up to 5 MPa, rigidly fixed along the perimeter, the radius of curvature of the shell is taken equal to $R = 3$ m, the radius of the base of the shell is taken equal to $a = 1{,}5$ m, and a hoist arrow – $f = 0{,}4$ m.

The location of any point on the median surface of a spherical shell is determined by a Gaussian coordinate system α_1, α_2, and the position of an arbitrary point in thickness is determined by the coordinate α_3, considering that u – horizontal displacements along a radial coordinate r (the projection α_1), ϑ – radial displacements, w – vertical displacements (deflections) under the action of a lateral load q. The design scheme of the shell is shown in the figure 1.

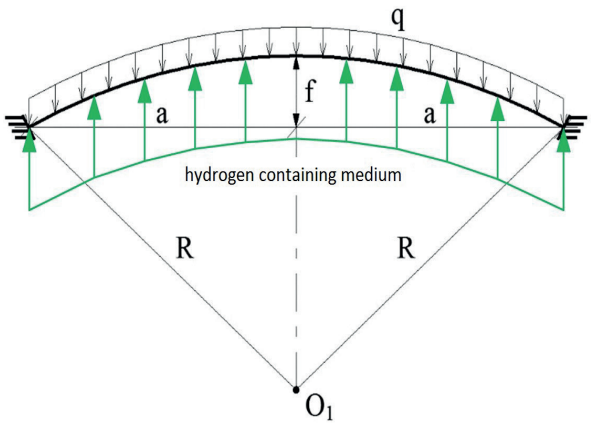

Figure 1. The design scheme of the shell

For a flat spherical shell, the constancy of the main radius of curvature of its middle surface within the plan is valid:

$$R_1 = R_2 = R, \quad (1)$$

$k_1 = k_2 = k = 1/R$ – main curvature.

Consider the equilibrium of a spherical shell with thickness $h = 0,05$ m, under the influence of a transverse axisymmetric uniformly distributed load q and a hydrogen-containing medium with a concentration λ. We accept the kinetic potential of deformations in the form [9, 10]:

$$W_1 = (A_e(\lambda) + B_e(\lambda)\xi)\sigma^2 + (C_e(\lambda) + D_e(\lambda)\xi + E_e(\lambda)\eta Cos3\varphi)\tau^2 + [(A_p(\lambda) + B_p(\lambda)\xi)\sigma^2 + (C_p(\lambda) + D_p(\lambda)\xi + E_p(\lambda)\eta Cos3\varphi)\tau^2]^n, \quad (2)$$

where $A_e(\lambda)$, $B_e(\lambda)$, $C_e(\lambda)$, $D_e(\lambda)$, $E_e(\lambda)$, $A_p(\lambda)$, $B_p(\lambda)$, $C_p(\lambda)$, $D_p(\lambda)$, $E_p(\lambda)$ – functions that determine the physical and mechanical characteristics of the material that appear in the recording of the potential of the quasilinear and nonlinear parts and depend on the degree of hydrogen saturation. The quantitative characteristics of the stress state are determined by the modulus of the total stress vector on the deviator site:

$$S_0 = \sqrt{\sigma^2 + \tau^2},$$

but a quality picture – is determined by the normalized stresses on this site, which depend on the angle ψ between normal and vector S_0, and also the harmonic phase invariant φ:

$$\xi = \cos\psi = \sigma / S_0; \quad \eta = \sin\psi = \tau / S_0;$$
$$\cos 3\varphi = \sqrt{2}\det(S_{ij}) / \tau^3,$$

where $\sigma = \sigma_{ij}\delta_{ij}/3$ – medium stress or normal octahedral; $\tau = (S_{ij}S_{ij}/3)^{1/2}$ – tangential octahedral stress; δ_{ij} – the Kronecker symbol; $S_{ij} = \sigma_{ij} - \delta_{ij}\sigma$ – stress deviator $i, j = (1, 2, 3)$.

The dependences of the mechanical properties on the degree of hydrogenation of the material are presented in the form of a polynomial expansion of the coefficients of the kinetic potential in powers of the concentration of the medium λ, and the expansion coefficients of the polynomials are determined by least-squares processing of empirical data on the deformation of titanium alloy specimens to axial tension and compression at different levels λ (0; 0,02; 0,04 и 0,08%), which for the VT1-0 alloy take the form:

$$V_{ek}(\lambda) = e_{0k} + e_{1k}\cdot\lambda + e_{2k}\cdot\lambda^2;$$
$$V_{pk}(\lambda) = p_{0k} + p_{1k}\cdot(p_{2k})^{\lambda}; \quad (3)$$
$$A_e(\lambda) = V_{e1}(\lambda); \quad B_e(\lambda) = V_{e3}(\lambda);$$
$$C_e(\lambda) = V_{e2}(\lambda); \quad D_e(\lambda) = V_{e4}(\lambda);$$
$$E_e(\lambda) = V_{e5}(\lambda);$$
$$A_p(\lambda) = V_{p1}(\lambda); \quad B_p(\lambda) = V_{p3}(\lambda);$$
$$C_p(\lambda) = V_{p2}(\lambda); \quad D_p(\lambda) = V_{p4}(\lambda);$$
$$E_p(\lambda) = V_{p5}(\lambda), \quad (4)$$

where e_{ik}, p_{ik} – polynomial coefficients, $i = 0...2$; $k = 1...5$ [9, 10].

Connections of strain and stress tensors are established from potential (2) using Castigliano's formulas:

$$e_{kk} = \frac{\partial W_1}{\partial \sigma_{kk}}; \quad \gamma_{ij} = \frac{\partial W_1}{\partial \tau_{ij}}; \quad (5)$$
$$(i, j, k = 1,2,3;\ i \neq j);$$

Taking into account the axisymmetry of the problem and the fact that the shell is subjected to pressure q on the outer surface of the shell, the geometric dependences take the form:

$$\varepsilon_1 = u_{,1} - kw + 0{,}5(w_{,1})^2; \quad \varepsilon_2 = \frac{u}{r} - kw;$$
$$\chi_1 = -w_{,11}; \quad \chi_2 = -\frac{w_{,1}}{r}; \qquad (6)$$
$$e_{11} = \varepsilon_1 + z\chi_1; \quad e_{22} = \varepsilon_2 + z\chi_2,$$

where ε_1, ε_2 – relative deformations in the middle surface; χ_1, χ_2 – mid-surface curvatures.

Considering equations (2) - (6) and Kirchhoff-Lav's hypotheses, the relationship between the simplified form of deformations and stresses is represented in the form:

$$\begin{Bmatrix} e_{11} \\ e_{22} \end{Bmatrix} = [\mathrm{A}] \begin{Bmatrix} \sigma_{11} \\ \sigma_{22} \end{Bmatrix}; \; [\mathrm{A}] = \begin{bmatrix} A_{11}(\lambda) & A_{12}(\lambda) \\ A_{21}(\lambda) & A_{22}(\lambda) \end{bmatrix}. \qquad (7)$$

Inverting matrix equations (7), we obtain the dependences of stresses on deformations:

$$\begin{Bmatrix} \sigma_{11} \\ \sigma_{22} \end{Bmatrix} = [\mathrm{B}] \begin{Bmatrix} e_{11} \\ e_{22} \end{Bmatrix}; \; [\mathrm{B}] = \begin{bmatrix} B_{11}(\lambda) & B_{12}(\lambda) \\ B_{21}(\lambda) & B_{22}(\lambda) \end{bmatrix}, \qquad (8)$$

where $[\mathrm{B}] = [\mathrm{A}]^{-1}$; A_{11}, A_{12}, … – components of the symmetric compliance matrix [A], which are functions containing the deformation potential W_1 (2), depending on the type of stress state and the degree of hydrogenation of the titanium alloy.

These components are determined according to [9, 10] as follows:

$$A_{11}(\lambda) = \{2[R_1(\lambda) + 2R_3(\lambda)]/3 + R_2(\lambda)\xi[3 - 2\xi^2]/3 + R_4(\lambda)[\xi(2-\eta^2)/3 + 4(\sigma_{11} - 2\sigma_{22})/9S_0] + R_5(\lambda)[\eta Cos3\varphi(1+\xi^2) + 2\sqrt{2}\xi - 2Cos3\varphi - \sqrt{2}\sigma_{22}/S_0]\}/3;$$
$$A_{12}(\lambda) = \{2[R_1(\lambda) - R_3(\lambda)]/3 + [R_2(\lambda) + R_4(\lambda)/3]\xi + R_5(\lambda)[Cos3\varphi(1-\eta) - \sqrt{2}\xi]\}/3;$$
$$A_{22}(\lambda) = \{2(R_1(\lambda) + 2R_3(\lambda))/3 + R_2(\lambda)\xi[3 - 2\xi^2]/3 + R_4(\lambda)[\xi(2-\eta^2) + 4(\sigma_{22} - 2\sigma_{11})/9S_0] + R_5(\lambda)[\eta Cos3\varphi(1+\xi^2) + 2\sqrt{2}\xi - 2Cos3\varphi - \sqrt{2}\sigma_{22}/S_0]\}/3;$$
$$A_{12}(\lambda) = A_{21}(\lambda);$$
$$R_k(\lambda) = L_{ek}(\lambda) + n[(A_p(\lambda) + B_p(\lambda)\xi)\sigma^2 + \left(C_p(\lambda) + D_p(\lambda)\xi + E_p(\lambda)\eta\cos 3\varphi\right)\tau^2]^{n-1} L_{pk}(\lambda);$$
$$L_{m1}(\lambda) = A_m(\lambda); \quad L_{m2}(\lambda) = B_m(\lambda);$$
$$L_{m3}(\lambda) = C_m(\lambda); \quad L_{m4}(\lambda) = D_m(\lambda);$$
$$L_{m5}(\lambda) = E_m(\lambda); \quad m = e, p; \quad k = 1,2,3.$$

The forces and moments are determined by integrating the stresses across the shell thickness in the traditional way:

$$N_1 = \int_{-h/2}^{h/2} \sigma_{11} dz; \quad N_2 = \int_{-h/2}^{h/2} \sigma_{22} dz;$$
$$M_1 = \int_{-h/2}^{h/2} \sigma_{11} z dz; \quad M_2 = \int_{-h/2}^{h/2} \sigma_{22} z dz. \qquad (9)$$

The moments and forces are expressed in terms of the components of the deformations of the middle surface of the shell in the following way:

$$\begin{aligned} N_1 &= K_{11}(\lambda)\varepsilon_1 + K_{12}(\lambda)\varepsilon_2 + P_{11}(\lambda)\chi_1 + P_{12}(\lambda)\chi_2; \\ N_2 &= K_{12}(\lambda)\varepsilon_1 + K_{22}(\lambda)\varepsilon_2 + P_{21}(\lambda)\chi_1 + P_{22}(\lambda)\chi_2; \\ M_1 &= P_{11}(\lambda)\varepsilon_1 + P_{12}(\lambda)\varepsilon_2 + D_{11}(\lambda)\chi_1 + D_{12}(\lambda)\chi_2; \\ M_2 &= P_{12}(\lambda)\varepsilon_1 + P_{22}(\lambda)\varepsilon_2 + D_{21}(\lambda)\chi_1 + D_{22}(\lambda)\chi_2, \end{aligned} \qquad (10)$$

where the integral characteristics of material functions, taking into account the influence of the degree of hydrogenation, are calculated through its concentration λ as follows:

$$K_{ij} = \int_{-h/2}^{h/2} B_{ij}(\lambda) dz, \quad P_{ij} = \int_{-h/2}^{h/2} B_{ij}(\lambda) z dz;$$
$$D_{ij} = \int_{-h/2}^{h/2} B_{ij}(\lambda) z^2 dz.$$

In connection with the triple nonlinearity of the problem, the resolving equations are formulated in a linearized form using the two-step method of sequential perturbations of the parameters of V.V. Petrov [7]. Physical dependencies are presented in the following linearized form:

$$\delta e_{11} = \frac{\partial e_{11}}{\partial \sigma_{11}}\delta\sigma_{11} + \frac{\partial e_{11}}{\partial \sigma_{22}}\delta\sigma_{22};$$
$$\delta e_{22} = \frac{\partial e_{22}}{\partial \sigma_{11}}\delta\sigma_{11} + \frac{\partial e_{22}}{\partial \sigma_{22}}\delta\sigma_{22}; \qquad (11)$$
$$\delta\varepsilon_1 = \delta u_{,1} - k\delta w + w_{,1}\,\delta w_{,1}; \quad \delta\varepsilon_2 = \frac{\delta u}{r} - k\delta w;$$
$$\delta\chi_1 = -\delta w_{,11}; \; \delta\chi_2 = \frac{-\delta w_{,1}}{r}.$$

The inversion of relations (11) leads to the following dependences of stresses on deformations in increments of the following form:

$$\delta\sigma_{11} = B_{11}(\lambda)\delta e_{11} + B_{12}(\lambda)\delta e_{22};$$
$$\delta\sigma_{22} = B_{21}(\lambda)\delta e_{11} + B_{22}(\lambda)\delta e_{22}, \qquad (12)$$

where $B_{11}(\lambda) = \frac{\Delta_{22}}{\Delta}$;

$$B_{12}(\lambda) = B_{21}(\lambda) = -\frac{\Delta_{21}}{\Delta} = -\frac{\Delta_{12}}{\Delta};$$
$$B_{22}(\lambda) = \frac{\Delta_{11}}{\Delta}; \quad \Delta_{11} = \frac{\partial e_{11}}{\partial \sigma_{11}}; \quad \Delta_{22} = \frac{\partial e_{22}}{\partial \sigma_{22}};$$
$$\Delta_{12} = \Delta_{21} = \frac{\partial e_{11}}{\partial \sigma_{22}} = \frac{\partial e_{22}}{\partial \sigma_{11}}; \quad \Delta = \Delta_{11}\Delta_{22} - \Delta_{12}\Delta_{21};$$

Dependences of deformation increments at a point on the deformation increments of the middle surface $\delta\varepsilon_1$ and $\delta\varepsilon_2$ and it's curvature $\delta\chi_1$, $\delta\chi_2$ are presented in the form:

$$\delta e_{11} = \delta\varepsilon_1 + z\delta\chi_1; \quad \delta e_{22} = \delta\varepsilon_2 + z\delta\chi_2 .$$

Then the equations for the connection of efforts with deformations of the middle surface in increments have the form:

$$\delta N_1 = K_{11}(\lambda)\delta\varepsilon_1 + K_{12}(\lambda)\delta\varepsilon_2 + P_{11}(\lambda)\delta\chi_1 + P_{12}(\lambda)\delta\chi_2;$$
$$\delta N_2 = K_{12}(\lambda)\delta\varepsilon_1 + K_{22}(\lambda)\delta\varepsilon_2 + P_{21}(\lambda)\delta\chi_1 + P_{22}(\lambda)\delta\chi_2; \qquad (13)$$
$$\delta M_1 = P_{11}(\lambda)\delta\varepsilon_1 + P_{12}(\lambda)\delta\varepsilon_2 + D_{11}(\lambda)\delta\chi_1 + D_{12}(\lambda)\delta\chi_2;$$
$$\delta M_2 = P_{12}(\lambda)\delta\varepsilon_1 + P_{22}(\lambda)\delta\varepsilon_2 + D_{21}(\lambda)\delta\chi_1 + D_{22}(\lambda)\delta\chi_2,$$

The axial symmetry of the problem under consideration makes it possible to simplify the equilibrium equations in increments as follows:

$$\delta M_{1,11} - \delta M_{2,1}/r + 2\delta M_{1,1}/r + k(\delta N_1 + \delta N_2) + \delta N_1 w_{,11} + N_1\delta w_{,11} = -\delta q;$$
$$\delta N_{1,1} + (\delta N_1 - \delta N_2)/r - k[\delta M_{1,1} + (\delta M_1 - \delta M_2)/r] = 0. \qquad (14)$$

Integrating equations (12) over the thickness of the shell according to the rules (9), and introducing the results into equilibrium equations (14), we arrive at two linearized differential equations in displacements:

$$2r^2 D_{12,11}\,\delta w_{,1} + 2r^2 D_{12,1}\,\delta w_{,11} - 2r^2 P_{12,11}\,\delta u - 2r^2 P_{12,1}\,\delta u_{,1} + 2rP_{22,1}\,\delta u + 2rP_{22}\delta u_{,1} - 2P_{22}\delta u - 2rD_{22,1}\,\delta w_{,1} - 2rD_{22}\delta w_{,11} + 2D_{22}\delta w_{,1} - 4r^2 P_{11,1}\,\delta u_{,1} - 4r^2 P_{11}\delta u_{,11} + 4r^2 D_{11,1}\,\delta w_{,11} + 4r^2 D_{11}\delta w_{,111} - 2r^3 P_{11,11}\,\delta u_{,1} - 4r^3 P_{11,1}\,\delta u_{,11} - 2r^3 P_{11}\delta u_{,111} + 2r^3 P_{11}(\delta w_{,11})^2 + 2r^3 D_{11,11}\,\delta w_{,11} + 4r^3 D_{11,1}\,\delta w_{,111} + 2r^3 D_{11}\delta w_{,1111} - 2r^3 kK_{11}w_{,1}\,\delta w_{,1} - 2r^3 kK_{12}w_{,1}\,\delta w_{,1} + 2r^3\delta w_{,11}\,K_{11}k\delta w - 2r^3\delta w_{,11}\,K_{11}w_{,1}\,\delta w_{,1} + 2r^3\delta w_{,11}\,K_{12}k\delta w + 2r^3\delta w_{,11}\,K_{11}kw + 2r^3\delta w_{,11}\,K_{12}kw - 2r^3 kK_{12}\delta u_{,1} + 2r^3 K_{22}k^2\delta w - 2r^3\delta w_{,11}\,K_{11}\delta u_{,1} - 2r^3\delta w_{,11}\,K_{11}u_{,1} - r^3\delta w_{,11}\,K_{11}w_{,1}^{\,2} - 4r^2 P_{11}w_{,1}\,\delta w_{,11} - 2r^2 kK_{12}\delta u - 2r^2 kK_{22}\delta u - 2r^2\delta w_{,11}\,K_{12}\delta u + 2r^2\delta w_{,11}\,P_{12}\delta w_{,1} - 2r^2\delta w_{,11}\,K_{12}u + 2r^2 P_{12,1}\,k\delta w + 2r^2 P_{12,1}\,w_{,1}\,\delta w_{,1} + 4r^2 P_{12}k\delta w_{,1} + 2r^2 P_{12}w_{,11}\,\delta w_{,1} + 4r^2 P_{12}w_{,1}\,\delta w_{,11} -$$

$$
\begin{gathered}
-2r^2P_{22},_1\,k\delta w+4r^2P_{11},_1\,k\delta w-4r^2P_{11},_1\,w,_1\,\delta w,_1+\\
+4r^2P_{11}k\delta w,_1-4r^2P_{11}w,_{11}\,\delta w,_1+\\
+2r^3P_{11},_{11}\,k\delta w-4r^3P_{11},_1\,w,_{11}\,\delta w,_1-2r^3P_{11,11}w,_1\,\delta w,_1+\\
+4r^3P_{11},_1\,k\delta w,_1-4r^3P_{11},_1\,w,_1\,\delta w,_{11}+\\
+4r^3P_{11}k\delta w,_{11}-2r^3P_{11}w,_{111}\,\delta w,_1-2r^3P_{11}w,_{11}\,\delta w,_{11}-\\
-2r^3P_{11}w,_1\,\delta w,_{111}+2r^3P_{12},_{11}\,k\delta w+\\
+4r^3P_{12},_1\,k\delta w,_1+4r^3P_{12}k\delta w,_{11}-2r^3kK_{11}\delta u,_1+\\
+2r^3K_{11}k^2\delta w+4r^3K_{12}k^2\delta w=2r^3\delta q\,;\quad (15)\\
r^2\left(kD_{11}-P11\right)\delta w,_{111}-\\
-\left(rP_{11},_1-krD_{11},_1+r\left(kP_{11}-K11\right)w,_1-kD_{11}+P_{11}\right)r\delta w,_{11}-\\
-r^2\left(kP_{11}-K_{11}\right)\delta u,_{11}-\\
-\delta w,_1\,r^2\left(kP_{11}-K_{11}\right)w,_{11}+\\
+kr^2\left(k\delta w-w,_1\,\delta w,_1-\delta u,_1\right)P_{11},_1-\\
-r^2\left(k\delta w-w,_1\,\delta w,_1-\delta u,_1\right)K_{11},_1+\\
+r\left(-\delta w,_1+k\left(kr\delta w-\delta u\right)\right)P_{12},_1+\\
+\left(-kr^2\delta w+r\delta u\right)K_{12},_1+\delta w,_1\,D_{12},_1\,kr+\\
+\left(-r\left(kP_{11}-kP_{12}-K_{11}+K_{12}\right)w,_1\right)\delta w,_1+\\
(k^2P_{11}r^2+k^2P_{12}r^2-kr^2K_{11}-kr^2K_{12}-kD_{22}+P_{22})\delta w,_1-\\
-r\left(kP_{11}-K_{11}\right)\delta u,_1+\delta wP_{11}k^2r-\\
-\delta wK_{11}kr-\left(kr\delta w-\delta u\right)\left(kP_{22}-K_{22}\right)=0\,.
\end{gathered}
$$

The resulting gradient system of equations (15) needs to be supplemented with boundary conditions in increments. Due to the axial symmetry of the problem, at the center of the shell the rotation of the normal to the middle surface, radial displacements and their increments will be equal to zero ($w,_1=0$, $u=0$, $\delta w,_1=0$, $\delta u=0$).

In the process of chemical adsorption, hydrogen molecules disintegrate into atoms that diffuse deep into the material [9, 10]. The flux density J is proportional to the spatial concentration gradient λ, the diffusion equation takes the form:

$$J=-Dgrad\lambda=-D\frac{\partial\lambda}{\partial z},\qquad (16)$$

where $D=const$ – diffusion coefficient, z – coordinate in the direction of diffusion that corresponds to the axis α_3.

In accordance with the experimental data presented in [11], as well as in connection with unidirectional diffusion, the kinetic equation of hydrogenation corresponds to Fick's second law, and its solution is known due to the double Fourier transform (direct and inverse), the result of which has the form:

$$\frac{\partial\lambda(z,t)}{\partial t}=D\frac{\partial^2\lambda(z,t)}{\partial z^2},\qquad (17)$$

where t – is a current time.

The solution of equation (17) for the process of one-sided diffusion has a well-known approximate analytical solution presented in the works [9, 10]:

$$
\begin{gathered}
\lambda(z,t)=\lambda_1+(\lambda_2-\lambda_1)z/h+\\
+(2/\pi)\sum_{i=1}^{\infty}\sin(i\cdot\pi\cdot z/h)\exp(-F_o\pi^2i^2)\times\\
\times[\lambda_2\cos(i\cdot\pi)-\lambda_1]/i,
\end{gathered}
$$

where $F_O=Dt/h^2$ – is a Fourier number; i – is a row member number; λ_1 and λ_2 – boundary values of the concentration of the medium on the lower and upper surfaces of the shell.

For the shell, the following boundary conditions are accepted: in the event of an aggressive medium acting on the side of the application of a power load:

$$\lambda(-h/2,t)=\lambda_\infty=\lambda_1,\quad \lambda(+h/2,t)=0=\lambda_2,$$

where λ_∞ – equilibrium concentration of a hydrogen-containing medium.

The initial conditions are:

$$\lambda(z,0)=0\,.$$

The calculations were performed using the MATLAB and Maple software packages. The results of calculating a spherical shell operating in an aggressive environment of hydrogen with various concentrations from 0 to 0.08% using the proposed model are presented below.

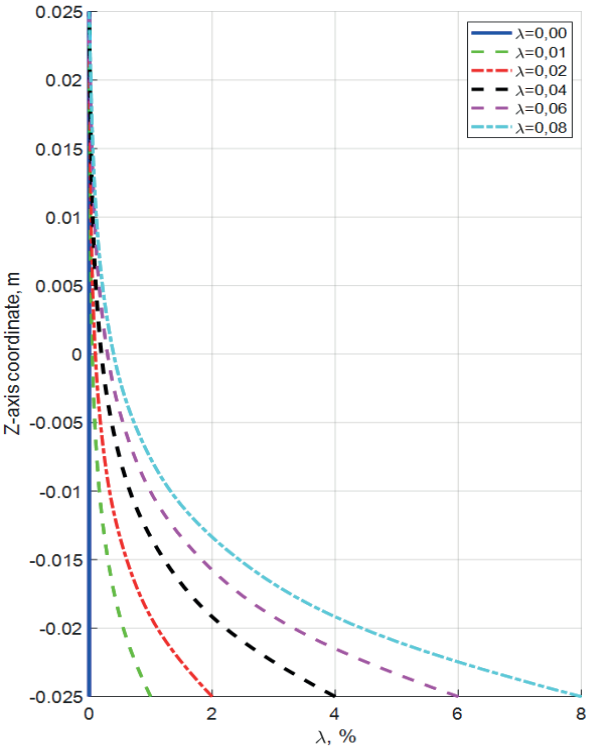

Figure 2. Distribution of hydrogen concentration by shell thickness

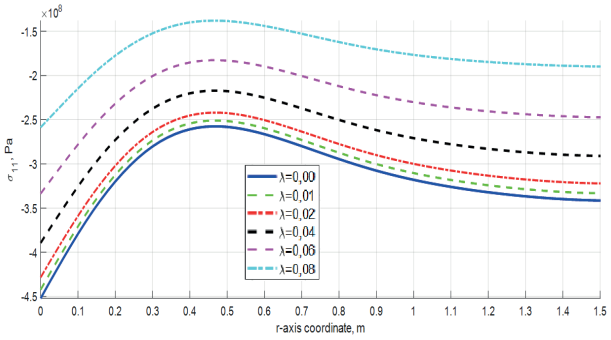

Figure 3. Stresses σ11 along the radius from below

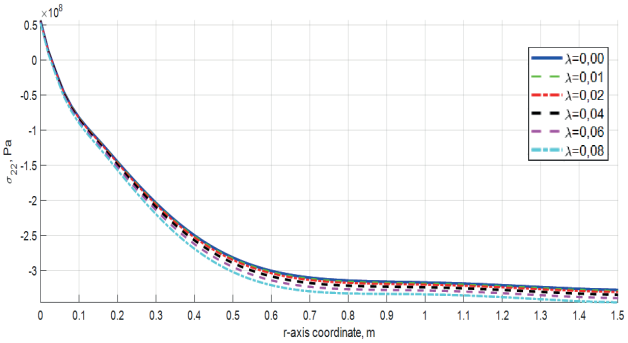

Figure 4. Stresses σ22 along the radius from above

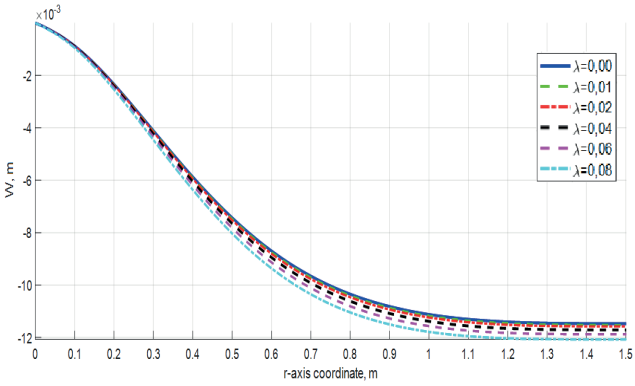

Figure 5. Deflections in the shell

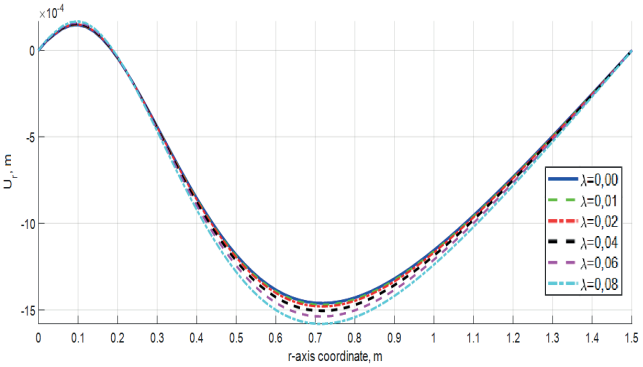

Figure 6. Horizontal displacements

CONCLUSION

After analyzing the presented graphs shown in figures 2 - 6, it is easy to note the similarity of the results calculated using the model considered in the presented article with classical nonlinear solutions without taking into account hydrogen saturation. The conducted research is fully consistent with the experimentally established facts, which shows that during a certain time interval corresponding to large gradients of hydrogen concentrations, there is an intense change in the nature of the stress-strain state of structures. In this case of a spherical shell, quantitative changes reach 20% for stresses in compressed and 24% in stretched zones. The control of the impact of an aggressive hydrogen environment in the work was organized on the basis of nonlinear relationships that consider the induced sensitivity to hydrogen saturation in a wide range of changes in the types of stress state [8, 9, 12, 13].

In this work, a mathematical model of the effect of hydrogen saturation on the stress-strain state of a shallow spherical shell is constructed and a numerical solution to the problem is presented with an illustration of deflections, displacements and stresses.

The model of the influence of gas saturation, constructed in this work, is based on the approaches to constructing constitutive relations for materials with different resistance, proposed in works [8, 9, 12, 13]. This approach uses a rather flexible mechanism for taking into account a variety of stress states and demonstrates a high accuracy of agreement between the results obtained and experimental data on the deformation of a wide range of materials under complex types of stress states. In turn, the model for accounting for materials with different resistance, proposed in the works of I.G. Ovchinnikov [1 – 4], is based on the simplest nonlinear theory of elasticity and is built considering the uniaxial stress state and, therefore, has an approximate mechanism of the influence of the type of stress state on the strength of materials.

ACKNOWLEDGEMENT

This research has been supported by the the grant of the Rector of TulSU, contract № 8898GRR of March 1, 2021 and also supported by a grant from the government of the Tula region in the field of science and technology, agreement № DS/284 of October 25, 2021.

REFERENCES

1. **Ovchinnikov I.G.** O metodologii postroeniya modelej konstrukcij, vzaimodejstvuyushchih s agressivnymi sredami [On the methodology for constructing models of structures interacting with aggressive media] / I.G.Ovchinnikov // Durability of materials and structural elements in aggressive and high-temperature media. – Saratov: Sarat. polytechnic institute, 1988, pp. 17-21 (in Russian).
2. **Ovchinnikov I.G.** Matematicheskoe modelirovanie processa vzaimodejstviya elementov konstrukcij s agressivnymi sredami [Mathematical modeling of the process of interaction of structural elements with aggressive media] / I.G.Ovchinnikov, V.V.Petrov // Deformation of materials and structural elements in aggressive media. - Saratov: Sarat. polytechnic in-t., 1983, pp. 3-11. (in Russian)
3. **Ovchinnikov I.G.** Analiz eksperimental'nyh dannyh po vliyaniyu vodoroda pri normal'nyh temperaturah na mekhanicheskie svojstva metallov i splavov k postroeniyu modeli vzaimodejstviya konstruktivnyh elementov s vodorodom **[**Analysis of experimental data on the effect of hydrogen at normal temperatures on the mechanical properties of metals and alloys for the construction of a model of the interaction of structural elements with hydrogen]. Part 1. The problem of the effect of hydrogen on metals and ways to solve it. Regularities of hydrogen penetration into structural elements / I.G.Ovchinnikov, A.B.Rassada. – Saratov: Sarat. polytechnic institute, 1989, 28 pages (in Russian).
4. **Ovchinnikov I.G.** Model' vzaimodejstviya nagruzhennyh elementov konstrukcij s vodorodosoderzhashchej sredoj i ee prilozheniya [Model of interaction of loaded structural elements with a hydrogen-containing medium and its applications] / I.G.Ovchinnikov, A.B.Rassada. // Applied problems of strength and stability of deformable systems in aggressive media. Saratov: Sarat. polytechnic institute, 1989, pp. 12-16 (in Russian).
5. **Rabotnov Yu.N.** O mekhanizme dlitel'nogo razrusheniya [On the mechanism of prolonged destruction] // Problems of strength of materials and structures. Moscow: Publishing House of the Academy of Sciences of the USSR, 1959, pp. 5-7 (in Russian).
6. **Rabotnov Yu.N.** Izbrannye trudy. Problemy mekhaniki deformiruemogo

tverdogo tela [Selected Works. Problems of solid mechanics]. Moscow: Science, 1991, 196 pages (in Russian).
7. **Petrov V.V.** Dvuhshagovyj metod posledovatel'nogo vozmushcheniya parametrov i ego primenenie k resheniyu nelinejnyh zadach mekhaniki deformiruemogo tverdogo tela [Tekst] [Two-step method of successive perturbations of parameters and its application to solving nonlinear problems of solid mechanics of deformable body [Text] / V.V.Petrov, I.G.Ovchinnikov, V.K.Inozemtsev // Problems of strength of structural elements under the action of loads and working media. – Saratov: SSTU, 2001, pp. 6-12 (in Russian).
8. **Treshchev A.A.** Izotropnye plastiny i obolochki, vypolnennye iz materialov, chuvstvitel'nyh k vidu napryazhennogo sostoyaniya: monografiya. [Isotropic plates and shells made of materials sensitive to the kind of the stress condition]. Moscow-Tula: RAABS-TulSU, 2013, 249 pages (in Russian).
9. **Korneev A.V.** Uchet vliyaniya vodorodosoderzhashchej sredy na napryazhenno-deformirovannoe sostoyanie materialov na osnove titanovyh splavov [Accounting for the influence of a hydrogen-containing medium on the stress-strain state of materials based on titanium alloys]. A.V.Korneev, A.A.Treshchev // Proceedings of universities. Building. – 2009, №3-4 (603-604), pp. 23-29. (in Russian).
10. **Treshchev A.A.** Teoriya deformirovaniya i prochnosti materialov s iznachal'noj navedyonnogo chuvstvitel'nost'yu k vidu napryazhyonnogo sostoyaniya. Opredelyayushchie sootnosheniya: monografiya. [The theory of deformation and durabilities for the materials with a primary and induced sensitivity to a kind of an stress condition. Defining correlations]: – Moscow - Tula: RAABS; TulSU, 2016, 328 pages (in Russian).
11. **Gervits T.Ya.** Vliyanie gazonasyshcheniya na staticheskuyu prochnost' titanovyh splavov [Influence of gas saturation on the static strength of titanium alloys] // FKhMM. 1981, № 2, pp. 45-48 (in Russian).
12. **Treshchev A.A.** Vliyanie izmeneniya koncentracii vodoroda vo vremeni na nds sfericheskoj obolochki iz titanovogo splava [Influence of changing the concentration of hydrogen during time on the structure of a spherical shell made of titanium alloy] / A.A.Treshchev, V.O.Kuznetsova // Expert: theory and practice, 2020, № 4 (7), pp. 72-81. doi: 10.24411/2686-7818-2020-10039. (in Russian).
13. **Matchenko, N.M.** Opredelyayushchie sootnosheniya izotropnyh raznosoprotivlya-yushchihsya sred. CH. 2. Nelinejnye sootnosheniya [Tekst] **[**Determining ratios of isotropic multi-resistive media. Part 2. Nonlinear ratios] / N.M.Matchenko, L.A.Tolokonnikov, A.A.Treshchev // News of the Academy of Sciences. Solid State Mechanics. – 1999, № 4, pp. 87-95 (in Russian).

СПИСОК ЛИТЕРАТУРЫ

1. **Овчинников И.Г.** О методологии построения моделей конструкций, взаимодействующих с агрессивными средами / И.Г.Овчинников // Долговечность материалов и элементов конструкций в агрессивных и высокотемпературных средах. – Саратов: Сарат. политехн. ин-т., 1988. С. 17-21.
2. **Овчинников И.Г.** Математическое моделирование процесса взаимодействия элементов конструкций с агрессивными средами / И.Г.Овчинников, В.В.Петров // Деформирование материалов и элементов конструкций в агрессивных средах. – Саратов: Сарат. политехн. ин-т., 1983. С. 3-11.
3. **Овчинников И.Г.** Анализ экспериментальных данных по влиянию водорода при

нормальных температурах на механические свойства металлов и сплавов к построению модели взаимодействия конструктивных элементов с водородом. Ч. 1. Проблема воздействия водорода на металлы и пути ее решения. Закономерности проникания водорода в конструктивные элементы / И.Г. Овчинников, А.Б. Рассада. – Саратов: Сарат. политехн. ин-т., 1989. 28 с.

4. **Овчинников И.Г.** Модель взаимодействия нагруженных элементов конструкций с водородососодержащей средой и ее приложения / И.Г.,Овчинников, А.Б.Рассада. // Прикладные проблемы прочности и устойчивости деформируемых систем в агрессивных средах. Саратов: Сарат. политехн. ин-т., 1989. С. 12-16.
5. **Работнов Ю.Н.** О механизме длительного разрушения // Вопросы прочности материалов и конструкций. М.: Изд-во АН СССР, 1959 С. 5–7.
6. **Работнов Ю.Н.** Избранные труды. Проблемы механики деформируемого твердого тела. М.: Наука, 1991 196 с.
7. **Петров В.В.** Двухшаговый метод последовательного возмущения параметров и его применение к решению нелинейных задач механики деформируемого твердого тела [Текст] / В.В.Петров, И.Г. Овчинников, В.К.Иноземцев // Проблемы прочности элементов конструкций под действием нагрузок и рабочих сред. – Саратов: СГТУ, 2001. – С. 6-12.
8. **Трещев А.А.** Изотропные пластины и оболочки, выполненные из материалов, чувствительных к виду напряженного состояния: монография. М.: Тула: РААСН; Изд-во ТулГУ, 2013. – 249 с.
9. **Корнеев А.В.** Учет влияния водородосодержащей среды на напряженно-деформированное состояние материалов на основе титановых сплавов / А.В. Корнеев, А.А. Трещев // Изв. вузов. Строительство. – 2009. – №3-4 (603-604). – С. 23–29.
10. **Трещев А.А.** Теория деформирования и прочности материалов с изначальной наведённого чувствительностью к виду напряжённого состояния. Определяющие соотношения: монография. – М.; Тула: РААСН; ТулГУ, 2016. – 328 с.
11. **Гервиц Т.Я.** Влияние газонасыщения на статическую прочность титановых сплавов / Г.Я.Гервиц // ФХММ. 1981. № 2. С. 45-48.
12. **Трещев А.А.** Влияние изменения концентрации водорода во времени на ндс сферической оболочки из титанового сплава / А.А. Трещев, В.О. Кузнецова // Эксперт: теория и практика. – 2020. – № 4 (7). – С. 72-81.
13. **Матченко Н.М.** Определяющие соотношения изотропных разносопротивляющихся сред. Ч. 2. Нелинейные соотношения [Текст] / Н.М. Матченко, Л.А. Толоконников, А.А. Трещёв // Изв. РАН. МТТ. – 1999. – № 4. – С. 87-95.

Aleksander A. Treshchev, Doctor of Technical Sciences, Professor, Head of the Department of Construction, Building Materials and Structures, Tula State University, Corresponding Member of RAACS; 300012, Russia, Tula, Lenin Ave. 92. Phone: +7 (905) 622-90-58. E-mail: taa58@yandex.ru.

Violetta O. Kuznetsova, graduate student of the department "Construction, building materials and structures" of Tula State University; 300012, Russia, Tula, Lenin Ave. 92. Phone: +7 (920) 759-52-80. E-mail: kuznecova_violetta@mail.ru.

Александр Анатольевич Трещев, доктор технических наук, профессор, зав. кафедрой «Строительство, строительные материалы и конструкции» Тульского Государственного Университета, член-корреспондент РААСН; 300012, Россия, г. Тула, пр. Ленина, 92. Тел. +7 (905) 622-90-58. E-mail: taa58@yandex.ru .

Виолетта Олеговна Кузнецова, аспирант кафедры «Строительство, строительные материалы и конструкции» Тульского Государственного Университета; 300012, Россия, г. Тула, пр. Ленина, 92. Тел. +7 (920) 759-52-80. E-mail: kuznecova_violetta@mail.ru.

International Journal for Computational Civil and Structural Engineering, 18(2) 131–142 (2022)

DOI:10.22337/2587-9618-2022-18-2-131-142

OPTIMIZATION OF BEARING STRUCTURES SUBJECT TO MECHANICAL SAFETY: AN EVOLUTIONARY APPROACH AND SOFTWARE

Anatoliy V. Alekseytsev [1], Al Ali Mohamad [2]

[1] Moscow State University of Civil Engineering (National Research University), Moscow, RUSSIA
[2] Technical University of Košice, Košice, SLOVAK REPUBLIC

Abstract. An approach to solving the urgent problem of optimizing the load-bearing structures of buildings and structures based on adapted genetic algorithms is presented. As a tool for finding a solution, iterative schemes are used, in which, in the classical approach to evolutionary modeling, a system of constraints is used that forms the operational requirements for reinforced concrete, steel and other structures. In this case, the value of the risk of material losses is used as one of the measures of the design optimality. This value is used to assess the feasibility of increasing the initial costs of manufacturing structures, taking into account the degree of their mechanical safety in case of emergency impacts. Groups of scenarios are considered as such impacts, including local damage to one or more load-bearing elements. A limitation is formed on the resistance to progressive collapse of the structure, which is interpreted as preventing large displacements and limiting deformations of certain parts or the structure as a whole. The magnitude of the risk is determined by a relative index determined as the ratio of the likely cost for damage from material loss to the initial cost of manufacturing the structure. The block diagrams that implement such iterative processes, information about the developed software and an example of optimization of the reinforced concrete supporting structure of the frame of an administrative multi-storey building are considered.

Keywords: genetic algorithms, evolutionary modeling, mechanical safety, optimization, progressive collapse, emergency actions, risk, software.

ОПТИМАЛЬНОЕ ПРОЕКТИРОВАНИЕ БЕЗОПАСНЫХ НЕСУЩИХ КОНСТРУКЦИЙ: ЭВОЛЮЦИОННЫЙ ПОДХОД И ПРОГРАММНОЕ ОБЕСПЕЧЕНИЕ

А.В. Алексейцев [1], Ал Али Мохамад [2]

[1] Национальный исследовательский Московский строительный университет, г. Москва, РОССИЯ
[2] Технический университет в Кошице, г. Кошице, СЛОВАКИЯ

Аннотация. Представлен возможный подход к решению актуальной задачи оптимизации конструктивных решений для несущих конструкций зданий и сооружений на основе адаптированных генетических алгоритмов. В качестве инструмента для поиска решения используются итерационные схемы, в которых при классическом подходе к эволюционному моделированию используется система ограничений, формирующая эксплуатационные требования к железобетонным, стальным и другим конструкциям. При этом в качестве одной из мер оптимальности конструкции используется величина риска материальных потерь. Эта величина используется для оценки целесообразности увеличения первоначальных затрат на изготовление конструкций с учетом степени их механической безопасности при запроектных воздействиях. Рассматриваются группы сценариев, включающие локальные повреждения одного или нескольких несущих элементов. При этом ставится ограничение на живучесть конструкции, которая трактуется как недопущение больших перемещений и предельных деформаций определенных частей или конструкции в целом. Величина риска определяется относительным индексом, определяемым соотношением вероятного ущерба от материальных потерь в стоимостном выражении к первоначальным затратам на изготовление конструкции. Рассматриваются блок-схемы, реализующие такие итерационные процессы, сведения о разработанном программном обеспечении и пример оптимизации железобетонной несущей конструкции каркаса административного многоэтажного здания.

Ключевые слова: генетические алгоритмы, эволюционное моделирование, механическая безопасность, оптимизация, живучесть, запроектные воздействия, риск, программное обеспечение.

INTRODUCTION

The problem of optimizing reinforced concrete and steel frames considering their safety level is mostly understudied. There are only a few studies that concern particular aspects of the problem to a different extent [1-4]. At the same time, some studies focus on both mechanical and technogenic safety [5]. As an example of optimizing, let's consider relatively simple objects, while hazards shall be excluded from a single iterative procedure. Structures safety is considered according to the values loss risk factor calculation [6-7]. In this regard, it may be difficult to optimise a design solution, considering costs of construction site life cycle stages in its in normal operations and considering its resistance to beyond design basis effects. Recent search schemes based on modern information technologies allows for getting better in solving this problem. Firstly, these are genetic algorithms [8-10], particle swarm methods [11-13], ant colony [14], and firefly's methods [15]. These algorithms may get accustomed to solving optimisation tasks both reinforced concrete, steel and other structures of various types. The article is concerned with the common approach to optimisation of reinforced concrete and steel load bearing structures considering the level of their mechanical safety, as well as evolutionary algorithms implementation for truss and plated and truss structures. It is proposed to introduce a measure of relative integral socio-economic losses risk as an estimate of safety level. The risk considers both normal operations of structural systems as part of a functional ongoing process in the building and emergency conditions related to mechanic damage of individual units or elements.

1. THE PROBLEM FORMULATION

As an optimal design goal, we'll use minimization of value terms of materials consumption of a structure, the labour intensity involved in its manufacture, and also safety level at emergency.

$$C\left(\{Y\}\right) \to \min; \quad \{Y\} = \left\{\{y\}_1, \{y\}_2, ..., \{y\}_{Np}\right\}, \tag{1}$$

where C is a notional value (conventional units), that considers the materials that make up the load bearing structure, manufacturing features and socio-economic losses risks; $\{Y\}$ is a set of design parameters that vary in search process, consisting of N_p disjoint subsets $\{y\}_{it}$, $it = (1,...,N_p)$; $\{y\}_{it}$ – a set of parameters consisting of parameter values admitted for selection in search process, corresponding to its it type.

This parameter type implies, for example, combinations of building element cross sections, position of structural joints, material classes of which it is made, plate width and etc.

Expressions for calculation of the value C for specific cases of structure optimisation have various notations, for example, for reinforced concrete frames [16]:

$$C = (P_c + P_r + P_f) \to P_{\min}, \tag{2}$$

where P_c, P_r, P_f – prime cost of materials and manufacture for concrete, fittings, casing and associated materials, respectively, $P_{\min}$ – some small real number;

– for steel frames [17]:

$$M = \rho \sum_{i=1}^{n} A_i l_i \to \min, \tag{3}$$

where ρ is steel density, A_i, l_i are area and length of structure element, respectively, and n *is* their number;

– for wood structures [18]:

$$f(\vec{X}) = \frac{C_{tim}V_{tim}(\vec{X}) + C_{pl}V_{pl}(\vec{X})}{a_n b_n} \to \min, \quad (4)$$

where $(\vec{X})$ is a vector of variables; $V_{tim}(\vec{X})$, $V_{pl}(\vec{X})$ are wood and plywood volumes in the fabricated structure; a_n, b_n are bay and width of a wood structure; C_{tim}, C_{pl} are weight coefficients for wood and plywood.

In solving the minimisation problem (1) by way of task (2) and (4), socio-economic losses risks is not considered in the goal function, that significantly diminishes the mechanical safety level of such optimized structures. The goal function is proposed as follows:

$$C = \left(C_S + R_S\right) \to \min,$$
$$R_S = \sum_{i=1}^{N}\sum_{j=1}^{M} p_{i,j}U_{i,j}, \quad (5)$$

C_S is a value related to costs for materials, structure fabrication, joint connection arrangement and etc.; R_S is the value terms of socio-economic losses risk defined by the probability $p_{i,j}$ for emergency j at stage i of structure life cycle. This probability can be determined based on the well-known Bayes' formula for conditional probability, N, M are a number of emergencies considered in optimisation for life cycle stages and those that may occur at this stage.

In solving load bearing structures optimisation problems, the following main active constraints are used:

– structure elements strength. This criterion can be expressed in strains, deformations and critical forces in dangerous cross section of a building element. These factors should not exceed the set design resistances, deformations, and forces;

– structure stiffness along linear displacements or angles of rotation;

– stability of system geometrical shape in the presence of its structural (topological) changes.

Passive constraints may be presented by conditions for ensuring structure overall stability, local durability of its structural elements, observing the requirements for unification of constructive solution, manufacturing or assembling processes.

It's obvious that the growing complexity of design solutions creates the necessity of varying dozens of design parameters. In this regard, manual approaches to optimisation become unacceptable, while gradient-based optimization algorithms are not efficient. With that said, methods evolve based on a combination of search algorithms, linear and non-linear mathematical programming. The major problem in implementation of such an optimisation approach for load bearing structures lies in the necessity of multiple automatic calculation at structure strain-stress distribution. Let us consider one of the variant for this calculation arrangement.

2. GENERAL SOLUTION SEARCH CIRCUIT

A number of basic stages is proposed for evolutionary algorithm implementation in terms of design solution.

2.1. Defining one or several optimisation criteria corresponding to problem solution goal. For example, cost minimum, ensuring strength, collapse resistance in emergency and etc. Here a decision is also taken about optimisation task decomposing, its phasing for a purpose of optimal topological synthesis, search for rational form. An example of such decomposition is addressed in work [19].

2.2. Formation of data on structure computational model, design parameter sets, force, kinematical, structural and technological constraints of the task.

2.3 Development or selection of a mathematical model for estimation of constraint satisfaction. A proven calculation model can be used for

bearing structures set forth in regulatory documents, and also computing model based on finite elements method. Moreover, for evolutionary approach implementation there is a problem for solver integration into the iterative search scheme. One of such methods will be stated in this paper.

2.4 Verification of constraint satisfaction, calculation of target function values and implementation of preserving the best solution for further reproduction and improvement of decisions. In using several optimality criteria, the target function value can be calculated based on weight coefficients x_k per each of the criteria:

$$C = \sum_{k=1}^{Nc} C_k x_k, \ \sum_k x_k = 1, \qquad (6)$$

where C_k is a goal function value upon criterion k, Nc is a number of criteria.

2.5 Verification of the condition of search process end. Provided that the condition for ending the iterations is satisfied the search is stopped. If it's not, then based on existing best solutions, structure options are modified by way of changing some varied parameters and proceeding to stage 2.4.

Some integral iteration number N_p is considered as a criterion of ending the iterations for genetic search during which no improvements occur in the iteration process:

$$N_p = {}^{n/3}\sqrt{mn!}, \qquad (7)$$

where n is a number of independently varied parameters; m is the arithmetic mean for values admitted for each parameter selection. Implementing the condition for ending the iterations is shown in Fig. 1.

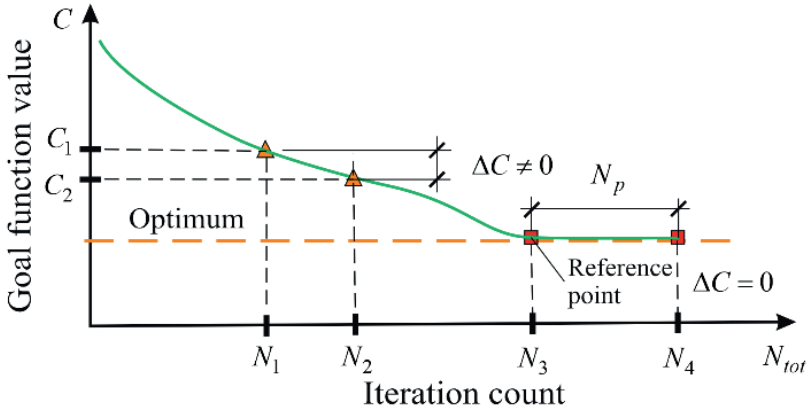

Figure 1. For realisation of iteration stopping criterion

Upon completion of iteration stopping, a decision obtained as a result of search is verified for satisfaction of passive (not considered during the iteration process) constraints.

Such constrains may include local durability of joint connection elements, design features related to ensuring structural support, local plate durability, ensuring necessary installation conditions and etc. Studies [20-23] explain in more detail the evolutionary algorithm in respect to individual types of load bearing building constructions. We'll demonstrate the content of stage 2.2 and stage 2.4 of evolutionary approach using the example of reinforced concrete simple beam (figures 2, 3). In this case, 4 parameters vary independently: higher and lower fitting diameters, concrete and fitting class. Some parameters may remain permanent.

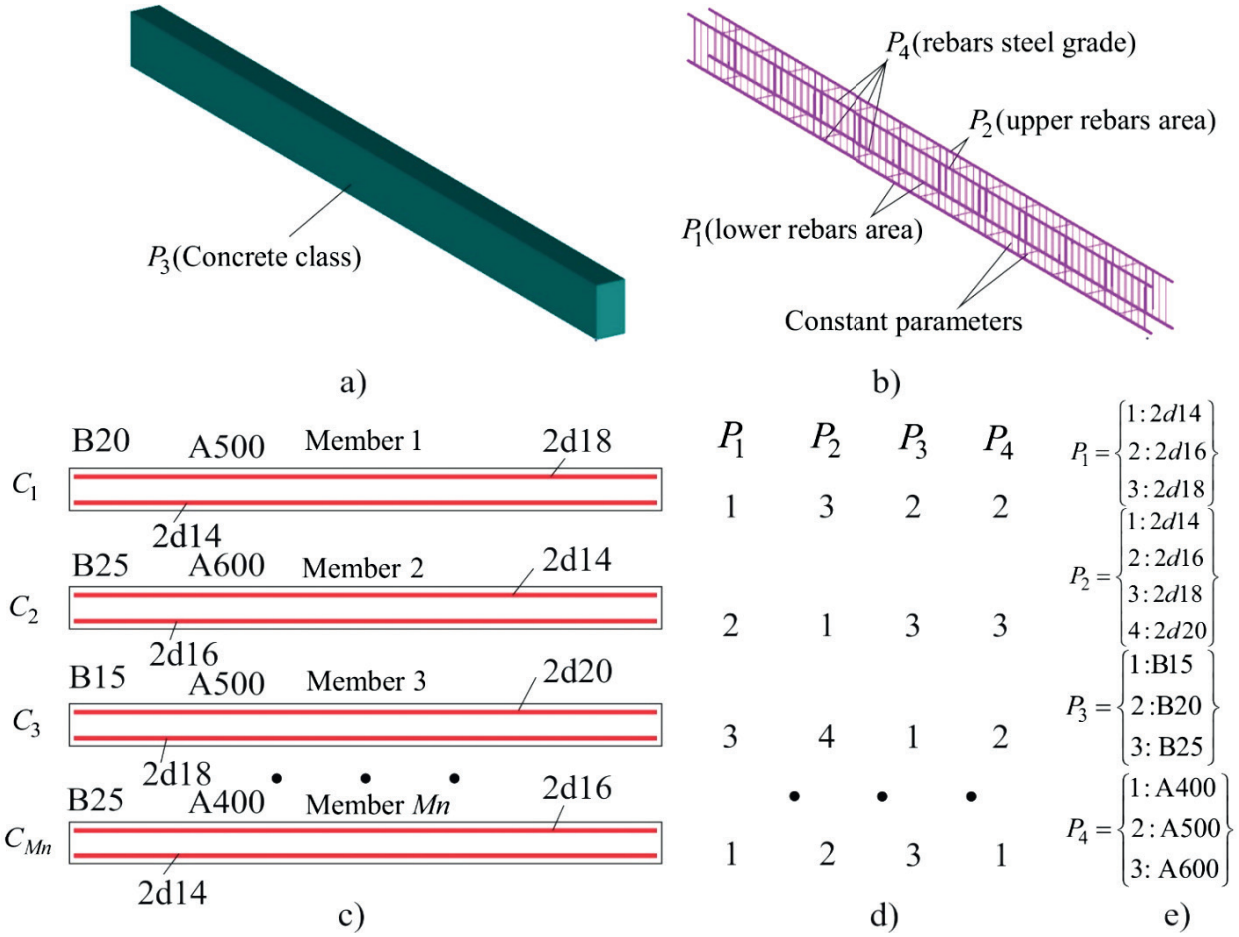

Figure 2. Presentation of reinforced concrete beam and sets of such structures in evolutionary approach: examples of setting varying and non-varying parameters (a), (b), vision of initial occasionally generated decision set (c), example of coding parameter values (d), set of permitted parameter values (e)

The choice of structure members for further solution improvement is made based on roulette-wheel selection method in fig. 3, a, where the choice probability is determined by the value:

$$l_i = f_i \Big/ \sum_{j=1}^{N} f_j,\ f_i = 1/C_i^I,\ I = 1..4, \qquad (8)$$

Structure modification is made based on operators, examples of which are shown in fig. 3, b, c. In making a decision about preservation of the best solution the following elitism EC criteria are used (fig. 3d):

$$\begin{cases} (\forall A_i \in \Pi_A)\exists A_i \notin \Pi_B \\ C(\forall A_i \in \Pi_A) \le C_{\max}(\tilde{A}_{\tilde{i}} \in \Pi_B) \end{cases} \Rightarrow, \qquad (9)$$
$$\Rightarrow \left(\tilde{A}_{\tilde{i}} \in \Pi_B\right) = \left(A_i \in \Pi_A\right).$$

The first condition in the system means absence in elite set Π_B a copy from the set Π_A, and second condition means that the meaning of a target criteria for a member from set Π_A must be less than maximum from the elite set. It should be noted that dimensions M_n of a current set and M_{ne} elite set of decisions may differ. Practical use of evolutionary approach showed that $M_n \in [15 \div 50]$, $M_{ne} \in [10 \div 25]$.

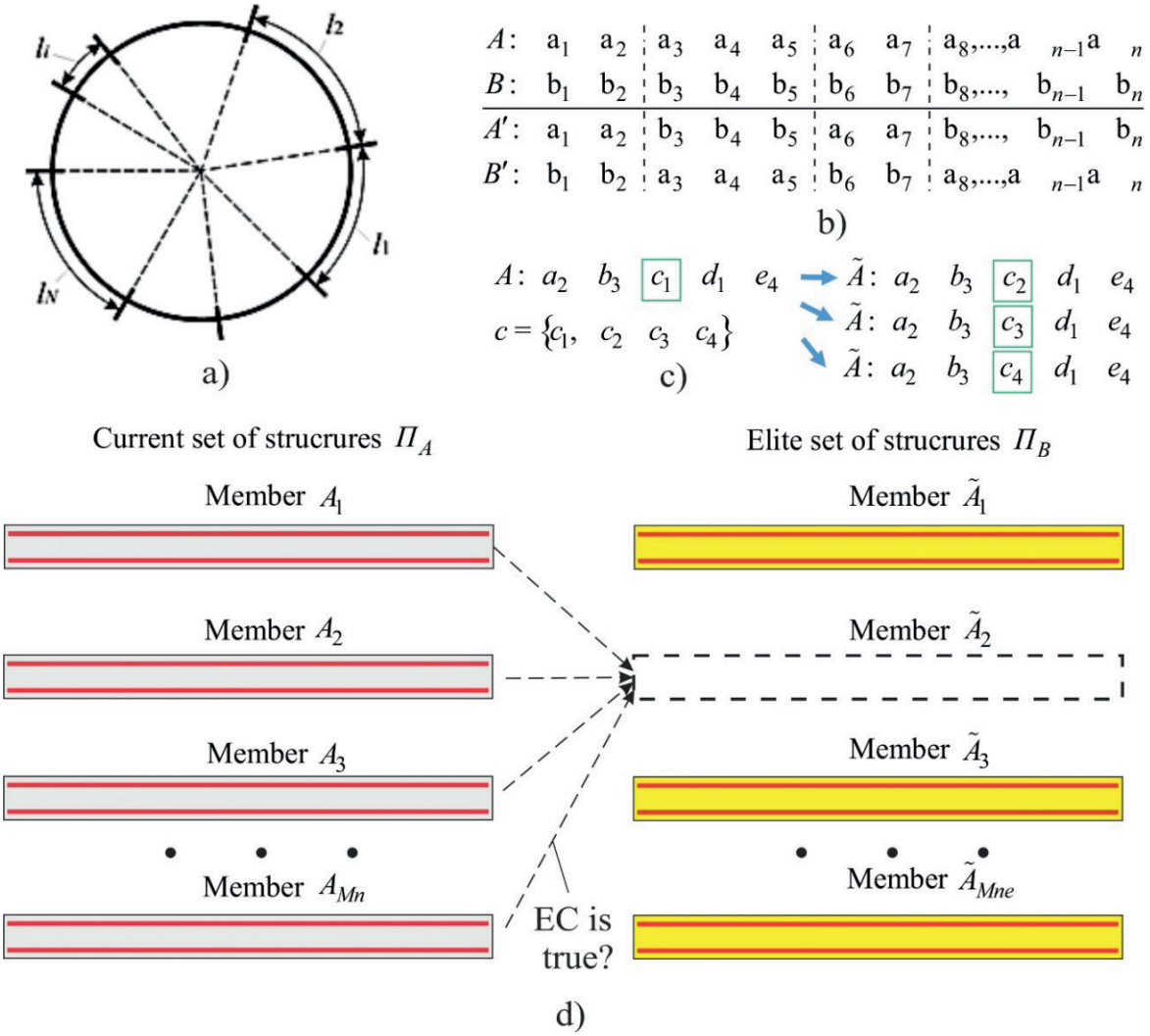

Figure 3. Evolutionary search components: roulette-wheel scheme (a), multipoint crossingover (b) and mutation (c) operators, elite population editing scheme on the basis of elitism criteria (EC) satisfaction

3. INTERACTION WITH PROGRAM COMPEX SOLVERS

Current requirements to structural designing assume the assessment of their strain-stress distribution taking into account physical, geometrical and constructive nonlinearity. It calls for using modern program complexes with a possibility of exchanging data with a solver and exterior programme developments. Simcenter "Femap". Preprocessor of this complex can integrate with all modern solvers, while we've used NX Nastran solver. The scheme of organisation of evolutionary search program interaction [24, 25] with Simcenter "Femap" is shown in fig. 4.

The operating system is used to exchange data between the finite element complex solver and the genetic search program. This is possible if there is an open format for the input / output file, as well as the ability to run the solver without using special pre / postprocessor commands.

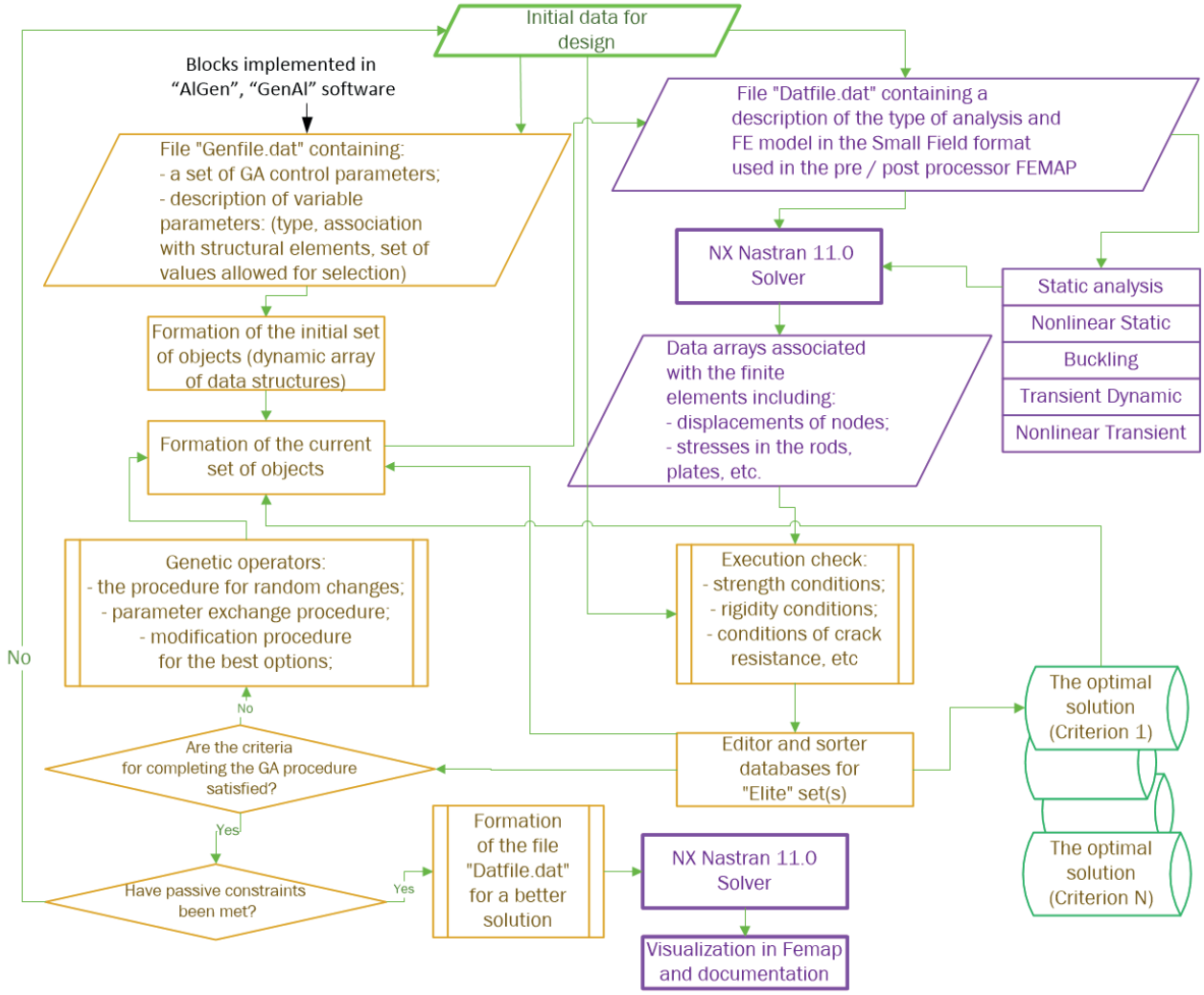

Figure 4. Structure of software employing the evolutionary process search for bearing structure optimization

4. EXAMPLE OF USING EVOLUTIONARY ALGORITHM IN VARIOUS APPROACHES TO DESIGNING

Let us consider the designing of the frame of half precast multi-storey civil building. Frame ceilings and finishes are precast. It is believed, that their parameters to be non-variable. It means, that they are not considered within the search.

There are three options of frame designing to be considered:

– using solutions given in typical design documentation (s. B1.020) allowing for normal operations (I);

– using evolutionary search with no regard for safety limits according to presentation (5) in $R_s = 0$ (II);

– using evolutionary algorithm in accordance with presentation with a possibility of considering emergencies $R_s \neq 0$ while ensuring mechanical safety at level $\zeta = R_s / C_s = 0.2$. Frame calculation scheme is shown in fig. 5, a. As an emergency script, it is offered to have an opportunity of excluding their design diagram one from columns K1-K7 as a result of local mechanical damage fig. 5, b.

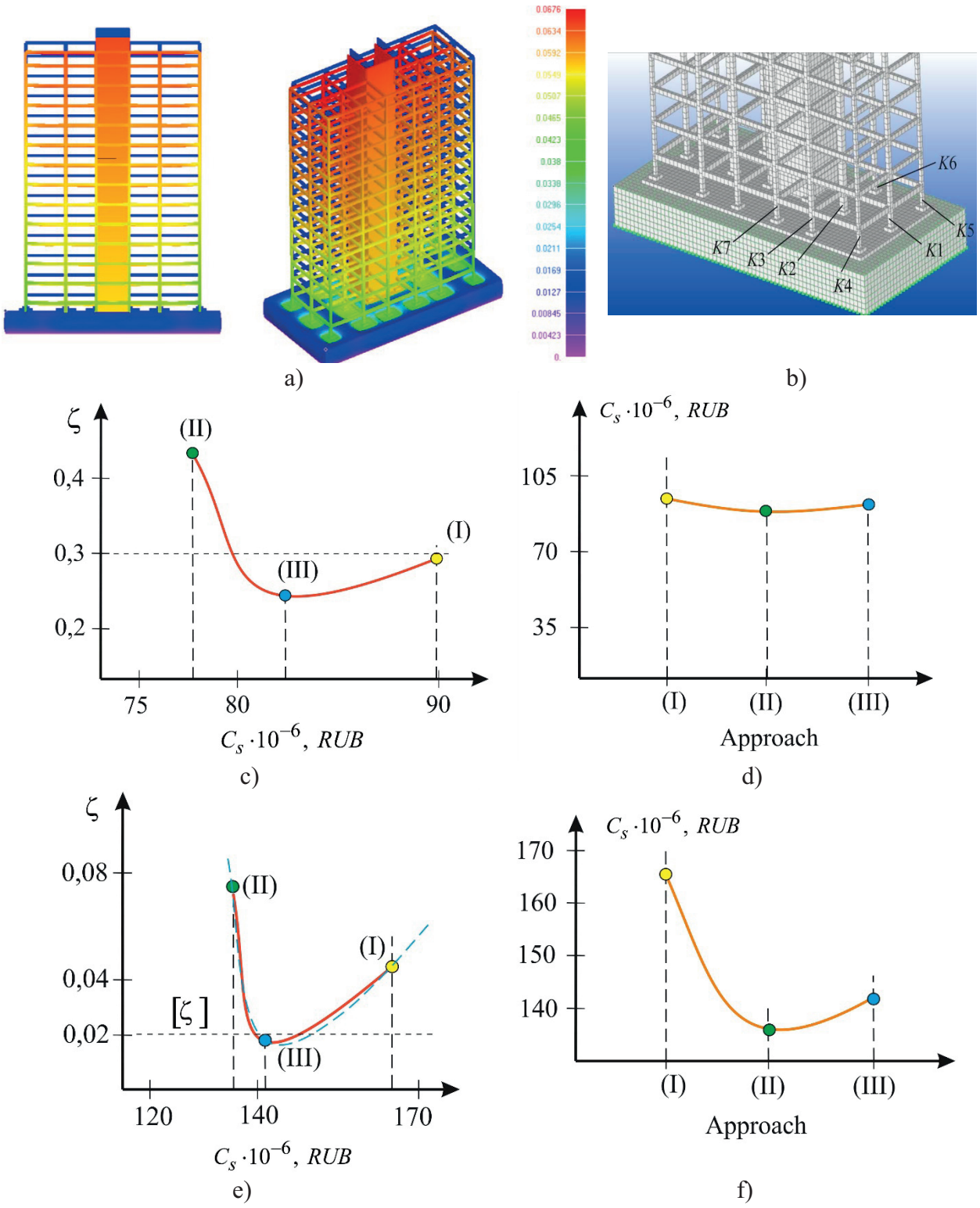

Figure 5. Results of building frame designing: design diagram including the map of vertical yield of the building foundation (a), emergency scripts (b), results of safety and cost estimation in normal operations (c, d) and emergency (e, f)

As the figure 5, c, d shows, in normal operations regardless of possible emergency conditions, the approach to designing according to rules (I) allows for gaining the structure value comparable to optimisation algorithms (II), (III). Moreover, structure cost-cutting using (II) approach significantly decreases its safety. Using constrains in view of the risks in optimisation algorithms (III), a 40% safer structure option has been obtained with very insignificant appreciation (to 10%) in comparison to approach (I).

DISCUSSION

Considering emergency condition scripts, conventional approach (I) does not allow for obtaining minimal design cost in reaching a relative level risk $\zeta \leq 0.2$. Utilising genetic search (II) in minimal cost may appear unacceptable due to a low safety level, which appeared to be almost 2 times lower than in approach (I). Approach (III) is the most cost-saving solution in constraints to safety level.

CONCLUSION

1. An approach has been developed to bearing structure parameter optimisation based on evolutionary algorithm.
2. Solving the problems of optimizing building load bearing structures of normal and advanced responsibility level must include a requirement for considering the risk of consequences from an accident.
3. A scheme of interaction of evolutionary search iteration procedure with modern program complexes.

ACKNOWLEDGEMENT

Authors are thankful to organisers of the conference “Tasks and methods of simulation of structures and constructions” (“Zolotovskie readings” – 2019) for an opportunity to test the basic results described herein.

REFERENCES

1. **Aoues Y., Chateauneuf A.** Reliability-based optimization of structural systems by adaptive target safety - Application to RC frames. Structural Safety. 2008; 30(2):144–61. doi: 10.1016/j.strusafe.2006.10.002
2. **Tamrazyan A., Alekseytsev A.** Strategy for the evolutionary optimization of reinforced concrete frames based on parallel populations evolving In: IOP Conference Series: Materials Science and Engineeringthis link is disabled, 2020, 869(5), 052019
3. **Lee C.K., Kim S.K.** GA-based algorithm for selecting optimal repair and rehabilitation methods for reinforced concrete (RC) bridge decks. Automation in Construction. 2007; 16(2):153–64. doi: 10.1016/j.autcon.2006.03.001
4. **Barone G., Frangopol D.M.** Life-cycle maintenance of deteriorating structures by multi-objective optimization involving reliability, risk, availability, hazard and cost. Structural Safety. 2014; 48:40–50. doi: 10.1016/j.strusafe.2014.02.002
5. **Yeo D., Potra F.A.** Sustainable design of reinforced concrete structures through CO2 emission optimization. Journal of Structural Engineering (United States). 2015; 141(3). doi: 10.1061/(ASCE)ST.1943-541X.0000888
6. **Gardoni P.** Risk and reliability analysis. In: Springer Series in Reliability Engineering. 2017. p. 3–24. doi: 10.1007/978-3-319-52425-2_1
7. **Beck A.T., Verzenhassi C.C.** Risk optimization of a steel frame communications tower subject to tornado winds. Latin American Journal of Solids and Structures. 2008; 5(3):187–203.
8. **Coello Coello C.A.** Multi-objective optimization. In: Handbook of Heuristics. 2018. p. 177–204. doi: 10.1007/978-3-319-07124-4_17
9. **Greiner D., Periaux J., Emperador J.M., Galván B., Winter G.** Game Theory Based Evolutionary Algorithms: A Review with

Nash Applications in Structural Engineering Optimization Problems. Archives of Computational Methods in Engineering. 2017; 24(4):703–50. doi: 10.1007/s11831-016-9187-y

10. **Abdi M., Ashcroft I., Wildman R.** Topology optimization of geometrically nonlinear structures using an evolutionary optimization method. Engineering Optimization. 2018; 50(11):1850–70. doi: 10.1080/0305215X.2017.1418864
11. **Lin J.P., Wang G., Xu R.** Particle Swarm Optimization-Based Finite-Element Analyses and Designs of Shear Connector Distributions for Partial-Interaction Composite Beams. Journal of Bridge Engineering. 2019; 24(3). doi: 10.1061/(ASCE)BE.1943-5592.0001371
12. **Alekseytsev A.V., Al Ali M.** Optimization of hybrid I-beams using modified particle swarm method // Magazine of Civil Engineering. 2018; 83(7):175-185. doi: 10.18720/MCE.83.16.
13. **Lalwani S., Sharma H., Satapathy S.C., Deep K., Bansal J.C.** A Survey on Parallel Particle Swarm Optimization Algorithms. Vol. 44, Arabian Journal for Science and Engineering. 2019. p. 2899–923. doi: 10.1007/s13369-018-03713-6
14. **Manju M., Kant C.** Ant Colony Optimization: A Swarm Intelligence based Technique. International Journal of Computer Applications. 2013; 73(10):30–3. doi: 10.5120/12779-9387
15. **Durbhaka G.K., Selvaraj B., Nayyar A.** Firefly Swarm: Metaheuristic Swarm Intelligence Technique for Mathematical Optimization. In: Advances in Intelligent Systems and Computing. 2019. p. 457–66. doi: 10.1007/978-981-13-1274-8_34
16. **Tamrazyan A.G., Konovalova O.O.** Optimization of design parameters of monolithic slabs supported along the contour using genetic algorithms. Safety of the building fund of Russia. Problems and solutions. Materials of the International Academic Readings. 2020. C. 115-122.
17. **Grebenyuk G.I., Dmitriev P.A., Zhadanov V.A., Astashenkov G.G.** Design, calculation and optimization of combined ribbed structures based on wood. Izvestiya vuzov. Building. 2013. No. 11-12. S. 48-56.
18. **Serpik I.** Discrete size and shape optimization of truss structures based on job search inspired strategy and genetic operations. Periodica Polytechnica: Civil Engineering. 2020. T. 64. № 3. C. 801-814.
19. **Alekseytsev A.V.** Two-stage synthesis of structural structures using the genetic algorithm and Delaunay tetrahedrization. International Journal for Computational Civil and Structural Engineering. 2013. vol. 9. No. 4. pp. 83-91.
20. **Balling R., Briggs R., Gillman K.** Multiple optimum size/shape/topology designs for skeletal structures using a genetic algorithm // Journal of Structural Engineering. ASCE. – 2006. – Vol. 132. – P. 1158 -1165.
21. **Alekseytsev A.V., Gaile L., Drukis P.** Optimization of steel beam structures for frame buildings subject to their safety requirements. Magazine of Civil Engineering. 2019. № 7 (91). C. 3-15.
22. **Kaveh A., Ghafari M.H., Gholipour Y.** Optimum seismic design of steel frames considering the connection types. Journal of Constructional Steel Research. 2017; 130:79–87. doi: 10.1016/j.jcsr.2016.12.002
23. **Alekseytsev, A.V.** Mechanical safety of reinforced concrete frames under complex emergency actions. Magazine of Civil Engineering, 2021, 103(3), 10306
24. **Tamrazyan A.G., Alekseytsev A.V.** Genetic algorithm for optimization of reinforced concrete beam structures "Algen". Certificate of registration of the computer program RU 2019612582, 22.02.2019.
25. **Tamrazyan A.G., Alekseytsev A.V.** Genetic algorithm for Reinforced Concrete Slab Optimization "Genal". Certificate of registration of the computer program RU 2019612583, 22.02.2019. Application No. 2019611393 dated 15.02.2019.

СПИСОК ЛИТЕРАТУРЫ

1. **Aoues Y., Chateauneuf A.** Reliability-based optimization of structural systems by adaptive target safety - Application to RC frames. Structural Safety. 2008; 30(2):144–61. doi: 10.1016/j.strusafe.2006.10.002
2. **Tamrazyan A., Alekseytsev A.** Strategy for the evolutionary optimization of reinforced concrete frames based on parallel populations evolving In: IOP Conference Series: Materials Science and Engineeringthis link is disabled, 2020, 869(5), 052019
3. **Lee C.K., Kim S.K.** GA-based algorithm for selecting optimal repair and rehabilitation methods for reinforced concrete (RC) bridge decks. Automation in Construction. 2007; 16(2):153–64. doi: 10.1016/j.autcon.2006.03.001
4. **Barone G., Frangopol D.M.** Life-cycle maintenance of deteriorating structures by multi-objective optimization involving reliability, risk, availability, hazard and cost. Structural Safety. 2014; 48:40–50. doi: 10.1016/j.strusafe.2014.02.002
5. **Yeo D., Potra F.A.** Sustainable design of reinforced concrete structures through CO2 emission optimization. Journal of Structural Engineering (United States). 2015; 141(3). doi: 10.1061/(ASCE)ST.1943-541X.0000888
6. **Gardoni P.** Risk and reliability analysis. In: Springer Series in Reliability Engineering. 2017. p. 3–24. doi: 10.1007/978-3-319-52425-2_1
7. **Beck A.T., Verzenhassi C.C.** Risk optimization of a steel frame communications tower subject to tornado winds. Latin American Journal of Solids and Structures. 2008; 5(3):187–203.
8. **Coello Coello C.A.** Multi-objective optimization. In: Handbook of Heuristics. 2018. p. 177–204. doi: 10.1007/978-3-319-07124-4_17
9. **Greiner D., Periaux J., Emperador J.M., Galván B., Winter G.** Game Theory Based Evolutionary Algorithms: A Review with Nash Applications in Structural Engineering Optimization Problems. Archives of Computational Methods in Engineering. 2017; 24(4):703–50. doi: 10.1007/s11831-016-9187-y
10. **Abdi M., Ashcroft I., Wildman R.** Topology optimization of geometrically nonlinear structures using an evolutionary optimization method. Engineering Optimization. 2018; 50(11):1850–70. doi: 10.1080/0305215X.2017.1418864
11. **Lin J.P., Wang G., Xu R.** Particle Swarm Optimization-Based Finite-Element Analyses and Designs of Shear Connector Distributions for Partial-Interaction Composite Beams. Journal of Bridge Engineering. 2019; 24(3). doi: 10.1061/(ASCE)BE.1943-5592.0001371
12. **Alekseytsev A.V., Al Ali M.** Optimization of hybrid I-beams using modified particle swarm method // Magazine of Civil Engineering. 2018; 83(7):175-185. doi: 10.18720/MCE.83.16.
13. **Lalwani S., Sharma H., Satapathy S.C., Deep K., Bansal J.C.** A Survey on Parallel Particle Swarm Optimization Algorithms. Vol. 44, Arabian Journal for Science and Engineering. 2019. p. 2899–923. doi: 10.1007/s13369-018-03713-6
14. **Manju M., Kant C.** Ant Colony Optimization: A Swarm Intelligence based Technique. International Journal of Computer Applications. 2013; 73(10):30–3. doi: 10.5120/12779-9387
15. **Durbhaka G.K., Selvaraj B., Nayyar A.** Firefly Swarm: Metaheuristic Swarm Intelligence Technique for Mathematical Optimization. In: Advances in Intelligent Systems and Computing. 2019. p. 457–66. doi: 10.1007/978-981-13-1274-8_34
16. **Тамразян А.Г., Коновалова О.О.** Оптимизация проектных параметров опертых по контуру монолитных перекрытий с использованием генетических алгоритмов // Безопасность строительного фонда России. Проблемы

и решения. Материалы Международных академических чтений. 2020. С. 115-122.
17. **Гребенюк Г.И., Дмитриев П.А., Жаданов В.А., Асташенков Г.Г.** Конструирование, расчет и оптимизация совмещенных ребристых конструкций на основе древесины [Текст] / Г.И. Гребенюк, // Известия вузов. Строительство. – 2013. – №11-12. – С. 48-56.
18. **Serpik I.** Discrete size and shape optimization of truss structures based on job search inspired strategy and genetic operations. Periodica Polytechnica: Civil Engineering. 2020. Т. 64. № 3. С. 801-814.
19. **Алексейцев А.В.** Двухэтапный синтез структурных конструкций с использованием генетического алгоритма и тетраэдризации Делоне. Международный журнал по расчету гражданских и строительных конструкций. 2013. Т. 9. № 4. С. 83-91.
20. **Balling R., Briggs R., Gillman K.** Multiple optimum size/shape/topology designs for skeletal structures using a genetic algorithm // Journal of Structural Engineering. ASCE. – 2006. – Vol. 132. – P. 1158 -1165.
21. **Alekseytsev A.V., Gaile L., Drukis P.** Optimization of steel beam structures for frame buildings subject to their safety requirements. Magazine of Civil Engineering. 2019. № 7 (91). С. 3-15.
22. **Kaveh A., Ghafari M.H., Gholipour Y.** Optimum seismic design of steel frames considering the connection types. Journal of Constructional Steel Research. 2017; 130:79–87. doi: 10.1016/j.jcsr.2016.12.002
23. **Alekseytsev, A.V.** Mechanical safety of reinforced concrete frames under complex emergency actions. Magazine of Civil Engineering, 2021, 103(3), 10306
24. **Тамразян А.Г., Алексейцев А.В.** Генетический алгоритм оптимизации железобетонных балочных конструкций "Алген". Свидетельство о регистрации программы для ЭВМ RU 2019612582, 22.02.2019.
25. **Тамразян А.Г., Алексейцев А.В.** Генетический алгоритм оптимизации железобетонных плит "Генал". Свидетельство о регистрации программы для ЭВМ RU 2019612583, 22.02.2019. Заявка № 2019611393 от 15.02.2019.

Anatoly V. Alekseytsev, docent, candidate of technical sciences, associated professor of the department "Reinforced concrete and stone structures"; National Research Moscow State Technical University (NRU MGSU), Russia, Moscow, Yaroslavskoe sh., 26, Scopus ID: 57191530761, Researcher ID: I-3663-2017, ORCID: 0000-0002-4765-5819, tel .: +7 (495) 287-49-14. E-mail: alekseytsevav@mail.ru.

Al Ali Mohamad, Ph.D. tech. Sci., Head of the Department of Steel and Wooden Structures, Technical University of Kosice, Slovakia, Researcher ID: AAH-5275-2019, Scopus ID: 55516059900. ORCID:0000-0001-7866-8156. Letná 9 042 00 Košice Slovak Republic E-mail: alali@tuke.sk

Алексейцев Анатолий Викторович, доцент, кандидат технических наук, доцент кафедры «Железобетонные и каменные конструкции»; Национальный исследовательский московский государственный технический университет (НИУ МГСУ), Россия, г. Москва, Ярославское ш., 26, Scopus ID: 57191530761, Researcher ID: I-3663-2017, ORCID: 0000-0002-4765-5819, тел.: +7(495)287-49-14. E-mail: alekseytsevav@mail.ru.

Ал Али Мохамад, канд. техн. наук., заведующий кафедрой «Стальные и деревянные конструкции», Технический университет г. Кошице, Словакия, Researcher ID: AAH-5275-2019, Scopus ID: 55516059900. ORCID:0000-0001-7866-8156. Letná 9 042 00 Košice Slovak Republic. E-mail: alali@tuke.sk

International Journal for Computational Civil and Structural Engineering, 18(2) 143–155 (2022)

DOI:10.22337/2587-9618-2022-18-2-143-155

THE USE OF COPPER NANOMODIFIED CALCIUM CARBONATE AS A BACTERICIDAL ADDITIVE FOR CONCRETE

Kamil B. Sharafutdinov [1], Kseniya A. Saraykina [1], Galina G. Kashevarova [1], Vladimir T. Erofeev [2]

[1] Perm National Research Polytechnic University, Perm, RUSSIA
[2] Ogarev Mordovia State University, Saransk, RUSSIA

Abstract: Experimental studies of the resistance of cement stone and concrete to the influence of mold fungi have been carried out. The effectiveness of the use of nanomodified calcium carbonate and the PHMG biocide as bactericidal additives for concrete has been investigated. The influence of Glenium and C-3 plasticizers on the effectiveness of the action of bactericidal additives has been investigated. Both investigated biocidal additives showed a fungicidal effect on concrete specimens. The use of nanomodified calcium carbonate as a bactericidal additive for concrete is effective as the use of PHMG biocide. The introduction of this bactericidal additives does not reduce the strength of the hardened concrete.

Keywords: concrete, mold fungi, biocidal additives, PHMG, calcium carbonate.

ПРИМЕНЕНИЕ НАНОМОДИФИЦИРОВАННОГО КАРБОНАТА КАЛЬЦИЯ В КАЧЕСТВЕ БАКТЕРИЦИДНОЙ ДОБАВКИ ДЛЯ БЕТОНА

К.Б. Шарафутдинов [1], К.А. Сарайкина [1], Г.Г. Кашеварова [1], В.Т. Ерофеев [2]

[1] Пермский национальный исследовательский политехнический университет, г. Пермь, РОССИЯ
[2] Мордовский государственный университет им. Н.П. Огарева, г. Саранск, РОССИЯ

Аннотация: Проведены экспериментальные исследования стойкости образцов из цементного камня и бетона к воздействию плесневых грибов. Исследована эффективность применения наномодифицированного карбоната кальция и биоцида ПГМГ-ГХ в качестве бактерицидных добавок для бетона. Дополнительно исследовано влияние пластификаторов Glenium и С-3 на эффективность действия бактерицидных добавок. Обе исследованные биоцидные добавки показали фунгицидный эффект на бетоне. Применение наномодифицированного карбоната кальция в качестве бактерицидной добавки для бетона не менее эффективно, чем применение биоцида ПГМГ-ГХ. Введение исследованных биоцидных добавок не снижает прочность затвердевшего бетона.

Ключевые слова: бетон, плесневые грибы, биоцидные добавки, ПГМГ, карбонат кальция.

INTRODUCTION

Biocorrosion is an important problem in modern construction. The growth of organisms such as bacteria, lichens and building materials can negatively effect on the structure of reinforced concrete. Microbes destroy the building material, not only manifesting themselves on its surface. They reduce strength characteristics of reinforced concrete penetrating inside the structure and causing metal corrosion. The destruction of structures by biocorrosion can cause colossal damage and repairing of such structures leads to high financial costs [1,2].

The degree of mold growth depends on environmental factors, material properties and the characteristics of the mold itself. Biocorrosion research aims to predict whether mold will grow

on a specific material under favorable conditions, certain humidity and temperature. To prevent the growth of mold fungi, such research must be carried out at the stage of development of new building materials and must be considered in the design, construction and operation of the building. The knowledge gained will help to protect the future building structure from biocorrosion.

The most susceptible building materials to mold are wooden structures. Sugar and starch in the wood are suitable for the growth and reproduction of fungi [3, 4]. But it is necessary to understand that fungal mycelium can become a breeding ground for other fungi or for other microorganisms. The destructive effect of this microorganisms will manifest itself on other materials, in particular on concrete. There are foreign studies of biocorrosion of concrete structures, which show that the most dangerous for cement are sulfur-oxidizing and sulfate-reducing bacteria [5, 6].

Molds reproduct by spores, so it is usual to Cladosporium, Penicillium and Aspergillus to have their spores in the air. Mold fungi can stay on the surface of the material for a long time in the form of spores and do not appear in any way until conditions for their favorable development arise. The most important factor for the development of mold fungi is the humidity of the environment, which depends not only by the climatic features, but also by the operating conditions of the rooms in buildings or by short-term exposure to moisture on the building structure [7, 8]. Indoor mold growth is also harmful to humans and it can cause adverse health effects.

A large number of works are devoted to the study of the biological resistance of cement composites aimed of the effect of the type of binders, fillers and biocidal additives on the mold fouling and resistance of materials to molds [9, 10, 11].

Theme of bacterial protection became especially relevant in 2020, when the epidemic of the SARS-CoV-2 virus had arrived. Scientists were faced with the need to create antibacterial surfaces capable of destroying bacteria [14]. Chinese scientists [12] conducted an analysis of studies of inorganic and organic antibacterial additives, which showed that inorganic additives with metal ions are more effective than organic due to a longer duration of action. It was concluded that the use of antibacterial nanoadditives is a promising way to increase the biostability of building materials [13].

Antibacterial nanoadditives contain nanoparticles of heavy metals in their composition. However, in some cases, the resulting product becomes toxic and unusable that is why the most common metals are silver or copper. Copper and silver nanoparticles show a complete absence of toxic effects on humans [15]; therefore, the use of copper ions is most promising for the development of bactericidal nanoadditives. Copper has not only antibacterial but also antiviral properties. [16,17]. British scientists [18] conducted a study showing that no viable SARS-CoV-2 was found on the copper surface after 4 hours.

Modern nanotechnology makes it possible to increase the resistance of the material to biodegradation that will lead to increasing the durability of the concrete structure.

Carbonate rocks are the basis for the production of building materials. Introduction of carbonate into the composition of concrete does not reduce its strength [19, 20]. Calcium carbonate nanomodified with copper particles can become a promising bactericidal nanoadditive for mortars. This additive is currently used in the production of antibacterial silicone rubber and plastics. The surfaces of materials made with this additive will retain antibacterial properties until the copper nanoparticles are not removed mechanically.

MATERIALS AND METHODS

The purpose of this experimental study was to determine the effectiveness of the use of nanomodified calcium carbonate as a bactericidal additive for concrete. The effectiveness of the additive was researched through the determination of the resistance of cement stone and concrete to the effect of mold fungi.

For experimental specimens, Portland cement CEM I 42.5 R produced by LLC

«Gornozavodskcement» was used as a binder. Fine-grained river sand sifted to a fraction of 0.315-0.2 mm was used as a fine aggregate for concrete. Plasticizing additives «Glenuim ACE 440» manufactured by LLC «BASF» and plasticizer «C-3» manufactured by JSC «GK Polyplast» were introduced in the dosage recommended by manufacturers into concrete compositions together with mixing water. All experimental compositions had a normal solution consistency according to GOST 310.4-81 standart, because the type of plasticizer influenced to the W/C ratio of solution.

Researched antibacterial additive was a calcium carbonate modified with copper nanoparticles manufactured by GV Holdings Co (South Korea). This additive was used as the main bactericidal nanoadditive for the research. As an alternative bactericidal additive, the additive «PHMG» produced by LLC «Alterkhim-Pro» (Dzerzhinsk, Russia) was chosen. To ensure uniform distribution of the additives in the concrete mixture, they were previously introduced into the mixing water. The number of components by weight is given for 1 kg of cement in table 1.

Concrete specimens were molded in the form of small briquette bars with size dimensions 1x1x3 cm. This size of specimens allows to put them in Petri dishes for testing for fungal resistance and then use to determine the strength of hardened concrete. For the manufacture of formwork these forms were modeled in the Autodesk 3dsmax software (Fig. 1A). The created model was printed (Fig. 1B) on a 3d-printer in the laboratory of Perm Polytechnic University (Perm, Russia). The use of additive technologies made possible to reduce the cost of molds production and increased the accuracy of the concrete specimen. Forming of concrete specimen was carried out in the laboratory of Perm Polytechnic University (Perm, Russia).

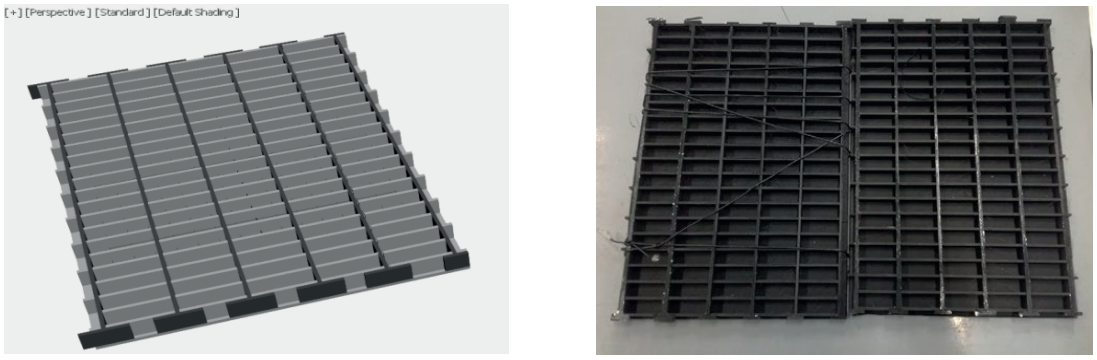

Figure 1. 3D model of formwork and 3D printed formworks

Table 1. Types of experimental compositions

№	C, kg	S, kg	W, kg	Plastisizer		Antibacterial additive		Type of composition
				type	mass, kg	type	mass, kg	
1	1		0,32					Cements stone – no additives
2	1		0,32			CaCO3	0,005	Cements stone with 0,5%C CaCO3
3	1	3	0,34	Glenium	0,01	CaCO3	0,005	Experimental compositions with 0,5%C dosage of additive
4	1	3	0,34	Glenium	0,01	PHMG	0,005	
5	1	3	0,36	C-3	0,005	CaCO3	0,005	
6	1	3	0,36	C-3	0,005	PHMG	0,005	
7	1	3	0,34	Glenium	0,01			Concrete – no additives
8	1	3	0,36	C-3	0,005			
9	1	3	0,34	Glenium	0,01	PHMG	0,02	Experimental compositions with 2%C dosage of additive
10	1	3	0,34	Glenium	0,01	CaCO3	0,02	

After 28 days of hardening, the concrete specimens were packed into groups according to the compositions and then transported to the laboratory of microbiological analysis of Lobachevsky University (Nizhny Novgorod, Russia). They were tested for resistance to mold fungi.

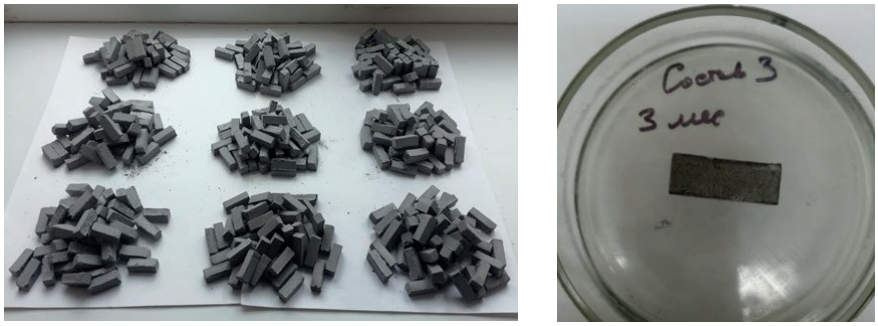

Figure 2. Concrete specimens before experiment and in Petri dish

The tests were carried out in accordance to GOST 9.049-91 according to methods 1 and 3. When tested according to method 1, the material is contaminated with mold spores in water and placed in a sterile Petri dish. In this case, molds grow only on the nutrients contained in the material. If the material is not a nutrient medium for molds, then the growth of molds will not occur, therefore, the material is fungus-resistant. When tested according to method 3, the material is contaminated with mold spores and then exposed in a Petri dish with a nutrient medium for fungi. In this case, fungi will grow on the nutrient medium, but if the material is fungicidal, then mold fungi will not grow on it, and as a result of the diffusion of the biocide into the nutrient medium, an inhibition zone is formed in which mold growth will not be observed.

Specimens were exposured in Petri dishes for 1 and 3 months at temperature 28 ± 2 °C and humidity of more than 90%. Thus, the specimens were kept in an environment favorable for the development of molds. 5 concrete specimens were taken for each composition and method.

After the experiment each of the tested groups was packed separately according to the methods and transported to Ogarev Mordovia University (Saransk, Russia), where the specimens were tested for compressive strength.

Figure 3. Mold fungi growth

The compressive strength of the samples was determined from the results of testing 5 specimens for each composition. Specimens were placed in a special tooling that allowed the specimens of this size to be tested using standard test equipment. Flexural strength was not determined due to the low strength of the fine-grained concrete specimens caused by their small size. The average compressive strength of the 5 specimens tested is taken to display the result.

RESULTS

Results according to method 1 testing show that all researched compositions of concrete and cement stone were found to be fungus-resistant. This happened because cement stone and

concrete are not a breeding ground for molds, therefore, their growth was not observed on the specimens. But the fungal resistance of a material does not itself guarantee that the material will be protected from mold. During the operation of the concrete structure, various contaminants brought by water and winds settle on the surface of material. Thus, various bacteria, algae and other contaminants can appear on the surface of the concrete and they will already be a breeding ground for mold. They will contribute to biocorrosion and destruction of building material, therefore it is important to provide the building material to be not only fungal resistant, but also fungicidal. That can be determined by method 3 experiment.

Table 2 shows the results of testing specimen according to method 3. The points indicate the degree of mold fungi growth, where R is the size of zone of inhibition in the presence of a fungicidal effect. The introduction of biocidal additives caused a fungicidal effect.

Table 2. Results after 4 weeks of exposition in mold fungi by methods 1 and 3

№	Type: Cem - cement C – conctrete A - additive	Plasticizer	Antibacterial additive		Degree of mold fungi growth, points		Result
			Type	%C	M 1	M 3	
1	Cem				0 - 1	2	Fungi resistant
2	Cem + A		CaCO3	0,5	0	0 (R = 4-5 mm)	Fungicidal
3	C + A	Glenium	CaCO3	0,5	0	0 (R = 2-4 mm)	Fungicidal
4	C + A	Glenium	PHMG	0,5	0	0 (R = 8-10 mm)	Fungicidal
5	C + A	C-3	CaCO3	0,5	0 - 1	0 (R = 1-5 mm)	Fungicidal
6	C + A	C-3	PHMG	0,5	0	0 (R = 12-15 mm)	Fungicidal
7	C	Glenium			0	0 (R = 1-2 mm)	Fungi resistant
8	C	C-3			0 - 1	2	Fungi resistant
9	C + A	Glenium	PHMG	2	0	0 (R = 8-15 mm)	Fungicidal
10	C + A	Glenium	CaCO3	2	0 - 1	0 (R = 1-4 mm)	Fungicidal

The degree of mold growth after 4 months of exposure can be observed in photos of Petri dishes with the studied specimens. The most indicative result of the effect of nanomodified calcium carbonate is noticeable on specimens of cement stone.

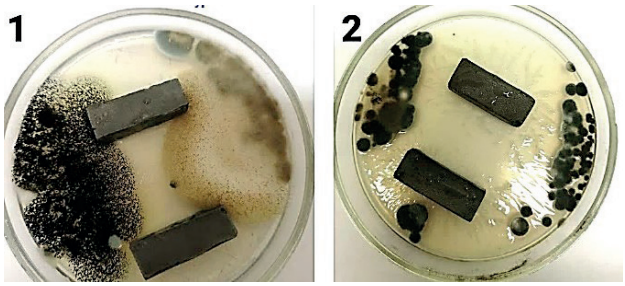

Figure 4. Degree of mold growth on cement stone: 1 – no additive, 2 – with nanomodified $CaCO_3$

Photos are shown Specimens with the biocidal nanomodified calcium carbonate show a fungicidal effect with an inhibition zone of 4-5 mm after 1 month of exposure. After 3 months of exposure, the inhibition zone decreased to 2-3 mm, however, the specimens continued to demonstrate fungicidal effect. Compositions No.3- No.10 were a specimens of concrete with a plasticizer. This building material is used in building structures, therefore the results of testing of these specimens for fungal resistance will be more practically applicable. Compositions No.7 and No.8 were prepared to assess the effect of the plasticizing additive on fungal resistance. Fig.5 shows the results of mold growth of concrete specimens made with different plasticizers but without biocidal additives.

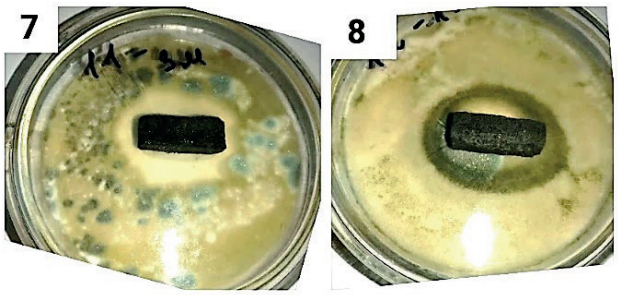

Figure 5. Degree of mold growth on concrete:
7 – plasticizer Glenium ACE 440;
8 – plasticizer C-3

The results show that Glenium ACE 440 polycarboxylate superplasticizer performs much better than C-3 plasticizer. Specimens with Glenium plasticizer showed a negligible fungicidal effect with an inhibition zone of 1-2 mm, while specimens with C-3 plasticizer show a mold growth rate of up to 2 points according to method 3. Concrete with C-3 plasticizer is fungus resistant, but it is no longer fungicidal, like concrete with Glenium plasticizer.

For experimental compositions No.3- No.6, the dosage of biocidal additives was chosen the same and equal to 0.5% of the cement mass (0,5%C). This made it possible to assess the effect of the additive on the fungicidal properties of concrete with a plasticizer. Despite the fact that concrete with a plasticizer Glenium and without a biocidal additive already shows a fungicidal effect, it was important to find out how the joint introduction of biocidal additives and plasticizers will affect the fungicidal properties of concrete. The results in Table 2 show that concrete with both types of additives show a fungicidal effect, but in compositions with PHMG (No.4 and No.6) the zone of inhibition is much larger and reaches 15 mm.

For compositions with nanomodified CaCO3, the inhibition zone does not exceed 5 mm. This difference is also noticeable in the photographs shown in Fig.6 and Fig.7.

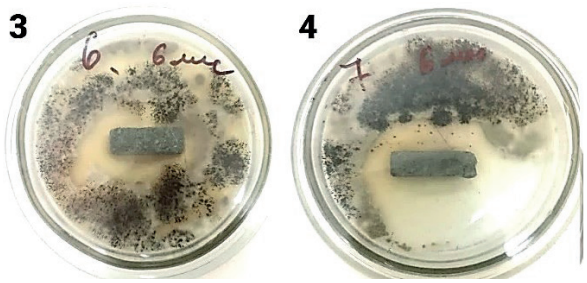

Figure 6. Degree of mold growth on concrete with a Glenium plasticizer:
3 – nanomodified $CaCO_3$ additive;
4 – PHMG additive

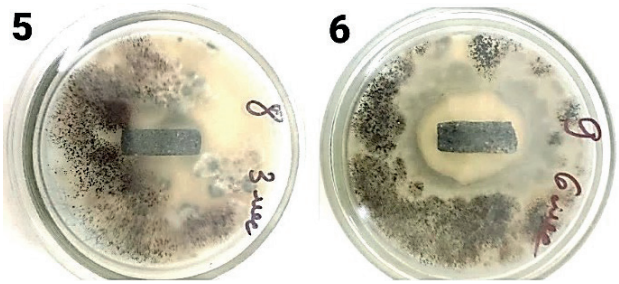

Figure 7. Degree of mold growth on concrete with a C-3 plasticizer:
5 – nanomodified $CaCO_3$ additive;
6 – PHMG additive

For experimental compositions No.9 and No.10, an increased dosage of biocidal additives was chosen. It was equal to 2% by weight of the cement. These 2 compositions were made in order to understand the effect of an increased dosage of a biocidal additive on the fungicidal properties of concrete. Concrete specimen were made with Glenium plasticizer. The results in Table 2 show that increasing the dosage of the biocidal additive does not enhance the fungicidal effect on concrete. The inhibition zone did not exceed 5 mm with an increase in the dosage of nanomodified calcium carbonate. With an increased dosage of the PHMG biocide, the inhibition zone was 8-15 mm, which also corresponds to the result obtained at a dosage of 0.5%. It can be assumed that the increasing of dosage of researched additive does not make sense, since positive results have already been obtained with dosages of 0.5% of additive.

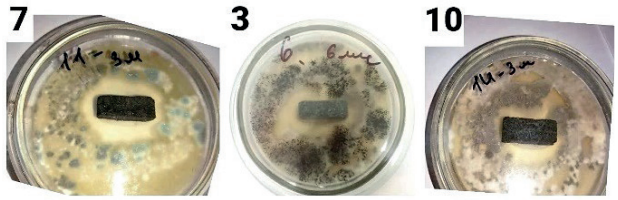

Figure 8. Degree of mold growth on concrete with a Glenium plasticizer with antibacterial $CaCO_3$ additive dosage: 7 – 0%; 3 – 0,5%C; 10 – 2%C

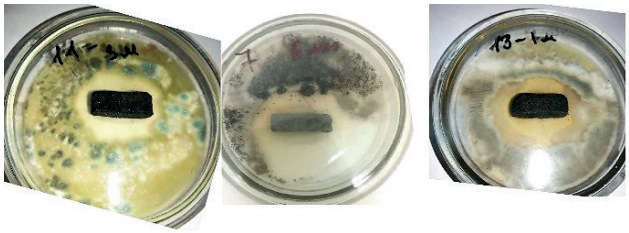

Figure 9. Degree of mold growth on concrete with a Glenium plasticizer with PHMG additive dosage: 7 – 0%; 4 – 0,5%C; 9 – 2%C

Fig.8 and Fig.9 clearly demonstrate that the degree of mold growth does not depend on the dosage of the bactericidal additive in the selected ranges of 0.5–2%. For a visual comparison, the figures show the test results of specimen from the composition No.7, where only the Glenium plasticizer was used and no biocidal additives were introduced.

Mold growth rate depends on the exposure time. All of the above results describe the degree of mold growth after 4 weeks of exposure. This time is sufficient to assess the fungicidal properties of the material in accordance to GOST 9.049-91. In practice, mold growth can manifest itself at a much later time, since mold, like any living creature, will adapt to environmental conditions for some time and then grow and develop over time. Fungicidal properties of the material may appear in the form of a zone around the specimen only at the early time of exposure, but later this zone may overgrow, since one species of fungi will become a breeding ground for other type of fungi. In this case, the fungicidal property of the material will not allow mold fungi to cause biocorrosion.

In this study, Petri dishes with specimens of compositions No.3- No.6 were additionally photographed after 3 months of exposure. This allows a visual assessment of the growth rate of molds over time. Fig.10 and Fig.11 show that concrete compositions with Glenium plasticizer and two investigated biocidal additives after 3 months of exposure continue to demonstrate a fungicidal effect. No significant mold growth was observed in the inhibition zone and mold did not grow on the specimens themselves. This allows us to conclude that the nanomodified CaCO3 additive shows the same efficiency as the PHMG biocidal additive even after 3 months of exposure to molds. Fig.12 show that the composition of concrete with the plasticizer C-3 and the nanomodified CaCO3 after 3 months show a fungicidal effect, but there is noticeable overgrowing of the zone after 3 months. If PHMG was chosen as a biocidal additive, even after 3 months, there is a clear absence of additional mold growth after 3 months. It can be concluded that the combined use of PHMG and the Glenium plasticizer is the most effective way for ensuring the durability of a concrete structure to the extent of its resistance to the destructive effects of molds.

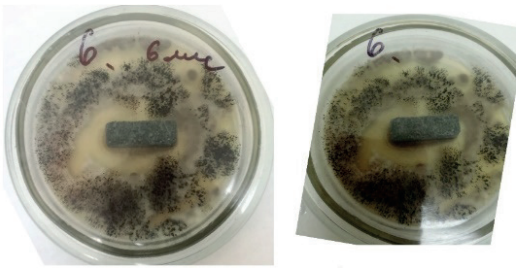

A *B*

Figure 10. Degree of mold growth on concrete with a Glenium plasticizer with antibacterial CaCO3 additive (composition No.3). A – after 1 month, B – after 3 months

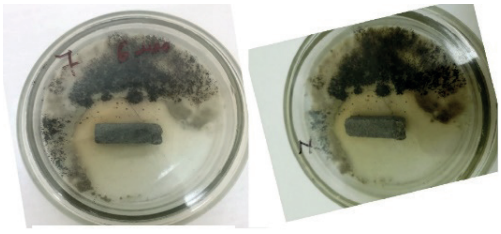

A *B*

Figure 11. Degree of mold growth on concrete with a Glenium plasticizer with antibacterial PHMG additive (composition No.4). A – after 1 month, B – after 3 months

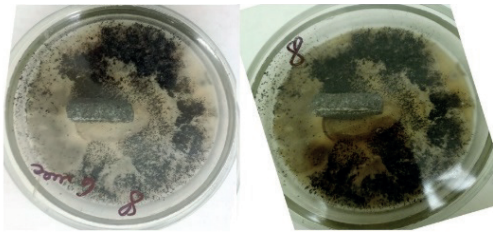

A *B*

Figure 12. Degree of mold growth on concrete with a C-3 plasticizer with antibacterial CaCO3 additive (composition No.5). A – after 1 month, B – after 3 months

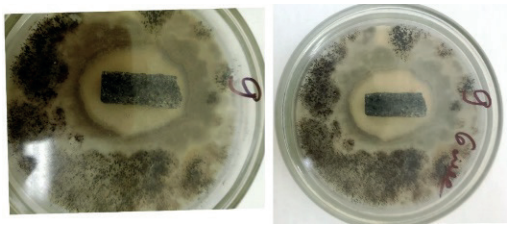

A *B*

Figure 13. Degree of mold growth on concrete with a C-3 plasticizer with antibacterial PHMG additive (composition No.6). A – after 1 month, B – after 3 months

But we should know that PHMG can be toxic for human and cannot be used in construction, that is why nanomodified CaCO3 can be used to protect concrete structure.

Compressive strength is an important characteristic of concrete. Biocorrosion leads to a deterioration of the strength characteristics of concrete structures. The decrease in strength of a structure from the effects of mold can pass slowly and imperceptibly. If it is not detected in time, the destruction of the structure can occur suddenly. In this study, all tested concrete specimens proved to be fungus-resistant after 1 month of exposure. Therefore, a noticeable decrease in the strength of the samples as a result of the destructive effect of molds should not be observed.

For the practical applicability of this study and substantiation of the effectiveness of the use of nanomodified additives, the compressive strength of specimens from all compositions was additionally investigated. Due to small size of the tested specimens (1x1cm), the results obtained are relative, however, they allow to make a comparative analysis.

Specimens were divided into 3 groups. The first and second group of specimens after 28 days of hardening were exposed to mold fungi according to methods 1 and 3, respectively. The third group of samples after 28 days of hardening was left for storage at a temperature of 20 ± 2 °C and a humidity of 60%.

After the experiment on fungal resistance with specimens of groups 1 and 2, specimens of all groups were tested for compressive strength at one day. For compositions No.3- No.6, samples were additionally tested after 3 months of exposure. Fig.14 show the compressive strength results of samples stored in room conditions compared to samples stored in a Petri dish at 28 ± 2 °C and humidity of above 90%.

The increased temperature and humidity during tests according to methods 1 and 3 led to an acceleration of the compressive strength of concrete. That is evident from the results of tests of specimens tested according to method 1, where the compressive strength increased by 3-6 times compared to specimens stored at room temperature.

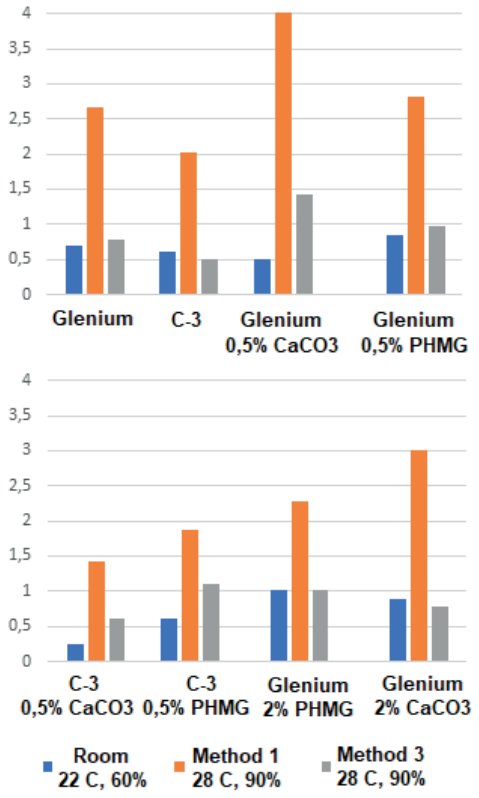

Figure 14. Relative compressive strength of concrete specimens

Concrete with C-3 plasticizer has lower compressive strength compared to concrete with Glenium plasticizer. This is clearly seen on compositions with a biocidal additive at a dosage of 0.5%C. Compositions with Glenium plasticizer have 1.2 - 2.5 times greater compressive strength than compositions with C-3 plasticizer. This is observed both on specimens stored at room temperature and on specimens exposed to mold, where much better conditions for the concrete curing were created.

The introduction of biocidal additives together with the Glenium plasticizer leads to a slight increase in the compressive strength of the concrete.

For compositions No.3 - No.6 were obtained results that allow to compare the compressive strength of the specimens after 1 and 3 months of exposure. The results show that the additional increasing of strength of the specimens during the second and third months of exposure is already insignificant and at 3 months of exposure all compositions have the same strength as they had after 1 month of exposure. Glenium plasticizer accelerates early strength development, which is also evident in the results of these tests. Strength diagrams are shown in Fig. 15.

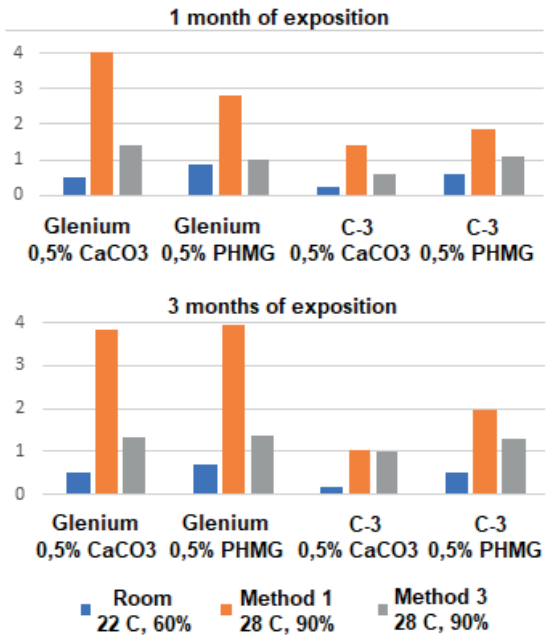

Figure 15. Relative compressive strength of specimens

DISCUSSION

The results of the study show the effectiveness of usage of each type of additive as a bactericidal additive and as a hardening additive.

Cement stone specimens showed a fungicidal effect, so the introduction of nanomodified calcium carbonate into the cement stone can be effective.

Composition of concrete with Glenium ACE 440 plasticizer also showed a fungicidal effect, which can be explained by the high quality of this type of plasticizer. The manufacturer indicates that this plasticizer increases the durability of concrete structures, therefore, it is likely that the manufacturer includes fungicidal additives to the plasticizer, which led to an insignificant fungicidal effect of concrete. Mold already begun to grow up to 2 points on concrete specimens only with C-3 plasticizer and while tested according to method 3.

The introduction of PHMG into the concrete composition gives greater efficiency than the introduction of nanomodified calcium carbonate in the same dosage. This is noticeable from the results of measuring the zone of inhibition. All compositions with PHMG show an inhibition zone of up to 15 mm, while concrete samples with the addition of nanomodified calcium carbonate show fungicidal activity with an inhibition zone of maximum 5 mm.

Increasing of the fungicidal effect is not observed while increasing of the dosage of biocidal additives above 0.5%. Concrete retained its fungicidal properties, but the inhibition zone of the material remained the same size as it was at a dosage of 0.5%. Therefore, increasing the dosage of the biocidal additive above 0.5% is not advisable.

The compressive strength of concrete specimens with Glenium plasticizer is in all cases higher than the strength of specimens made of concrete with C-3 plasticizer. This can be explained by the high quality of the plasticizer and the presence of hardening accelerators in its composition.

The introduction of PHMG slightly increases the compressive strength of concrete specimens,

which corresponds to the manufacturer's description. However, the 2-3 times increase in compressive strength declared by the manufacturer was not achieved. At a dosage of PHMG equal to 0.5% - 2%, the strength of concrete specimens increased by an average of 14-18%.

CONCLUSION

In this study the resistance to mold fungi was determined for cement stone specimens and samples of concrete with different plasticizing additives. Two types of antibacterial additives were investigated: calcium carbonate modified with copper nanoparticles and the biocidal additive PHMG. All studied specimens were found to be fungus resistant. Concrete compositions with biocidal additives are fungicidal or at least fungistatic for 1 month of exposure.

The introduction of nanomodified additives into concrete may be relevant from the point of view of novelty, however, this study shows that the introduction of the biocidal additive PHMG on the studied concrete compositions gives the same. At the same time, an increase in the dosage of biocides is not advisable since it will only lead to an increase in the cost of concrete. Its compressive strength and biocidal characteristics will remain the same.

In further studies, reduced dosages of biocidal additives and various plasticizing additives for concrete should be considered, since they can affect the biocidal properties of the concrete in different ways. Polymeric materials are actively used in modern construction. The use of nanomodified additives can be effective precisely in them; however, this topic requires further research.

REFERENCES

1. **Rodin A.I., Erofeev V.T., Pustovgar A.P., Eremin A.V., Pashkevich S.A., Bogatov A.D., Kaznacheev, S.V., Adamtsevich A.O.** Kinetika nabora prochnosti biotsidnikh tsementov [Kinetics of strengthening of biocidal cements]. // *Vestnik MGSU,* 2014, Volume 12, pp. 88-98 (in Russian).
2. **Dergunova A., Piksaykina A., Bogatov A., Salman Al.D.S.D., Erofeev V.** The economic damage from biodeterioration in building sector. // IOP Conference Series: Materials Science and Engineering, 2019, Volume 698(7), 077020.
3. **Zhao J., Csetenyi L., Gadd G. M.** Biocorrosion of copper metal by Aspergillus niger. // International Biodeterioration & Biodegradation, 2020, Volume 154, 105081.
4. **Salem M. Z. M.** EDX measurements and SEM examination of surface of some imported woods inoculated by three mold fungi. // Measurement, 2016, Volume 86, pp. 301–309.
5. **Hager W.H., Boes R.M.** Hydraulic structures: a positive outlook into the future. // Journal of Hydraulic Research, 2014, Volume 52, pp. 299-310.
6. **Cai W., Li Y., Niu L., Zhang W., Wang C., Wang P., Meng F.** New insights into the spatial variability of biofilm communities and potentially negative bacterial groups in hydraulic concrete structures. // Water Research, 2017, Volume 123, pp. 495–504.
7. **Salonen H., Lappalainen S., Lindroos O., Harju R., Reijula K.** Fungi and bacteria in mould-damaged and non-damaged office environments in a subarctic climate. // Atmospheric Environment, 2007, Volume 41(32), pp. 6797–6807.
8. **Tischer C.G., Heinrich J.** Exposure assessment of residential mould, fungi and microbial components in relation to children's health: Achievements and challenges. // International Journal of Hygiene and Environmental Health, 2013 Volume 216(2), pp. 109–114.
9. **Erofeev V., Rodin A., Rodina N., Kalashnikov V., Irina E.** Biocidal Binders

for the Concretes of Underground Constructions. // Procedia Engineering, 2016, Volume 165, pp. 1448-1454.
10. **Travush V.I., Karpenko N.I., Erofeev V.T., Rodin A.I., Smirnov V.F., Rodina N.G.** Development of Biocidal Cements for Buildings and Structures with Biologically Active Environments. // Power Technology and Engineering, 2017, Volume 51(4), pp. 377-384.
11. **Svetlov D.A., Svetlova E.D., Svetlov D.D., Egorova T.S.** Research into Antibacterial Activity of Novel Disinfectants Derived from Polyhexamethylene Guanidine Hydrochloride. // IOP Conference Series Materials Science and Engineering, 2021, Volume 1079(6), 062017.
12. **Qiu L., Dong S., Ashour A., Han B.** Antimicrobial concrete for smart and durable infrastructures: A review. // Construction and Building Materials, 2020, Volume 260, 120456.
13. **Noeiaghaei T., Mukherjee A., Dhami N., Chae S.-R.** Biogenic deterioration of concrete and its mitigation technologies. // Construction and Building Materials, 2017, Volume 149, pp. 575–586.
14. **Sportelli M.C., Izzi M., Kukushkina E.A., Hossain S.I., Picca R.A., Ditaranto N., Cioffi N.** Can Nanotechnology and Materials Science Help the Fight against SARS-CoV-2? // Nanomaterials, 2020, Volume 10(4), 802.
15. **Slepiˇcka P, Slepiˇcková N. K., Siegel J., Kolská Z., Švorˇcík V**. Methods of Gold and Silver Nanoparticles Preparation. // Materials. 2020. Volume 13(1), 1.
16. **Tavakoli A, Sadegh M.H.** Inhibition of herpes simplex virus type 1 by copper oxide nanoparticles. // Journal of Virological Methods, 2019, 275:113688.
17. **Grass G, Rensing C, Solioz M.** Metallic Copper as an Antimicrobial Surface. // Applied and environmental microbiology, 2011, Volume 77(5), pp. 1541–1547.
18. **Doremalen N, Bushmaker T, Morris D.H., Holbrook M.G., Gamble A., Williamson B.N., Tamin A., Harcourt J.L., Thornburg N.J., Gerber S.I., Lloyd-Smith J.O., Emmie de Wit, Vincent J.** Aerosol and surface stability of HCoV-19 (SARS-CoV-2) compared to SARS-CoV-1. // The New England Journal of Medicine, 2020, 382, pp. 1564-1567.
19. **Zakrevskaya L.V., Khudyakova K.A.** Dobavki karbonatnykh porod v stroitel'nyye kompozitsionnyye materialy [Additives of carbonate rocks in building composite materials]. // Innovatsionnyye tekhnologii sovremennoy nauchnoy deyatel'nosti: strategiya, zadachi, vnedreniye. // Sbornik statey Mezhdunarodnoy nauchno-prakticheskoy konferentsii, Penza, May 14th 2020, pp 23-27 (in Russian).
20. **Koren'kova S.F., Bezgina L.N, Zimina V.G., Renkas Ye.V.** Vliyaniye mikrodispersnogo karbonata kal'tsiya na formirovaniye adgezionnoy prochnosti v betonakh razlichnogo sostava [Influence of microdispersed calcium carbonate on the formation of adhesive strength in concretes of various compositions]. // News of higher educational institutions. Construction, 2007, Issue 10 (586), pp.10-16 (in Russian).

СПИСОК ЛИТЕРАТУРЫ

1. **Родин А.И., Ерофеев В.Т., Пустовгар А.П., Еремин А.В., Пашкевич С.А., Богатов А.Д., Казначеев С.В., Адамцевич А.О.** Кинетика набора прочности биоцидных цементов. // Вестник МГСУ, 2014, том 12, с. 88-98.
2. **Dergunova A., Piksaykina A., Bogatov A., Salman Al.D.S.D., Erofeev V.** The economic damage from biodeterioration in building sector. // IOP Conference Series: Materials Science and Engineering, 2019, Volume 698(7), 2019, 077020.
3. **Zhao J., Csetenyi L., Gadd G. M.** Biocorrosion of copper metal by Aspergillus niger. // International

Biodeterioration & Biodegradation, 2020, Volume 154, 105081.
4. **Salem M.Z.M.** EDX measurements and SEM examination of surface of some imported woods inoculated by three mold fungi. // Measurement, 2016, Volume 86, pp. 301–309.
5. **Hager W.H., Boes R.M.** Hydraulic structures: a positive outlook into the future. // Journal of Hydraulic Research, 2014, Volume 52, pp. 299-310.
6. **Cai W., Li Y., Niu L., Zhang W., Wang C., Wang P., Meng F.** New insights into the spatial variability of biofilm communities and potentially negative bacterial groups in hydraulic concrete structures // Water Research, 2017, Volume 123, pp. 495–504.
7. **Salonen H., Lappalainen S., Lindroos O., Harju R., Reijula K.** Fungi and bacteria in mould-damaged and non-damaged office environments in a subarctic climate // Atmospheric Environment, 2007, Volume 41(32), pp. 6797–6807.
8. **Tischer C.G., Heinrich J.** Exposure assessment of residential mould, fungi and microbial components in relation to children's health: Achievements and challenges. // International Journal of Hygiene and Environmental Health, 2013 Volume 216(2), pp. 109–114.
9. **Erofeev V., Rodin A., Rodina N., Kalashnikov V., Irina E.** Biocidal Binders for the Concretes of Underground Constructions // Procedia Engineering, 2016, Volume 165, pp. 1448-1454.
10. **Travush V.I., Karpenko N.I., Erofeev V.T., Rodin A.I., Smirnov V.F., Rodina N.G.** Development of Biocidal Cements for Buildings and Structures with Biologically Active Environments // Power Technology and Engineering, 2017, Volume 51(4), pp. 377-384.
11. **Svetlov D.A., Svetlova E.D., Svetlov D.D., Egorova T.S.** Research into Antibacterial Activity of Novel Disinfectants Derived from Polyhexamethylene Guanidine Hydrochloride // IOP Conference Series Materials Science and Engineering, 2021, Volume 1079(6), 062017.
12. **Qiu L., Dong S., Ashour A., Han B.** Antimicrobial concrete for smart and durable infrastructures: A review. // Construction and Building Materials, 2020, Volume 260, 120456.
13. **Noeiaghaei T., Mukherjee A., Dhami N., Chae S.-R.** Biogenic deterioration of concrete and its mitigation technologies. // Construction and Building Materials, 2017, Volume 149, pp. 575–586.
14. **Sportelli M.C., Izzi M., Kukushkina E.A., Hossain S.I., Picca R.A., Ditaranto N., Cioffi N.** Can Nanotechnology and Materials Science Help the Fight against SARS-CoV-2? // Nanomaterials, 2020, Volume 10(4), 802.
15. **Slepiˇcka P, Slepiˇcková N. K., Siegel J., Kolská Z., Švorˇcík V**. Methods of Gold and Silver Nanoparticles Preparation // Materials. 2020. Volume 13(1), 1.
16. **Tavakoli A, Sadegh M.H.** Inhibition of herpes simplex virus type 1 by copper oxide nanoparticles // Journal of Virological Methods, 2019, 275:113688.
17. **Grass G, Rensing C, Solioz M.** Metallic Copper as an Antimicrobial Surface. // Applied and environmental microbiology, 2011, Volume 77(5), pp. 1541–1547.
18. **Doremalen N, Bushmaker T, Morris D.H., Holbrook M.G., Gamble A., Williamson B.N., Tamin A., Harcourt J.L., Thornburg N.J., Gerber S.I., Lloyd-Smith J.O., Emmie de Wit, Vincent J.** Aerosol and surface stability of HCoV-19 (SARS-CoV-2) compared to SARS-CoV-1 // The New England Journal of Medicine, 2020, 382, pp. 1564-1567.
19. **Закревская Л.В., Худякова К.А.** Добавки карбонатных пород в строительные композиционные материалы // Инновационные технологии современной научной деятельности: стратегия, задачи, внедрение. Сборник статей

Международной научно-практической конференции, 14 мая 2020 г., Пенза, с.23-27.
20. **Коренькова С.Ф., Безгина Л.Н, Зимина В.Г., Ренкас Е.В.** Влияние микродисперсного карбоната кальция на формирование адгезионной прочности в бетонах различного состава. // Известия высших учебных заведений. Строительство, 2007, том 10 №586, с.10-16.

Kamil B. Sharafutdinov. post-graduate student of department of Building Constructions and Computational Mechanics, Perm National Research Polytechnic University; Russia, 614010, Perm, ul. Kuibyshev, 109; phone +79063745012, e-mail: kamil_sh@bk.ru

Kseniya A Saraykina. Head of Building department, Ph.D. in Engineering Science, senior lecturer of department of Construction Engineering and Materials Science, Perm National Research Polytechnic University; Russia, 614010, Perm, ul. Kuibyshev, 109; phone +73422198172, e-mail: k.a.saraykina@pstu.ru

Galina G. Kashevarova. Corresponding Member of Russian Academy of Architecture and Construction Sciences, Professor, Dr.Sc., Head of department of Building Constructions and Computational Mechanics, Perm National Research Polytechnic University; Russia, 614010, Perm, ul. Kuibyshev, 109; phone +73422198361, e-mail: ggkash@mail.ru.

Vladimir T. Erofeev. member of Russian Academy of Architecture and Construction Sciences, Professor, Dr.Sc., Head of department of Faculty of Architecture and Civil Engineering and Head of department of Building materials and technologies Ogarev Mordovia State University; Russia; 430000, Saransk, ul. Sovetskaya, 24; phone +78342474019, e-mail: fac-build@adm.mrsu.ru

Шарафутдинов Камил Булатович - аспирант кафедры строительных конструкций и вычислительной механики Пермского национального исследовательского политехнического университета; Россия 614010, г. Пермь, ул. Куйбышева, 109; тел. +79063745012, e-mail: kamil_sh@bk.ru.

Сарайкина Ксения Александровна - декан строительного факультета к.т.н., доцент кафедры "Строительный инжиниринг и материаловедение" Пермского национального исследовательского политехнического университета; Россия, 614010, г. Пермь, ул. Куйбышева, 109; тел. +73422198172, e-mail: k.a.saraykina@pstu.ru

Кашеварова Галина Геннадьевна - член-корреспондент РААСН, доктор технических наук, профессор, заведующая кафедрой «Строительные конструкции и вычислительная механика» Пермского национального исследовательского политехнического университета; Россия 614010, г. Пермь, ул. Куйбышева, 109; тел. +73422198361, e-mail: ggkash@mail.ru.

Ерофеев Владимир Трофимович - доктор технических наук, профессор, член РААСН, декан архитектурно-строительного факультета и заведующий кафедрой «Строительные материалы и технологии» Национального исследовательского Мордовского государственного университета им. Н. П. Огарёва; Россия, 430000, г.Саранск, ул. Советская, 24; тел.+78342474019, e-mail: fac-build@adm.mrsu.ru

International Journal for Computational Civil and Structural Engineering, 18(2) 156–162 (2022)

DOI:10.22337/2587-9618-2022-18-2-156-162

METHOD FOR EXTRACTING DIAGNOSTIC FEATURES OF THE FACILITIES TECHNICAL CONDITION IN THE SYSTEM FOR MONITORING

Vladislav A. Kats, Liubov A. Adamtsevich

National Research Moscow State University of Civil Engineering, Moscow, RUSSIA

Abstract: Technical diagnostics of facilities is an urgent problem during its operation. An integral part of the implementation of diagnostic monitoring systems is the development of a decision support system (DSS) based on the analysis of acoustic emission (AE) diagnostic data and machine learning methods. A necessary condition for the application of machine learning methods in the development of DSS is the process of extracting diagnostic features from the AE signal. In the present work, an improved method is proposed for extracting diagnostic features from time series of AE signals. This includes two successive steps. At the first step, the frequency and frequency-time characteristics are calculated in a sliding window of short duration, which describe local changes in the shape and structure of single pulses. At the second step, the resulting matrix of informative features is aggregated by calculating statistical moments of various orders, which makes it possible to effectively detect long-term trends in the AE signal changes emitted by the defect. Verification of the proposed method was carried out on a full-scale control object of the oil tank RVS No. 3 ("NTEK LLC"). Based on the results obtained, a conclusion was made about the effectiveness of the proposed method in the development of diagnostic monitoring systems based on acoustic emission data.

Keywords: acoustic emission, decision support system, feature extraction, digital signal processing, feature dimension reduction.

СПОСОБ ИЗВЛЕЧЕНИЯ ДИАГНОСТИЧЕСКИХ ПРИЗНАКОВ В СИСТЕМЕ МОНИТОРИНГА ТЕХНИЧЕСКОГО СОСТОЯНИЯ СТРОИТЕЛЬНЫХ ОБЪЕКТОВ

В.А. Кац, Л.А. Адамцевич

Национальный исследовательский Московский государственный строительный университет, г. Москва, РОССИЯ

Аннотация: Техническая диагностика строительных объектов в процессе их эксплуатации является актуальной проблемой. Неотъемлемой частью реализации систем диагностического мониторинга является разработка системы поддержки принятия решения (СППР), основанной на анализе данных акустико-эмиссионной (АЭ) диагностики и методах машинного обучения. Необходимым условием применения методов машинного обучения при разработке СППР является процесс извлечения диагностических признаков из сигнала АЭ. В настоящей работе предложен улучшенный способ извлечения диагностических признаков из временных рядов АЭ-сигналов, включающий в себя два последовательных шага. На первом шаге вычисляются частотные и частотно-временные характеристики в скользящем окне малой длительности, описывающие локальные изменения формы и структуры единичных импульсов. На втором шаге полученная матрица информативных признаков агрегируется посредством расчета статистических моментов различных порядков, что позволяет эффективно детектировать долговременные тренды изменения сигнала АЭ, излучаемые дефектом. Верификация предложенного способа проведена на натурном объекте контроля – нефтеналивном резервуаре РВС №3 («ООО НТЭК»). На основе полученных результатов сделан вывод об эффективности предложенного способа при разработке систем диагностического мониторинга, основанных на данных акустической эмиссии.

Ключевые слова: акустическая эмиссия, система поддержки принятия решения, извлечение признаков, цифровая обработка сигнала, редукция размерности признаков.

INTRODUCTION

Diagnostics of the technical condition of facilities without its decommissioning is an urgent problem. Its solution deals with the need to continuously monitor the technical condition of building structures, develop integrated diagnostic monitoring systems, as well as effectively manage the risks of accidents at control objects. As a part of the practical implementation of the diagnostic monitoring system, an important task is to predict the failure of an object and assess the possible damage caused by an emergency situation at a construction site using the decision support system (DSS) [1].

Machine learning methods are widely used in modern DSS. It is noted that these methods promise assessing the technical condition using the data of instrumental non-destructive testing, in particular, the results of acoustic emission (AE) diagnostics [1].

A necessary condition for the use of machine learning to assess the hazard class is the extraction of a set of informative features characterizing the evolution of defects ("feature extraction") from the registered AE signal [2]. A useful AE signal has a number of features that complicate the task of feature extraction:

a) Data from sensors (AE transducers) are usually recorded with a high sampling rate of at least 1-2 MHz, which entails a large amount of monitoring data. In this regard, of particular importance is the provision of compression of the initial data when extracting features and, on the other hand, the sensitivity of the informative features themselves to changes in the local structure of the AE time series when a single pulse of short duration appears.

b) The evolution of defects-sources of acoustic emission is slow [1].

The characteristic time for the development of defects before the onset of a pre-destructive state ranges from several weeks to several years, depending on the technical condition of a particular building structure and its operating conditions. At the same time, in order to determine the hazard class of AE source defects and to reveal the kinetics of their evolution, it becomes necessary to register and analyze long-term trends of the corresponding informative features.

The present work proposes an improved method for extracting features from the time series of acoustic emission signals by means of sliding time windows of different widths with overlaps. This method can be used for the analysis of experimental AE time series of long duration obtained during the diagnostics of full-scale building objects.

METHODS

In this paper, we study a method for extracting diagnostic features of the defect's presence in a structural member, based on the calculation of a number of statistical values that are directly related to the shape parameters and the local structure of the sequence of acoustic emission and noise pulses recorded during the control of the technical condition of a building structure. It is essential that the registration of noisy time series of acoustic emission in this case should be implemented in such a way that ensures the identification of the true shape of the useful AE signal against the background of noise. This condition is satisfied if recording noisy AE data using a non-threshold method [4].

At the first step, informative features in the frequency and time domains are calculated in sliding windows with overlaps in order to identify local changes in the signal shape on a small-time scale, which are associated with the occurrence of signal source defects. The length of such an analyzing window is chosen from the following considerations. On the one hand, the window length should be small enough to ensure the stationarity of the noisy signal and its spectrum within the window. On the other hand, the window length should be large enough to ensure the representativeness of the calculation of statistical features in the time domain and the required spectral resolution in the frequency domain respectively.

Based on the results of preliminary studies of experimental AE time series, it was found that the most informative on small time scales is the

following set of features in the time and frequency domains:

1) Spectral centroid.

It is defined as the weighted average amplitude of the frequency spectrum of the signal:

$$C_i = \frac{\sum_{k=1}^{W_L} kX_i(k)}{\sum_{k=1}^{W_L} X_i(k)},$$

where W_L is a number of Fourier transform coefficients

$X_i(k)$ is magnitude of k^{th} transform coefficient

i is the index of time window

The centroid is a measure of the shape of the spectrum. The growth of the centroid indicates the predominance of high-frequency components in the spectrum of the noisy signal, due to the presence of interference.

2) Range factor.

This factor describes the standard deviation of the spectrum, which is related to the width and position on the frequency axis of the signal bandwidth [6]:

$$S_i = \sqrt{\frac{\sum_{k=1}^{N} (k - C_i)^2 X_i(k)}{\sum_{k=1}^{N} X_i(k)}}.$$

Noise pulses usually have a larger peak-to-peak factor, while the appearance of AE pulses associated with a structural defect leads to a small spectral spread and a corresponding decrease in the peak-to-peak factor.

3) Spectrum attenuation factor.

This factor determines the frequency below which the q^{th} fraction of the area under the spectrum amplitude distribution function is concentrated (the corresponding frequency is analogous to the percentile in statistics [7]):

$$\sum_{k=1}^{R_i} X_i(k) = q \sum_{k=1}^{N} X_i(k)$$

The attenuation coefficient also describes the shape of the spectrum and can be used to differentiate the useful AE signal and noise, as well as signals related to source defects of various hazard classes.

4) Spectral flux density (sequence) of pulses.

It is defined as the square of the difference between the normalized magnitudes of the spectra of two successive time windows:

$$S_i = \sqrt{\frac{\sum_{k=1}^{N} (k - C_i)^2 X_i(k)}{\sum_{k=1}^{N} X_i(k)}}.$$

$$F_{(i,i-1)} = \sum_{k=1}^{N} \left(EN_i(k)_L - EN_{i-1}(k)_L \right)^2,$$

where $EN_i(k)_L = \frac{X_i(k)_L}{\sum_{m=1}^{N} X_i(m)_L}$,

L is the basis length of Fast Fourier Transform for spectrum calculation

This measure is sensitive to local changes in the amplitude of the spectrum associated with the dynamics of the evolution of the shape of the AE time series during the occurrence and development of AE source defects that belong to different hazard classes.

At the second step, the features calculated at the first step are aggregated over time to identify patterns of useful AE pulses due to the development of defects. Aggregation is carried out in sliding windows up to several seconds wide by averaging over a number of statistical parameters: mathematical expectation, standard deviation, median, extreme values, coefficients of variation, skewness and kurtosis.

The width of the aggregating window is chosen from the following considerations. The window length should be small enough to reveal the differences between the noise and signal components and, on the other hand, large enough to reveal the differences between the signal components of different hazard classes that arise in the process of long-term evolution of AE signal source defects.

For each averaging parameter, a time series is formed, consisting of samples, the value of each

of which is determined by a single aggregating window of a given width. Combining these series into a two-dimensional array forms a matrix of informative features. The resulting matrix is used further as input data for the application of machine learning algorithms in classifying the detected defects by hazard classes.

RESULTS AND DISCUSSION

Verification of the proposed approach was carried out on the data of experimental time series of acoustic emission obtained during the diagnostics of the technical condition of the oil tank RVS No. 3, containing defects of various hazard classes, located in the control object.

Figure 1 shows graphs of the differential distribution function of a number of informative features that describe the shape of the AE signal and its change during the transition from one hazard class of the AE source defect to another. As an example, the calculation results are shown for three features in the frequency domain - the spectral centroid and the spectral density of the AE pulse flux. In this case, the following parameters were used for the calculation on a small-time scale (analyzing windows): the width of the sliding time window is 18 ms, the overlap is 14 ms, the width of the spectral window in calculations in the frequency domain is 32768 samples, the type of the spectral window is the Hamming weight function [6].

It follows from Figure 1 that the probability distribution densities of the statistical features listed in the previous section significantly depend on the hazard class of the AE source defect and, accordingly, on the shape of the generated acoustic emission signal: the spectral flux distribution mode (Fig. 3a) shifts towards higher values with an increase in the hazard class from the first to the third, however, the magnitude of the shift is weakly expressed. In this case, the value of the distribution density corresponding to the mode, on the contrary, increases significantly. The distribution mode of the spectral centroid (Fig. 3b) changes in the opposite way, namely, the value of the distribution density corresponding to the mode remains practically unchanged, and the mode itself noticeably shifts to the region of large values of the centroid frequency with an increase in the hazard class. At the same time, the value of the asymmetry coefficient increases.

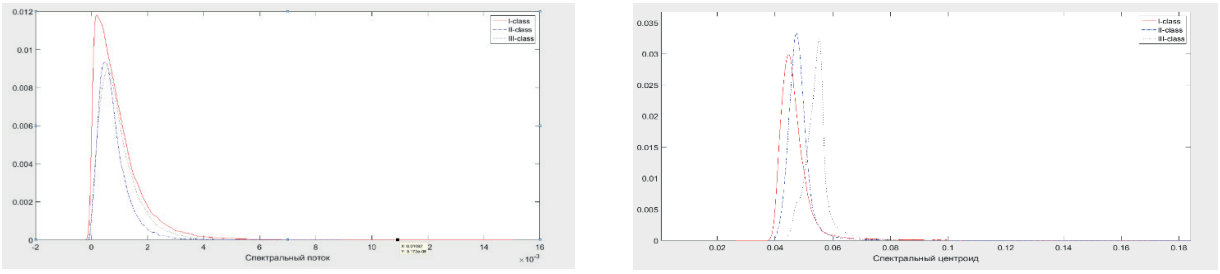

a *b*

Figure 1. Probability distribution densities of statistical signs of local changes in the shape of the AE signal for defects-sources of acoustic emission of I, II, III hazard classes: a) spectral flux density; b) spectral centroid

Table 1 summarizes the results of the calculation of statistical parameters at short time intervals. From the analysis of the data presented in Table 1, it follows that the probability density of the distribution of the selected features correlates with the hazard class. Accordingly, there is reason to believe that the time series of feature values corresponding to the obtained distribution functions can be used as input data at the second step of the proposed method, while it is advisable to use the parameters shown in Table 1 for averaging.

Table 1. Statistical values of the distribution function of diagnostic features for different hazard classes

Informative feature / distribution function parameter	Defect hazard class	Mode	Median	Skewness	Kurtosis
Spectral flux	I-class	0.0002	0.0007	2.8611	18,8905
	II-class	0.0005	0.0006	2.1951	12.4415
	III-class	0.0006	0.0008	2.3149	14.1484
Spectral centroid	I-class	0.0448	0.0452	8.5160	95.4774
	II-class	0.0473	0.0473	11.2270	176.0832
	III-class	0.0552	0.0541	9.2873	133.9230

To assess the degree of information content of the signs, a priori information about the hazard classes of AE source defects, obtained, as noted above, by an independent control method, was used. Figure 2 shows the results of feature calculation in the space of two SNE components. The points corresponding to the aggregation window, which belongs to a certain hazard class of the AE source defect, are marked in one color: green - the first class, yellow - the second, red - the third. It follows from Figure 2 that the grouping of features in the SNE-component space generally agrees with the color coding by hazard classes, while the classification error estimated using the "Accuracy" metric [14] does not exceed 2.5%. Thus, the proposed set of features and the method of its calculation make it possible to correctly divide acoustic emission signals into groups in accordance with the hazard class of AE source defects.

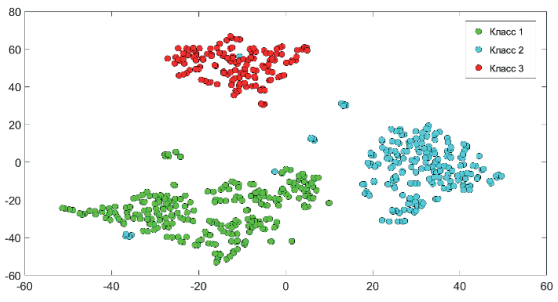

Figure 2. Averaged statistical signs of acoustic emission for the control object with sources of three hazard classes in the space of two SNE components

CONCLUSIONS

The paper presents a method for extracting diagnostic features from time series of acoustic emission signals in order to build on its basis a decision support system that provides diagnostic monitoring of the technical condition of facilities.

As diagnostic features, it is proposed to use a set of statistical parameters that are calculated in the frequency and time domains and describe the shape and local structure of the AE signal sequence: spectral centroid, flux, peak-to-peak coefficient, and spectrum attenuation coefficient.

The proposed approach was tested on a real test object - a vertical steel tank containing a defective weld. Based on a numerical comparison of the classification results in a two-dimensional feature space with a priori known from the experiment grouping of signals according to the hazard classes of AE source defects, it was found that the proposed set of features and the method of its calculation make it possible to establish a correspondence between the numerical values of the feature vector and the hazard class.

Thus, these diagnostic features can be used to describe the process of evolution of AE source defects in the control object from one hazard class to another and can be effectively used in building a decision support system as part of diagnostic monitoring systems for building structures.

REFERENCES

1. **Calabrese L., Campanella G., Proverbio E.** Noise removal by cluster analysis after long time AE corrosion monitoring of steel reinforcement in concrete // Construction and Building Materials. – 2012. – V. 34. – P. 362-371.
2. **Aggelis D.G.** Acoustic Emission Analysis for NDE in Concrete // Innovative AE and NDT Techniques for On-Site Measurement of Concrete and Masonry Structures. – 2016. – V. 20. – P. 69-88.
3. **Tzanetakis G., Cook P.** Musical genre classification of audio signals // IEEE Transactions on Speech and Audio Processing. - 2002. – V. 10. – P. 293–302.
4. **Kuzmin A.N., Inozemtsev V.V., Prokhorovsky A.S., Akselrod E.G., Kats V.A.** Tekhnologiya besporogovoj registracii dannyh akusticheskoj emissii pri kontrole promyshlennyh ob"ektov [Technology of non-threshold recording of acoustic emission data in the control of industrial facilities] // Himicheskaya tekhnika. – 2018. – No. 3. – P. 10-16. (in Russian).
5. **Inozemtsev V.V., Prokhorovsky A.S., Kuzmin A.N., Axelrod E.G.** Sposob registracii i analiza signalov akusticheskoj emissii [Method for registration and analysis of acoustic emission signals] // RF Patent No. 2570592. (in Russian).
6. **Proakis J.G., Manolakis D.K.** Digital Signal Processing. – 4 изд. – London: Pearson Education, 2009. – 1104 c.
7. **Giannakopoulos T., Pikrakis A.** Introduction to Audio Analysis - A MATLAB Approach. 2014. – Elsevier Ltd. – 262 c.
8. **Kuzmin A.N., Akselrod E.G., Kats V.A.** Akustiko-emissionnyj kontrol' pri ocenke tekhnicheskogo sostoyaniya oborudovaniya neftegazovogo kompleksa [Acoustic emission control in assessing the technical condition of the oil and gas complex equipment] // V Mire NK. – 2017. – V. 1 – P. 71-80. (in Russian).
9. **Moradian Z., Li B.Q.** Hit-Based Acoustic Emission Monitoring of Rock Fractures: Challenges and Solutions // Advances in Acoustic Emission Technology. - 2017. – V. 179. – P. 357-370.
10. **Ogura N., Yatsumoto H., Chang K.C., Shiotani T.** Development of Damage Evaluation Method for Concrete in Steel Plate-Bonded RC Slabs // Advances in Acoustic Emission Technology. – 2017. – V. 179. – P. 321-334.
11. **Vafa Soltangharaei, Rafal Anay, Nolan W. Hayes, Lateef Assi, Yann Le Pape, Zhongguo John Ma, Paul Ziehl.** Damage Mechanism Evaluation of Large-Scale Concrete Structures Affected by Alkali-Silica Reaction Using Acoustic Emission // Applied Sciences. – 2018. - №8. – P. 2148-2167.
12. **L.P. van der Maaten, Hinton G.E.** Visualizing High-Dimensional Data Using t-SNE // Journal of Machine Learning Research. – 2008. – V. 9. – P. 2579-2605.
13. **Barnes J., Hut P.** A hierarchical O(N log N) force-calculation algorithm // Nature. – 1986. – V. 324. - P. 446–449.
14. **Bishop C.M.** Pattern Recognition and Machine Learning (Information Science and Statistics). - 2 ed. - New York: Springer, 2007. - 738 p.

СПИСОК ЛИТЕРАТУРЫ

1. **Calabrese L., Campanella G., Proverbio E.** Noise removal by cluster analysis after long time AE corrosion monitoring of steel reinforcement in concrete // Construction and Building Materials. – 2012. – V. 34. – P. 362-371.
2. **Aggelis D.G.** Acoustic Emission Analysis for NDE in Concrete // Innovative AE and NDT Techniques for On-Site Measurement of Concrete and Masonry Structures. – 2016. – V. 20. – P. 69-88.
3. **Tzanetakis G., Cook P.** Musical genre classification of audio signals // IEEE

Transactions on Speech and Audio Processing. – 2002. – V. 10. – P. 293–302.
4. **Кузьмин А.Н., Иноземцев В.В., Прохоровский А.С., Аксельрод Е.Г., Кац В.А.** Технология беспороговой регистрации данных акустической эмиссии при контроле промышленных объектов // Химическая техника. – 2018. – №3. - С. 10-16.
5. **Иноземцев В.В., Прохоровский А.С., Кузьмин А.Н., Аксельрод Е.Г.** Способ регистрации и анализа сигналов акустической эмиссии // Патент РФ №2570592.
6. **Proakis J.G., Manolakis D.K.** Digital Signal Processing. – 4 изд. – London: Pearson Education, 2009. – 1104 c.
7. **Giannakopoulos T., Pikrakis A.** Introduction to Audio Analysis - A MATLAB Approach. 2014. – Elsevier Ltd. – 262 c.
8. **Кузьмин А.Н., Аксельрод Е. Г., Кац В. А.** Акустико-эмиссионный контроль при оценке технического состояния оборудования нефтегазового комплекса. // В Мире НК. – 2017. – Т. 1 – С. 71-80.
9. **Moradian Z., Li B.Q.** Hit-Based Acoustic Emission Monitoring of Rock Fractures: Challenges and Solutions // Advances in Acoustic Emission Technology. - 2017. – V. 179. – P. 357-370.
10. **Ogura N., Yatsumoto H., Chang K.C., Shiotani T.** Development of Damage Evaluation Method for Concrete in Steel Plate-Bonded RC Slabs // Advances in Acoustic Emission Technology. – 2017. – V. 179. – P. 321-334.
11. **Vafa Soltangharaei, Rafal Anay, Nolan W. Hayes, Lateef Assi, Yann Le Pape, Zhongguo John Ma, Paul Ziehl.** Damage Mechanism Evaluation of Large-Scale Concrete Structures Affected by Alkali-Silica Reaction Using Acoustic Emission // Applied Sciences. – 2018. - №8. – P. 2148-2167.
12. **L.P. van der Maaten, Hinton G.E.** Visualizing High-Dimensional Data Using t-SNE // Journal of Machine Learning Research. – 2008. – V. 9. – P. 2579-2605.
13. **Barnes J., Hut P.** A hierarchical O(N log N) force-calculation algorithm // Nature. – 1986. – V. 324. - P. 446–449.
14. **Bishop C.M.** Pattern Recognition and Machine Learning (Information Science and Statistics). - 2 ed. - New York: Springer, 2007. - 738 p.

Vladislav A. Kats. PhD student of the department of Informational technology, systems and automatization in construction of the National Research Moscow State University of Civil Engineering; 129337, Russia, Moscow, Yaroslavskoe shosse, 26. E-mail: vladislavkats1894@gmail.com

Liubov A. Adamtsevich. Candidate of Technical Sciences, Associate Professor, Associate Professor of the department of Informational technology, systems and automatization in construction of the National Research Moscow State University of Civil Engineering; 129337, Russia, Moscow, Yaroslavskoe shosse, 26. E-mail: AdamtsevichLA@mgsu.ru.

Кац Владислав Анатольевич, аспирант кафедры Информационных систем, технологий и автоматизации в строительстве Национального исследовательского Московского государственного строительного университета, 129337, Москва, Ярославское ш., д. 26, e-mail: vladislavkats1894@gmail.com

Адамцевич Любовь Андреевна, кандидат технических наук, доцент, доцент кафедры Информационных систем, технологий и автоматизации в строительстве Национального исследовательского Московского государственного строительного университета, 129337, Москва, Ярославское ш. ,д.26; тел. +7495-287-49-14 доб. 30-42, e-mail: AdamtsevichLA@mgsu.ru; ORCID: 0000-0002-5843-0076M

International Journal for Computational Civil and Structural Engineering, 18(2) 163–174 (2022)

DOI:10.22337/2587-9618-2022-18-2-163-174

STRENGTH MODEL FOR CALCULATING CENTRALLY COMPRESSED CONCRETE ELEMENTS WITH COMPOSITE REINFORCEMENT, TAKING INTO ACCOUNT THE SPACING OF STIRRUPS

Ashot G. Tamrazyan, Andrey E. Lapshinov

National Research Moscow State University of Civil Engineering, Moscow, RUSSIA

Abstract. The article discusses the relevance of developing techniques for confined elements with FRP reinforcement. The method for calculating centrally confined concrete columns with non-metallic GFRP reinforcement (without regard to its compression work) is proposed for the first time in the Russian Federation. The strength model was developed based on the well-known theoretical model of confined concrete. The article considers the effect of strengthening the concrete core of the columns, which is obtained due to the more frequent placement of both transverse and longitudinal reinforcement. The dependence of the bearing capacity of concrete columns on the strength of the transverse reinforcement material is shown. It was proved that with a decrease in the spacing of the longitudinal reinforcement, the area of the effectively confined concrete core inside the reinforcement cage increases. It was shown that, due to the low compressive modulus of elasticity of the FRP reinforcement, the stress in it will be comparable to the concrete stress. Therefore, the compressive strength of the FRP reinforcement can be neglected in the case of determining the bearing capacity of centrally confined concrete elements. As a result, a strength model for calculating confined concrete elements with FRP reinforcement was proposed, considering the spacing of transverse reinforcement, the longitudinal and transverse reinforcement ratio, and the strength of the material of transverse reinforcement. The developed strength model can be applied not only for square, but also for columns of round and rectangular sections.

Keywords: confinement, stirrups, GFRP, spacing, reinforcement ratio.

ПРОЧНОСТНАЯ МОДЕЛЬ ДЛЯ РАСЧЕТА ЦЕНТРАЛЬНО СЖАТЫХ БЕТОННЫХ ЭЛЕМЕНТОВ С КОМПОЗИТНОЙ АРМАТУРОЙ С УЧЕТОМ ШАГА ПОПЕРЕЧНЫХ СТЕРЖНЕЙ

А.Г. Тамразян, А.Е. Лапшинов

Национальный исследовательский московский государственный строительный университет, г. Москва, РОССИЯ

Аннотация. В статье обсуждается актуальность разработки методики для элементов с эффективно обжатым ядром и армированием стеклокомпозитной арматурой. Впервые в Российской Федерации предложен метод расчета центрально сжатых бетонных колонн с неметаллической стеклокомпозитной арматурой (без учета ее работы на сжатие). Модель прочности была разработана на основе хорошо известной теоретической модели обжатого бетона. В статье рассматривается эффект усиления бетонного ядра колонн, который образуется за счет более частого размещения как поперечной, так и продольной арматуры. Показана зависимость несущей способности бетонных колонн от прочности материала поперечной арматуры. Было доказано, что с уменьшением расстояния между продольной арматурой площадь эффективно обжатого ядра бетона внутри арматурного каркаса увеличивается. Было показано, что из-за низкого модуля упругости при сжатии арматуры из стеклопластика напряжение в ней будет сопоставимо с напряжением в бетоне. Следовательно, прочностью на сжатие стеклокомпозитной арматуры можно пренебречь в случае определения несущей способности центрально сжатых бетонных элементов. В результате была предложена модель прочности для расчета сжатых бетонных элементов с армированием композитной арматурой с учетом расстояния между поперечной арматурой, процента армирования продольной и поперечной

арматуры, а также материала поперечной арматуры. Разработанная прочностная модель может быть применена не только для квадратных, но и для колонн круглого и прямоугольного сечения.

Ключевые слова: обжатие, хомуты, стеклокомпозит, шаг, процент армирования.

INTRODUCTION

In recent years, studies of confined concrete are becoming more and more widespread [1,2]. It was noted that concrete works most efficiently under three-dimensional stress, which led to the appearance of structures with both various types of confinement reinforcement and an increased spacing of transverse reinforcement [3]. The advantages of increasing the bearing capacity of columns by creating a three-dimensional stress state with the use of transverse reinforcement are obvious and have great potential [4]. There is also a whole spectrum of compressive members suffering from reinforcement corrosion, where the use of steel reinforcement leads to early failure of the structure due to corrosion and shortens the life cycle. In such harsh conditions (for example, in tanks, silos, bunkers, reservoirs) columns with non-metallic FRP reinforcement can be successfully used, increasing the life cycle of structures, their overhaul intervals and reducing capital repair costs.

However, a strength model that would consider the effect of an increased spacing of transverse reinforcement on the strength of centrally confined elements has not been introduced in the Russian Federation so far. There is still no methodology for calculating centrally confined columns reinforced with longitudinal and transverse FRP reinforcement in our country. In the modern design standards of the Russian Federation [7], the design resistance of FRP reinforcement for compression is taken equal to 0. In the design standards of different countries, FRP reinforcement as compression reinforcement is also not considered [8, 9]. Canadian researchers [10] proposed the following formula (1) for calculating centrally confined circular elements considering confined GFRP reinforcement:

$$P_0 = 0.85 f_c^{'}(A_g - A_F) + \alpha_g f_{fu} A_F, \qquad (1)$$

where 0.85 – coefficient defined as the ratio between the strength of concrete in a structure and the cylindrical strength of concrete;

f'_c – cylinder strength of concrete;

A_g – column cross-section area;

A_F – cross-sectional area of confined FRP reinforcement;

α_g – a new coefficient that considers the compressive strength of FRP reinforcement depending on its tensile strength.

f_{fu} – tensile strength of FRP reinforcement.

From formula (1), it can be established that with the strength of FRP reinforcement of 1000 Mpa and a coefficient of α_g = 0.3, the strength of composite reinforcement considered in the design will be 300 Mpa.

It is known that the design compressive strength of reinforcement is determined to a greater extent by the ultimate compressibility of concrete $\varepsilon_{bu}=2\cdot10^{-3}$. The ultimate compressibility of concrete depends on the strength of the concrete, its grade, composition, and the duration of the load application. With an increase in the grade of concrete, the ultimate deformations decrease, however, with an increase in the duration of the load application, they increase.

Since, due to bond, the reinforcement deforms with the concrete $\varepsilon_{sc}= \varepsilon_{bu}$, the limiting stresses in it are determined by the formula of Hooke's law:

$$\sigma_{sc} = \varepsilon_{sc} E_s \qquad (2)$$

where E_s – modulus of elasticity of the reinforcement. Therefore, the design resistance of the steel reinforcement will be equal to $R_{sc}=400$ *МПа*, which is accepted in modern

design standards for traditional reinforced concrete structures.

Using Hooke's law (2) it can be obtained that the limiting stresses in the FRP reinforcement at the compressive modulus of elasticity 30 000 MPa and standard strain values for concrete 0,2% achieved only around 50-60 *МПа*, which can be comparable to the compressive stresses of concrete. Under such stresses, considering the ratio of reinforcement in confined structures (usually no more than 2-3%), the share of FRP reinforcement in the bearing capacity of the column will be very small, comparable to the computational error, which greatly limits the prospects for its use in confined elements.

Thus, the stresses in confined FRP reinforcement, due to the low modulus of elasticity, cannot reach such high values proposed by Canadian researchers; therefore, this approach is practically inapplicable. In addition, this strength model ignores the influence of the transverse reinforcement parameters (diameter, spacing, strength) on the strength of a confined element, which, as studies show [11, 12], is incorrect. The results of studies carried out with the usual, not frequent spacing of the stirrup [13], show no increase in the strength of the samples. Therefore, it is necessary to develop a methodology that considers the step of the transverse reinforcement, the ratio of longitudinal and transverse reinforcement, and the strength of the stirrups.

METHODS

During the development of the strength model, general scientific research methods were used (analysis and synthesis, methods of generalization, induction, and deduction). To develop the calculation methodology, the well-known model of confined concrete proposed by Mander et al in 1988 [14] was taken and adapted for columns with FRP reinforcement.

A comparative stress-strain diagram is shown in Figure 1. This figure shows two curves. One curve is for unconfined concrete (bottom), the other is for confined (top). The upper curve has 2 branches - ascending and descending. The ascending branch has a variable slope and starts at a point with a value E_b. Further, the slope of the curve decreases until it reaches the value of the maximum limited strength R_{cb}, ε_{cb}. Thereafter, a descending branch begins with a slight negative slope, reflecting plastic behavior. The end of the curve has a point with maximum deformation ε_{bu}, in which the destruction of the first stirrup occurs. The bottom curve reflects the behavior of unconfined concrete. It has the same ascending branch as the confined concrete curve, with a peak value f'_c (R_b), ε_{c0}. Then, the descending branch follows to the value $1,5...2\varepsilon_{c0}$. Further, the dependence is a straight line until zero strength is reached when cracks appear (ε_{sp}). In our case, it is extremely important to find the dependence for determining the stress-strain state of a limited concrete core inside the stirrups.

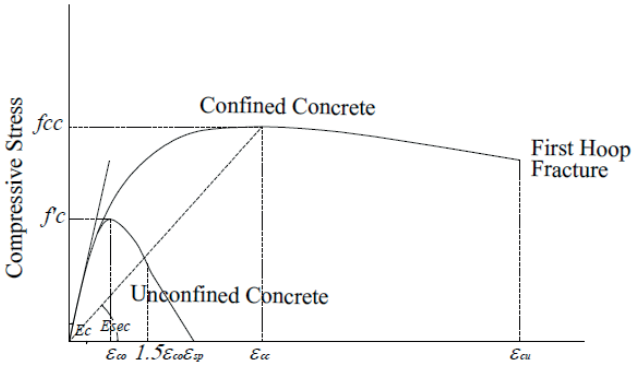

Figure 1. Axial Stress-Strain Model proposed by Mander et al. (1988) for monotonic loading

A distinctive feature of the methods for calculating structures with a triaxial stress state of the inner core is considering the increased strength of concrete in the longitudinal direction.

When comparing the efficiency of structural elements with different methods of reinforcement, the factors of the efficiency of concrete work is η and the efficiency of the structural element as a whole - *m*.

$$\eta = \sigma_b / R_b \quad (3)$$

$$m = N / R_s A_s + R_b A_b \quad (4)$$

where σ_b – longitudinal stresses in concrete at the moment of failure;
N – bearing capacity of the element.

For elements reinforced only with longitudinal reinforcement and the usual standard spacing of transverse reinforcement $\eta = m = 1$, previously conducted experiments [15] found that the efficiency of confined concrete largely depends on the method of reinforcement (Table 1).

Table 1. The dependence of the efficiency factors of concrete μ and the structural element m on the reinforcement method

Type of element, reinforcement	μ	m
Steel tube confined concrete (STCC)	1,5…2,0	3,0…4,2
With reinforcement		
Spiral	1,2…1,4	1,4…1,8
Mesh	1,3…1,5	1,4…1,8
List	1,2…1,4	1,4…1,7
Angle (L-shape)	1,1…1,2	1,2…1,5

The efficiency of a confined concrete core operating in confined conditions can vary significantly depending on the type of concrete. So, for example, for steel tube confined concrete (STCC) concrete η varies from 3.0 for lightweight aggregate concrete to 4.2 for conventional concrete; for elements with mesh and spiral reinforcement - from 1.4 to 1.8, respectively; with corner reinforcement - from 1.2 to 1.5.

Columns of circular cross-section are rarely used in structures for industrial and civil construction therefore, for further research, we will use columns of square and rectangular cross-section.

For the calculation of traditional tube confined concrete structures with a reinforcing cage inside the tube, previously it was proposed to distinguish three characteristic zones in its cross section, which are in different stress-strain state [3].

In our case, due to the frequent setting of transverse reinforcement, only 2 characteristic zones can be considered in the cross section of the element – *A1* inside the reinforcement cage and *A2* from the outer edge of the column to the inner edge of the reinforcing cage (Figure 2).

Inside of the A*1* zone concrete works under conditions of a biaxial stress state, while in the zone *A2* the stressed state of concrete can be characterized as uniaxial compression.

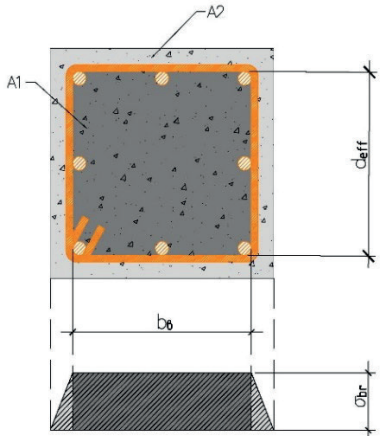

Figure 2. Plot of lateral pressure over the core

For the rest, the calculation is proposed to be carried out by analogy with square-section concrete not taking the steel shell into account.

RESULTS

The strength of the concrete core of a composite reinforcing cage element operating under

volumetric compression is determined as the average value of the strength of the peripheral and central zones:

$$R_{b3,m} = \frac{R_{b3,f} A_{s,z} + R_b (A - A_{s,z})}{A}, \qquad (5)$$

where $R_{b3,f}$ – the compressive strength of the central zone of a concrete core having indirect reinforcement in the form of frequently installed transverse FRP reinforcement. $A_{s,z}$ – area of the zone inside the stirrups.

Strength of concrete reinforced core $R_{b3,f}$ is determined by the formula (6) with replacement of R_b by $R_{b,s}$ and $\overline{\sigma}$ by $\overline{\sigma}_s$ (or $\overline{\sigma}_f$). In our case $\overline{\sigma}_s$ - the relative value of the lateral pressure in the limiting state from the side of the reinforcing cage on the concrete core and $R_{b,s}$ – compressive strength of concrete with indirect reinforcement with stirrups.

$R_{b,3f}$ is calculated by the formula:

$$R_{b,3f} = R_b \left[1 + \left(0.5\overline{\sigma_{fc}} + \frac{\overline{\sigma_{fc}} - 2}{4} + \sqrt{\left(\frac{\overline{\sigma_{fc}} - 2}{4} \right)^2 + \frac{\sigma_{fc}}{b_1}} \right) \right] \qquad (6)$$

where $\overline{\sigma}_{sc}$ - relative radial stresses inside the reinforcement cage.

The value of $\overline{\sigma}_s$ is calculated by the following formula [6,13]:

$$\overline{\sigma} = 0{,}48 e^{-1{,}5b1} \rho^{0{,}8} \qquad (7)$$

In the formula (7) the structural element ρ is replaced by ρ_f, defined as follows:

$$\rho_f = \frac{\sigma_{y,p} A_p}{R_{b,s} A} \qquad (8)$$

The value of $\overline{\sigma}_{fc}$ is calculated by the following formula:

$$\overline{\sigma}_{fc} = \frac{\mu_{fc} \sigma_{y,sc}}{R_b}, \qquad (9)$$

where $\sigma_{y,sc}$ - spiral yield strength;

μ_{fc} - transverse reinforcement ratio with stirrups.

The transverse reinforcement ratio with stirrups depends on the area of the stirrup A_{fc}, the area limited by the diameter of the spiral d_{eff} and spacing of stirrups s. μ_{fc} is calculated according to the formula:

$$\mu_{fc} = \frac{2A_{fc}}{d_{eff} s} \qquad (10)$$

Formulas (9) and (10) reflect the previously made assumption that the smaller the spacing of transverse reinforcement, the higher the relative radial stresses inside the reinforcement cage and, therefore, the higher the strength of the concrete core.

In our case, in formula (9) instead of the yield point of steel $\sigma_{y,sc}$ it is necessary to use the tensile strength of the material from which the stirrups are made, namely GFRP reinforcement.

In current construction practice, bent steel rods are already shipped to site prefabricated or bent on site. Unlike the FRP reinforcement, steel has an elastoplastic nature and, therefore, can be easily fixed to “cold”. Current design codes specify bending radius for steel reinforcement from 2,5d_s for mild steel, which corresponds to a maximum deformation of 20%. In the case of FRP reinforcement, there may be problems with potential buckling of the fibers on the inner (compressed) side. Besides that, the typical ultimate strain of composites ranges from 1% to 2.5%, therefore strains in the fibers must be controlled to avoid early failure of the entire rebar. As a result, the cold bending of composite rebar requires larger radius than steel rebar.

It is believed that the bending strength of FRP reinforcement bars is lower than the strength of a straight bar [16, 17]. The key factor is the parallelism of the fibers. So, for fibers, the

decrease in strength begins for angles from 5º. For laminates with an angle of inclination of the fibers from the b-axis 30º strength is only 10% of the initial (Figure 3).

The compromise between mechanical properties, ease of manufacture and use of composite stirrups is a bend diameter 7 times larger than the stirrup diameter [18]. In addition, some researchers [19] obtained graphs of the dependence of the strength of FRP reinforcement rods on the angle of inclination of the fibers (Figure 4).

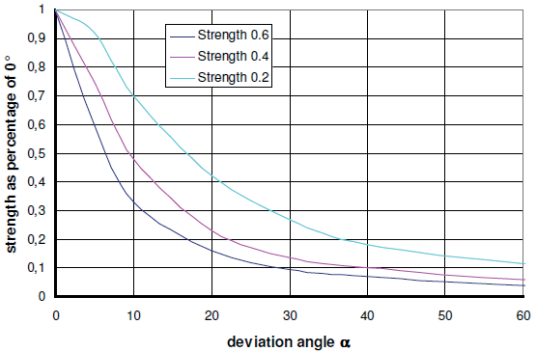

Figure 3. The influence of deviation angle of fibers to strength of UD laminates for different fiber contents [19]

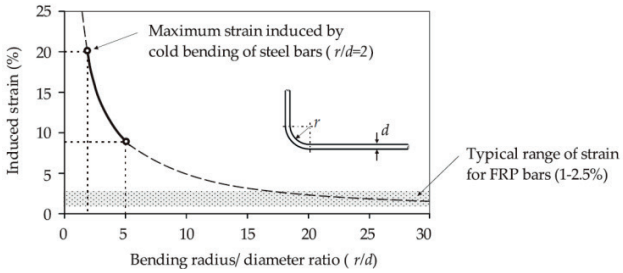

Figure 4. Induced strain values in cold bent bars [18]

Considering the above, we can conclude that for composite stirrups the strength of the rebars on the bends critically depends on the angle of inclination of the fibers. This fact is reflected in the design standard of the Russian Federation for structures reinforced with FRP reinforcement [7]. So, according to clause 5.2.10 [7], the design value R_{fw} of the resistance of FRP reinforcement to tensile at the bend radius of stirrups made of rebars with a diameter d_{fw}, equal to at least $6d_{fw}$ should be defined by the formula:

$$R_{fw} = 0.004E_f \le 0{,}5R_f \qquad (11)$$

Thus, at the most common value of the tensile elastic modulus of GFRP reinforcement *50 000 MIIa* it is necessary to substitute values no more than R_{fw}=*200 MPa* in the formula (11) instead of $\sigma_{y,sc}$.

It is also important to determine the area of the effectively confined core of the section. According to [4], the area of an effectively limited concrete core A_e is less than the area of the core inside the center lines of the stirrups, excluding the area of the longitudinal reinforcement A_{fc}. The confined concrete zone is assumed to be the area within the center lines of the stirrup's perimeter (Figure 5).

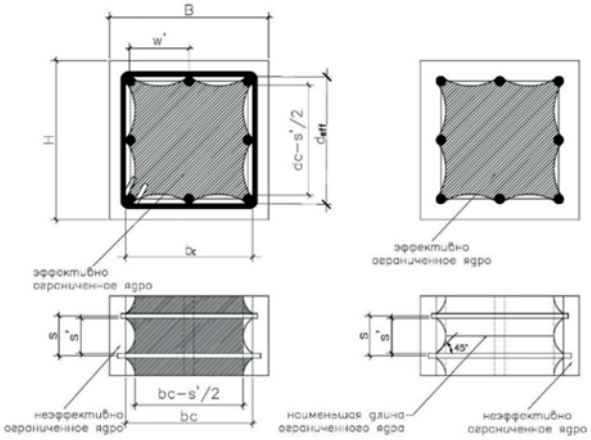

Figure 5. Zone of confined concrete for square columns

The total ineffective area of the confined core at the level of the stirrups, taken that their number is *n*:

$$A_i = \sum_{i=1}^{n} \frac{\left(w_i'\right)^2}{6} \qquad (12)$$

Considering that the boundary of effectively confined concrete between two adjacent stirrups has the shape of a square parabola with an initial angle of inclination 45º, the ratio of the area of

effectively confined concrete to the area of the core will be as follows:

$$\lambda = \frac{\left(A_{et} - \sum_{i=1}^{n} \frac{\left(w_i^{'}\right)^2}{6} \right)}{A_{et}} \qquad (13)$$

As can be seen from Fig. 5, the contour of an effectively limited core is not square or rectangular, as it was assumed earlier [20]. From the equation of the area of a square parabola, the ordinate of the parabola depends on the abscissa (the spacing of the longitudinal reinforcement). That is, with a decrease in the distance between the bars of the longitudinal reinforcement, the ordinate of the parabola also decreases. At the same time, the area of unconfined concrete is reduced, and the area of efficiently confined concrete is increased. Based on the above, we can conclude that saturation with longitudinal reinforcement, i.e., an increase in its spacing, directly affects the area of an effectively confined core enclosed inside the stirrups and, as a result, affects an increase in the bearing capacity of the centrally compressed element.

Thus, the area of confined concrete in the section is determined in the middle between two adjacent stirrups:

$$A_{emt} = \left(b_c - \frac{s'}{2} \right)\left(d_c - \frac{s'}{2} \right) = b_c d_c \left(1 - \frac{s'}{2b_c} \right)\left(1 - \frac{s'}{2d_c} \right) \qquad (14)$$

Accordingly, the effective area in the middle section is calculated as follows:

$$A_e = \lambda b_c d_c \left(1 - \frac{s'}{2b_c} \right)\left(1 - \frac{s'}{2d_c} \right) = \\ = \frac{1}{b_c d_c} \left(b_c d_c - \sum_{i=1}^{n} \frac{\left(w_i^{'}\right)^2}{6} \right) b_c d_c \left(1 - \frac{s'}{2b_c} \right)\left(1 - \frac{s'}{2d_c} \right) \qquad (15)$$

$$A_e = \left(b_c d_c - \sum_{i=1}^{n} \frac{\left(w_i^{'}\right)^2}{6} \right)\left(1 - \frac{s'}{2b_c} \right)\left(1 - \frac{s'}{2d_c} \right) \qquad (16)$$

It can be seen from the formula above that the smaller the spacing of the transverse reinforcement, the larger the area of effectively confined concrete in the core of the section will be and, therefore, the higher the bearing capacity of the centrally compressed element will be. This proves the previously stated assumption that with a decrease in the spacing of the transverse reinforcement, the bearing capacity of a confined concrete element increases with FRP reinforcement. In addition, the spacing of the longitudinal reinforcement also affects the area of the effectively compressed core of the section. The more often the longitudinal reinforcement is installed in the section, the smaller the variable w' will be, the larger the area of the effectively compressed core and, therefore, the greater the bearing capacity of the element will be.

DISCUSSION

As a result, the bearing capacity of a compressed element with FRP reinforcement can be represented as following:

$$N_{ult,3f} = R_{b3,f} A_e + R_b (A - A_e) \qquad (17)$$

This formula takes into account the increased strength of an effectively confined core $R_{b3,f}$ whereas the compressive strength of the FRP reinforcement is not taken into account.

Generally, the method takes into account the spacing of the transverse reinforcement, the saturation of the longitudinal and transverse reinforcement, the strength of the material of the transverse reinforcement (stirrups).

It can be noted that the developed model can be adapted for round and rectangular columns as well. Only in the case of columns with a circular cross-section, the efficiency of using FRP reinforcement should be higher due to the greater strength of the transverse reinforcement material without bends.For comparison with the experimental data, a comparison was made with the research results obtained in [11,12,21]. The comparison results (table 2 and figure 6) shows good correlation between theoretical and experimental values.

Table 2. Experimental results and model prediction for GFRP reinforced compressed members

№	Specimen	b(d), mm	w', mm	s, mm	R_b, MPa	$R_{b,3f}$, MPa	N^{exp}	N^{theor}	$\frac{N^{exp}}{N^{theor}}$
1	**2**		**3**	**4**	**5**	**6**	**7**	**8**	**9**
Lapshinov, Madatyan [12]	CB 1-1	200	75	500	14,9	15,65	615,1	646	0,95
	CB 2-1	200	75	500	14,9	15,22	504,5	624,9	0,81
	CB 1-2	200	75	250	14,9	16,36	600,1	640	0,94
	CB 2-2	200	75	250	14,9	15,53	532,2	626,8	0,85
	CB 1-3	200	75	167	15,9	18,05	738,3	689,6	1,07
	CB 1-4	200	75	100	15,2	18,59	746,1	688,6	1,08
	CB 2-4	200	75	100	15,9	16,67	619,8	680,1	0,91
	CB 1-1	200	75	500	14,9	15,63	568,4	650,4	0,87
	CG 2-1	200	75	500	14,9	15,22	561,1	628	0,89
	CG 1-2	200	75	250	14,9	16,35	583,3	643	0,91
	CG 2-2	200	75	250	14,9	15,52	491,2	629,8	0,78
	CG 1-3	200	75	167	14,9	17,05	586,1	641,4	0,91
	CG 1-4	200	75	100	15,2	18,64	798,4	678,6	1,18
	CG 2-4	200	75	100	15,2	16,74	726,2	646,4	1,12
Lapshinov, Tamrazyan [11]	CG 2-3	200	74	167	19,73	21,9	849,6	818,6	1,04
	CG 2-4-6	200	74	100	19,73	23,18	901,3	839,1	1,07
	CG 2-4-3	200	74	100	19,73	23,18	901,3	839,1	1,07
	CG 2-4-4	200	148	100	19,73	23,18	849,6	779,1	1,09
	CC 1-4	200	74	100	19,73	23,79	1042,3	848	1,23
	CS 1-4	200	74	100	19,73	23,79	1091	1210	0,9
	CS 1-5	200	74	50	19,73	27,14	1140	1270,7	0,9
	CS 1-5	200	74	50	19,73	27,14	1042,2	908,7	1,15
	CS 2-5	200	74	50	19,73	26,08	993,6	891,5	1,11
	CS 2-5-4	200	74	50	19,73	26,08	901,3	891,5	1,01
	CS 2-5-6	200	75	50	19,73	26,08	936,5	890,4	1,05
Lapshinov, et al [21]	C.4Ø10-50-1	150	100	50	22,4	35,95	670,5	541,4	1,24
	C.4Ø10-50-2	150	100	50	27,8	41,97	652,3	664,6	0,98
	C.4Ø10-100-1	150	100	100	20,1	27,68	501,5	471,2	1,06
	C.4Ø10-100-2	150	100	100	20,1	27,68	538,9	471,2	1,14
	C.8Ø10-50-1	150	50	50	26,2	40,20	721,6	666,8	1,08

In the table 2: CB – columns with BFRP rebars, CG – columns with GFRP rebars, CC – columns with CFRP rebars, CS – columns with steel rebars, C.4Ø – columns with GFRP rebars.

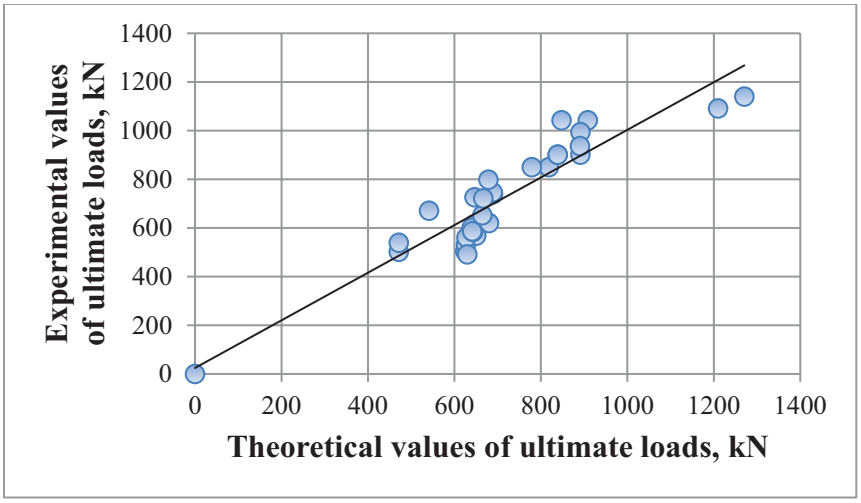

Figure 6. Comparison of calculated and experimental strength data of the author's tests [11,12,21]

CONCLUSION

1. Based on the above-described model of confined concrete, a model for calculating the strength of a centrally compressed concrete element with FRP reinforcement has been adapted and proposed for the first time in RF.
2. The proposed method considers the effect of the frequent spacing of the transverse reinforcement and saturation of longitudinal reinforcement on the strength of centrally confined concrete elements with FRP reinforcement.
3. The influence of the strength of the transverse reinforcement material on the bearing capacity of the centrally compressed concrete element has been justified.
4. An increase in the bearing capacity of confined elements with a decrease in the spacing of transverse reinforcement and saturation of the amount of longitudinal reinforcement is theoretically justified.

ACKNOWLEDGMENT

This work was carried out with the financial support of the Ministry of Science and Higher Education of the Russian Federation (project "Theoretical and experimental design of new composite materials to ensure safety during the operation of buildings and structures in conditions of man-made and biogenic threats" No. FSWG-2020-0007).

REFERENCES

1. **Tamrazyan A.G., Fedorov V.S., Kharun M.** The effect of increased deformability of columns on the resistance to progressive collapse of buildings // IOP Conference Series: Materials Science and Engineering, 2019, 675 012004, DOI: 10.1088/1757-899X/675/1/012004.
2. **Tamrazyan A., Avetisyan L.** Comparative analysis of analytical and experimental results of the strength of compressed reinforced concrete columns under special combinations of loads // MATEC Web of Conferences, 2016, 86(1):01029, DOI: 10.1051/matecconf/20168601029
3. **Krishan A.L., Astaf'eva M.A.** Silovoe soprotivlenie trubobetonnyh kolonn vysotnyh zdanij [Force resistance of pipe-concrete columns of high-rise buildings]. – Magnitogorsk: Izd-vo Magnitogorsk. gos. tekhn. un-ta im. G.I. Nosova, 2015 (in Russian).
4. **Tamrazyan A.G.** K raschetu nesushchej sposobnosti zhelezobetonnyh kolonn s uchetom diagrammy deformirovaniya ogranichennogo betona [To calculate the bearing capacity of reinforced concrete

columns taking into account the deformation diagram of limited concrete] // no. *Tekhnologiya tekstil'noj promyshlennosti*, 2018, 5 (377), pp. 217-220 (in Russian).

5. **Ahmed E., Dulude C. & Benmokrane B.** Construction and monitoring of the GFRP-reinforced flat slabs of the Hotel de Ville Parking Garage in Quebec City, 2011 Canada. Technical Rep., City of Québec, Quebec.
6. **Hamdy M. Mohamed, Benmokrane B.** Design and Performance of Reinforced Concrete Water Chlorination Tank Totally Reinforced with GFRP Bars: Case Study // Journal of Composites for Construction, 2014, Vol. 18, Issue 1, pp. 05013001. DOI: 10.1061/(ASCE)CC.1943-5614.0000429.
7. **SP 295.1325800.2017** Concrete structures reinforced with fibre-reinforced polymer bars. Design rules
8. **ACI 440.1R-15** (ACI Committee 440, 2015). «Guide for the Design and Construction of Concrete Reinforced with Fiber-Reinforced Polymer Bars». American Concrete Institute, Farmington Hills, MI, 88 pp.
9. **CAN/CSA S806-12** (2012). «Design and Construction of Building Components with Fiber Reinforced Polymers», Canadian Standards Association, Rexdale, ON, Canada.
10. **Afifi M.Z., Mohamed H.M. & Benmokrane B.** Axial capacity of circular concrete columns reinforced with GFRP-bars and spirals // Journal of Composites for Construction, ASCE, Volume 18, no. 1, Feb. 2014, p. 04013017. DOI:10.1061/(ASCE)CC.1943-5614.0000438
11. **Lapshinov A.E., Tamrazyan A.G.** K vliyaniyu poperechnogo armirovaniya na prochnost' i deformativnost' szhatyh betonnyh elementov, armirovannyh kompozitnoj polimernoj armaturoj [To the Effect of Transverse Reinforcement on the Strength and Deformability of Compressed Concrete Elements reinforced with composite Polymer Reinforcement] // *Stroitel'stvo i rekonstrukciya*. 2018. no. 4 (78). pp. 20-30 (in Russian).
12. **Lapshinov A.E., Madatyan S.A.** (2013). Concrete columns reinforced with GFRP and BFRP // 11th International Conference on Fiber Reinforced Polymers in Reinforced Concrete Structures. Guimaraes, Portugal.
13. **Oreshkin D.A., Bondarenko YU.V., Spirande K.V., Mol'skij M.M.** (2016) Eksperimental'nye issledovaniya prochnosti i deformativnosti stekloplastikovoj armatury pri szhatii i szhatyh stekloplastbetonnih elementov [Experimental studies of the strength and deformability of fiberglass reinforcement under compression and compressed fiberglass concrete elements]. *Naukovij visnik budivnictva*, 2016, no. 2, pp. 250-258. (in Russian).
14. **Mander J.B., Priestley M.J.N. & Park R.** Theoretical Stress-Strain Model for Confined Concrete // Journal of Structural Engineering, ASCE. Volume 114, no. 8, August 1988, pp. 1827...1849.
15. **Gvozdev A.A.** Prochnost', strukturnye izmeneniya i deformacii betona [Strength, structural changes and deformations of concrete]. Moscow, Strojizdat, 1978. – 296 p.
16. **Bank L.** Composites for construction Structural Design with FRP Materials. Chapter 6. FRP Shear Reinforcement, Wiley, 2006.
17. **Gizdatullin A.R., Hozin V.G., Kuklin, A.N., Husnutdinov, A.M.** Osobennosti ispytanij i harakter razrusheniya polimerkompozitnoj armatury [Features of testing and the nature of destruction of polymer composite reinforcement] // *Inzhenerno-stroitel'nyj zhurnal,* 2014, no. 3, pp. 40-50 (in Russian).
18. **Imjai T., Guadagnini M. & Pilakoutas K.** Bend strength of FRP bars: Experimental investigation and bond modeling // J.

Mater. Civ. Eng., 2017, vol. 29, no. 7, DOI: 10.1061/(ASCE)MT.1943-5533.0001855.
19. **Menges, G.** Kunststoff verarbeitung Umdruck zur Vorlesung (printed lecture notes ed. Menges G. IKV), Aachen, 1980.
20. **Ahmed Mohsen Abd El Fattah.** PhD thesis. – Kansas state university, USA, 2012 pp. 318…324, 341…348.
21. **Lapshinov A.E., Kakusha V.A., Gorbunov I.A.** Strength Investigation of Short Concrete Columns Reinforced with GFRP Reinforcement II Scientific Conference «MODELLING AND METHODS OF STRUCTURAL ANALYSIS», Moscow State University of Civil Engineering, 2021.

СПИСОК ЛИТЕРАТУРЫ

1. **Tamrazyan A.G., Fedorov V.S., Kharun M.** The effect of increased deformability of columns on the resistance to progressive collapse of buildings // IOP Conference Series: Materials Science and Engineering, 2019, 675 012004, DOI: 10.1088/1757-899X/675/1/012004.
2. **Tamrazyan A., Avetisyan L.** Comparative analysis of analytical and experimental results of the strength of compressed reinforced concrete columns under special combinations of loads // MATEC Web of Conferences, 2016, 86(1):01029, DOI: 10.1051/matecconf/20168601029
3. **Кришан А.Л., Астафьева М.А.** Силовое сопротивление трубобетонных колонн высотных зданий / А.Л. Кришан,. – Магнитогорск: Изд-во Магнитогорск. гос. техн. ун-та им. Г.И. Носова, 2015.
4. Тамразян А.Г. К расчету несущей способности железобетонных колонн с учетом диаграммы деформирования ограниченного бетона // № 5 (377) Технология текстильной промышленности. – 2018. – С. 217-220.
5. **Ahmed E., Dulude C. & Benmokrane B.** Construction and monitoring of the GFRP-reinforced flat slabs of the Hotel de Ville Parking Garage in Quebec City, 2011 Canada. Technical Rep., City of Québec, Quebec.
6. **Hamdy M. Mohamed, Benmokrane B.** Design and Performance of Reinforced Concrete Water Chlorination Tank Totally Reinforced with GFRP Bars: Case Study // Journal of Composites for Construction, 2014, Vol. 18, Issue 1, pp. 05013001. DOI: 10.1061/(ASCE)CC.1943-5614.0000429.
7. **SP 295.1325800.2017** Concrete structures reinforced with fibre-reinforced polymer bars. Design rules
8. **ACI 440.1R-15** (ACI Committee 440, 2015). «Guide for the Design and Construction of Concrete Reinforced with Fiber-Reinforced Polymer Bars». American Concrete Institute, Farmington Hills, MI, 88 pp.
9. **CAN/CSA S806-12** (2012). «Design and Construction of Building Components with Fiber Reinforced Polymers», Canadian Standards Association, Rexdale, ON, Canada.
10. **Afifi M.Z., Mohamed H.M. & Benmokrane B.** Axial capacity of circular concrete columns reinforced with GFRP-bars and spirals // Journal of Composites for Construction, ASCE, Volume 18, no. 1, Feb. 2014, p. 04013017. DOI:10.1061/(ASCE)CC.1943-5614.0000438
11. **Лапшинов А.Е., Тамразян А.Г.** К влиянию поперечного армирования на прочность и деформативность сжатых бетонных элементов, армированных композитной полимерной арматурой // Stroitel'stvo i rekonstrukciya. 2018. № 4 (78). S. 20-30.
12. **Lapshinov A.E., Madatyan S.A.** Concrete columns reinforced with GFRP and BFRP // 11th International Conference on Fiber Reinforced Polymers in Reinforced Concrete Structures. Guimaraes, Portugal. 2013.
13. **Орешкин Д.А., Бондаренко Ю.В., Спиранде К.В., Мольский М.М.**

Экспериментальные исследования прочности и деформативности стеклопластиковой арматуры при сжатии и сжатых стеклопластбетонних элементов // Науковий вісник будівництва, 2016. № 2. с. 250 -258.
14. **Mander J.B., Priestley M.J.N. & Park R.** Theoretical Stress-Strain Model for Confined Concrete // Journal of Structural Engineering, ASCE. Volume 114, no. 8, August 1988, pp. 1827...1849.
15. **Гвоздев А.А.** Прочность, структурные изменения и деформации бетона. – М.: Стройиздат, 1978. – 296 с.
16. **Bank L.** Composites for construction Structural Design with FRP Materials. Chapter 6. FRP Shear Reinforcement, Wiley, 2006.
17. **Гиздатуллин А.Р., Хозин В.Г., Куклин, А.Н., Хуснутдинов, А.М.** Особенности испытаний и характер разрушения полимеркомпозитной арматуры // Инженерно-строительный журнал, 2014, № 3. – С. 40-50.
18. **Imjai T., Guadagnini M. & Pilakoutas K.** Bend strength of FRP bars: Experimental investigation and bond modeling // J. Mater. Civ. Eng., 2017, vol. 29, no. 7, DOI: 10.1061/(ASCE)MT.1943-5533.0001855.
19. **Menges, G.** Kunststoff verarbeitung Umdruck zur Vorlesung (printed lecture notes ed. Menges G. IKV), Aachen, 1980.
20. **Ahmed Mohsen Abd El Fattah.** PhD thesis. – Kansas state university, USA, 2012 pp. 318…324, 341…348.
21. **Lapshinov A.E., Kakusha V.A., Gorbunov I.A.** Strength Investigation of Short Concrete Columns Reinforced with GFRP Reinforcement II Scientific Conference «MODELLING AND METHODS OF STRUCTURAL ANALYSIS», Moscow State University of Civil Engineering, 2021.

Ashot G. Tamrazyan, Head of the Department of Reinforced Concrete and Masonry Structures of the National Research Moscow State University of Civil Engineering, Doctor of Technical Sciences, Professor, Full Member of the Russian Academy of Engineering (RIA), Advisor to the RAASN. 129337, Russia, Moscow, Yaroslavskoe highway, 26, tel. +79037305843, e-mail: tamrazian@mail.ru.

Andrey E. Lapshinov, senior lecturer, Head of the Laboratory for the Inspection of Buildings and Structures of the National Research Moscow State University of Civil Engineering. 129337, Russia, Moscow, Yaroslavskoe highway, 26, tel. +74952874914 (ext.555), e-mail: La686@ya.ru.

Тамразян Ашот Георгиевич, заведующий кафедрой железобетонных и каменных конструкций ФГБОУ ВО «Национальный исследовательский Московский государственный строительный университет», доктор технических наук, профессор, действительный член Российской инженерной академии (РИА), советник РААСН. 129337, Россия, г. Москва, Ярославское шоссе, д. 26, телефон +79037305843, e-mail: tamrazian@mail.ru.

Лапшинов Андрей Евгеньевич, старший преподаватель, заведующий лабораторией обследования зданий и сооружений (ЛОЗиС) ФГБОУ ВО «Национальный исследовательский Московский государственный строительный университет». 129337, Россия, г. Москва, Ярославское шоссе, д. 26, телефон +79265659080 (доб.555), e-mail: La686@ya.ru. Россия, г. Москва, Ярославское шоссе, д. 26, телефон +74952874914, e-mail: La686@ya.ru

International Journal for Computational Civil and Structural Engineering, 18(2) 175–183 (2022)

DOI:10.22337/2587-9618-2022-18-2-175-183

RELATIONSHIP BETWEEN STRENGTH AND DEFORMATION CHARACTERISTICS OF HIGH-STRENGTH SELF-COMPACTING CONCRETE

Igor M. Bezgodov [1], Semyon S. Kaprielov [2], Andrey V. Sheynfeld [2,]

[1] Research and testing center «MGSU STORY-TEST» National Research Moscow State University of Civil Engineering, Mytishchi, RUSSIA

[2] «Research Institute for Concrete and Reinforced Concrete» named after A.A. Gvozdev, Moscow, RUSSIA

Abstract. The paper provides data on the strength and deformation characteristics of heavy self-compacting concrete of classes B30-B100 with a cubic compressive strength of 36.5-114.8 MPa. It has been established that the values of the concrete prism compressive strength (36.2-104.2 MPa) are 42-64% higher than the normalized values given in the building code of the Russian Federation SP 63.13330.2018. The values of the static modulus of elasticity for high-strength concretes of classes B80-B100 are 44.1-48.1 GPa and exceed by 5-12% the values given in SP 63.13330.2018. The ultimate compressive strains of concrete of classes B30-B100 are in the range from 261×10^{-5} to 326×10^{-5} and exceed the value of 200×10^{-5} given in SP 63.13330.2018. Complete deformation diagrams of self-compacting concretes of classes B30-B100 have been constructed. The nonlinearity of these ones decreases with increasing concrete strength. The descending branch of the σ-ε diagram is observed only for concrete of a class below B55 with a total relative compressive strain of 403.3×10^{-5} under a loading level of $0.85R_b$. Concrete of classes B55-B100 has no descending branch. Previously established dependencies are refined for the analytical description of strains and stresses at any stages of loading structures.

Keyword. High-strength self-compacting concrete, complete strain diagrame, deformation characteristics, Poisson's ratio, ultimate compressive strains, compressive strength, static modulus of elasticity.

ВЗАИМОСВЯЗЬ ПРОЧНОСТНЫХ И ДЕФОРМАЦИОННЫХ ХАРАКТЕРИСТИК ВЫСОКОПРОЧНЫХ САМОУПЛОТНЯЮЩИХСЯ БЕТОНОВ

И.М. Безгодов[1], С.С. Каприелов [2], А.В. Шейнфельд [2]

[1] Научно-исследовательский и испытательный центр «МГСУ СТРОЙ-ТЕСТ» Национальный исследовательский Московский Государственный Строительный Университет, г. Мытищи, РОССИЯ

[2] Научно-исследовательский, проектно-конструкторский и технологический институт бетона и железобетона им. А.А. Гвоздева, г. Москва, РОССИЯ

Аннотация. Получены данные о прочностных и деформационных характеристиках тяжёлых самоуплотняющихся бетонов классов В30-В100 с кубиковой прочностью на сжатие 36,5-114,8 МПа. Установлено, что значения призменной прочности бетонов на сжатие (36,2-104,2 МПа) на 42-64 % превосходят нормируемые показатели, приведенные в своде правил РФ СП 63.13330.2018. Значения статического модуля упругости, для высокопрочных бетонов классов В80-В100 составляют 44,1-48,1 ГПа и превышают на 5-12 % значения, приведенные в СП 63.13330.2018. Предельные относительные деформации сжатия бетонов классов В30-В100 находятся в диапазоне от 261×10^{-5} до 326×10^{-5} и превышают значение 200×10^{-5}, приведенное в СП 63.13330.2018. остроены полные диаграммы деформирования самоуплотняющихся бетонов классов В30-В100, нелинейность которых уменьшается по мере роста прочности бетона. Нисходящая ветвь диаграммы σ-ε наблюдается только у бетона класса ниже В55 с суммарной относительной деформацией сжатия $403,3\times10^{-5}$ при уровне нагружения $0,85R_b$. У бетонов классов В55-В100 нисходящая ветвь отсутствует. Уточнены ранее установленные зависимости для аналитического описания относительных деформаций и напряжений на любых этапах нагружения конструкций.

Ключевые слова: Высокопрочный самоуплотняющийся бетон, полная диаграмма деформирования, деформационные характеристики, коэффициент Пуассона, предельные относительные деформации сжатия, прочность на сжатие, статический модуль упругости.

INTRODUCTION

All regulatory documents for the calculation of reinforced concrete structures both in Russia (set of rules SP 63.13330.2018) and abroad (international standard Model Code MC 2010, European standard EN 1992-1-1: 2004 Eurocode 2) are based on the relationship between the strength and deformation characteristics of concrete.

In Russia, the generalized strength parameter is the compressive strength class of concrete determined by the values of cubic (R) and prism (R_b) compressive strength. Among several normalized deformation characteristics of concrete, the most significant is the static modulus of elasticity (E_b), which according to SP 63.13330.2018 "Concrete and reinforced concrete structures. General Provisions", depends mainly on the classes and types of concrete. The remaining deformation characteristics are either depends on the elastic modulus (shear modulus ($G=0,4 \cdot E_b$), or are taken constant (transverse strain coefficient - Poisson's ratio $\nu_b=0.2$; ultimate strain for axial compression under short-term load $\varepsilon_{b0}=0.002$).

At the same time, foreign standards give strength and deformation characteristics (except for Poisson's ratio) for each class of concrete.

An analysis of the existing concrete strain diagrams under compression in Russian and foreign regulatory documents has shown that the ultimate compressive strain of concrete in many countries is taken as a variable. And non-linear dependences of strain diagrams are proposed, considering the ascending and descending branches [1]. In addition, the values on the ascending branch of the corresponding cylindrical strength and the total strain, taking into account the descending branch, are determined for each class.

However, the application of the dependencies given in foreign standards and literature is difficult in Russia, since the methods for determining the main characteristics of concrete have significant differences regarding the shape and size of the samples, the conditions for their maintenance, the speed and discreteness of loading, etc.

A number of studies [2-9] showed that the experimentally obtained dependences between the strength and deformation characteristics of ordinary concrete with a compressive strength not exceeding 40 MPa cannot always be used for high-strength concrete with a strength of 60-120 MPa.

Therefore, the study of the relationship between the strength and the complex of deformation characteristics of both ordinary and high-strength concretes with the construction of complete strain diagrams (including the descending branch) and the refinement of the previously obtained dependencies is an urgent task. This is of particular interest for concretes made of self-compacting mixtures, the volume of which is growing.

The purpose of the research was to determine the relationship between the strength and deformation characteristics of concrete classes from B30 to B100, prepared from self-compacting mixtures, with the refinement of previously obtained dependencies

To achieve the purpose, the following tasks were solved:

- determination of strength (cubic and prismatic compressive strength) and deformation (static modulus of elasticity, Poisson's ratio, ultimate compressive strains) characteristics of five compositions of self-compacting concrete of classes B30-B100;
- construction of complete concrete deformation diagrams, including the descending branch;

- refining of the previously established in [8, 9] dependences of the deformation characteristics of concretes on their prism compression strength;
- comparing of the obtained results with the standard values given in the building code of the Russian Federation SP 63.13330.2018.

MATERIALS AND TEST METHODS

Applied materials

The materials (cement, modifier, microfiller, sand and crushed stone), which satisfy the standards of the Russian Federation and applied in the production of self-compacting concrete mixes for construction projects at the Moscow-City MIBC, were used for the preparation of concrete in laboratory conditions.

The characteristics of the materials were as follows:

- Portland cement CEM I 52.5 N, corresponding to GOST 31108;
- organomineral concrete modifier MB10-50C A-II-2, including microsilica (45%), fly ash (45%) and superplasticizer (10%) [10], corresponding to GOST R 56178;
- micro-filler - non-activated mineral powder MP-1 (ground limestone) with a particle size of less than 1.25 mm, corresponding to GOST R 52129 and GOST R 56592;
- superplasticizer SikaPlast E4 based on a mixture of modified lignosulfonates and polycarboxylate esters, corresponding to GOST 24211;
- class I quartz sand with fineness modulus M_{cr}=2.55, corresponding to GOST 8736;
- crushed granite fraction 5-10 mm, corresponding to GOST 8267;
- water for mixing concrete mixtures, corresponding to GOST 23732.

Compositions and Properties of Concrete Mixes

In laboratory conditions, 5 concrete compositions were prepared using self-compacting mixtures with a cement consumption of 287 to 482 kg/m^3 with the addition of MB modifier and micro-filler at a water-binding ratio W / (C + MB) from 0.25 to 0.69.

The compositions of self-compacting concrete mixtures are presented in table 1.

Table 1. Composition of self-compacting concrete mixtures

No composition	Composition of self-compacting concrete mixes, kg/m^3						
	C	MB	MP-1	FA	CA	SP	W
1	287	-	148	822	871	3,53	198
2	305	29	167	836	836	-	177
3	349	65	150	818	838	-	161
4	423	70	101	826	846	-	161
5	482	131	50	733	904	-	151

Note: C - Portland cement; MB - modifier; MP-1 - microfiller; FA - sand; CA - crushed stone; SP - superplasticizer; W - water.

Concrete mixtures were prepared in a 25-liter forced-action mixer with mixing of each batch for 5 minutes. The results of tests of concrete mixtures showed that their mobility, determined by the spread of a normal cone [11], is in the range from 55 to 65 cm.

Object of Research and Test Methods

Samples were formed from the prepared concrete mixtures: 3 cubes with a size of 100 × 100 × 100 mm to determine the cubic compressive strength of concrete (R) according to Russian standards GOST 10180 and GOST 31914; 6 prisms with a size of 100 × 100 × 400 mm to

determine the prism compressive strength of concrete, the static modulus of elasticity, Poisson's ratio according to the standards of the Russian Federation GOST 24452 and GOST 31914; 3 prisms with size of 70.7 × 70.7 × 280 mm to establish complete strain diagrams of concrete according to the method [13, 14].
Control specimens were stored for 28 days under normal conditions (temperature plus 20 ± 2 °C, humidity 95 ± 5%) before testing. The loading of the prisms was carried out in steps equal to $0{,}1R_b$ with holding at each step for 5 minutes until the destruction of the specimens. The static modulus of elasticity and Poisson's ratio were determined at a loading level of 30-40% of the prism strength.

TEST RESULTS AND DISCUSSION

Table 2 presents concrete test results in terms of: concrete class (B), cubic (R) and prism (R_b) compressive strength, static modulus of elasticity (E_b), Poisson's ratio (ν_b), ultimate compressive strain (ε_{b0}). And figure 1 shows complete strain diagrams of concrete.

Table 2. Strength and short-term deformation characteristics of concrete

No	Strength and deformation characteristics of concrete						
	B, MPa	R, MPa	R_b, MPa	E_b, MPa	ν_b	$\varepsilon_{b0} \times 10^5$	$\varepsilon_{b0}^{-0,85} \times 10^5$
1	B30	36.5	36.2	32.5	0.206	261	403
2	B55	61.8	56.0	39.2	0.214	276	-
3	B70	80.2	74.5	40.5	0.198	299	-
4	B80	92.5	85.3	44.1	0.205	294	-
5	B100	114.8	104.2	48.1	0.230	326	-

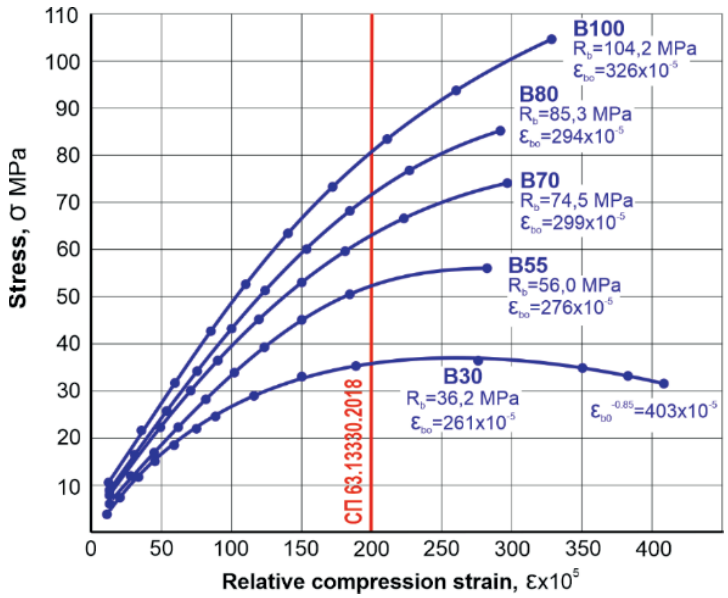

Figure 1. Complete concrete compressive strain diagrams σ–ε

Compressive Strength

The cubic compressive strength (R) for all concretes at the age of 28 days is in the range from 36.5 to 114.8 MPa and corresponds to concrete compressive strength classes from B30 to B100. The prismatic compressive strength of concrete (R_b) at the age of 28 days is in the range from 36.2 to 104.2 MPa. Evaluation of the above results according to the criterion of the prism strength coefficient, determined by the ratio of the prismatic compressive strength of concrete to cubic strength ($K_{pp} = R_b / R$) shows that its actual values are in the range from 0.91 to 0.99 and significantly exceed the values of this coefficient calculated according to the parameters given in the building code of Russian Federation SP 63.13330.2018 (from 0.71 to 0.73).

Static Modulus of Elasticity

The static modulus of elasticity of concretes of classes B30-B100 with prismatic strength from 36.2 to 104.2 MPa is in the range from 32.5 to 48.1 GPa (see Table 2). Figure 2 shows the dependence between the static modulus of elasticity and the prismatic compressive strength of concrete.

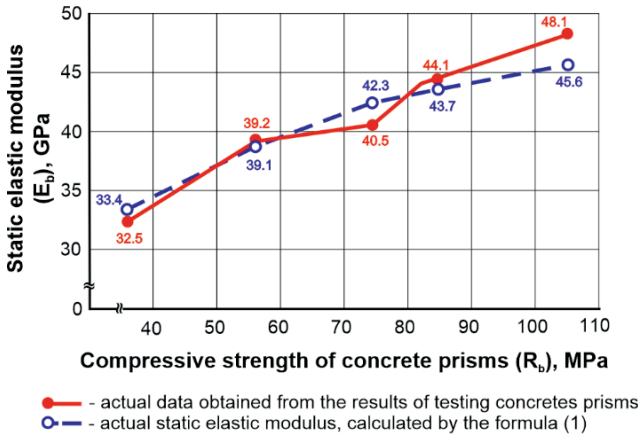

Figure 2. Static elastic modules vs compressive strength of concretes prisms

The obtained results (see Fig. 2) show that the static modulus of elasticity of concrete is proportional to the prismatic strength and can be determined by the corrected formula [8] in the form:

$$E_b = \frac{52000 \cdot R_b}{23 + 0.92 R_b} \quad (1)$$

Comparison of the calculated results and those obtained experimentally shows (see Figure 2) that this formula can be used to determine the static modulus of elasticity of concrete, since the calculation error does not exceed 5%.

Comparison of the experimentally obtained values of E_b with normalized values showed that the static modulus of elasticity of high-strength concretes of classes B80-B100 exceeds by 5 ... 14% the values given in SP 63.13330.2018, corresponds to Model Code MC 2010 and is consistent with previously obtained results [4-6, 15, 16].

Poisson's ratio

Poisson's ratio of heavy concretes of classes B30-B100 is in the range from 0.198 to 0.230 (see Table 2) and, in general, corresponds to the normalized value of the coefficient of transverse deformations $\nu_{b,P}$= 0.2 according to the building code of the Russian Federation SP 63.13330.2018.

Ultimate compressive strain

Ultimate compressive strains of concrete of classes B30-B100 with prismatic strength from 36.2 to 104.2 MPa are in the range from 261×10^{-5} to 326×10^{-5} (see Table 2) and exceed the value of 200×10^{-5} given in SP 63.13330.2018. The complete strain diagrams of concrete under compressive show (see Fig. 1) that the descending branch is observed only in class B30 concrete with a prism strength of 36.2 MPa, where the total relative compressive strain was 403.3×10^{-5} at the level of $0.85R_b$ of the descending branch. For concretes with higher strength, there is no descending branch, which corresponds to the results obtained in [9].

Figure 3 shows the dependence between the ultimate strain and the prismatic compression strength of concrete.

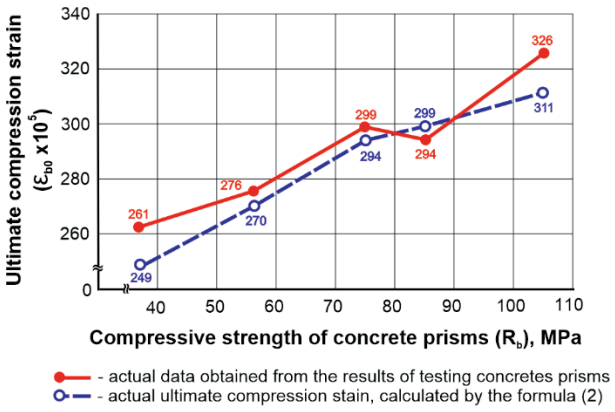

Figure 3. Ultimate compressive strain vs compressive strength of concretes prisms

The obtained results (see Fig. 3) show that the ultimate strain of concrete increase with an increase in prismatic strength and can be determined by the corrected formula [8, 9] in the form:

$$\varepsilon_{b0} = 0.024 \sqrt[3]{\frac{R_b}{E_b}} \qquad (2)$$

Comparison of the calculated results and those obtained experimentally shows (see Fig. 3) that this formula can be used to determine the limiting relative deformations of concrete, since the calculation error does not exceed 5%.

Relationship between Strains and Stresses

It is necessary to determine the values of strains or stresses at any stage of loading or deformation of structures when calculating or testing. For an analytical description of relative strains and stresses at any stages of loading, it is proposed to use the refined equations [8, 9] in the form:

$$\varepsilon_\eta = \varepsilon_{b0} \cdot \left(1 \pm \sqrt[n]{1 - \frac{\sigma}{R_b}}\right) \qquad (3)$$

$$\sigma_\eta = R_b - \left|1 - \frac{\varepsilon_\eta}{\varepsilon_{b0}}\right|^n \cdot R_b \qquad (4)$$

where:

ε_η is strain at a given stress level;

σ_η is the stress at given strain, MPa;

η is the loading level equal to the ratio of stresses to prismatic strength (σ/R_b);

ε_{b0} is ultimate compressive strain;

R_b is the prismatic compressive strength of concrete, MPa;

n is the degree of non-linearity of the concrete strain diagram, which depends on its strength and can be determined by the formula:

$$n = 3.5 - \frac{R_b \cdot 10^3}{E_b} \qquad (5)$$

The dependence between the degree of nonlinearity of deformation diagrams and the prism compressive strength of concrete is shown in Figure 4, from which it can be seen that with increasing strength, the degree of nonlinearity decreases and tends to unity. This confirms the results of previous studies [8, 17].

It should be noted that when determining the strain in the descending branch of the diagram σ–ε, the sign in front of the root of the second polynomial in formula (3) should be replaced from minus to plus.

Comparison of the strainf of self-compacting concretes of classes B30-B100, obtained experimentally, with the results calculated from the analytical dependence (3) showed satisfactory convergence, which makes it possible to use equations (3) and (4) to assess strains and stresses at all stages of loading structures.

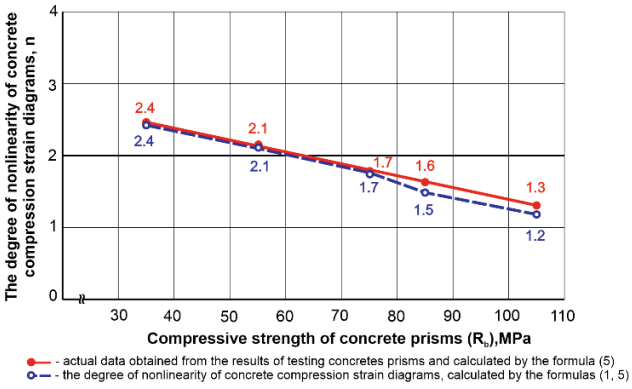

Figure 4. The degree of nonlinearity of concrete compressive strain diagrams vs compressive strength of concretes prisms

CONCLUSIONS

1. Strength (cubic and prismatic compressive strength) and deformation (static modulus of elasticity, Poisson's ratio, ultimate compressive strains) characteristics of five compositions of self-compacting concretes of classes B30-B100 were determined using standard and special methods.
2. The obtained results show that the values of the strength and deformation characteristics of high-strength self-compacting concrete of classes B80-B100 exceed the standard values given in the building code of the Russian Federation SP 63.13330.2018.
3. Complete strain diagrams of self-compacting concretes of classes B30-B100 are constructed. The nonlinearity of these diagrams decreases as the strength of concrete increases. The descending branch of the σ-ε diagram is observed only for concrete of classes below B55 with a prism strength of 36.2 MPa, while it is absent for concrete of classes B55-B100 with a prism strength of 56.0-104.2 MPa.
4. Previously established dependences for determining the static modulus of elasticity, ultimate compressive strains and analytical expressions for strains and stresses at any stages of loading the structures made of self-compacting concrete of classes B30-B100 have been refined.

REFERENCES

1. **Panfilov D.A., Pischulev A.A., Dimadetdinov K.I.** Review of existing diagrams of deformation of concrete under compression in domestic and foreign regulatory documents // Industrial and civil construction. - 2013. - No. 3. - pp.34-36 (in Russian).
2. **Sviridov N.V., Kovalenko M.G., Chesnokov V.M.** Mechanical properties of especially strong cement stone // Concrete and reinforced concrete. 1991. No. 2. pp. 7-9 (in Russian).
3. **Beshr H., Almusallam A.A., Maslehuddin M.** Effect of coarse aggregate quality on the mechanical properties of high strength concrete // Construction and Building Materials. - 2003. - No. 97-103. - pp. 97-103.
4. **Kaprielov S., Karpenko N., Sheinfeld A., Kouznetsov E.** Influence of multicomponent modifier containing silica fume, fly ash, superplasticizer and air-entraining agent on structure and deformability of high-strength concrete // Seventh CANMET/ ACI International Conference on Superplasticizers and other chemical admixtures in concrete. Berlin, Germany, 2003, p.p.99-107
5. **Kaprielov S., Karpenko N., Sheinfeld A.** On Controlling Modulus of Elasticity and Creep in High-Strength Concrete with Multicomponent Modifier // Eighth CANMET/ACI International Conference on Fly ash, Silica Fume, Slag and Natural Pozzolans in Concrete, Las Vegas, May 23-29, 2004, Supplementary Papers, p.p.405-421
6. **Karpenko N.I., Kaprielov S.S., Kuznetsov E.N., Sheinfeld A.V., Bezgodov I.M.** Creep measures for high-strength concretes based on MB / RAASN, Bulletin of the Department of Building Sciences. Issue. 8. - M., 2004. - pp.203-214 (in Russian).
7. **Byung Jae Lee, Seong-Hoon Kee, Taekeun Oh, Yun-Yong Kim** Effect of Cylinder Size on the Modulus of Elasticity and Compression Strength of Concrete from Static and Dynamic Tests // Hindawi Publishing Corporation Advances in Materi-als Science and Engineering. - 2015. - No. ID 580638. - 12 p.
8. **Bezgodov I.M.** On the issue of evaluation, the ultimate compression strain for various classes of concrete // Concrete and reinforced concrete. - No. 15. - 2015. - pp.9-11 (in Russian).
9. **Bezgodov I.M., Dmitrenko E.N.** Improvement of curvilinear diagrams of concrete deformation // Industrial and civil

construction. - No. 8. – 2019. – pp.99-104 (in Russian).
10. **Kaprielov S., Sheinfeld A.** Influence of Silica Fume / Fly Ash / Superplasticizer Combinations in Powder-like Complex Modifiers on Cement Paste Porosity and Concrete Properties. // Sixth CANMET/ACI International Conference on Superplasticizers and other Chemical Admixtures in Concrete. Nice, France, October 2000. Proceedings, p.p. 383-400.
11. EN 12350-8: 2010 Testing fresh concrete - Part 8: Self compacting concrete - Slump-flow test.
12. EN 206: 2013 Concrete - Specification, performance, production and conformity.
13. **Bezgodov I.M., Levchenko P.Yu.** On the issue of the method of obtaining complete strain concrete diagrams // Tekhnologii betonov. - No. 10. - 2013. - pp.34-36 (in Russian).
14. **Bezgodov I.M.** Methodological features of the study of complete strain diagrams and stress relaxation in concrete // Tekhnologii betonov. - No. 11-12. - 2020. - pp.39-44 (in Russian).
15. **Sviridov N.V.** Extra strong cement concrete // Energy construction. - No. 8. - 1991. - P.21-29 (in Russian).
16. **Sviridov N.V., Kovalenko M.G.** Concrete with a strength of 150 MPa on ordinary Portland cements // Concrete and reinforced concrete. - No. 2. - 1990. - pp.21-22 (in Russian).
17. **Mkrtchan A.M., Aksenov V.M.** Analytical description of the diagram of deformation of high-strength concretes // Inzhenerny Bulletin of the Don. - 2013. - No. 3. URL: http://www.ivdon.ru/magazin/archive/n3y2013/1818 (in Russian).

СПИСОК ЛИТЕРАТУРЫ

1. **Панфилов Д.А., Пищулев А.А., Димадетдинов К.И.** Обзор существующих диаграмм деформирования бетонов при сжатии в отечественных и зарубежных нормативных документах // Промышленное и гражданское строительство. – 2013. - №3. - С.34-36.
2. **Свиридов Н.В., Коваленко М.Г., Чесноков В.М.** Механические свойства особо прочного цементного камня // Бетон и железобетон. 1991. № 2. С .7-9.
3. **Beshr H., Almusallam A.A., Maslehuddin M.** Effect of coarse aggregate quality on the mechanical properties of high strength concrete // Construction and Building Materials. - 2003. - №97-103. - C. 97-103.
4. **Kaprielov S., Karpenko N., Sheinfeld A., Kouznetsov E.** Influence of multicomponent modifier containing silica fume, fly ash, superplasticizer and air-entraining agent on structure and deformability of high-strength concrete // Seventh CANMET/ACI International Conference on Superplasticizers and other chemical admixtures in concrete. Berlin, Germany, 2003, p.p.99-107
5. **Kaprielov S., Karpenko N., Sheinfeld A.** On Controlling Modulus of Elasticity and Creep in High-Strength Concrete with Multicomponent Modifier // Eighth CANMET/ACI International Conference on Fly ash, Silica Fume, Slag and Natural Pozzolans in Concrete, Las Vegas, May 23-29,2004, Supplementary Papers, p.p.405-421
6. **Карпенко Н.И., Каприелов С.С., Кузнецов Е.Н., Шейнфельд А.В., Безгодов И.М.** Меры ползучести высокопрочных бетонов на основе МБ // РААСН, Вестник отделения строительных наук. Вып. 8. - М., 2004. - С.203-214.
7. **Byung Jae Lee, Seong-Hoon Kee, Taekeun Oh, Yun-Yong Kim** Effect of Cylinder Size on the Modulus of Elasticity and Compressive Strength of Concrete from Static and Dynamic Tests // Hindawi Publishing Corporation Advances in Materials Science and Engineering. - 2015. - №ID 580638. – 12 p.

8. **Безгодов И.М.** К вопросу оценки предельной относительной деформации бетона при сжатии для различных классов бетона // Бетон и железобетон. – №5. – 2015. – С.9-11.
9. **Безгодов И.М., Дмитренко Е.Н.** Совершенствование криволинейных диаграмм деформирования бетона // Промышленное и гражданское строительство. – №8. – 2019. – С.99-104.
10. **Kaprielov S., Sheinfeld A.** Influence of Silica Fume / Fly Ash / Superplasticizer Combinations in Powder-like Complex Modifiers on Cement Paste Porosity and Concrete Properties // Sixth CANMET/ACI International Conference on Superplasticizers and other Chemical Admixtures in Concrete. Nice, France, October 2000. Proceedings, p.p.383-400.
11. EN 12350-8: 2010 Testing fresh concrete - Part 8: Self compacting concrete - Slump-flow test.
12. EN 206: 2013 Concrete - Specification, performance, production and conformity.
13. **Безгодов И.М., Левченко П.Ю.** К вопросу о методике получения полных диаграмм деформирования бетона // Технологии бетонов. – №10. – 2013. – С.34-36.
14. **Безгодов И.М.** Методические особенности исследования полных диаграмм деформирования и релаксации напряжений в бетоне / Технологии бетонов. – №11-12. – 2020. – С.39-44.
15. **Свиридов Н.В.** Особо прочный цементный бетон / Энергетическое строительство. - №8. – 1991. - С.21-29.
16. **Свиридов Н.В., Коваленко М.Г.** Бетон прочностью 150 МПа на рядовых портландцементах / Бетон и железобетон. - №2. – 1990. - С.21-22.
17. **Мкртчан А.М., Аксенов В.М.** Аналитическое описание диаграммы деформирования высокопрочных бетонов // Инженерный вестник Дона. – 2013. - №3. URL:http://www.ivdon.ru/magazin/archive/n3y2013/1818.

Simyon S. Kaprielov, Eng.Sc.D., head of laboratory №16 "Research Institute for Concrete and Reinforced Concrete" named after A.A. Gvozdev, JSC Research Center of Construction, 2-nd Institutskaya str., 6, Moscow, 109428, Russian Federation, tel. +7 (499) 171-0573, e-mail: kaprielov@masterbeton-mb.ru.

Andrey V. Sheynfeld, Eng.Sc.D., deputy head of laboratory №16 "Research Institute for Concrete and Reinforced Concrete" named after A.A. Gvozdev, JSC Research Center of Construction, 2-nd Institutskaya str., 6, Moscow, 109428, Russian Federation, tel. +7 (499) 174-7635, e-mail: sheynfeld@masterbeton-mb.ru.

*Igor M. Bezgodov***,** engineer, Moscow State University of Civil Engineering (National Research University), Moscow, Russian Federation, Olimpiyskiy avenue, 50/25, Mytishchi, Moscow oblast, 141006, Russian Federation, tel. +7 (495) 542-97-42, e-mail: ibezgodov52@yandex.ru

Каприелов Семен Суренович, доктор технических наук, заведующий лабораторией №16 НИИЖБ им. А.А. Гвоздева АО «НИЦ Строительство», 109428 Москва, 2-я Институтская ул., д.6, кор.5, тел. +7-499-171-0573, e-mail: kaprielov@masterbeton-mb.ru.

Шейнфельд Андрей Владимирович, доктор технических наук, зам. заведующего лабораторией №16 НИИЖБ им. А.А. Гвоздева АО «НИЦ Строительство», 109428 Москва, 2-я Институтская ул., д.6, кор.5, тел. +7-499-174-7635, e-mail: sheynfeld@masterbeton-mb.ru.

Безгодов Игорь Михайлович, инженер, Научно-исследовательский и испытательный центр «МГСУ СТРОЙ-ТЕСТ» Национальный исследовательский Московский Государственный Строительный Университет, 141006 г. Мытищи, Московская область, Олимпийский проспект, вл.50, стр. 25, УЛК СТиЖБК, +7-495-542-9742, e-mail: ibezgodov52@yandex.ru

DOI:10.22337/2587-9618-2022-18-2-184-193

FORMATION OF COMPUTATIONAL SCHEMES OF ADDITIONAL TARGETED CONSTRAINTS THAT REGULATE THE FREQUENCY SPECTRUM OF NATURAL OSCILLATIONS OF ELASTIC SYSTEMS WITH A FINITE NUMBER OF DEGREES OF MASS FREEDOM, THE DIRECTIONS OF MOVEMENT OF WHICH ARE PARALLEL, BUT DO NOT LIE IN THE SAME PLANE PART 1: THEORETICAL FOUNDATIONS

Leonid S. Lyakhovich [1], ***Pavel A. Akimov*** [2]
[1] Tomsk State University of Architecture and Civil Engineering, Tomsk, RUSSIA
[2] National Research Moscow State University of Civil Engineering, Moscow, RUSSIA

Abstract: For some elastic systems with a finite number of degrees of freedom of masses, in which the directions of mass movement are parallel and lie in the same plane (for example, rods), special methods have been developed for creating additional constraints, the introduction of each of which purposefully increases the value of only one natural frequency and does not change any from the natural modes. The method of forming a matrix of additional stiffness coefficients that characterize such targeted constraint in this problem can also be applied when solving a similar problem for elastic systems with a finite number of degrees of mass freedom, in which the directions of mass movement are parallel, but do not lie in the same plane (for example, plates). At the same time, for such systems, only the requirements for the design schemes of additional targeted constraints are formulated, and not the methods for their creation. The distinctive paper proposes an approach that allows researcher to create computational schemes for additional targeted constraints for such systems. A variant of the computational scheme, represented by a rod system with one degree of activity, is considered. Some special properties of such targeted constraints are revealed. When forming the computational scheme, the material consumption for creating a constraint is minimized, and design restrictions are taken into account. Particular attention is paid to the modification of the computational scheme of the constraint, when, during its formation, rods appear that "pass" through the original system.

Keywords: natural frequency, natural modes, generalized additional targeted constraint, stiffness coefficients

ФОРМИРОВАНИЕ РАСЧЕТНЫХ СХЕМ ДОПОЛНИТЕЛЬНЫХ СВЯЗЕЙ, ПРИЦЕЛЬНО РЕГУЛИРУЮЩИХ СПЕКТР ЧАСТОТ СОБСТВЕННЫХ КОЛЕБАНИЙ УПРУГИХ СИСТЕМ С КОНЕЧНЫМ ЧИСЛОМ СТЕПЕНЕЙ СВОБОДЫ МАСС, У КОТОРЫХ НАПРАВЛЕНИЯ ДВИЖЕНИЯ ПАРАЛЛЕЛЬНЫ, НО НЕ ЛЕЖАТ В ОДНОЙ ПЛОСКОСТИ ЧАСТЬ 1: ТЕОРЕТИЧЕСКИЕ ОСНОВЫ

Л.С. Ляхович [1], ***П.А. Акимов*** [2]
[1] Томский государственный архитектурно-строительный университет, г. Томск, РОССИЯ
[2] Национальный исследовательский Московский государственный строительный университет, г. Москва, РОССИЯ

Аннотация: Для некоторых упругих систем с конечным числом степеней свободы масс, у которых направления движения масс параллельны и лежат в одной плоскости, (например, стержни) разработаны

методы создания дополнительных связей, введение каждой из которых прицельно увеличивает значение только одной собственной частоты и не изменяет ни одну из форм собственных колебаний. Метод формирования матрицы дополнительных коэффициентов жесткости, характеризующих в этой задаче такую прицельную связь, может быть применен и при решении аналогичной задачи для упругих систем с конечным числом степеней свободы масс, у которых направления движения масс параллельны, но не лежат в одной плоскости (например, пластины). Вместе с тем для таких систем сформулированы лишь требования к расчетным схемам дополнительных прицельных связей, а не методы их создания. В данной статье предлагается подход, позволяющий создавать расчётные схемы дополнительных прицельных связей и для таких систем. Рассмотрен вариант расчётной схемы связи, представленный стержневой системой с одной степенью активности. Выявлены некоторые особые свойства таких прицельных связей. При формировании расчётной схемы выполняется минимизация расхода материала на создание связи, учитываются конструктивные ограничения. Особое внимание уделено модификации расчётной схемы связи, когда при ее формировании появляются стержни, «проходящие» сквозь исходную систему.

Ключевые слова: частота собственных колебаний, форма собственных колебаний, обобщенная прицельная дополнительная связь, коэффициенты жесткости

As is known [1, 2, 3, 4, 5, 6], introduction of generalized targeted constraints is one of the methods for freeing a given interval of the natural frequency spectrum from one or more of natural frequencies.

Original solutions of problems of forming a matrix of additional stiffness and creating on the basis of this matrix of the computational scheme of the corresponding targeted constraints are presented in [1, 2, 3, 4]. These solutions are based on the displacement method for systems with a finite number of degrees of freedom of masses, in which the directions of mass movement are parallel and lie in the same plane.

It was shown in [5, 6] that the method of forming a matrix of additional stiffness coefficients can also be applied in solving a similar problem for elastic systems with a finite number of mass degrees of freedom, in which the directions of mass movement are parallel, but do not lie in the same plane. Besides, the requirements for the computational schemes of additional targeted constraints were formulated in [5, 6] in relation to this problem.

Let us give the order of formation of the matrix of additional stiffness in relation to the considering systems.

In the papers mentioned above, the main system of the displacement method [7] was chosen, which was obtained by introducing linear relations in the direction of mass movement. For example, for the plate [8, 9] shown in Figure 1*a*, the main system is shown in Figure 1*b*.

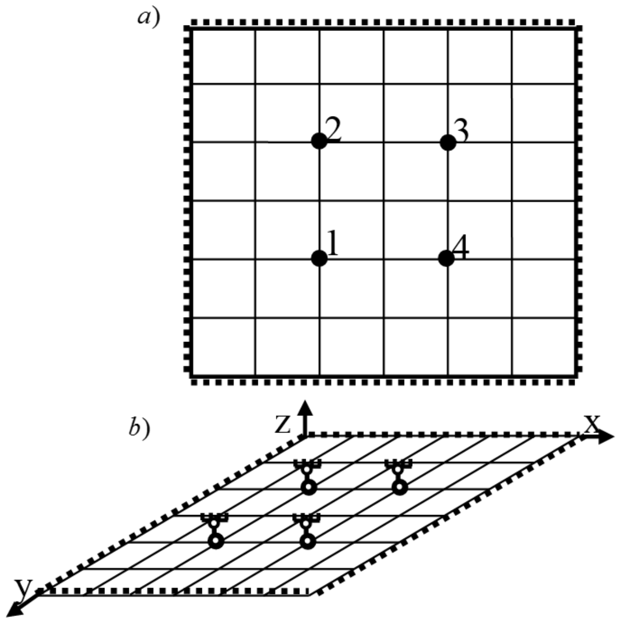

Figure 1. Sample of structure.

The displacement method equations were written in the conventional form for systems with a finite number of degrees of freedom:

$$\begin{cases} (r[1,1]+m[1]\omega^2)v[1,j]+r[1,2]v[2,j]+ \\ \quad +\ldots+r[1,q]*v[q,j]+\ldots+r[1,n]*v[n,j]=0 \\ r[2,1]v[1,j]+(r[2,2]+m[2]\omega^2)v[2,j]+ \\ \quad +\ldots+r[2,q]*v[q,j]+\ldots+r[2,n]*v[n,j]=0 \\ \ldots\ldots\ldots\ldots\ldots\ldots\ldots\ldots\ldots\ldots\ldots\ldots \\ r[n,1]v[1,j]+r[n,2]v[2,j]+ \\ \quad +\ldots+r[n,q]v[q,j]+ \\ \quad +\ldots+(r[n,n]+m[n]*\omega^2)*v[n,j]=0 \end{cases} \qquad (1)$$

In (1) the values $r[i,k]$ form a matrix of stiffness coefficients $A=\|r[i,k]\|$; $m[i]$ are the mass values, forming a diagonal matrix $M=\|m[i]\|$; ω is the frequency of natural oscillations of the system; $v[k,j]$ are displacements in the direction of mass movement in the j-th natural mode $(j=1,2,..,q,,..,n)$ (forms of natural oscillations). Equation roots

$$\left|A-\omega^2 M\right|=0 \qquad (2)$$

determine the frequency spectrum of natural oscillations of the system

$$\omega[1],\omega[2],...,\omega[q-1],\omega[q],\omega[q+1],...,\omega[n] \qquad (3)$$

It is shown that the creation of generalized targeted constraint that increases only one frequency of natural oscillations (for example, $\omega[q]$) to a predetermined value and does not change any of the natural modes and the values of the remaining frequencies of the spectrum is based on the formation of a matrix of additional stiffness coefficients:

$$A_0=A_{SO}A_S=A_{SO}\|a_0[i,k]\|_{i,k=1}^{n}, \qquad (4)$$

where we have

$$A_S=\|a_0[i,k]\|_{i,k=1}^{n}. \qquad (5)$$

The matrix A_0 must have special properties. If the introduced constraint is "targeted" at the (q)-th frequency of natural oscillations, then the stiffness coefficients $\|a_0[i,k]\|_{i,k=1}^{n}$ should be orthogonal to the coordinates of the natural modes of the remaining $(n-1)$ frequencies of the spectrum, that is

$$\sum_{k=1}^{n}a_0[i,k]v[k,j]=0, \quad i=1,2,..,n,\quad j=1,2,..,(q-1),(q+1),..,n). \qquad (6)$$

With respect to the (q)-th natural frequency, at which the introduced constraints is "targeted", the coefficients are not orthogonal, that is,

$$\sum_{k=1}^{n}a_0[i,k]v_\omega[k,q]\neq 0,\quad (i=1,2,..,n). \qquad (7)$$

It can be shown that conditions (6) and (7) will be satisfied by the coefficients

$$a_0[i,k]=m[i]m[k]v_\omega[i,q]v_\omega[k,q]. \qquad (8)$$

The value of the multiplier is defined as the root of the equation

$$\left|(A-\omega_S^2 M)+A_{SO}A_S\right|=0. \qquad (9)$$

Since the (q)-th natural mode of the original system remains its natural mode after the introduction of the targeted constraint and at a frequency ω_S, the factor A_{SO} can be found as

$$A_{SO}=\frac{-\sum_{i=1}^{n}\sum_{k=1}^{n}(a[i,k]-\omega_S^2 m[i,k])v_\omega[i,q]v_\omega[k,q]}{\sum_{i=1}^{n}\sum_{k=1}^{n}a_0[i,k]v_\omega[i,q]v_\omega[k,q]}. \qquad (10)$$

The result of solving the equation

$$\left|(A+A_{SO}A_S)-\omega^2 M\right|=0. \qquad (11)$$

must confirm that the natural modes have not changed, and the "targeted" frequency has increased to ω_S.

The support device, to which the matrix of additional stiffness coefficients A_0 will correspond, must provide the ratio between the nodal displacements the same as between the coordinates of the (q)-th natural mode of the original system. It is shown that such a ratio will be realized if the additional support system transfers forces

to the nodes of the main rod system, the ratios between which are proportional to the values

$$R_0[i] = m[i]v[i,(q)]. \quad (12)$$

In [5, 6], the requirements for the computational schemes of additional targeted constraints were formulated in relation to systems with a finite number of degrees of freedom of masses, in which the directions of mass movement are parallel, but do not lie in the same plane.

For such systems, the generalized targeted constraint should correspond to the matrix of additional stiffness coefficients A_0 (4). If the computational scheme of constraint is represented by a variant of the hinged-rod system, then it should be once statically indeterminate, in the nodes of the system where the masses are located, vertical members are installed in the direction of movement of the masses, and the prestress of any one constraint member causes forces $Nst[i](i = 1,..,n)$ in these vertical members, the relationship between which are proportional to the ratios between the forces $R_0[i]$ (11). In this case, the constraint structure should not have any connections with the original system, except for vertical members installed in the nodes where the masses are located.

It was noted in [5, 6] that the computational schemes of generalized targeted constraint that meet the above requirements are multivariant and depend on the geometry of the original system, the location of the masses, and some other characteristics of the considering object.

In particular, it is possible to accept the computational scheme of the targeted constraint in the form of a once statically indeterminate hinge-rod system, the geometry of which is determined both by the lengths of the main vertical members installed in the nodes in the direction of mass movement $lst[i]\,(i = 1,2,..,n)$ and by the given lengths of additional rods $ld[k]\,(k = 1,2,..,n_1)$, that have no connections with the original system.

Then, after forming the matrix of additional stiffnesses A_0 (4), computing the values A_{SO} (10) and $R_0[i]$ (12), the problem is reduced to finding the lengths $lst[i]\,(i = 1,2,..,n)$ from the conditions for the occurrence in the main vertical members of forces $Nst[i](i = 1,..,n)$, the ratios between which will be proportional to the ratios between the forces $R_0[i]\,(i = 1,.., n)$.

Below, one of the options for finding the lengths of the rods will be presented, which determine the geometry of the targeted constraint, in which the necessary ratios between the forces in the main vertical members are provided.

The considering variant is based on methods for minimizing the square of the difference between the forces arising in the main vertical members $Nst[i](i = 1,..,n)$ in the process of forming the targeted constraint and the values $R_0[i]\,(i = 1,.., n)$.

Thus, we have the problem of minimization of the function

$$fo = \sum_{i=1}^{i=n} (Nst[i] - R_0[i])^2. \quad (13)$$

in the parameter space $lst[i]\,(i = 1,2,..,n)$.

In accordance with the above requirements, a computational scheme of the targeted constraint is created in the form of a once statically indeterminate hinge-rod system, in which the length of one of the main racks (for example, g -th) is specified. Let's call this vertical member the base one $lst[g] = lst0[g]$. According to the design conditions, the lengths of additional rods $\bar{l}d[k]\,(k = 1,2,..,n1)$ are selected, which do not vary during the formation of the scheme of the targeted constraint. The initial values of the remaining variable lengths

$$\bar{l}st[i]\,(i = 1,2,..,(g-1),(g+1),..,n)$$

are also set. These actions determine the initial geometry of the computational scheme of the targeted constraint. Since the computational scheme of the targeted constraint is once statically indeterminate, the force in one of the main vertical members (for example, in q -th) is set. .

The method of searching for the minimum of the objective (target) function (13) in the space of variable lengths (the steepest descent, random search, etc.) is selected.

Let us consider an algorithm for implementing actions to form a computational scheme for targeted constraint.

We recommend application of special algorithm, presented below.

1. In accordance with the chosen method of searching for the minimum of the objective function, increments to variable lengths

$$lst[i] = \bar{l}st[i] + \Delta l(i = 1,2,..,(g-1),(g+1),..,n)$$

are set and the geometry of the computational scheme of the targeted constraint is updated.

2. A system of equilibrium equations is constructed in order to determine the forces in the rods of targeted constraint. Since it was assumed that $Nst[q] = R_0[q]$, now the number of unknown forces in the rods of the targeted constraint is equal to the number of equilibrium equations.

3. Unknown forces in the rods of the targeted constraint are determined from the equations of equilibrium with allowance for $Nst[q] = R_0[q]$.

4. The value of the objective function is computed

$$fo = \sum_{i=1}^{i=n} (Nst[i] - R_0[i])^2 .$$

5. If we have $f_O > OOO$, then in accordance with the chosen method of searching for the minimum of the objective function (12), the increments $\Delta l[i]$ are corrected (values $\Delta l[i]$ and ratios between them are changed). We have

$$\bar{l}st[i] = lst[i](i = 1,2,..,(g-1),(g+1),..,n).$$

Then the transition to the third step (item 3) is made. and the process continues.

6. If the value f_O is less than a preselected small value OOO, then the process ends, and the computational scheme of the targeted constraint is formed with a given error (OOO) provided that the length of the base rack is accepted $lst[g] = lst0[g]$.

The cross-sectional areas of the rods of targeted constraint are found from the condition that its stiffness coincides with the stiffness determined by matrix $A_0 = A_{S0} \cdot A_S = A_{S0} \cdot \| a_0[i,k] \|_{i,k=1}^{n}$ (4).

Targeted constraint is constructed on the basis of forces $R_0[i]$, which correspond to the forces in the main vertical members $Nst[i] = R_0[i](i = 1,2,..,n)$, in additional vertical members $Nd[k]\,(k = 1,2,..,n1)$ and in the rods of the belt of constraint $N_P[j](j = 1,2,..,n2)$.

The derivation of the dependency that determines the area of the cross-sections of the rods of targeted constraint for the systems, in which the directions of mass movement are parallel and lie in the same plane, is given in [4]. This dependence with allowance for some modifications, can also be applied to the system under consideration

$$A_{SO}\Big(\sum_{i=1}^{n} \frac{N_{st}^2[i] \cdot |lst[i]|}{E \cdot F_{st}[i]} + \sum_{j=1}^{n2} \frac{N_P^2[j] \cdot l_P[j]}{E \cdot F_P[j]} + \sum_{j=1}^{n1} \frac{N_d^2[k] \cdot ld[k]}{E \cdot F_d[k]}\Big) = 1, \quad (14)$$

where

$$F_{st}[i] = F \cdot \alpha[i]; \quad F_P[j] = F \cdot \beta[j]; \quad F_d[k] = F \cdot \gamma[k] \quad (15)$$

are respectively, the cross-sectional area of the vertical members, belts and additional rods of the targeted constraint; E is the modulus of elasticity of the material of the rods. The coefficients $\alpha[i]$, $\beta[j]$ and $\gamma[k]$ determine the ratios between the cross-sectional areas in the rods of targeted constraint.

The value F is determined by dependence

$$F = A_{SO}\Big(\sum_{i=1}^{n} \frac{N_{st}^2[i] \cdot |lst[i]|}{E \cdot \alpha[i]} + \sum_{j=1}^{n2} \frac{N_P^2[j] \cdot l_P[j]}{E \cdot \beta[j]} + \sum_{j=1}^{n1} \frac{N_d^2[k] \cdot l_P[k]}{E \cdot \gamma[k]}\Big). \quad (16)$$

The length of the base vertical member

$$lst[g] = lst0[g]$$

and the values $\alpha[i]$, $\beta[j]$ and $\gamma[k]$ depending on the design conditions, can either be set or found by minimizing the volume of material of the targeted constraint.

If the volume of material of the targeted constraint is minimized, then the objective function (volume of material of the targeted constraint V_{SV}) has the form:

$$V_{SV} = F \cdot \{\sum_{i=1}^{n} \alpha[i] \cdot |lst[i]| + \\ + \sum_{k=1}^{n2} \beta[j] \cdot l_P[j] + \sum_{k=1}^{n1} \gamma[k] \cdot ld[k]\}. \quad (17)$$

When constructing the computational scheme of the targeted constraint, the values of some variable lengths may turn out to be negative. Therefore, absolute values of variable lengths $|lst[i]|$ are introduced into (14), (16) and (17).

When constructing the computational scheme of the targeted constraint and minimizing the function (17), the limitations of the variable values can be taken into account. Restrictions on the values of $\alpha[i]$, $\beta[j]$ and $\gamma[k]$ are related to the conditions of strength, stiffness, and stability of the rods. These restrictions are not considered in the distinctive paper. The restrictions on the lengths of the main vertical members can be written in the following form:

$$l\max \geq lst[i] \geq l\min, (i = 1,2,..,n), \quad (18)$$

where $lst[i]$ are the lengths of the main vertical members; $l\min$ and $l\max$ are respectively their allowable minimum and maximum values.

Since the ratios between the forces

$$Nst[i] = R_0[i] (i = 1,2,..,n)$$

do not change during the construction of the targeted constraint at $f_O \leq OOO$, the ratios between the lengths of the variable values do not change when the length of the base vertical member changes. This circumstance allows us to attribute restrictions (18) to one variable length – the length of the base vertical member $lst[g] = lst0[g]$. If for $f_O \leq OOO$ among the main vertical members the largest length is equal to $lst[k1]$, and the smallest is equal to $lst[k2]$, then, denoting $\chi 1 = lst[g]/lst[k1]$ and $\chi 2 = lst[g]/lst[k2]$, expression (18) can be rewritten as:

$$l\max 0 \geq lst0[g] \geq l\min 0, \quad (19)$$

where we have

$$l\max 0 = l\max^* \chi 1; \quad l\min 0 = l\min^* \chi 2.$$

Now, when searching for the minimum of function (13), the range of acceptable values $lst0[g]$ is determined by dependence (19).

Constraints in the form (18), (19) are used provided that the signs of the lengths of all main vertical members are positive. If the signs of the lengths of all main vertical members are negative, then the sign of the coordinate in the direction of the vertical members is reversed.

There are cases in construction of computational scheme of the targeted constraint, when the values of the lengths of some main vertical members turn out to be positive, while others are negative. Structurally, such a scheme requires an ideally free "passage" of a part of the rods of targeted constraint "through" the original system, which is almost unrealizable. In these cases, the targeted constraint should be shifted in the direction of movement of the masses in a positive or negative direction by an amount at which the values of all the lengths of the main vertical members will be of the same sign.

Let us designate by $lst[i]\max$ the largest length among the "positive vertical members" at $f_O \leq OOO$, and by $lst[k]\min$ the largest absolute value among the "negative lengths".

If the targeted constraint is moved in a positive direction, then the shift value must be greater than

$$Z_V = lst[k]\min + l\min .$$

Obviously, in this case, the lengths of all vertical members will be "positive". In this case, the vertical member of the smallest length will be in the node where the vertical member was with $lst[k]\min$. Now the length of the vertical member in this node will be equal to $l\min$. The longest length of vertical member will be at the node where the vertical member was with $lst[i]\max$. Now the length of the vertical member in this node will be equal to

$$lst[i]\max + lst[k]\min + l\min .$$

If the targeted constraint is moved in a negative direction, then the shift value must be greater than

$$Z_N = lst[i]\max + l\min .$$

Obviously, in this case, the lengths of all vertical members will be "negative". In this case, the vertical member with the smallest absolute value of the length will be in the node where the vertical member was with $lst[i]\max$. Now the absolute value of the length of the vertical member in this node will be equal to $l\min$. The largest absolute length of the vertical member will be at the node where the vertical member was with $lst[k]\min$. Now the absolute value of the vertical member length in this node will be equal to

$$lst[i]\max + lst[k]\min + l\min .$$

In these cases, the restrictions on the lengths of the vertical members take the form

$$l\max \geq (lst[i]\max + lst[k]\min + l\min) . \quad (20)$$

As noted above, at $f_O \leq OOO$, the ratios between the lengths of the variable quantities do not change. This circumstance allows us to attribute restrictions (20) to one variable length – the length of the base vertical member $lst[g] = lst0[g]$. Using (20) we get

$$l\max - l\min \geq lst[i]\max + lst[k]\min$$

or

$$\frac{l\max - l\min}{lst0[g]} \geq \frac{lst[i]\max}{lst0[g]} + \frac{lst[k]\min}{lst0[g]} . \quad (21)$$

Since the ratios

$$\frac{lst[i]\max}{lst0[g]} \text{ and } \frac{lst[k]\min}{lst0[g]}$$

remain constant when the length $lst0[g]$ changes, then we have

$$\frac{lst[i]\max}{lst0[g]} + \frac{lst[k]\min}{lst0[g]} = \frac{lst[i]\max + lst\min}{lst0[g]} = \frac{1}{\chi 3}, \quad (22)$$

where

$$\chi 3 = \frac{lst0[[g]}{lst[i]\max + lst[k]\min} . \quad (23)$$

remains constant when changing $lst0[g]$.
Thus, constraint (20) can be represented as:

$$(l\max - l\min) * \chi 3 \geq lst0[g] . \quad (24)$$

Now, when searching for the minimum of function (17), the range of acceptable values $lst0[g]$ for cases where the lengths of the main vertical member turn out to be of different signs is determined by dependence (24).
The choice of , and does not affect the computational scheme of the targeted constraint, but only affects the values of the

cross-sectional areas of its rods. The value of the length of the base vertical member affects both the geometry of the computational scheme of the targeted constraint and the cross-sectional areas of its rods.

Let's consider the procedure for implementing actions to minimize the volume of material of targeted constraint.

If the values , and are set according to the design conditions, then, after determining the initial values of the cross-sectional areas of the rods of targeted constraint, we can determine the length of the base vertical member, at which the objective function (17) takes minimum value in the range of permissible values of this length ((19) or (24)). It can be done by the above algorithm and one of the variants of the one-dimensional search method.

If the values , and are also determined from the conditions of the minimum material of the targeted constraint, then in this case one of the variants of the method of successive approximations can be used. The initial values , and are preliminarily selected, and the initial values of the cross-sectional areas of the rods of targeted constraint are determined. Each approximation of the method consists of two successive steps:

1. On the basis of the algorithm given above and the one-dimensional search method, with known , and the length of the base vertical member is determined, at which the objective function V_{SV} (17) takes the minimum value in the range of allowable length values $lst0[g]$ ((19) or (24)).

2. One of the methods for finding the minimum of the objective function (17) (the steepest descent, random search, and others) in the space of variable values , and continues the process of minimizing the function (17).

Approximations of the method (the first and the second steps) are repeated until the difference between the weight functions (17) of two neighboring approximations becomes less than a sufficiently small preselected value.

REFERENCES

1. **Nudelman Ya.L., Lyakhovich L.S., Giterman D.M.** O Naibolee Podatlivyh Svjazjah Naibol'shej Zhestkosti [About the Most Pliable Bonds of the Greatest Rigidity]. // Issues of applied mechanics and mathematics. Tomsk, TSU Publishing House, 1981, pp. 113-126 (in Russian).
2. **Giterman D.M., Lyakhovich L.S., Nudelman Ya.L.** Algoritm Sozdanija Rezonansno-Bezopasnyh Zon pri Pomoshhi Nalozhenija Dopolnitel'nyh Svjazej [Algorithm for Creation of Resonantly Safe Zones by Applying Additional Constraints]. // "Dynamics and strength of machines", Vol. 39. Kharkov, "Vishcha schkola", 1984, pp. 63-69 (in Russian).
3. **Lyakhovich L.S., Maletkin O.Yu.** O Pricel'nom Regulirovanii Sobstvennyh Chastot Uprugih Sistem [On Targeted Control of Natural Frequencies of Elastic Systems. // Izvestiya vuzov. Construction and architecture, 1990, No. 1, pp. 113-117 (in Russian).
4. **Lyakhovich L.S.** Osobye Svojstva Optimal'nyh Sistem i Osnovnye Napravlenija ih Realizacii v Metodah Rascheta Sooruzhenij [Special Properties of Optimal Systems and the Main Directions of Their Implementation in the Methods of Calculation of Structures]. Tomsk, Tomsk State University of Architecture and Construction, 2009, 372 pages (in Russian).
5. **Lyakhovich L.S., Akimov P.A.** Aimed control of the frequency spectrum of eigenvibrations of elastic plates with a finite number of degrees of freedom of masses by superimposing additional constraints. // International Journal for Computational Civil and Structural Engineering, 2021, Volume 17, Issue 2, pp. 76-82.
6. **Akimov P.A., Lyakhovich L.S.** Pricel'noe Regulirovanie Spektra Chastot Sobstvennyh Kolebanij Uprugih Plastin s Konechnym Chislom Stepenej Svobody Mass Putem Vvedenija Dopolnitel'nyh Obobshhennyh Svjazej i Obobshhennyh Kinematicheskih

Ustrojstv [Precision Control for Eigen-Frequency of Elastic Plates with Finite Number of Mass Degrees of Freedom by Using Additional Generalized Connections and Kinematic devices]. // Vestnik Tomskogo gosudarstvennogo arkhitekturno-stroitel'nogo universiteta. Journal of Construction and Architecture, 2021, Volume 23, Issue 4, pp. 57-68 (in Russian).

7. **Akimov P.A., Lyakhovich L.S.** Aimed Control of the Frequency Spectrum of Eigenvibrations of Elastic Plates with a Finite Number of Degrees of Mass Freedom by Introducing Additional Generalized Kinematic Devices. // International Journal for Computational Civil and Structural Engineering, 2021, Volume 17, Issue 4, pp. 181-187.
8. **Shitikova M.V., Krusser A.I.** Force Driven Vibrations of Nonlinear Plates on a Viscoelastic Winkler Foundation Under the Harmonic Moving Load. // International Journal for Computational Civil and Structural Engineering, 2021, Volume 17, Issue 4, pp. 161-180.
9. **Akimov P.A., Mozgaleva M.L., Kaytukov T.B.** Numerical Solution of the Problem of Isotropic Plate Analysis with the Use of B-Spline Discrete-Continual Finite Element Method. // International Journal for Computational Civil and Structural Engineering, 2020, Volume 16, Issue 4, pp. 14-28.
10. **Manuylov G.A., Kosytsyn S.B., Grudtsyna I.E.** Influence of Buckling Forms Interaction of Stiffened Plate Bearing Capacity. // International Journal for Computational Civil and Structural Engineering, 2020, Volume 16, Issue 2, pp. 83-93.
11. **Mozgaleva M.L., Akimov P.A., Kaytukov T.B.** Localization of Solution of the Problem of Isotropic Plate Analysis with the Use of B-Spline Discrete-Continual Finite Element Method. // International Journal for Computational Civil and Structural Engineering, 2021, Volume 17, Issue 1, pp. 55-74.

СПИСОК ЛИТЕРАТУРЫ

1. **Нудельман Я.Л., Ляхович Л.С., Гитерман Д.М.** О наиболее податливых связях наибольшей жесткости. // Вопросы прикладной механики и математики. – Томск: Издательство ТГУ, 1981, с. 113-126.
2. **Гитерман Д.М., Ляхович Л.С., Нудельман Я.Л.** Алгоритм создания резонансно-безопасных зон при помощи наложения дополнительных связей. // Динамика и прочность машин», Вып. 39. – Харков: «Вища школа», 1984, с. 63-69.
3. **Ляхович Л.С., Малеткин О.Ю.** О прицельном регулировании собственных частот упругих систем. // Известия вузов. Строительство и архитектура, 1990, №1, с. 113-117.
4. **Ляхович Л.С.** Особые свойства оптимальных систем и основные направления их реализации в методах расчета сооружений. – Томск: Издательство Томского государственного архитектурно-строительного университета, 2009. – 372 с.
5. **Lyakhovich L.S., Akimov P.A.** Aimed control of the frequency spectrum of eigenvibrations of elastic plates with a finite number of degrees of freedom of masses by superimposing additional constraints. // International Journal for Computational Civil and Structural Engineering, 2021, Volume 17, Issue 2, pp. 76-82.
6. **Акимов П.А, Ляхович Л.С.** Прицельное регулирование спектра частот собственных колебаний упругих пластин с конечным числом степеней свободы масс путем введения дополнительных обобщенных связей и обобщенных кинематических устройств. // Вестник Томского государственного архитектурно-строительного университета, 2021, Том 23, №4, с. 57-67.
7. **Akimov P.A., Lyakhovich L.S.** Aimed Control of the Frequency Spectrum of Eigenvibrations of Elastic Plates with a Finite Number of Degrees of Mass Freedom by

Introducing Additional Generalized Kinematic Devices. // International Journal for Computational Civil and Structural Engineering, 2021, Volume 17, Issue 4, pp. 181-187.

8. **Shitikova M.V., Krusser A.I.** Force Driven Vibrations of Nonlinear Plates on a Viscoelastic Winkler Foundation Under the Harmonic Moving Load. // International Journal for Computational Civil and Structural Engineering, 2021, Volume 17, Issue 4, pp. 161-180.
9. **Akimov P.A., Mozgaleva M.L., Kaytukov T.B.** Numerical Solution of the Problem of Isotropic Plate Analysis with the Use of B-Spline Discrete-Continual Finite Element Method. // International Journal for Computational Civil and Structural Engineering, 2020, Volume 16, Issue 4, pp. 14-28.
10. **Manuylov G.A., Kosytsyn S.B., Grudtsyna I.E.** Influence of Buckling Forms Interaction of Stiffened Plate Bearing Capacity. // International Journal for Computational Civil and Structural Engineering, 2020, Volume 16, Issue 2, pp. 83-93.
11. **Mozgaleva M.L., Akimov P.A., Kaytukov T.B.** Localization of Solution of the Problem of Isotropic Plate Analysis with the Use of B-Spline Discrete-Continual Finite Element Method. // International Journal for Computational Civil and Structural Engineering, 2021, Volume 17, Issue 1, pp. 55-74.

Ляхович Леонид Семенович, академик РААСН, профессор, доктор технических наук, профессор кафедры строительной механики, Томский государственный архитектурно-строительный университет; 634003, Россия, г. Томск, Соляная пл. 2;
E-mail: lls@tsuab.ru

Акимов Павел Алексеевич, академик РААСН, профессор, доктор технических наук; ректор Национального исследовательского Московского государственного строительного университета; 129337, г. Москва, Ярославское шоссе, д. 26; тел. +7(495) 651-81-85;
Email: AkimovPA@mgsu.ru, pavel.akimov@gmail.com.

Leonid S. Lyakhovich, Full Member of the Russian Academy of Architecture and Construction Sciences, Professor, DSc, Head of Department of Structural Mechanics, Tomsk State University of Architecture and Building; 2, Solyanaya St., 2, Tomsk, 634003, Russia;
E-mail: lls@tsuab.ru

Pavel A. Akimov, Full Member of the Russian Academy of Architecture and Construction Sciences, Professor, Dr.Sc.; Rector of National Research Moscow State University of Civil Engineering; 26, Yaroslavskoe Shosse, Moscow, 129337, Russia; phone +7(495) 651-81-85;
Email: AkimovPA@mgsu.ru, pavel.akimov@gmail.com.